Nanospintronics with Molecular Magnets - Tunneling and Spin-Electric Coupling

Nossa Márquez, Javier Francisco

2013

Nanospintronics With Molecular Magnets. Tunneling And Spin-Electric Coupling

JAVIER NOSSA | DIVISION OF SOLID STATE PHYSICS | LUND UNIVERSITY

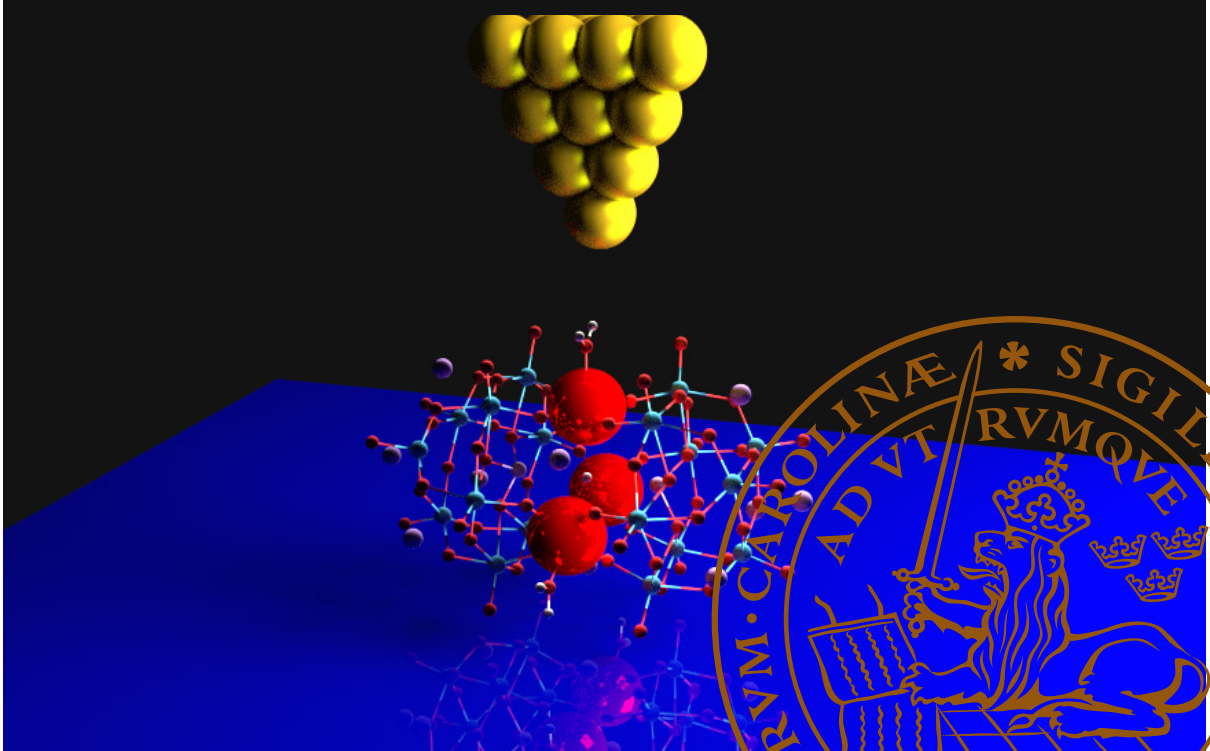

Nanospintronics with molecular magnets. Tunneling and spin-electric coupling.

Javier Nossa

Lund University

Division of Solid State Physics
Lund Institute of Technology
Lund University

Lund, Sweden 2013

ISBN 978-91-7473-547-5
ISBN 978-91-7473-548-2
Printed in Sweden by Mediatryck, Lund 2013.

Nanospintronics with molecular magnets. Tunneling and spin-electric coupling.

Javier Nossa

Division of Solid State Physics
Lund Institute of Technology
Lund University, Sweden

Thesis for the degree of
Doctor of Philosophy in Engineering

Thesis Advisor: Prof. Carlo M. Canali
Linnaeus University, Kalmar, Sweden

Faculty Opponent: Prof. Stefano Sanvito
Trinity College Dublin, Dublin, Ireland

Academic dissertation which, by due permission of the Faculty of Engineering at Lund University, will be publicly defended on Thursday, September 12th, 2013, at 13.00 in room Ny227, Kalmar-Nyckel, at Linnaeus university, Gröndalsvägen 19, for the degree of Doctor of Philosophy in Engineering.

Organization
LUND UNIVERSITY
Division of Solid State Physics,
Lund Institute of Technology,
Box 118,
SE-221 00 Lund, SWEDEN

Author(s)
Javier Francisco Nossa Marquez

Document name
DOCTORAL DISSERTATION

Date of issue
September 2013

Sponsoring organization

Title and subtitle
Nanospintronics with molecular magnets. Transport and spin-electric coupling.

Abstract
This dissertation investigates theoretically electric control of the magnetic properties of molecular magnets. Two classes of magnetic molecules are considered. The first class consists of molecules that are spin frustrated. As a consequence of the frustration, the ground-state manifold of these molecules is characterized by states of different spin chirality, which can be coupled by an external electric field. Electric control of these spin states can be used to encode and manipulate quantum information. The second class comprises molecules known as single-molecule magnets, which are characterized by a high spin and a large magnetic anisotropy. Here the main goal is to control and manipulate the magnetic properties, such as the anisotropy barriers, by adding and subtracting individual electrons, as achieved in tunneling transport.

Papers I, II and III deal with spin-electric coupling in spin frustrated molecules. Spin density functional theory is used to evaluate the parameters that control the strength of this coupling. Paper I reports the electronic and magnetic properties of the triangular antiferromagnet Cu_3. It is found that an external electric field couples to the spin chirality of the system. The strength of this coupling is large enough to allow efficient spin-electric manipulation with electric fields generated by a scanning tunneling microscope.

Paper II investigates the zero-field splitting in the ground-state manifold of the triangular Cu_3 molecular magnet caused by the Dzyaloshinskii-Moriya (DM) interaction. It employs a Hubbard model approach to elucidate the connection between the spin-orbit and the DM interaction. It is shown that the DM interaction constant D can be expressed in terms of the microscopic Hubbard-model parameters, which are calculated by first principles methods.

Paper III investigates systematically the spin-electric coupling in several triangular molecular magnets, such as V_3 and Cu_3O, and its dependence on different types of magnetic atoms, distances between magnetic centers and exchange paths between magnetic atoms. A generalization of the spin-electric coupling for a V_{15} molecular magnet, comprising fifteen magnetic centers, is also reported in this paper.

In Paper IV first-principles methods are employed to study theoretically the properties of an individual Fe_4 single-molecule magnet attached to metallic leads in a single-electron transistor geometry. It is demonstrated that an external electric potential, modeling a gate electrode, can be used to manipulate the magnetic properties of the system by adding or subtracting electrons to the molecule.

In Paper IV quantum transport via a triangular molecular magnet such as Cu_3 is investigated. It is proposed that Coulomb-blockade transport experiments can be used to determine the spin-electric coupling strength in triangular molecular magnets. The theoretical analysis, based on a Hubbard model, is supported by master-equation calculations of quantum transport in the cotunneling regime.

Key words
Molecular magnets, spin exchange, spin-orbit interaction, magnetic anisotropy, spin frustration, spin chirality, spin-electric control, quantum transport, Coulomb blockade, density functional theory, quantum master equation.

Classification system and/or index terms (if any)

Supplementary bibliographical information

Language
English

ISSN and key title

ISBN
978-91-7473-547-5
978-91-7473-548-2

Recipient´s notes

Number of pages 223

Price

Security classification

I dedicate this thesis to my parents.
They have given me the inspiration and motivation
to tackle any task with enthusiasm and determination.
They have supported me all the way since the
beginning of my studies.

Abstract

This dissertation investigates theoretically electric control of the magnetic properties of molecular magnets. Two classes of magnetic molecules are considered. The first class consists of molecules that are spin frustrated. As a consequence of the frustration, the ground-state manifold of these molecules is characterized by states of different spin chirality, which can be coupled by an external electric field. Electric control of these spin states can be used to encode and manipulate quantum information. The second class comprises molecules known as single-molecule magnets, which are characterized by a high spin and a large magnetic anisotropy. Here the main goal is to control and manipulate the magnetic properties, such as the anisotropy barriers, by adding and subtracting individual electrons, as achieved in tunneling transport.

Papers I, II and III deal with spin-electric coupling in spin frustrated molecules. Spin density functional theory is used to evaluate the parameters that control the strength of this coupling. Paper I reports the electronic and magnetic properties of the triangular antiferromagnet $\{Cu_3\}$. It is found that an external electric field couples to the spin chirality of the system. The strength of this coupling is large enough to allow efficient spin-electric manipulation with fields generated by a scanning tunneling microscope.

Paper II investigates the zero-field splitting in the ground-state manifold of the triangular $\{Cu_3\}$ molecular magnet caused by the Dzyaloshinskii-Moriya (DM) interaction. It employs a Hubbard model approach to elucidate the connection between the spin-orbit and the DM interaction. It is shown that the DM interaction constant D can be expressed in terms of the microscopic Hubbard-model parameters, which are calculated by first-principles methods.

Paper III investigates systematically the spin-electric coupling in several triangular molecular magnets, such as $\{V_3\}$ and $\{Cu_3O\}$, and its dependence on different types of magnetic atoms, distances between magnetic centers and exchange paths between magnetic atoms. A generalization of the spin-electric coupling for a $\{V_{15}\}$ molecular magnet,

comprising fifteen magnetic centers, is also reported in this paper.

In Paper IV first-principles methods are employed to study theoretically the properties of an individual $\{Fe_4\}$ single-molecule magnet attached to metallic leads in a single-electron transistor geometry. It is demonstrated that an external electric potential, modeling a gate electrode, can be used to manipulate the magnetic properties of the system by adding or subtracting electrons to the molecule.

In Paper V quantum transport via a triangular molecular magnet such as $\{C_3\}$ is investigated. It is proposed that Coulomb-blockade transport experiments can be used to determine the spin-electric coupling strength in triangular molecular magnets. The theoretical analysis, based on a Hubbard model, is supported by master-equation calculations of quantum transport in the cotunneling regime.

Keywords: Molecular magnets, spin exchange, spin-orbit interaction, magnetic anisotropy, spin frustration, spin chirality, spin-electric control, quantum transport, Coulomb blockade, density functional theory, quantum master equation.

Populärvetenskaplig Sammanfattning

I denna avhandling undersöker vi hur man med hjälp av externa elektriska fält kan manipulera de magnetiska egenskaper som finns hos molekylära magneter. Denna manipulation förmedlas av antingen spinn-elektrisk koppling eller den magnetiska anisotropin hos den molekylära magneten. För att förstå vad detta betyder så ska vi först förklara vissa grundläggande begrepp om magnetism. Vi kommer att börja med att förklara vad en molekylär magnet är. Tänk dig att du har ett antal atomer av övergångsmetaller, såsom järn, kobolt, nickel eller mangan, arrangerade på ett sådant sätt att samspelet mellan dem får dem att hålla ihop och ge magnetiska egenskaper till molekylen. Vi kommer att kalla detta arrangemang *den magnetiska kärnan* av den molekylära magneten. Tänk dig nu att denna kärna är omgiven av andra atomer (oorganiska ligander) som kan vara utformade för att säkerställa att molekylen binder på ytor eller i knutpunkter. Vi kommer att kalla denna sköld *det oorganiska skalet*.

Men varför kan en molekyl kallas för molekylär magnet? Till att börja med är en molekyl en samling av atomer. Varje atom har elektroner. Elektroner i universum innehar magnetiska egenskaper, närmare bestämt en inneboende rörelsemängdsmoment som genererar ett magnetiskt moment. I stort sett skulle man kunna se dem som mycket små stavmagneter, det vill säga att de har nord- och sydpoler. Denna inneboende egenskap kallas *spinn*. I verkligheten är spinn ett rent kvantmekaniskt objekt som kommer från losningen av den relativistiska Dirac ekvationen inom kvantmekaniken. Ofta representeras det av en pil som pekar antingen upp eller ner vilket illustrerar riktningen på det magnetiska flätet (Fig. 1 a). Då en elektron är placerad i ett magnetfält, anpassas dess spinn till det magnetfältet. En välbekant effekt kan ses när en kompassnål faller in i linje med det magnetiska fältet på jorden (se Fig. 1. c)).

Detta tankesätt kan användas för att fröstå både magnetiska material och magnetiska molekyler. Ett magnetiskt material skapas när elektronernas spinn i huvuddelen av materialet är i linje med varandra. Samma effekt syns på molekylär nivå där magnetiska moment

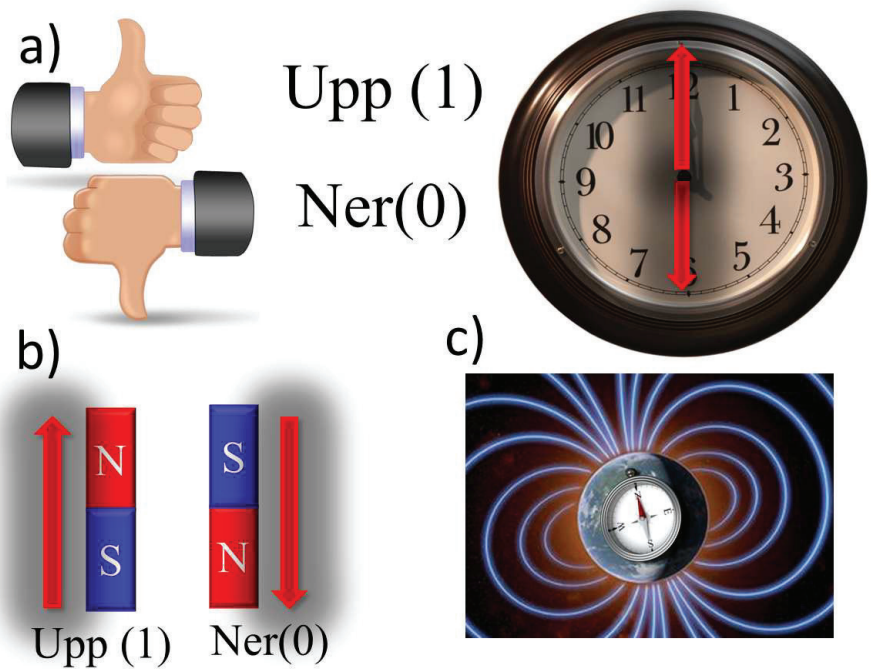

Figure 1: Tecknad av spinn av en elektron. a) Den spin kan klassiskt ses som en tumme upp eller ner. En annan representation är att tänka det som en pil som pekar mot nummer tolv i en klocka (spinn upp) eller antalet sex (spinn ner). Det är också ofta kallas som 0 eller 1 i binära siffror. b) Snurra linjer upp med orienteringen av en stavmagnet. c) De spin ställer upp med ett magnetfält precis som en linjer kompassnålen upp med jordmagnetiska fältet.

skapas genom att elektronernas spinn i en samling av atomer blir parallella. En magnetisk molekyl egenskaperna likt en klassik magnet, men uppvisar även kvantmekaniska egenskaper på grund av sin minimala storlek, uppvisar den också kvantmekaniska egenskaper. Notera att så här långt har vi inte använt något yttre magnetfält för att ordna molekylens spinn, denna uppställning har ett rent kvantmekaniskt ursprung. I en molekylär magnet styrs spinnens riktning av interaktionen mellan elektronens spinn och elektronens omloppsbana i den molekylära strukturen. Denna egenskap kallas magnetisk anisotropi och det beror på den komplicerade bindning av de magnetiska atomerna i kärnan med de icke-magnetiska atomerna i strukturen. Numera kan denna bindning till viss del vara utformad i laboratoriet vilket ger oss möjlighet att skapa molekyler med specifika egenskaper. Mängden parallella spinn i en molekylär magnet bestämmer hur robust det magnetiska beteendet är: Ju fler parallella spinn, desto mer magnetisk är molekylen.

Hittills har vi definierat vad molekylära magneter är. Låt oss nu tala om hur vi kan manipulera deras magnetiska egenskaper. Man skulle kunna se en molekylär magnet som en samling parallella spinns eller som ett gigantiskt spinn som representerar alla spinn på en gång. Det magnetiska beteendet hos en molekylär magnet styrs av detta gigantiska spinn. Genom att manipulera molekylernas spinn kan man styra dess magnetiska egenskaper. Traditionellt så manipuleras spinn med hjälp av externa magnetfält vilket emellertid är problematiskt på molekylär nivå. Den typiska storleken på en molekylär magnet är några nanometer, en nanometer är en miljard gånger mindre än en meter och det är därför mycket svårt att tillämpa magnetfält lokalt på den nivån. Magnetfält ger långsam växling, dessutom är det svårt att uppbåda ett tillräckligt kraftfullt magnetfält. Åandra sidan, starka elektriska fält kan enkelt åstadkommas och kan utan vidare tillämpas lokalt på nanoskala. De kan också slås på och av mycket snabbt. Därför är manipulation av de magnetiska egenskaperna hos molekylära magneter med hjälp av ett elektriskt fält en intressant och lovande tutveckling.

I denna avhandling studeras två metoder för hur man med hjälp av elektriska fält kan manipulera magnetiska egenskaper hos molekylära magneter. I den första metoden undersöker vi kopplingen av spinn hos en molekylär magnet med det externa elektriska fältet. Vi beaktar en särskild klass av molekylär magnet med intressanta och specifika egenskaper i sitt lägsta energitillstånd (grundtillstånd). På grund av den molekylära magnetens speciella geometri, kan ett elektriskt fält kopplas ihop med spinnet i systemet. Genom att manipulera riktningen och styrkan hos det elektriska fältet kan man därför manipulera den molekylära magnetens spinn. I den andra metoden manipulerar vi den magnetiska

anisotropin hos den molekylära magneten. I detta fall kan vi använda en annan typ av molekylär magnet som kännetecknas av sin stora magnetiskt anisotropiska energi, vilket är den energi det krävs för att ñdra molekylens spinns. Genom att manipulera denna energibarriär kan man styra de magnetiska egenskaperna hos systemet. Vi undersöker den molekylära magnets anisotropin genom att addera eller subtrahera en elektron till systemet. Ett yttre elektriskt fält kan driva elektroner in eller ut ur den molekylära magneten.

Det är relevant att understryka varför att vi studerar manipulation av magnetiska egenskaperna hos molekylära magneter: Dagens teknik måste hitta effektivare sätt att lagra och bearbeta digital information. Detta kan uppnås genom att använda kvantdatorer istället för konventionella datorer. Kvantdatorer skulle kunna lagra och bearbeta data med hjälp av kvantmekaniska tillstånd som kallas kvantum bitar eller kvantbitar vilket i sin tur skulle kunna öka beräkningskraften drastiskt. Konventionella datorer byggs av kiselkretsar, som innehåller miljontals transistorer, där var och en av dem representerar en bit av informationen som antingen kan vara noll eller ett (binära siffror). En bit skulle kunna representeras av ett spinn som pekar uppåt eller nedåt så som visas i Fig. 1 a) eller som timvisaren på kl 12 och kl 6 på en klocka i Fig. 1 b).

För att förmedla en tydligare innebörd tar vi en blick på den grundläggande skillnaden mellan konventionella datorer och kvantdatorer. Tänk att du har en klocka framför dig (se Fig. 1 b)) och timvisaren pekar mot tolvan, som i detta fall motsvarar *ett* i digital information. Tänk dig nu att timvisaren pekar mot sexan, i detta fall motsvarar det *noll* i digital information. I konventionella datorer kan timvisaren bara peka mot antingen 12 (*ett*) eller 6 (*noll*), det vill säga utföra operationer med klassiska bitar. Till skillnad från detta kan timvisaren i en kvantdator peka mot ett annat nummer. Den skulle kunna peka mot siffrorna 3, 5, 11 eller någon punkt mellan dem, på detta vis uppnås överlagring av informationen. En kvantdator utför dessutom operationer som använder kvantum (kvantbitar), som magiskt nog kan vara *noll* och *ett* samtidigt. De är i ett tillstånd av kvantum superposition, detta är vad som ger en kvantdator dess överlägsna beräkningskraft.

En molekyls spinn är allts̊ ett kvantum objekt som kan användas som en kvantbit, det kan vara upp (*ett*), nedåt (*noll*) eller båda på en gång. Om en molekylär magnet kan fungera som en pytteliten magnet, kan man därför använda den för att lagra information. Man skulle kunna föreställa sig att ha antingen en bit eller kvantbit per molekyl. Man skulle också kunna föreställa sig en molekylär magnet som en strömbrytare, precis som en transistor; en molekylär transistor, där elektricitet antingen kan vara av eller på. Eftersom molekylära magneter är ungefär tio gånger mindre än de nuvarande minsta transistorerna,

skulle det avsevärt öka mängden transistorer i en krets. Dessutom kan de två spinntillstånden i en molekylär magnet användas för att koda en kvantbit. Det har sagts att varje gång en kvantum bit sätts till en kvantdator, fördubblas datorns beräkningskraft. Man har förutspått att en kvantdator på 300-kvantbitar skulle vara mer kraftfull än dagens alla datorer sammantaget vilket illustrerar kraften i kvantmekaniska beräkningar. Elektrisk kontroll av dessa magnetiska molekyler kan följaktligen vara ett steg mot utvecklandet av en helt ny och mycket kraftfull typ av datorer.

Popular Scientific Summary

In this thesis we investigate the manipulation of the magnetic properties of molecular magnets by means of external electric fields. This manipulation is mediated by either the spin-electric coupling or the magnetic anisotropy of the molecular magnet. In order to understand what this means, let us first explain some basic concepts about magnetism. We will start explaining what a molecular magnet is. Imagine you have a bunch of transition metal atoms, such as iron, cobalt, nickel or manganese, arranged in such a way that the interaction between them makes them stick together and provide magnetic features to the molecule. We will call this arrangement the *magnetic core* of the molecular magnet. Now imagine this core to be surrounded by other atoms (inorganic ligands) that can be designed to ensure the molecule binds on surfaces or into junctions. We will call this shield *inorganic shell*.

But why a molecule can be called a molecular magnet? First of all, a molecule is a collection of atoms. Each atom has electrons. Electrons in the universe have internal magnetic properties, more precisely an intrinsic angular momentum that generates a magnetic moment. One could think that they are basically like little tiny bar magnets, one of those with north and south poles. This intrinsic property is called the *spin*. Although in reality the spin is purely a quantum mechanical object that comes from the solution of the relativistic Dirac's equation in quantum mechanics, it is commonly represented by an arrow pointing either up or down. A representation of the spin orientation is shown in Fig. 2 a). The up or down illustrates the orientation of the tiny little magnet (see Fig 2 b)). When an electron is placed in a magnetic field, its spin lines up with that field. A familiar effect can be viewed when a compass needle lines up with the magnetic field of the earth (see Fig. 2 c)).

From magnetic materials to molecular magnets one can follow this trend of thoughts. A magnetic material is created when the spins (intrinsic magnetic fields) of the electrons in the bulk of material are all aligned. The same happens in a finite system, a magnetic

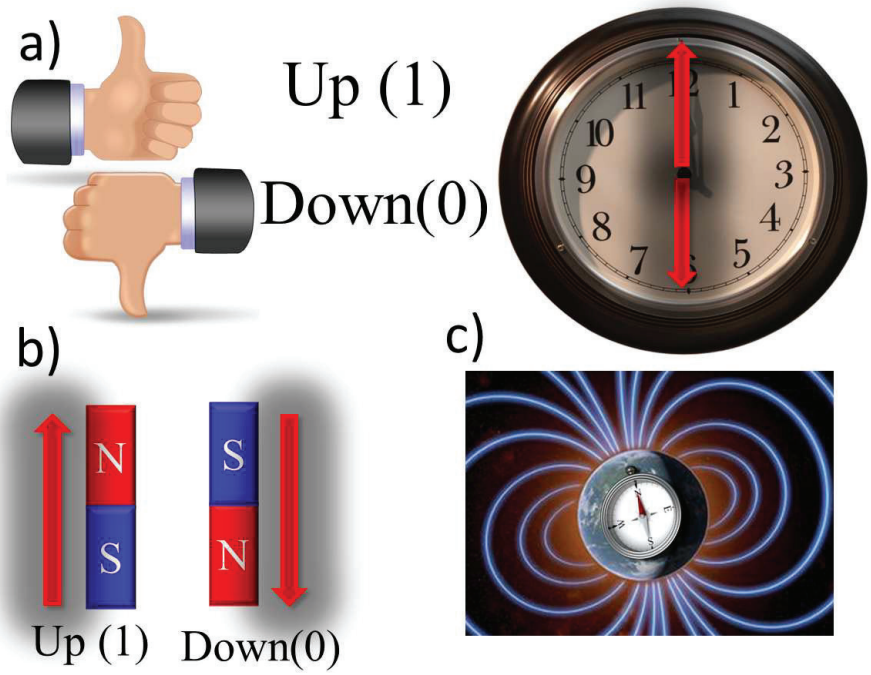

Figure 2: Cartoon of the spin of an electron. a) The spin can be classically viewed as a thumb up or down. Another representation is to think it as an arrow pointing towards the number twelve in a clock (spin up) or the number six (spin down). It is also commonly referred as 0 or 1 in binary digits. b) Spin lines up with the orientation of a bar magnet. c) The spin lines up with a magnetic field just like a compass needle lines up with the earth magnetic field.

domain is created when the spins of a number of electrons in a collection of atoms become parallel. Now, down to the molecular size, when the spins of two or more electrons in the atoms of a molecule line up with each other, a magnetic molecule is created. It exhibits the classical properties of a magnet, but because of its little tiny size, it also exhibits quantum properties. Note that, so far, we have not used any external magnetic field to line up the spins of the molecule. This alignment has purely quantum mechanical origin. In a molecular magnet the orientation of this aligned spin along a particular direction is determined by the interaction of the electron spin and the electron orbital motion in the molecular structure. This property is called magnetic anisotropy and it depends on the complicated bonding of the magnetic atoms of the core with the non-magnetic atoms of the structure. Nowadays this bonding can be, to a certain extent, designed in the laboratory. It gives us the opportunity of create molecules with particular properties. The amount of parallel spins in a molecular magnet determines the robustness of its magnetic behavior: the larger the number of parallel spins, the more magnetic the molecule is.

So far, we have defined what molecular magnets are. Now, let us talk about how we can manipulate their magnetic properties. One could think a molecular magnet as a collection of parallel spins or as a giant spin representing all the spins at once. In the latter case, the magnetic behavior of a molecular magnet comes from its (giant) spin. One could control the magnetic properties of the molecular magnets by means of the manipulations of its spin. Traditionally the spin is manipulated by means of magnetic fields. This manipulation has, however, some challenges when it comes to the molecular size. The typical size of a molecular magnet is about few nanometers. A nanometer is one billion times smaller than one meter. Therefore, it is very difficult to apply magnetic fields locally at this nanoscale regime. Magnetic fields present slow switching. In addition, it is hard to obtain a very strong magnetic field. On the other hand, strong electric fields are easy to obtain and can readily be applied locally on the nanoscale. They can also be turned on and off very fast. Therefore, the manipulation of the magnetic properties of molecular magnets by means of an electric field is an interesting and promising field of study.

In this thesis we study two methods of manipulating the magnetic properties of molecular magnets by means of an external electric field. In the first method we investigate the coupling of the spin of a molecular magnet with the external electric field. We consider a special class of molecular magnet with interesting and particular properties of its ground state. The ground state tells us how the molecule is when it is in its lowest energetic

state. Due to the special molecular magnet geometry, an electric field can couple with the spin of the system. Therefore, manipulating the orientation and strength of the electric field, one could manipulate the spin of the molecular magnet. In the second method, we manipulate the magnetic anisotropy of the molecular magnet. In this case we use another type of molecular magnet characterized for its large magnetic anisotropy energy, which is the energy that it takes to rotate the total spin of the molecule away from its preferential direction. By manipulating this energy barrier one could control the magnetic properties of the system. We investigate the control of the molecular magnet anisotropy by means of adding or subtracting an electron to the system. An external electric field is able to drive electrons in or out of the molecular magnet.

We consider relevant to underline the reasons we study the manipulation of the magnetic properties of molecular magnets. Today's technology needs to find more efficient ways to store and process digital information. This can be achieved using quantum computers instead of conventional computers. Quantum computers store and process data using quantum mechanical states called quantum bits or qubits that might increase massively computer power. Conventional computers are built from silicon chips, which contain millions of transistors. Each one of them represents a bit of information, which can either be zero or one (binary digits). A bit could be represented by a spin pointing up or down as shown in Fig. 2 a) or as the hour hand at 12 and at 6 in a clock in Fig. 2 b).

In order to convey a more clear meaning we take a glance at the basic difference between conventional and quantum computers. Imagine you are in front of a clock (see Fig. 2 b)) and the hour hand points towards the 12. That is the *one* in digital information. Now imagine it pointing towards the 6. That is the *zero* of digital information. In a classical computer the hour hand can only point towards either 12 or 6. Conventional computers perform operations using classical bits. On the other hand, in a quantum computer the hour hand can point towards any other number. It could point towards the numbers 3, 5, 11 or any point between them. It can be in a superposition of both bits of information. A quantum computer performs operations using quantum bits or qubits. They can be magically *zero* and *one* at the same time. They are in a quantum superposition of states. This is what gives a quantum computer its superior computing power.

As a final remark, the spin of a molecular magnet is a quantum object that can be used as a qubit. It can be up (*one*), down (*zero*) or both at once. If a molecular magnet can function as a little tiny magnet, then one could use it to store information. One could think to have either one bit or qubit per molecule. One could think a molecular magnet

as a switching device, just like a transistor: a molecular transistor, where electricity can either flow or stop. Since molecular magnets are about ten times smaller than the present smallest transistors, it could increase considerably the amount of transistors in a chip. Additionally, the two spin states in a molecular magnet can be used to encode a qubit. It has been said that every time a quantum bit is added to a quantum computer, it doubles its computational power. It has been predicted that by having a 300-qubit quantum computer it would be more powerful than all the world computers connected together. That is the power of quantum computation. Therefore, controlling the magnetic properties of molecular magnets electrically could take us to the next computer generation.

List of publications

Parts, but far from all, of the contributions presented in this thesis have previously been accepted to conferences or submitted to journals.

- M. Fhokrul Islam, **Javier F. Nossa**, Carlo M. Canali and Mark Pederson, "First-principles study of spin-electric coupling in a Cu_3 single molecular magnet," in Phys. Rev. B **82**, 155446 (2010)
  Contribution: I participated in the planning of this study. I did all the DFT calculations. I participated in the analysis of the results.
- **J. F. Nossa**, M. F. Islam, C. M. Canali and M. R. Pederson, "First-principles studies of spin-orbit and Dzyaloshinskii-Moriya interactions in the Cu_3 single-molecule magnet," in Phys. Rev. B **85**, 085427 (2012)
  Contribution: I participated in the planning of this study. I carried out all the DFT calculations. I participated in the analysis of the results and in writing the paper.
- **J. F. Nossa**, M. F. Islam, C. M. Canali and M. R. Pederson, "Electric control of spin states in frustrated triangular molecular magnets," in manuscript
  Contribution: I was a participant in the planning of this study. I did all the calculations. I participated in the analysis of the results and in writing the paper.
- **J. F. Nossa**, M. F. Islam, C. M. Canali and M. R. Pederson, "Electric control of a Fe_4 single-molecule magnet in a single-electron transistor," submitted to Phys. Rev. B (2013)
  Contribution: I participated in the planning of this study. I performed all the DFT calculations. I played a role in the analysis of the results and in writing the paper.

- ▷ **J. F. Nossa** and C. M. Canali, "Cotunneling signatures of Spin-Electric coupling in frustrated triangular single-molecule magnets," in manuscript
  Contribution: I participated in the planning of this study. I did all the transport calculations. I was engaged in the analysis of the results and I wrote the paper.

Acknowledgments

I am grateful to the following people for what they have done for me, for my career, and for this thesis.

First and foremost I offer my sincerest gratitude to my supervisor, Dr Carlo M. Canali for his insightful advise, for his patience, and for his unsurpassed willingness to discuss Physics and other subjects. Without his excellent guidance I would not have been able to complete this thesis. I am deeply grateful to Dr. Mark Pederson for the long discussions, enthusiasm and encouragement that helped me sort out the technical details of my thesis. I would like to express my gratitude to Dr. Fhokrul Islam for his good advice, support and friendship, which have been invaluable on both an academic and a personal level, for which I am extremely grateful. I am most grateful to Dr. Magnus Paulsson for providing me with computational advice through my studies. His endless held guided me to write computer codes necessary for the development of this thesis.

In my daily work I have been blessed with a friendly and cheerful group of fellow students, colleagues and friends. I am grateful to all of them. I would like to thank Dr. Susan Canali for her help with the English language. I likewise thank to Caroline Berglund Pilgrim for her translation of the scientific popular summary to Swedish.

I would like to acknowledge with much appreciation to my parents for their endless love, support and encouragement to chase my dreams. I would like to express my very great appreciation and deepest gratitude to my lovely wife Carolina Camacho for her support, unwavering love, advice, encouragement, cheering and patience. Her excellent influence in my life makes me a better person and parent.

Last but not the least, I want to thank my little one, Lukas, for all the happiness that he has brought to my life.

Javier Nossa
Kalmar, August 2013

Contents

List of Figures

Part I

INTRODUCTION

Introduction

Today most technological gadgets are based on taking electrons and moving them all around small electronic devices made of circuits, transistors, diodes, resistors, etc. The main role in such devices is played by the electron charge. On the other hand, the spin of the electron does not play a role in such devices. The spin of the electron, as an individual intrinsic property of the electron, has been ignored in microelectronics for more than 60 years. It is, however, effectively used in information storage by magnetic materials in the form of regions that contain many spins all aligned.

Twenty years ago it was realized that one could use the spin, still in the form of magnetized regions, to control the current in a circuit. This was the first example of a spin-electronics device. The first discovery of this new area is the giant magneto resistance (GRM), in which the change in electrical resistance of magnetic metallic multi-layers in response to an applied magnetic field can be observed. The GMR is a result of spin-dependent scattering by defects and interfaces. In a GMR device the spin is used to control information processes rather than storing information. It has been used to control the functionality of microelectronic devices, namely the resistance.

GRM was discovered by Albert Fert [1] and Peter Grünberg [2] who were awarded the Nobel Prize in Physics in 2007. Ever since, GMR has generated a lot of interest due to the deep fundamental physics that governs this phenomenon and the broad applications to information technology such as magnetic recording, storage and sensor industries [3].

The field that studies the manipulation of the electron spin in contrast to its charge is called spin-electronics or *spintronics*. It is an emerging new area of technology that could revolutionize the way conventional electronic devices work. In spintronics the spin of a particle is taken into account as a quantum variable that can exist in a superposition of states of spin up and spin down. One goal in this new area is to understand how to control such a superposition in different kinds of materials. Spintronics is a wide field of research and technology which goes from the control of single localized spins regarded as

spin qubits to spin transport and spin dynamics in macroscale systems [4]. In addition to the enormous technological applications, the spin of the electron is essentially a quantum-mechanical object and its interaction with the electron charge or the environment gives us a unique opportunity to understand more in depth the quantum nature of matter.

The success of spintronics devices has been mostly limited to inorganic metals and semiconductors. Nevertheless, a new spintronics sub-area has emerged in the last years, namely *molecular spintronics* [5–11]. It deals with the overlap between spintronics, molecular electronics and molecular magnetism. Therefore it combines the classical macroscale properties of a magnet with the quantum properties of a nanoscale object [12]. Chemists and physicists collaborate very closely with the goal of designing, synthesizing, characterizing and manipulating magnetic and electrical properties (spins and charges) of molecular-based materials. This collaboration has generated advances in chemical design and synthesis, which allow the realization of interesting magnetic molecules with desired electronic and magnetic properties. A second essential feature of ongoing research is the improved ability of integrating individual magnetic molecules into solid state nano-electronic devices.

Molecular magnets (MMs) consist of a magnetic core surrounded by organic ligands that allow the molecule to bind to surfaces or junctions [13]. Unlike traditional bulk magnetic materials, molecular magnetic materials can be magnetized in a magnetic field without any interaction between the individual molecules. This magnetization is a property of the molecules themselves. Typically magnetic molecules have long spin-relaxation times, which can be utilized in high-density information storage. They are also usually characterized by a weak hyperfine interaction with the environment, resulting in long spin coherence times, which is an essential property for applications in quantum information processing. MMs display a variety of non-trivial quantum effects such as quantum tunneling of the magnetization [14, 15], Berry phase interference [16] and quantum spin coherence [8, 10, 17]. Due to their double nature, classic macroscale properties of a magnet and quantum properties of a nanoscale entity, MMs are ideal systems to investigate decoherence and the interplay between classical and quantum behavior [17].

The miniaturization of spintronics devices down to molecular spintronics, namely the use of molecular magnets, allows us to have more devices in a smaller space. The manipulation of the magnetic properties of molecular magnets by magnetic fields is straightforward but, in practice, cannot be realized easily with molecular-size spatial resolution, and at fast temporal scales. Unlike magnetic fields, electric fields are easily produced,

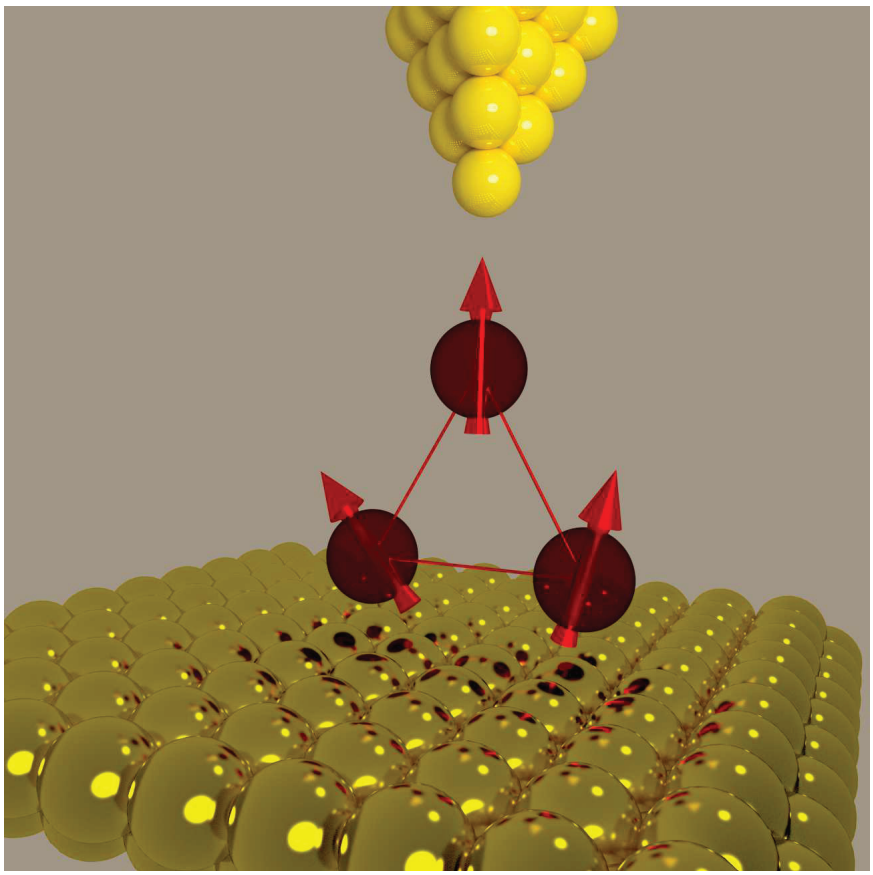

Figure 3: Schematic representation of a triangular molecular magnet in a scanning tunneling microscope tip device.

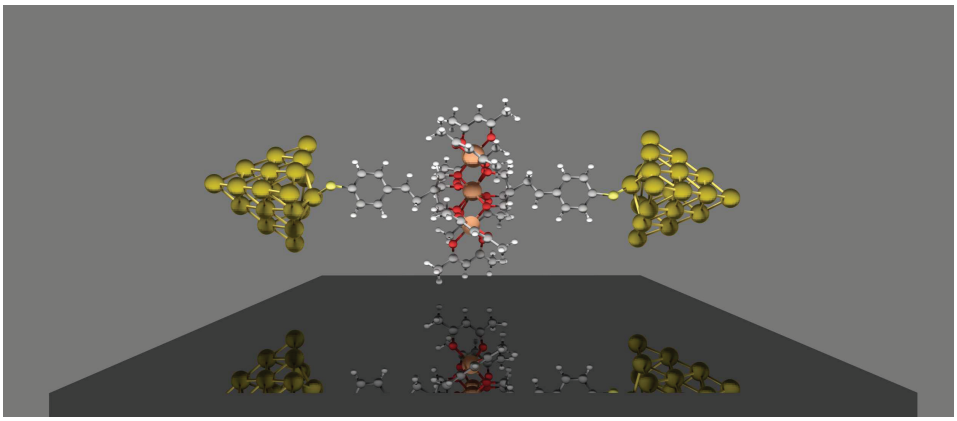

Figure 4: Schematic representation of a $\{Fe_4\}$ single-molecule magnet in a single-electron transistor device.

quickly switched, and can be applied locally at the nanoscale and molecular scale. Therefore, manipulation of the properties of molecular magnets by external electric fields is an attractive and promising alternative. In the last ten years theoretical and experimental efforts towards this goal have considered different classes of magnetic molecules and strategies to incorporate them into electric nano-circuits [18–23].

In this thesis we investigate the electric control of the magnetic properties of nanospintronics devices such as molecular magnets. The magnetic properties of such systems can be *indirectly* modified by an electric field by simply modifying the spin-orbit interaction. This manipulation, however, may not be efficient since the spin-orbit effects scale with the size of the system. Thus, additional mechanisms must be found to efficiently couple the spin of the system and applied electric fields.

Throughout this thesis we study two classes of magnetic molecules and the manipulation of their magnetic properties by an external electric field. We consider molecules that are spin frustrated systems and, consequently, have special ground state manifold properties. The other class of molecules investigated in this thesis are molecules that are known as single-molecule magnets (SMMs) and they are characterized by a large magnetic anisotropy. But why are we interested in these molecules? In principle, all molecules are "magnetic" because they do respond to a magnetic field. Then what is important here is what kind of response is found in the molecule or what kind of zero-field properties are present in these molecules. In the case of frustrated molecules there is an interesting

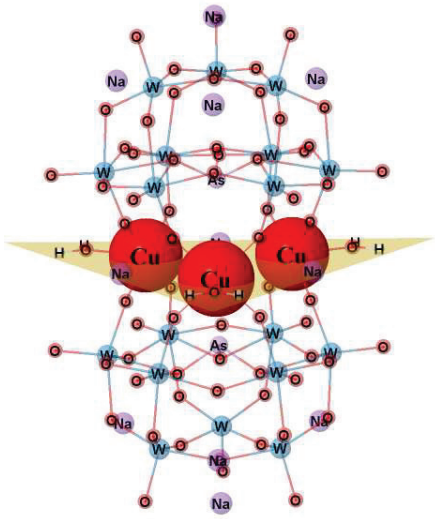

(a) $\{Cu_3\}$

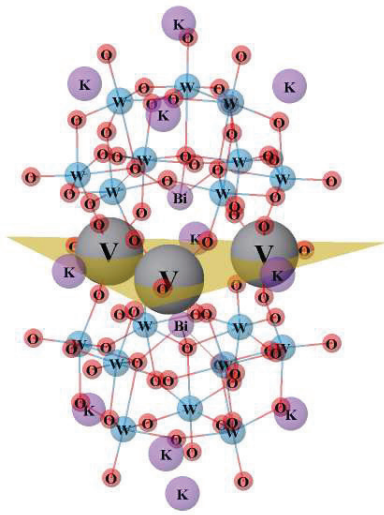

(b) $\{V_3\}$

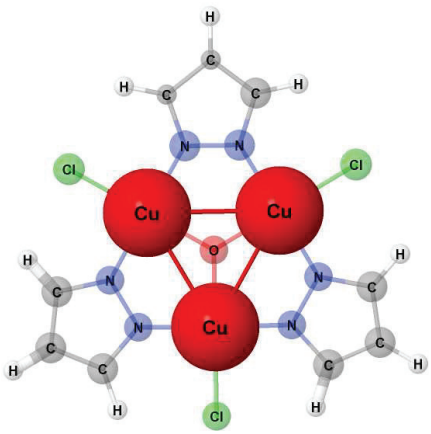

(c) $\{Cu_3O\}$

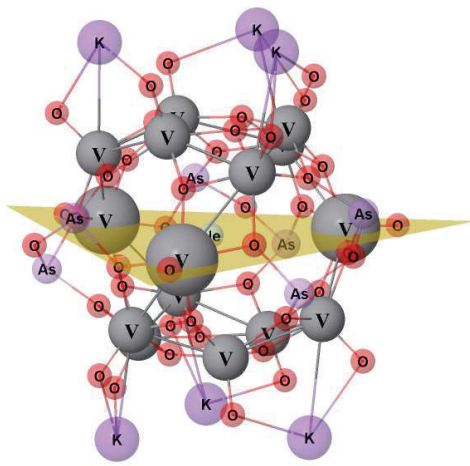

(d) $\{V_{15}\}$

Figure 5: Ball-stick view of the spin frustrated molecular magnets studied in this thesis.

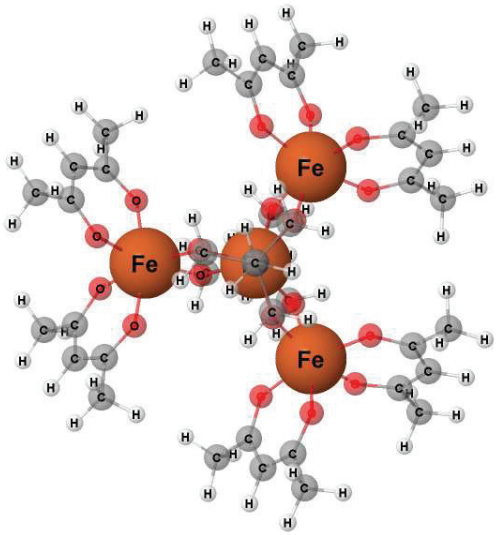

Figure 6: Ball-stick top view of an isolated $\{Fe_4\}$ single-molecule magnet (SMM).

double degeneracy in the spin ground state that is characterized by the chirality of the system. The manipulation of the quantum spin states can be used to encode a qubit. In the case of SMMs there is a zero field splitting called anisotropy. Because of this large barrier, separating the spin up and spin down states, the molecule could be used to store information classically.

Now, how do we manipulate the magnetic properties of these molecules electrically? In the case of spin frustrated molecular magnets, we study an efficient spin-electric coupling mechanism. It is based on an interplay of spin exchange, spin-orbit interaction, and lack of inversion symmetry. This is shown in Chapter 1. The ground state of a spin frustrated molecular magnet is characterized by two two-fold degenerate states of opposite chirality but same spin. An external electric field can couple these states through the spin induced dipole moment of the molecule. We investigate spin frustrated molecules such as $\{Cu_3\}$, $\{V_3\}$, $\{Cu_3O\}$ and $\{V_{15}\}$ (see Fig. 5). A schematic representation of such system is shown in Fig. 3. In Chapter 3 we address a Coulomb blockade methodology based on a master equation to calculate experimentally this induced dipole moment in a cotunneling measurement.

In the case of SMMs we control the magnetic anisotropy of the molecule by charging it positively and negatively in a single-electron transistor device. A schematic representation

Mol	NA	D (Å)	S	CC
$\{Cu_3\}$	110	4.88	D_{3h}	$Na_{12}[Cu_3(AsW_9O_{33})_2\cdot\ 3H_2O]\cdot 32H_2O$ [24]
$\{V_3\}$	104	5.70	D_{3h}	$K_{12}[(VO)_3(BiW_9O_{33})_2\cdot 29H_2O$ [25]
$\{Cu_3O\}$	31	3.29	D_{3h}	$Cu_3Cl_3N_6C_9H_9O$ [26]
$\{V_{15}\}$	70	7.00	D_3	$K_6[V_{15}As_6O_{42}(H_2O)]8H_2O$ [27]
$\{Fe_4\}$	122	3.18,5.5 (*)	D_3	$Fe_4C_{76}H_{132}O_{18}$. [28]

Table 1: Number of atoms (NA), distance between magnetic centers (D) in angstroms, point group symmetry (S) and chemical composition (CC) of the molecular magnets study in this thesis. (*) central-vertex and vertex-vertex Fe-Fe distances.

of such device is shown in Fig. 4. In Chapter 2 we study how the magnetic anisotropy is calculated. For this kind of molecule we investigate a $\{Fe_4\}$ SMM (see Fig. 6). In Table 1 we show the number of atoms, the distance between magnetic centers, point group symmetry and the chemical composition of the molecular magnets that are investigated in this thesis.

In the final chapter of the theory part of this thesis, we present an outlook where we show several prospects for ideas to be developed and implemented both in ab-initio calculations and quantum transport in molecular magnets.

In the development of this thesis we found it useful to write three appendices. These are important since they present essential concepts and tools used to conduct our research. In Appendix A we study basic concepts of group theory that are necessary to understand the spin-electric coupling in frustrated molecular magnets. In Appendix B we explicitly derive cotunneling transition rates using a regularization scheme that are used in Chapter 3. Finally, but not less important, in Appendix C we introduce the computational tool that we have used in most of this thesis: NRLMOL (the Naval Research Laboratory Molecular Orbital Library). It is a massively parallel code for electronic structure calculations on large molecules and clusters based on spin density functional theory.

As a final remark we would like to emphasize that this thesis has been divided in four parts, namely, the introduction, the theory, the appendices and the papers. The theory and appendices are meant to provide the reader with the necessary concepts and tools to understand the main procedures and findings of the papers.

Part II

THEORY

1

Spin-Electric Coupling in Molecular Magnets

In this chapter we present a detailed description of the spin-electric coupling in a molecular magnet (MM), more specifically, a spin frustrated triangular $\{Cu_3\}$ MM. This is motivated by the original work published in 2008 by Trif *et al.* [18]. Here we follow the procedures carried out in Ref. [19].

The lower energy regime of a spin frustrated triangular magnet (see Fig. 1.1) is composed of two two-fold degenerate chiral states. Based on a spin model and symmetry properties (see Appendix A) of the triangular molecule, one can demonstrate that electric fields can couple states of opposite chirality through the spin induced dipole moment. The strength of this spin-electric dipole coupling constant, d, determines the effectiveness of the manipulation of the spin states by electric fields. A precise estimate of this strength constant cannot be obtained analytically and has to be determined by ab-initio calculations or through experiments.

In our first paper (see Sec. 5) we calculate this parameter using NRLMOL (see Ap-

pendix C) in a $\{Cu_3\}$ MM. The spin-electric strength, d, is found to be 3.38×10^{-33}C·m (=0.001 Debye, three orders of magnitude lower than the dipole moment of the water molecule, 1.85 Debye), where e is the electron charge and a the Cu-Cu separation. The molecule response to an applied electric field shows that this spin-electric coupling mechanism is of potential interest for the use of MMs in quantum information processing as fast switching devices.

In the second paper (see Sec. 6) we include the effect of the spin-orbit interaction (SOI). It introduces a splitting in the ground-state manifold of the $\{Cu_3\}$ MM via the Dzyaloshinskii-Moriya interaction (DMI). We employ a Hubbard-model approach to elucidate the connection between the SOI and the DMI. This allows us to express the DMI constant, D, in terms of the microscopic Hubbard-model parameters, such as the effective hopping integral between magnetic sites t, the on-site repulsion energy U, and the strength of the spin orbit interaction $\lambda_{\rm SOI}$. The small splitting that we find for the $\{Cu_3\}$ MM is consistent with experimental results.

In a third paper (see Sec. 7) we study the spin-electric coupling in other triangular MMs and discuss the underlying mechanism leading to an enhanced coupling, which can be used as a convenient guide to synthesize MMs that can respond more efficiently to an external electric field. We investigate the dependence of spin-electric coupling on types of magnetic atoms, the distance between magnetic centers and the role of the exchange path between magnetic atoms. We choose three different MMs: $\{V_3\}$ and $\{Cu_3O\}$ triangular MMs which have three magnetic centers and $\{V_{15}\}$ which has fifteen magnetic atoms. Unlike $\{V_3\}$ and $\{Cu_3O\}$ MMs, the construction of the ground state for the $\{V_{15}\}$ MM requires some generalization as it involves fifteen magnetic centers. We describe a method for constructing the degenerate ground state of the $\{V_{15}\}$ molecule and calculation of the spin-electric coupling in this generalized ground state.

1.1 Spin-Electric Coupling

Recently, a mechanism of spin-electric coupling in antiferromagnetic (AFM) molecular magnets (MMs), characterized by a lack of inversion symmetry and spin frustration, has been proposed [18]. An example of such a system is a triangular spin $s = 1/2$ ring with AFM coupling, realized for example in the $\{\mathrm{Cu_3}\}$ and $\{\mathrm{V_3}\}$ MMs [25, 29]. The low energy physics of this system can be described by a three-site spin $s = 1/2$ Heisenberg

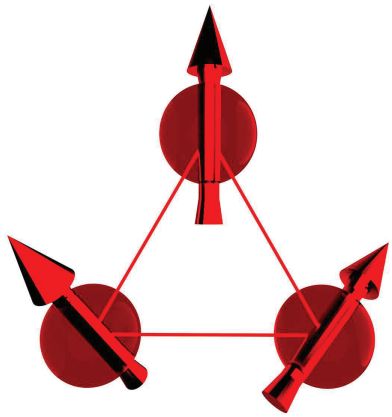

Figure 1.1: Schematic representation of a triangular molecule.

Hamiltonian:

$$H_0 = \sum_{i=1}^{3} J_{i,i+1}\mathbf{s}_i \cdot \mathbf{s}_{i+1} + \sum_{i=1}^{3} \mathbf{D}_{i,i+1} \cdot \mathbf{s}_i \times \mathbf{s}_{i+1}\,, \tag{1.1}$$

where $J_{i,i+1}$ is the exchange parameter between the spins $\mathbf{s}_i$ and $\mathbf{s}_{i,i+1}$, $\mathbf{D}$ is the Dzyaloshinskii vector, $\mathbf{s}_i$ are three 1/2-spins located at the Cu sites, and $\mathbf{s}_4 \equiv \mathbf{s}_1$. The first term in the Hamiltonian, Eq. (1.1), represents the isotropic Heisenberg exchange Hamiltonian, and the second term is the anisotropic Dzyaloshinskii-Moriya (DM) exchange interaction originated from the presence of spin-orbit interaction (SOI). The point group symmetry of this molecule is $D_{3\mathrm{h}}$, which imposes the following restrictions on the spin Hamiltonian parameters: $J_{i,i+1} \equiv J$ and $D^x_{i,i+1} = D^y_{i,i+1} = 0$, and $D^z_{i,i+1} \equiv D_z$. The strength of the DM vector $|\mathbf{D}_{i,i+1}|$ is at least one-order of magnitude smaller than the isotropic exchange constant $J_{i,i+1}$, and we will disregard it for the moment.

The ground state of the Hamiltonian Eq. (1.1) is a total spin $S = 1/2$ manifold, which is composed of two degenerate (total) spin $S = 1/2$ doublets spanned by the symmetry-adapted states $|\chi\pm, S_z\rangle$ that can be written as a linear combination of three different spin configurations (see Fig. 1.2):

$$|\pm 1, +\frac{1}{2}\rangle = \frac{1}{\sqrt{3}}\big(|\downarrow\uparrow\uparrow\rangle + \epsilon_{\pm}|\uparrow\downarrow\uparrow\rangle + \epsilon_{\mp}|\uparrow\uparrow\downarrow\rangle\big)\,, \tag{1.2}$$

$$|\pm 1, -\frac{1}{2}\rangle = \frac{1}{\sqrt{3}}\big(|\uparrow\downarrow\downarrow\rangle + \epsilon_{\pm}|\downarrow\uparrow\downarrow\rangle + \epsilon_{\mp}|\downarrow\downarrow\uparrow\rangle\big)\,, \tag{1.3}$$

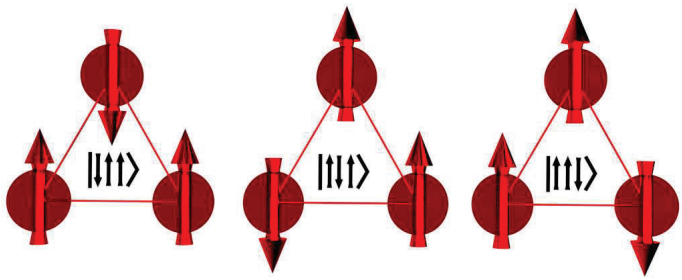

Figure 1.2: Linear combination of spin configurations associated with total spin projection $S_z = 1/2$.

where the quantum numbers $\chi = \pm 1$ specify the so-called handness or chirality of the state, S_z is the total z spin projection and $\epsilon_\pm = \exp(\pm 2\pi i/3)$. The many-body states $|\alpha_1\alpha_2\alpha_3\rangle$ are products of spin-orbital states $\alpha_i = \uparrow, \downarrow$ $(i = 1, 2, 3)$ localized on the three magnetic ions of the molecules. Eqs. (1.2) and (1.3) are eigenstates of the chirality operator

$$C_z = \frac{4}{\sqrt{3}} \mathbf{s}_1 \cdot \mathbf{s}_2 \times \mathbf{s}_3 \ , \tag{1.4}$$

where $\mathbf{s}_i$ (i =1,2,3) is the spin of the ith atom. It is useful to introduce also the other two components of the chiral vector operator

$$C_x = -\frac{2}{3}(\mathbf{s}_1 \cdot \mathbf{s}_2 - 2\mathbf{s}_2 \cdot \mathbf{s}_3 + \mathbf{s}_3 \cdot \mathbf{s}_1) \ , \tag{1.5}$$

$$C_y = \frac{2}{\sqrt{3}}(\mathbf{s}_1 \cdot \mathbf{s}_2 - \mathbf{s}_3 \cdot \mathbf{s}_1) \ , \tag{1.6}$$

and the ladder operators $C_\pm \equiv C_x \pm iC_y$. Note that $[C_l, C_m] = i2\epsilon_{lmn}C_n$ and $[C_l, S_m] = 0$. Here ϵ_{lmn} is the Levi-Civita symbol. The ladder operators reverse the chirality of the states: $C_\pm|\chi\mp, S_z\rangle = |\chi\pm, S_z\rangle$. They also have the property that $C_\pm|\chi\pm, S_z\rangle = 0$. Thus $\mathbf{C}$ behaves exactly like the operator $\mathbf{S}$ (for $S = 1/2$) in chiral space.

A triangular spin-1/2 antiferromagnet such a the $\{Cu_3\}$ MM belongs to the class of antiferromagnetic rings with an odd number of half-integer spins [30, 31]. In these systems, the lack of inversion symmetry of the molecule as a whole implies that the ground-state is a four-dimensional manifold, whose basis states $|\chi = \pm 1, S_z = \pm 1/2\rangle$ are characterized by the spin projection $S_z = \pm 1/2$ and by the chirality $C_z = \pm 1$. In contrast, antiferromagnetic rings with an even number of spins have non-degenerate

$S = 0$ singlet ground state. In odd-spin triangular rings, the two states of opposite chirality $|\chi = \pm 1, S_z = M\rangle$ can be coupled linearly by an external electric field, even in the absence of spin-orbit interaction.

We focus now on the spin-electric coupling of states with different chirality but the same total spin projection, Eq. (1.2). In the presence of an external electric field $\boldsymbol{\varepsilon}$, the Hamiltonian acquires the additional electric-dipole term $H_\varepsilon = \sum_i e\mathbf{r}_i \cdot \boldsymbol{\varepsilon} = e\mathbf{R}\cdot\boldsymbol{\varepsilon}$, where e is the electron charge, $\mathbf{r}_i$ is the coordinate of the ith electron and $\mathbf{R} = \sum_{i=1}^{3} \mathbf{r}_i$. In the $D_{3\mathrm{h}}$ point group symmetry the z-component of $\mathbf{R}$ transforms as A_2'' irreducible representation (IR), while (x, y) transform as the two-dimensional E' IR. The chiral states, Eq. (1.2), span E' IR. For a transition to be allowed, the direct product of two wavefunctions and the dipole operator sandwiched between them must contain the A_1' irreducible representation. Transition selection rules for $D_{3\mathrm{h}}$ (see Appendix A) establish that the product of chiral states and (x, y) components of the dipole moment is different from zero[1]

$$\underbrace{E'}_{\langle\chi\pm S_z|} \otimes \underbrace{E'}_{(x,y)} \otimes \underbrace{E'}_{|\chi\pm S_z\rangle} \neq 0, \tag{1.7}$$

while the product of chiral states and the z-component of the dipole moment is zero[2]

$$\underbrace{E'}_{\langle\chi\pm S_z|} \otimes \underbrace{A_2''}_{z} \otimes \underbrace{E'}_{|\chi\pm S_z\rangle} = 0. \tag{1.8}$$

Therefore, general group theory arguments guarantee dipole matrix elements of the form

$$-\langle E'_+, S_z|ex|E'_-, S_z\rangle = -i\langle E'_-, S_z|ey|E'_+, S_z\rangle \equiv d \neq 0. \tag{1.9}$$

Here d is a real number that is referred to as spin electric-dipole coupling. Therefore an external electric field causes transitions between chiral states of opposite chirality, but with the same spin projection S_z. The value of d cannot be determined by symmetry properties and has been determined by ab-initio calculations in $\{Cu_3\}$ molecular magnets [32].

In the subspace of spin projection $S_z = 1/2$ of the ground-state manifold, which is invariant under the application of the operator H_ε, the perturbed Hamiltonian $H_0 + H_\varepsilon$

[1] $E' \otimes E' \otimes E'$ spans $3E' + A_2' + A_1'$. It does span A_1'. Therefore, the product may be different from zero.
[2] $E' \otimes A_2'' \otimes E'$ spans $E'' + A_2'' + A_1''$. It does not span A_1'. Therefore the product is zero by symmetry.

can be expressed in the basis of the chiral states as

$$\begin{aligned} H &= H_0 + H_\varepsilon \\ &= \begin{vmatrix} \langle\chi_+,+\frac{1}{2}|H_0|\chi_+,+\frac{1}{2}\rangle & \langle\chi_+,+\frac{1}{2}|H_\varepsilon|\chi_-,+\frac{1}{2}\rangle \\ \\ \langle\chi_-,+\frac{1}{2}|H_\varepsilon|\chi_+,+\frac{1}{2}\rangle & \langle\chi_-,+\frac{1}{2}|H_0|\chi_-,+\frac{1}{2}\rangle \end{vmatrix} . \end{aligned} \tag{1.10}$$

A similar expression holds for the $S_z = -1/2$ subspace. The eigenvalues of H are

$$E^{\pm}_{\frac{1}{2}}(\boldsymbol{\varepsilon}) = E^{\pm}_{\frac{1}{2}}(0) \pm |\mathbf{d}\cdot\boldsymbol{\varepsilon}| \, , \tag{1.11}$$

with $E^{\pm}_{\frac{1}{2}}(0) = \langle\chi_\pm,+\frac{1}{2}|H_0|\chi_\pm,+\frac{1}{2}\rangle$, and the corresponding eigenstates

$$\left|\chi^{\pm}_{\frac{1}{2}}(\boldsymbol{\varepsilon})\right\rangle = \frac{1}{\sqrt{2}}\left(|\chi_+,+\frac{1}{2}\rangle \pm \frac{|\mathbf{d}\cdot\boldsymbol{\varepsilon}|}{\mathbf{d}\cdot\boldsymbol{\varepsilon}}|\chi_-,+\frac{1}{2}\rangle\right) . \tag{1.12}$$

Here we have introduced the electric dipole matrix element $\mathbf{d}$, which couples states of opposite chirality (but with the same spin projection, see Eq. (1.9))

$$\mathbf{d} = \langle\chi_+,+\frac{1}{2}|e\mathbf{R}|\chi_-,+\frac{1}{2}\rangle \tag{1.13}$$

with $d \equiv |\mathbf{d}|$.

The matrix element in Eq. (1.13) is the key quantity in the spin-electric coupling mechanism, and we have calculated its value in Paper I (see Sec. 5). Substituting the expressions for the chiral states from Eq. (1.2) and using the orthogonality of spin states, we obtain

$$\mathbf{d} = \frac{1}{3}(\langle\downarrow\uparrow\uparrow\,|e\mathbf{R}|\,\downarrow\uparrow\uparrow\rangle + \epsilon_+\langle\uparrow\downarrow\uparrow\,|e\mathbf{R}|\,\uparrow\downarrow\uparrow\rangle + \epsilon_-\langle\uparrow\uparrow\downarrow\,|e\mathbf{R}|\,\uparrow\uparrow\downarrow\rangle). \tag{1.14}$$

Thus, evaluating the dipole matrix element between two states of opposite chirality is equivalent to calculating the dipole moment of each of the three spin configurations.

Now, the effect of the electric field on the low-energy spectrum of a triangular MM can be recast in the form of the effective spin model. The electric dipole operator has nonzero matrix elements only in the ground-state manifold, where it couples states with equal spin components and opposite chirality. In the excited $S = 3/2$ subspace all the matrix elements of the electric dipole operator, $e\mathbf{R}$, are identically zero. This is straightforward since $\langle\uparrow\uparrow\uparrow\,|e\mathbf{R}|\,\uparrow\uparrow\uparrow\rangle$ and $\frac{1}{3}(\langle\downarrow\uparrow\uparrow\,|e\mathbf{R}|\,\downarrow\uparrow\uparrow\rangle + \langle\uparrow\downarrow\uparrow\,|e\mathbf{R}|\,\uparrow\downarrow\uparrow\rangle + \langle\uparrow\uparrow\downarrow\,|e\mathbf{R}|\,\uparrow\uparrow\downarrow\rangle)$ are both zero by symmetry. Therefore, we expect that the spin-electric Hamiltonian, H_ε, can be rewritten as a linear combination of the ladder operators, $C_\pm$. By comparing the matrix

elements of H_ε given in Eqs. (1.9) and (1.13) with the action of $C_\pm$ on the chiral states, one can show that [19]

$$H_\varepsilon^{\text{eff}} = d\boldsymbol{\varepsilon}' \cdot \mathbf{C}_\parallel \,, \tag{1.15}$$

where $\boldsymbol{\varepsilon}' = R_z(\phi)(7\pi/6 - 2\theta)\boldsymbol{\varepsilon}$, with $R(\phi)$ being the matrix representing a rotation by an angle ϕ around the z-axis, and θ being the angle between the in-plane component $\boldsymbol{\varepsilon}_\parallel$ of the electric field and the bond $\mathbf{s}_1$-$\mathbf{s}_2$. Here we can write the $\mathbf{C}_\parallel$ components of the chiral operator in the form of projection operators as

$$C_x = \sum_m \left(|\chi_+, S_z\rangle \langle \chi_-, S_z| + |\chi_-, S_z\rangle \langle \chi_+, S_z| \right) \tag{1.16}$$

and

$$C_y = i \sum_m \left(|\chi_+, S_z\rangle \langle \chi_-, S_z| - |\chi_-, S_z\rangle \langle \chi_+, S_z| \right), \tag{1.17}$$

where $S_z = 1/2, -1/2$.

By using Eqs. (1.5) and (1.6) we can now rewrite $\mathbf{C}_\parallel = (C_x, C_y)$ in terms of spin-operators $\mathbf{s}_i$ [19]. Thus, Eq. (1.15) becomes

$$H_\varepsilon^{\text{eff}} = \sum_i^3 \delta J_{ii+1}(\boldsymbol{\varepsilon}) \mathbf{s}_i \cdot \mathbf{s}_j \,, \tag{1.18}$$

where the modified exchange parameters take the form [19]

$$\delta J_{ii+1}(\boldsymbol{\varepsilon}) = \frac{4d}{3\sqrt{2}} |\boldsymbol{\varepsilon}_\parallel| \cos\left(\frac{2\pi}{3} i + \theta \right) \,. \tag{1.19}$$

This expression of the effective electric-dipole Hamiltonian suggests a transparent physical interpretation of the spin-electric couping mechanism [18, 19]. An external electric field changes the charge distribution of the $\{Cu_3\}$ molecule which, in turn, changes the exchange interaction between neighboring atoms. Since the modified exchange interaction does not commute with H_0, it can cause transitions between chiral states within the ground-state manifold.

Here we, now, turn to the spin-orbit interaction (SOI) in the ground state as an effective Hamiltonian. In the $D_{3\text{h}}$ point group, the SOI in the low-energy regime reads [33]

$$H_{\text{SOI}} = \lambda_{\text{SOI}}^{\parallel} T_{A_2} S_z + \lambda_{\text{SOI}}^{\perp} \left(T_{E''_+} S_- + T_{E''_-} S+ \right) \tag{1.20}$$

where $\lambda_{\text{SOI}}^{\parallel}$ and the $\lambda_{\text{SOI}}^{\perp}$ are the SOI parameters for the A_2'' and $E_\pm''$ irreducible representation, respectively. Here $T_{A_2''}$ and $T_{E''_\pm}$ are the corresponding irreducible representation

tensor operators in the orbital space. Because of group theory properties for $D_{3\mathrm{h}}$ symmetry, the only possible nonzero matrix elements of this SOI Hamiltonian in the low-energy regime, namely $S = 1/2$ subspace (chiral states subspace), can be written as

$$\langle \chi_{\pm} S_Z \left| H_{\mathrm{SOI}} \right| \chi_{\pm} S_z' \rangle = \pm \lambda_{\mathrm{SOI}}^{\parallel} S_z \delta_{S_z S_z'}. \tag{1.21}$$

Consequently, the effective SOI Hamiltonian is written as

$$H_{\mathrm{SOI}}^{\mathrm{eff}} = \Delta_{\mathrm{SOI}} C_z S_z \tag{1.22}$$

where $\Delta_{\mathrm{SOI}} = \lambda_{\mathrm{SOI}}^{\parallel}$, $S_z = s_z^1 + s_z^2 + s_z^3$ is the total spin defined as the sum of the individual spins s_i, and C_z transfortms as T_{A_2} IR. Using the definition of the z-component of the chiral operator in Eq. (1.4), one can see that $H_{\mathrm{SOI}}^{\mathrm{eff}}$ is reduced to the Dzyaloshinskii-Moriya Hamiltonian given in the second term of the RHS Eq. (1.1). Experimentally the DM-induced splitting in $\{Cu_3\}$ is estimated to be small (approximately 0.5 K [29]) and is calculated by ab-initio methods in Paper II (see Sec. 6).

To complete the full spectrum of the low-energy regime, an external magnetic field can be introduced. It couples to the spin via the Zeeman term $H_{\mathrm{MF}} = \mathbf{B} \cdot \tilde{g} \mathbf{S}$. Because of the $D_{3\mathrm{h}}$ symmetry, the g-factor tensor is diagonal, as a result, $\tilde{g} = diag\{g_{\parallel}, g_{\parallel}, g_{\perp}\}$, where $g_{\parallel} = g_{xx} = g_{yy}$ is parallel to the triangle plane and $g_{\perp} = g_{zz}$ is normal to it. Finally, from Eqs. (1.15), (1.22) and H_{MF}, the low-energy effective Hamiltonian is written as

$$\begin{aligned} H^{\mathrm{eff}} &= H_{\varepsilon}^{\mathrm{eff}} + H_{\mathrm{MF}} + H_{\mathrm{SOI}}^{\mathrm{eff}} \\ H^{\mathrm{eff}} &= d\boldsymbol{\varepsilon}' \cdot \mathbf{C}_{\parallel} + \mathbf{B} \cdot \tilde{g} \mathbf{S} + \Delta_{\mathrm{SOI}} C_z S_z. \end{aligned} \tag{1.23}$$

An schematic representation of the interplay of the three terms in Eq. (1.23) is shown in Fig. 1.3. At zero-field, the four-fold degenerate chiral states, $|\chi_{\pm} S_z = \pm 1/2\rangle$, are split by the SOI in two chiral doublets: $|\chi_{-} S_z = \pm 1/2\rangle$ and $|\chi_{+} S_z = \pm 1/2\rangle$. Then, an external magnetic field lifts the degeneracy of each doublet. Finally, and external electric field couples states of opposite chirality but same spin. The strength of this coupling is given by the paramenter d (see Eq. (1.13)).

Note that in the absence of the SOI, the chiral and spin operators evolve indipentintly. However, when SOI is present it couples C and S operators. Also, while the magnetic field causes transitions between states of opposite spin projection S_z but with the same spin chirality C_z, the electric field causes transitions between states of opposite chirality C_z, but with the same spin S_z.

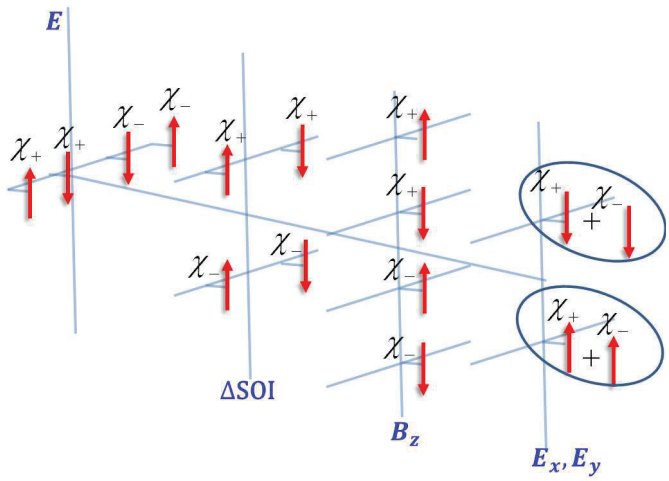

Figure 1.3: Splitting of the four-fold degenerate chiral states.

1.2 Parameters within the one-band Hubbard model approach

Spin Hamiltonians such as Eq. (1.1) are effective low-energy descriptions of the system, focusing only on the spin degrees of freedom. This assumption disregards completely the orbital degree of freedom. For the spin-electric coupling model, the orbital dynamics plays a fundamental role and has to be included to investigate the coupling constants. In this section we use the Hubbard model in order to include the orbital degree of freedom into the spin-electric coupling. This allows us to study intuitively the spin-electric coupling introduced by electric fields acting on the molecular orbitals. We follow here the procedure introduced in Ref. [19].

The second quantized one-band Hubbard Hamiltonian reads

$$H_U = -\sum_{i,j}\sum_{\alpha}\left\{t_{ij}c^{\dagger}_{i\alpha}c_{j\alpha} + \text{h.c.}\right\} + \frac{1}{2}U\sum_{i} n_{i\uparrow}\, n_{i\downarrow}\ , \tag{1.24}$$

where $c^{\dagger}_{i\alpha}$ ($c_{i\alpha}$) creates (destroys) an electron with spin α at site i, $n_{i\alpha} = c^{\dagger}_{i\alpha}c_{i\alpha}$ is the particle number operator and t_{ij} is a spin-independent hopping parameter. More precisely, the index i labels a Wannier function localized at site i. The first term represents the kinetic energy describing electrons hopping between nearest- neighbor sites i and j. For

$D_{3\mathrm{h}}$ symmetry this term is characterized by a hopping parameter $t_{ij} = t$. The second term is an on-site repulsion energy of strength U, which describes the energy cost associated with having two electrons of opposite spin on the same site. In this model the interaction energy between electrons which are not on the same site is completely neglected. The Hubbard model is the simplest model describing the fundamental competition between the kinetic energy and the interaction energy of electrons on a lattice.

The spin-orbit interaction in the Hubbard model is described by adding the following spin-dependent hopping term [19, 34–36]

$$H_{\mathrm{SOI}} = \sum_{i,j} \sum_{\alpha,\beta} \left\{ c^{\dagger}_{i\alpha} \Big(i \frac{\mathbf{P}_{ij}}{2} \cdot \boldsymbol{\sigma}_{\alpha\beta} \Big) c_{j\beta} + \mathrm{h.c.} \right\} , \tag{1.25}$$

where $\boldsymbol{\sigma} = \sigma_x \hat{x} + \sigma_y \hat{y} + \sigma_z \hat{z}$ is the vector of the three Pauli matrices. A commonly used notation for the Pauli matrices is to write the vector index i in the superscript, and the matrix indices as subscripts, so that the element in row α and column β of the ith Pauli matrix is $\sigma^i_{\alpha\beta}$, with $i = x, y, z$. Here the vector $\mathbf{P}_{ij}$ is proportional to the matrix element of $\boldsymbol{\nabla} V \times \mathbf{p}$ between the orbital parts of the Wannier functions at sites i and j; V is the one-electron potential and $\mathbf{p}$ is the momentum operator. Clearly the spin-orbit term has the form of a spin-dependent hopping, which is added to the usual spin-independent hopping proportional to t. In Eq. (1.25), spin-orbit coupling induces a spin precession about $\mathbf{P}_{ij}$ when an electron hops from site i to site j. This form of the spin-orbit interaction is a special case of Moriya's hopping terms [37] in the limit that all but one orbital energy is taken to infinity [35], and it is consistent with our choice of a one-band Hubbard model. The x and y components of $\mathbf{P}_{ij}$ describe processes with different spin, and because of the σ_{v} symmetry, $\mathbf{P}_{ij} = p\mathbf{e}_z$. Therefore, because of the symmetry of the molecule, the free Hubbard parameters are reduced to three, namely, t, U and p.

The final expression of the Hamiltonian that describes electrons in a triangular molecule, including the spin-orbit interaction is

$$\begin{aligned} H_{\mathrm{U+SOI}} \;=\; & \sum_{i,\alpha} \Big\{ c^{\dagger}_{i\alpha} \big(-t + i\lambda_{\mathrm{SOI}} \alpha \big) c_{i+1\alpha} + \mathrm{h.c.} \Big\} \\ & + \sum_{i,\alpha} \left(\epsilon_0 n_{i\alpha} + \frac{1}{2} U n_{i\alpha}\, n_{i\bar{\alpha}} \right) , \end{aligned} \tag{1.26}$$

where $\lambda_{\mathrm{SOI}} \equiv p/2 = \mathbf{P}_{ij}/2 \cdot \mathbf{e}_z$ is the spin-orbit parameter, ϵ_0 is the on-site orbital energy, and $\bar{\alpha} = -\alpha$.

We want to treat the two hopping terms perturbatively on the same footing, by doing an expansion around the atomic limit $t/U \ , \ \lambda_{\mathrm{SOI}}/U \to 0$. In many molecular magnets

$t \gg \lambda_{\mathrm{SOI}}$. This turns out to be the case also for $\{Cu_3\}$ [38]. In other molecules the two hopping parameters are of the same order of magnitude.

We are interested in the half-filling regime. From second-order perturbation theory in t/U, an antiferromagnetic isotropic exchange term emerges and splits the spin degeneracy of the low-energy sector of the Hubbard model, which is defined by the singly-occupied states. This action can be represented with an effective spin Hamiltonian, the isotropic Heisenberg model, with the exchange constant $J = 4t^2/|U|$ [39]. The perturbative method requires the definition of the unperturbed states being the one-electron states

$$|\phi_i^\alpha\rangle = c_{i\alpha}^\dagger |0\rangle , \tag{1.27}$$

singly-occupied three-electron states

$$|\psi_i^\alpha\rangle = \prod_{j=1}^{3} c_{j\alpha_j}^\dagger |000\rangle = \prod_{j=1}^{3} \left|\phi_j^{\alpha_j}\right\rangle , \tag{1.28}$$

with $\alpha_j = \alpha$ for $j \neq i$ and $\alpha_j = \bar{\alpha}$, for $j = i$. Finally the doubly-occupied three-electron states

$$\left|\psi_{ij}^\alpha\right\rangle = c_{i\uparrow}^\dagger c_{i\downarrow}^\dagger c_{j\alpha}^\dagger |000\rangle , \tag{1.29}$$

with $i = 1, 2, 3$ and $j \neq i$. The states in Eqs. (1.27)-(1.29) are eigenstates of the Hamiltonian, Eq. (1.26), only in the absence of the hopping and spin-orbit parameter. These states have the following energies, ϵ_0, $3\epsilon_0$ and $3\epsilon_0 + U$, respectively. These states are not yet symmetry adapted states of the $D_{3\mathrm{h}}$ point group. Symmetry adapted states can be found using the projector operator formalism [19, 33]. One-electron symmetry adapted states can be written as a linear combination of one-electron states, Eq. (1.27),

$$\left|\Phi_{A_1'}^\alpha\right\rangle = \frac{1}{\sqrt{3}} \sum_{i=1}^{3} |\phi_i^\alpha\rangle , \tag{1.30}$$

and

$$\left|\Phi_{E_\pm'}^\alpha\right\rangle = \frac{1}{\sqrt{3}} \sum_{i=1}^{3} \epsilon_{1,2}^{i-1} |\phi_i^\alpha\rangle , \tag{1.31}$$

where A_1' and $E_\pm'$ are one-dimensional and two-dimensional irreducible representations in the $D_{3\mathrm{h}}$ point group, respectively, and $\epsilon_{1,2}^k = \exp\left((2\pi i/3)^k\right)^{1,2}$. The three-electron symmetry adapted states for singly-occupied magnetic centers can be written as

$$\left|\psi_{A_1'}^{1\alpha}\right\rangle = \frac{1}{\sqrt{3}} \sum_{i=1}^{3} |\psi_i^\alpha\rangle , \tag{1.32}$$

and

$$\left|\psi^{1\alpha}_{E'_\pm}\right\rangle = \frac{1}{\sqrt{3}}\sum_{i=1}^{3}\epsilon_{1,2}^{i-1}\left|\psi_i^\alpha\right\rangle. \tag{1.33}$$

The states $|\psi^{1\,\alpha}_{E'_+}\rangle$ and $|\psi^{1\,\alpha}_{E'_-}\rangle$ have total spin $S = 1/2$ and z-spin projection $S_z = \pm 1/2$. These states are formally identical to the chiral states given in Eqs. (1.2) and (1.3) and are eigenstates of the Hubbard Hamiltonian when $t = \lambda_{\rm SOI} = 0$. The tunneling and SOI mix the singly-occupied and doubly-occupied states. Symmetry properties of the D_3h point group dictate that the tunneling and SOI terms in the Hubbard Hamiltonian transform as the irreducible representation A'_1. Therefore, only states transforming according to the same irreducible representations could be mixed. The first-order correction in t/U and $\lambda_{\rm SOI}$ is obtained by mixing in doubly-occupied states

$$|\Phi^{1\,\alpha}_{E'_\pm}\rangle \equiv |\psi^{1\,\alpha}_{E'_\pm}\rangle + \frac{(\epsilon_2^1-1)(t\pm\alpha\lambda_{\rm SOI})}{\sqrt{2}U}|\psi^{2\,\alpha}_{E'_1\pm}\rangle + \frac{3\epsilon_1^1(t\pm\alpha\lambda_{\rm SOI})}{\sqrt{2}U}|\psi^{2\,\alpha}_{E'_2\pm}\rangle, \tag{1.34}$$

where

$$|\psi^{2\,\alpha}_{E'_1\pm}\rangle = \frac{1}{\sqrt{6}}\sum_{i=1}^{3}\epsilon_{1,2}^{i-1}\left(|\psi^\alpha_{i1}\rangle + |\psi^\alpha_{i2}\rangle\right), \tag{1.35}$$

and

$$|\psi^{2\,\alpha}_{E'_2\pm}\rangle = \frac{1}{\sqrt{6}}\sum_{i=1}^{3}\epsilon_{1,2}^{i-1}\left(|\psi^\alpha_{i1}\rangle - |\psi^\alpha_{i2}\rangle\right), \tag{1.36}$$

are three-electron symmetry adapted states for doubly-occupied magnetic centers.

In the small t/U , $\lambda_{\rm SOI}/U$ limit, we can resort to a spin-only description of the low-energy physics of the system. The ground state manifold (corresponding to the states in Eq. (1.34)) is given by the two chiral spin states Eqs. (1.2), (1.3). In this low-energy regime the orbital states correspond to the singly-occupied localized atomic orbitals. The lowest energy states have total spin $S = 1/2$ and chirality $C_z = \pm 1$.

Now, we introduce the effect of the external electric field. An external electric field $\boldsymbol{\varepsilon}$ can couple to the molecule via two mechanisms. The first mechanism that we will study is by the modification of the on-site energies ϵ_0 via the Hamiltonian

$$H^0_{d-\varepsilon} = \sum_\alpha\sum_{i=1}^{3}\left(-e\mathbf{r}_i\cdot\boldsymbol{\varepsilon}\right)c^\dagger_{i\alpha}c_{i\alpha}, \tag{1.37}$$

where $\mathbf{r}_i$ is the coordinate vector of the *i*th magnetic center. From Fig. 1.4, the on-site

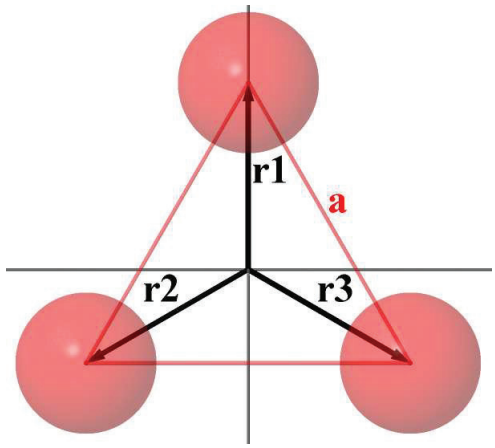

Figure 1.4: Coordinates of magnetic centers in a triangular molecule. $\mathbf{r}_i$ is the coordinate of the ith electron.

electric Hamiltonian can be written as

$$\begin{aligned} H^0_{d-\varepsilon} &= -ea\sum_\alpha \left[\frac{\varepsilon^y}{\sqrt{3}}c^\dagger_{1\alpha}c_{1\alpha} - \frac{1}{2}\left(\varepsilon^x + \frac{\varepsilon^y}{\sqrt{3}}\right)c^\dagger_{2\alpha}c_{2\alpha}\right. \\ &\left. +\frac{1}{2}\left(\varepsilon^x - \frac{\varepsilon^y}{\sqrt{3}}\right)c^\dagger_{3\alpha}c_{3\alpha}\right], \end{aligned} \tag{1.38}$$

where $\varepsilon_{x,y}$ are the in-plane coordinates of the electric field, e the electron charge and a the distance between magnetic centers.

The second mechanism is given by the modification of the hopping parameters t_{ii+1} and it can be written as

$$H^1_{d-\varepsilon} = \sum_\alpha \sum_{i=1}^{3} t^\varepsilon_{ii+1,\alpha} c^\dagger_{i\alpha} c_{i+1\alpha} + \text{H.c.}, \tag{1.39}$$

where $t^\varepsilon_{ii+1,\alpha} = -\left\langle \phi^\alpha_i | e\mathbf{r}\cdot\boldsymbol{\varepsilon} | \phi^\alpha_{i+1}\right\rangle$ are the modified hopping parameters due to the external electric field $\boldsymbol{\varepsilon}$, ϕ_i are the Wannier states localized on the ith magnetic center with spin α. These induced hopping parameters can be written as $t^{\boldsymbol{\varepsilon}}_{ii+1,\alpha} = \sum_q q^\alpha_{ii+1}\varepsilon_q$, with $q^\alpha_{ii+1} = -e\left\langle \phi^\alpha_i | q | \phi^\alpha_{i+1}\right\rangle$ and $q = x, y, z$. $D_{3\text{h}}$ point group symmetry properties given by the dipole selection rules reduce the number of free parameters induced by the electric field. Finding these free parameters is not an easy task when the basis set is composed of localized Wannier orbitals. In order to investigate the effect of the electric field on

the triangular molecule, we switch from the localized Wannier basis set to the symmetry adapted basis set $\Gamma = A_1', E_\pm'$. Then we apply the transition dipole selection rules to the new induced hopping parameters. In the symmetry adapted states, the hopping-Hamiltonian, Eq. (1.39), reads

$$H^1_{d-\varepsilon} = \sum_\alpha \sum_{\Gamma\Gamma'} t^{\boldsymbol{\varepsilon}}_{\Gamma,\Gamma',\alpha} c^\dagger_{\Gamma\alpha} c_{\Gamma'\alpha} + \text{H.c.}, \tag{1.40}$$

where $\Gamma, \Gamma' = A_1', E_+', E_-'$, $t^{\boldsymbol{\varepsilon}}_{\Gamma,\Gamma',\alpha} = \sum_q q^\alpha_{\Gamma\Gamma'} E_q$, with $q = x, y, z$ and $q^\alpha_{\Gamma\Gamma'} = -e \langle \phi^\alpha_\Gamma | q | \phi^\alpha_{\Gamma'} \rangle$. Here $c^\dagger_{\Gamma\alpha}(c_{\Gamma\alpha})$ creates (destroys) an electron in the adapted state Γ with spin α. Note that in Eq. (1.40) all the possible transitions are included, even those between states of the same symmetry adapted basis set. Dipole transition rules then will select the allowed transitions and the corresponding states. Although symmetry properties control the dipole transition rules, they do not allow us to calculate the strength of the transitions. Experiments or accurate ab-initio calculations have to be carried out to determine them. In the $D_{3\text{h}}$ point group, the (x, y) and z-coordinates span as the E' and the A_2'' irreducible representation, respectively. We have grouped x and y because they form a degenerate pair within the E' representation. From character tables of the $D_{3\text{h}}$ point group, we have the only allowed transitions correspond to

$$\begin{aligned}
\left\langle \phi^\alpha_{E_+'} \middle| x \middle| \phi^\alpha_{E_-'} \right\rangle &= -i \left\langle \phi^\alpha_{E_+'} \middle| y \middle| \phi^\alpha_{E_-'} \right\rangle \equiv -\frac{d_{EE}}{e} \\
\left\langle \phi^\alpha_{A_1'} \middle| x \middle| \phi^\alpha_{E_+'} \right\rangle &= -i \left\langle \phi^\alpha_{A_1'} \middle| y \middle| \phi^\alpha_{E_+'} \right\rangle \equiv -\frac{d_{AE}}{e} \\
\left\langle \phi^\alpha_{A_1'} \middle| x \middle| \phi^\alpha_{E_-'} \right\rangle &= i \left\langle \phi^\alpha_{A_1'} \middle| y \middle| \phi^\alpha_{E_-'} \right\rangle \equiv -\frac{d_{AE}}{e}
\end{aligned}$$

where d_{EE} and d_{AE} are the only two free parameters to be determined. Here we have used the symmetry rule that the product $f_1 \otimes f_2 \otimes f_3 \neq 0$ if it spans the A_1' representation. All the other transitions are not allowed within the $D_{3\text{h}}$ symmetry group. Inserting these allowed transitions into the Hamiltonian, Eq. (1.40), we have

$$H^1_{d-\varepsilon} = \sum_\alpha \left[d_{AE} \left(\bar{\mathcal{E}} c^\dagger_{A_1'\alpha} c_{E_-'\alpha} + \mathcal{E} c^\dagger_{A_1'\alpha} c_{E_+'\alpha} \right) + d_{EE} \bar{\mathcal{E}} c^\dagger_{E_-'\alpha} c_{E_+'\alpha} \right] + \text{H.c.}, \tag{1.41}$$

where $\mathcal{E} = \varepsilon^x + i\varepsilon^y$ and $\bar{\mathcal{E}} = \varepsilon^x - i\varepsilon^y$. Note that the parameters d_{AE} and d_{EE} tell us about the possible dipole-electric transitions between states that span A_1'-$E_\pm'$ and E_+'-E_-' IR, respectively. From Eq. (1.33) we can see that the chiral states also span $E_\pm$ IR.

To take even more advantage of the symmetry of the triangular molecule, we now write the relationship between the second quantized operators $c^\dagger_{i\alpha}, c_{i\alpha}$ and the symmetry

adapted operators $c^\dagger_{\Gamma\alpha}, c_{\Gamma\alpha}$. From Eqs. (1.27),(1.30) and (1.31), we have

$$\begin{pmatrix} c^\dagger_{A'_1\alpha} \\ c^\dagger_{E'_+\alpha} \\ c^\dagger_{E'_-\alpha} \end{pmatrix} = \begin{pmatrix} 1 & 1 & 1 \\ 1 & \epsilon & \epsilon^2 \\ 1 & \epsilon^2 & \epsilon \end{pmatrix} \begin{pmatrix} c^\dagger_{1\alpha} \\ c^\dagger_{2\alpha} \\ c^\dagger_{3\alpha} \end{pmatrix}, \tag{1.42}$$

where we have used $\epsilon^4 = \epsilon$. From the last equation we can write the localized second quantized operators as a linear combination of symmetry adapted operators

$$\begin{pmatrix} c^\dagger_{1\alpha} \\ c^\dagger_{2\alpha} \\ c^\dagger_{3\alpha} \end{pmatrix} = \begin{pmatrix} 1 & 1 & 1 \\ 1 & \epsilon^2 & \epsilon \\ 1 & \epsilon & \epsilon^2 \end{pmatrix} \begin{pmatrix} c^\dagger_{A'_1\alpha} \\ c^\dagger_{E'_+\alpha} \\ c^\dagger_{E'_-\alpha} \end{pmatrix}. \tag{1.43}$$

Now we can write the rest of the perturbed Hamiltonian, namely the $H^0_{d-\varepsilon}$ on-site electric field Hamiltonian (Eq. (1.38)) and $H_{\rm SOI}$ spin-orbit Hamiltonian (Eq. (1.25)), in terms of the symmetry adapted operators

$$H^0_{d-\varepsilon} = -\frac{iae}{2\sqrt{3}} \sum_\alpha \left[\bar{\mathcal{E}} c^\dagger_{E'_+\alpha} c_{A'_1\alpha} - \mathcal{E} c^\dagger_{E'_-\alpha} c_{A'_1\alpha} + \bar{\mathcal{E}} c^\dagger_{E'_-\alpha} c_{E'_+\alpha} \right] + \text{H.c.}, \tag{1.44}$$

and

$$H_{\rm SOI} = \sqrt{3}\lambda_{\rm SOI} \sum_\alpha \alpha \left(c^\dagger_{E'_-\alpha} c_{E'_-\alpha} - c^\dagger_{E'_+\alpha} c_{E'_+\alpha} \right). \tag{1.45}$$

Here one can notice that the spin-orbit interaction splits the chiral states without mixing them. After the use of symmetry properties in the D_{3h} point group, the Hubbard model with spin-orbit coupling and an external electric field finally has only five free parameters, namely t, U, $\lambda_{\rm SOI}$, d_{AE} and d_{EE}.

The electric dipole matrix elements between the perturbed chiral states of the $E_\pm$ IR have been determined previously in the limit of localized orbitals: $|ea| \gg d_{EE}, d_{AE}$ [19]. This leads to the following matrix elements of the electric dipole in the ground state

$$\left| \left\langle \Phi^{1\sigma}_{E'_-} \right| H^0_{d-\varepsilon} \left| \Phi^{1\sigma}_{E'_+} \right\rangle \right| \propto \left| \frac{t^3}{U^3} eEa \right|, \tag{1.46}$$

$$\left| \left\langle \Phi^{1\sigma}_{E'_-} \right| H^1_{d-\varepsilon} \left| \Phi^{1\sigma}_{E'_+} \right\rangle \right| \simeq \left| \frac{4t}{U} E d_{EE} \right|. \tag{1.47}$$

The off-diagonal matrix elements in Eqs. (1.46) and (1.47) represent a microscopic description of the electric dipole coupling introduced in Eq. (1.9) .

2

Magnetic anisotropy in a single-molecule magnet

Single-molecule magnets (SMMs) are a special class of spin-ordered and/or magnetically active molecules characterized by a relatively high molecular spin and large magnetic anisotropy energy [13]. The latter lifts the spin degeneracy even at zero magnetic field, and favors one particular alignment of the spin, making the molecule a nanoscale magnet. As a result, SMMs could be used to store information (spin up and down). A crucial requirement for this is the ability to control and manipulate the magnetic states of the SMM in an efficient way. Therefore, it is useful to be able to control the size of the magnetic anisotropy electrically. In Paper IV (Sec. 8) we investigate control of the magnetic anisotropy of a $\{Fe_4\}$ SMM in a single-electron transistor geometry by charging the molecule. We show that the spin ordering and the magnetic anisotropy of $\{Fe_4\}$ SMM remain stable in the presence of metallic leads. We also show the change in magnetic anisotropy for charged states both for the isolated molecule and molecule attached to the leads. Our calculations were done with NRLMOL (see Appendix C).

The energy barrier separating the states of spin up and spin down occurs via the spin-orbit interaction, which is a manifestation of relativistic effects in the electronic structure. Calculations of spin-orbit coupling have used a generalization of the standard spin-orbit coupling terms for spherical systems. In this chapter we follow a procedure used to calculate the magnetic anisotropy that goes beyond spherical systems [40] .

2.1 Magnetic Anisotropy

In the last two decades single-molecule magnets (SMMs) have attracted a lot of attention, in part, because of the possibility that these structures could represent the ultimate molecular-scale limit for magnetic units in high-density magnetic storage materials. More recently SMMs have been recognized as promising building blocks in molecular spintronics, the emerging field combining spintronics and molecular electronics [5, 7, 8, 41–43]. In particular, thanks to their long spin coherence time [17], SMMs are good candidates to realize spintronic devices that maintain, control and exploit quantum coherence of individual spin states. These devices could find important applications in the field of quantum information processing [44, 45].

Magnetic anisotropy of a molecular magnet comes from unpaired electrons in the material, molecules or cluster, which are not distributed equivalently in all directions in space. This phenomenon determines the formation of an energy barrier that separates different microstates with different spin magnetic moment. This energy barrier occurs via the spin-orbit interaction, which is a manifestation of relativistic effects in the electronic structure. Magnetic anisotropy determines the type of magnetization of a sample and fixes its easy, medium and hard magnetic axes. When the energy of the system depends only on the angle with respect to one specific axis, independently of the other two, the anisotropy is called uniaxial anisotropy and the axis is referred as “easy axis”. On the other hand, when the magnetization is free to rotate in a plane perpendicular to a given (fixed) direction, we say thqat the system is determine by an easy plane. Here we show the details of calculation on anisotropy parameters used in this thesis.

Single-molecule magnets (SMMs) can usually be described with a Heisenberg model. The isotropic Heisenberg Hamiltonian is given by

$$H = \sum_{ij} J_{ij} \mathbf{s}_i \cdot \mathbf{s}_j \ , \tag{2.1}$$

where $\mathbf{s}_i$ is the spin of the magnetic ion i and the constants J_{ij} describe the super-

exchange coupling between ions i and j. These terms break rotational invariance in spin space. Up to second-order perturbation theory, these terms, besides anisotropic corrections to the Heisenberg model, include the antisymmetric Dzyaloshinskii-Moriya spin exchange, and the single-ion magnetic anisotropy $H_{ia} = -\sum_i (\mathbf{d}_i \cdot \mathbf{s}_i)^2$. Because of these terms, the total spin is no longer a good quantum number. Within the giant-spin model of SMMs, where the isotropic exchange is the dominant magnetic interaction, the main effect of the spin-orbit interaction is to lift the spin degeneracy of the ground state (GS) multiplet. To second-order perturbation theory, this can be described by the following anisotropy Hamiltonian for the giant spin operator $\mathbf{S} = (S_x, S_y, S_z)$

$$\mathcal{H} = DS_z^2 + E(S_x^2 - S_y^2) \; . \tag{2.2}$$

The parameters D and E specify the axial and transverse magnetic anisotropy, respectively. If $D < 0$ and $|D| \gg |E|$, which define properties for SMMs, the system exhibits an easy axis in the z-direction. If $D > 0$ the systems has a quasi-easy plane perpendicular to the z-axis without energy barrier. In the absence of magnetic fields, and neglecting the small transverse anisotropy term, the GS of Eq. (2.2) is doubly degenerate and it corresponds to the eigenstates of S_z with eigenvalues $\pm S$. To go from the state $S_z = +S$ to the state $S_z = -S$ the system has to surmount a magnetic anisotropy energy barrier $\Delta E = |D|S^2$. In addition, transitions which change the axial quantum numbers require some type of carrier to balance the change in spin. When the transverse term is not negligible and S_z is not a good quantum number, we can still define an anisotropy barrier separating the two (degenerate) lowest energy levels as the energy difference between GS energy and the energy of the highest excited state. This is shown in Fig. 2.1. We have used, as an example, an isolated $\{Fe_4\}$ ($S = 5$) SMM. $D = -0.63$ K value has been taken from Paper IV (see Sec. 8). E values have been chosen in such way that the effect of the transverse term is clearly seen. Here we have plotted the energy E_n of the n state as a function of the expectation value of the spin projection $\langle n| S_z |n\rangle$. We can see that for $E = 0$ (left panel) the states are pure eigenstates of S_z, each of them corresponding to a different $m = -5, -4, \ldots, 4, 5$ value. As the value of E increases the eigenstates of the Hamiltonian become a linear combination of the m states (central and right panel). Therefore S_z is no longer a good quantum number. It can be also seen that when E becomes different from zero the splitting of the states close to $m = 0$, namely ± 1, is much larger than that of the ± 2 levels. This is because the E term mixes directly states which differ in m by ± 2 [13].

The anisotropy parameters D and E can be calculated within a self-consistent-field

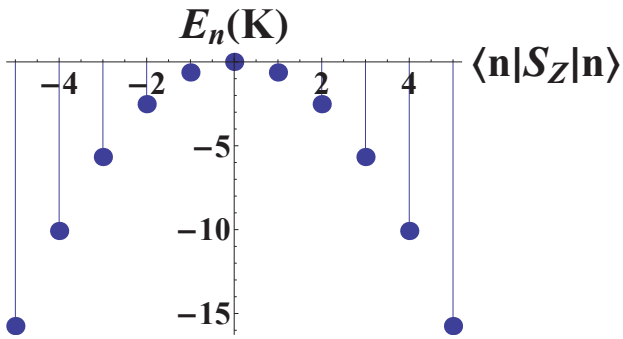

(a) E=0

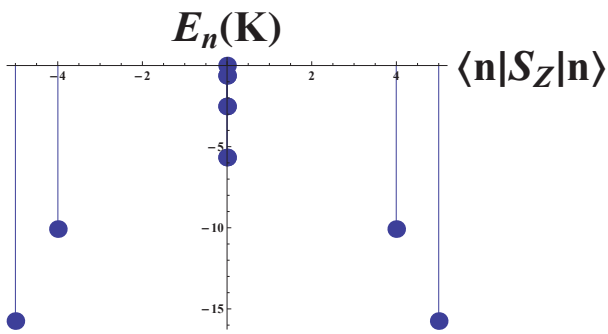

(b) E=D/10000 K

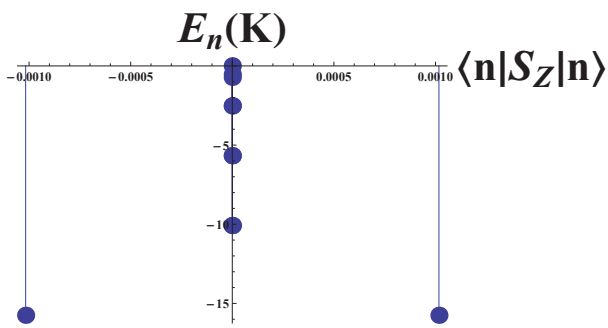

(c) E=D/100

Figure 2.1: Eigenvalues E_n of the Hamiltonian Eq. (2.2) as a function of the expectation value of the spin projection $\langle n|\, S_z\, |n\rangle$ of the corresponding n state for a $\{Fe_4\}$ ($S = 5$) single-molecule magnet. Here we have taken the value $D = -0.63$ K from Paper IV (see Sec. 8).

(SCF) one-particle theory (e.g. DFT or Hartree-Fock), by including the contribution of the spin-orbit interaction. Here we summarize the main steps of the procedure originally introduced in Ref. [46]. (For more recent reviews see Refs. [47, 48].)

The starting point are the matrix elements of the spin-orbit interaction (SOI) operator

$$U(\mathbf{r},\mathbf{p},\mathbf{S}) \quad = \quad -\frac{1}{2c^2}\mathbf{S}\cdot\mathbf{p}\times\boldsymbol{\nabla}\boldsymbol{\Phi}(\mathbf{r}), \tag{2.3}$$

where c is the speed of light, $\mathbf{S}$ is the spin moment, $\mathbf{p}$ is the momentum operator and $\boldsymbol{\Phi}$ is the Coulomb potential. For a spherically symmetry potential, the above expression can be rewritten as

$$U(r,\mathbf{L},\mathbf{S}) \quad = \quad \frac{1}{2c^2}\mathbf{S}\cdot\mathbf{L}\frac{1}{r}\frac{d\boldsymbol{\Phi}(r)}{dr}, \tag{2.4}$$

where $\mathbf{L}$ is the angular momentum. Although this approximation is widely used, it is valid only for spherical systems. However there are non spherical corrections that might be important for anisotropy energies.

Pederson *et al.* [46] have shown an exact simplified method for incorporating spin-orbit coupling into density functional theory calculations. This method requires the determination of single-electron wavefunctions. These wavefunctions can be expressed according to

$$\psi_{is}(\mathbf{r}) = \sum_{j\alpha} C_{j\alpha}^{is} f_j(\mathbf{r})\chi_\alpha \ , \tag{2.5}$$

where $f_j(\mathbf{r})$ is a spatial basis function, χ_α is either a majority or minority spinor, and $C_{j\alpha}^{is}$ are determined by effectively diagonalizing the Hamiltonian matrix. In order to calculate the effect of the SOI (Eq. (2.3)) it is necessary to calculate matrix elements of the form

$$\begin{aligned}
U_{j\alpha,k\alpha'} &= \langle f_j\chi_\alpha|\, U(\mathbf{r},\mathbf{p},\mathbf{S})\,|f_k\chi_{\alpha'}\rangle \\
&= \langle f_j\chi_\alpha|-\frac{1}{2c^2}\mathbf{p}\times\boldsymbol{\nabla}\boldsymbol{\Phi}(\mathbf{r})\cdot\mathbf{S}\,|f_k\chi_{\alpha'}\rangle \\
&= \sum_l \frac{1}{i}\,\langle f_j\chi_\alpha|-\frac{1}{2c^2}[\boldsymbol{\nabla}\times\boldsymbol{\nabla}\boldsymbol{\Phi}(\mathbf{r})]_l S_l\,|f_k\chi_{\alpha'}\rangle \\
&= \sum_l \frac{1}{i}\,\langle f_j|-\frac{1}{2c^2}[\boldsymbol{\nabla}\times\boldsymbol{\nabla}\boldsymbol{\Phi}(\mathbf{r})]_l\,|f_k\rangle \\
&\quad \times\langle\chi_\alpha|\,S_l\,|\chi_{\alpha'}\rangle \\
&= \sum_l \frac{1}{i}\,\langle f_j|\,V_l\,|f_k\rangle\,\langle\chi_\alpha|\,S_l\,|\chi_{\alpha'}\rangle\,,
\end{aligned} \tag{2.6}$$

where $l = x, y, z$, $\mathbf{p} = \boldsymbol{\nabla}/i$[1] and

$$\langle f_j | V_l | f_k \rangle = \langle f_j | - \frac{1}{2c^2} [\boldsymbol{\nabla} \times \boldsymbol{\nabla}\boldsymbol{\Phi}(\mathbf{r})]_l | f_k \rangle . \tag{2.7}$$

In order to find the most appropriate form of Eq. (2.7), we write one of its components as

$$\langle f_j | V_x | f_k \rangle = -\frac{1}{2c^2} \int d^3r f_j \left(\frac{d}{dy}\frac{d\Phi}{dz} - \frac{d}{dz}\frac{d\Phi}{dy} \right) f_k. \tag{2.8}$$

Each term of R.H.S. can be written as

$$f_j \frac{d}{dy}\frac{d\Phi}{dz} f_k = f_j \frac{d^2\Phi}{dydz} f_k + f_j \frac{d\Phi}{dz}\frac{d}{dy} f_k, \tag{2.9}$$

$$f_j \frac{d}{dz}\frac{d\Phi}{dy} f_k = f_j \frac{d^2\Phi}{dzdy} f_k + f_j \frac{d\Phi}{dy}\frac{d}{dz} f_k. \tag{2.10}$$

Inserting these two equations into Eq. (2.8), we get

$$\langle f_j | V_x | f_k \rangle = \frac{1}{2c^2} \int d^3r f_j \left(\frac{d\Phi}{dy}\frac{d}{dz} - \frac{d\Phi}{dz}\frac{d}{dy} \right) f_k. \tag{2.11}$$

Now, the factors in last equation can be written as

$$\begin{aligned} \int d^3r f_j \frac{d\Phi}{dy}\frac{d}{dz} f_k &= -\int d^3r \frac{d}{dy} f_j \Phi \frac{df_k}{dz} - \int d^3r \frac{df_j}{dy}\Phi\frac{df_k}{dz} \\ &\quad - \int d^3r f_j \Phi \frac{d^2 f_k}{dydz} \end{aligned} \tag{2.12}$$

and

$$\begin{aligned} \int d^3r f_j \frac{d\Phi}{dz}\frac{d}{dy} f_k &= -\int d^3r \frac{d}{dz} f_j \Phi \frac{df_k}{dy} - \int d^3r \frac{df_j}{dz}\Phi\frac{df_k}{dy} \\ &\quad - \int d^3r f_j \Phi \frac{d^2 f_k}{dzdy}. \end{aligned} \tag{2.13}$$

The first term in Eqs. (2.12) and (2.13) vanishes if the system is finite because the basis functions vanish at infinity. Inserting these equation into Eq. (2.11) we finally get

$$\langle f_j | V_x | f_k \rangle = \frac{1}{2c^2} \left(\left\langle \frac{df_j}{dz} \middle| \boldsymbol{\Phi} \middle| \frac{df_k}{dy} \right\rangle - \left\langle \frac{df_j}{dy} \middle| \boldsymbol{\Phi} \middle| \frac{df_k}{dz} \right\rangle \right). \tag{2.14}$$

The matrix elements for V_y and V_z are obtained by cyclical permutations of x, y and z in Eq. (2.14). This methodology for the SOI matrix does not require the determination

[1] Here we use $\hbar = 1$

of the electric field, it depends only the Coulomb potential and gradient of each basis function, and it is specially ideal for basis functions constructed from Gaussian-type orbitals, Slater-type functions, and plane waves. It is easier to take the derivative of the basis functions rather than that of the Coulomb potential.

Now we show a perturbative method for the determination of single-electron and collective shifts in total energies due to spin-orbit coupling [40]. Let us assume that in the absence of magnetic field and spin-orbit interaction, we have determined the unperturbed wave functions $\psi_{i\sigma}$ within a self-consistent field (SCF) approximation such a density functional theory (DFT). The SCF wave functions satisfy

$$H\left|\psi_{i\sigma}\right\rangle = \epsilon_{i\sigma}\left|\psi_{i\sigma}\right\rangle, \tag{2.15}$$

where $\left|\psi_{i\sigma}\right\rangle = \phi_{i\sigma}(\mathbf{r})\chi_{\sigma}$ is a simple product of a spatial function and spinor. Now, in the presence of spin-orbit interaction, the perturbed wave functions must satisfy

$$\left[H + \left(\frac{\mathbf{V}}{i} + \frac{1}{c}\mathbf{B}\right)\cdot\mathbf{S}\right]\left|\psi'_{i\sigma}\right\rangle = \epsilon'_{i\sigma}\left|\psi'_{i\sigma}\right\rangle, \tag{2.16}$$

where the operator $\mathbf{V}$ is defined in Eq. (2.14) and $\mathbf{B}$ is the magnetic field. Now we turn off the magnetic field and defined $\mathbf{M} = \mathbf{V}/i$ as a small perturbation. Then, from second order perturbation theory we have that the total energy of a system with arbitrary symmetry can be expressed as

$$\Delta^{(2)} = \mathbf{S_i}\cdot\overleftrightarrow{\mathcal{M}}\cdot\mathbf{S_j} = \sum_{\sigma\sigma'}\sum_{ij} M_{ij}^{\sigma\sigma'} S_i^{\sigma\sigma'} S_j^{\sigma\sigma'}, \tag{2.17}$$

where $i, j = x, y, z$,

$$S_i^{\sigma\sigma'} = \left\langle\chi_{\sigma}\left|S_i\right|\chi_{\sigma'}\right\rangle \tag{2.18}$$

is a spin integral, and

$$M_{ij}^{\sigma\sigma'} = -\sum_{l,k}\frac{\left\langle\phi_{l\sigma}\left|V_i\right|\phi_{k\sigma'}\right\rangle\left\langle\phi_{k\sigma'}\left|V_i\right|\phi_{l\sigma}\right\rangle}{\epsilon_{l\sigma} - \epsilon_{k\sigma'}}, \tag{2.19}$$

where $\phi_{l\sigma}$ and $\phi_{k\sigma'}$ are occupied and empty Kohn-Sham orbitals, respectively.

We now turn to the case of a closed-shell molecule with ΔN excess majority spin electrons. The above expression is valid for any set of spinors (χ_1, χ_2), which are constructed from a unitary transformation on the S_z eigenstates $(\left|\uparrow\right\rangle, \left|\downarrow\right\rangle)$ defined with respect to the z axis. The most general set of spinors can be generated from the following unitary transformation

$$\left|\chi_1\right\rangle \;=\; e^{i\alpha}\left[\cos\frac{\theta}{2}\left|\uparrow\right\rangle + e^{i\beta}\sin\frac{\theta}{2}\left|\downarrow\right\rangle\right], \tag{2.20}$$

$$|\chi_2\rangle \;=\; e^{-i\alpha}\left[-e^{-i\beta}\sin\frac{\theta}{2}\,|\uparrow\rangle+\cos\frac{\theta}{2}\,|\downarrow\rangle\right], \tag{2.21}$$

where θ and β are variational parameters and α is an ignorable parameter. The expectation values of a spin operator in the above basis is given by

$$\begin{aligned}
\langle\chi_1|S_x|\chi_1\rangle &= -\langle\chi_2|S_x|\chi_2\rangle = \frac{1}{2}\cos\beta\sin\theta\\
\langle\chi_1|S_y|\chi_1\rangle &= -\langle\chi_2|S_y|\chi_2\rangle = \frac{1}{2}\sin\beta\sin\theta\\
\langle\chi_1|S_z|\chi_1\rangle &= -\langle\chi_2|S_z|\chi_2\rangle = \frac{\cos\theta}{2}.
\end{aligned} \tag{2.22}$$

Therefore, the expectation value of a spin operator in a closed shell molecule with excess majority spin electrons ΔN is given by

$$\langle\chi_1|S_i|\chi_1\rangle \;=\; -\langle\chi_2|S_i|\chi_2\rangle = \frac{\langle S_i\rangle}{\Delta N} \tag{2.23}$$

and

$$\begin{aligned}
\langle\chi_1|S_i|\chi_2\rangle\langle\chi_2|S_j|\chi_1\rangle &= \langle\chi_1|S_i|\chi_1\rangle - \langle\chi_1|S_i|\chi_1\rangle\langle\chi_1|S_j|\chi_1\rangle\\
&= \langle\chi_1|S_iS_j|\chi_1\rangle - \frac{\langle S_i\rangle\langle S_j\rangle}{(\Delta N)^2}, \qquad (2.24)\\
\langle\chi_2|S_i|\chi_1\rangle\langle\chi_1|S_j|\chi_2\rangle &= \langle\chi_2|S_i|\chi_2\rangle - \langle\chi_2|S_i|\chi_2\rangle\langle\chi_2|S_j|\chi_2\rangle\\
&= \langle\chi_2|S_iS_j|\chi_2\rangle - \frac{\langle S_i\rangle\langle S_j\rangle}{(\Delta N)^2}, \qquad (2.25)
\end{aligned}$$

$$\begin{aligned}
\langle\chi_m|S_iS_i|\chi_m\rangle &= \frac{1}{4}, &(2.26)\\
\langle\chi_m|S_iS_j|\chi_m\rangle &= -\langle\chi_m|S_jS_i|\chi_m\rangle \text{ for } i\neq j, &(2.27)\\
\langle\chi_m|S_iS_j|\chi_m\rangle &= -\langle\chi_n|S_iS_j|\chi_n\rangle \text{ for } i\neq j. &(2.28)
\end{aligned}$$

where $\langle S_i\rangle$ is the ground state expectation value of the i^{th}-component of the total spin of the system for the given choice of the quantization axis. On the basis of a giant-spin model, $\langle S_i\rangle$ can be re-interpreted as the expectation values of the components of the giant-spin operator S for the spin-coherent state $|S,\hat{n}\rangle$ with $S=\Delta N/2$.

Now Eq. (2.17) can be rewritten as a diagonal part in the spin index plus the non-diagonal remainder according to:

$$\Delta^{(2)} = \sum_{\sigma}\sum_{ij} M_{ij}^{\sigma\sigma}S_i^{\sigma\sigma}S_i^{\sigma\sigma} + \sum_{\sigma\neq\sigma'}\sum_{ij} M_{ij}^{\sigma\sigma'}S_i^{\sigma\sigma'}S_i^{\sigma\sigma'} \tag{2.29}$$

Inserting Eqs. (2.24)-(2.28) into (2.29) we have

$$\begin{aligned}\Delta^{(2)} &= \sum_{ij}(M_{ij}^{11}+M_{ij}^{22}-M_{ij}^{12}-M_{ij}^{21})\frac{\langle S_i\rangle\langle S_j\rangle}{(\Delta N)^2} \\ &\quad +\frac{1}{4}\sum_{ii}(M_{ii}^{12}+M_{ii}^{21}) \end{aligned} \tag{2.30}$$

where $1 \equiv \chi_1$ and $2 \equiv \chi_2$. For uniaxial symmetry $M_{xx}^{\sigma\sigma'} = M_{yy}^{\sigma\sigma'}$ and running over i and j we get the total second order energy shift

$$\begin{aligned}\Delta^{(2)} &= (M_{xx}^{11}+M_{xx}^{22}+M_{zz}^{12}+M_{zz}^{21})\frac{\sin^2\theta}{4} \\ &\quad +(M_{zz}^{11}+M_{zz}^{22}+M_{xx}^{12}+M_{xx}^{21})\frac{\cos^2\theta}{4} \\ &\quad +\frac{1}{4}(M_{xx}^{12}+M_{xx}^{21}) \\ &= A+\frac{\gamma}{2}\left[\frac{\Delta N\cos\theta}{2}\right]^2 \end{aligned} \tag{2.31}$$

where $A = (M_{xx}^{11}+M_{xx}^{22}+M_{zz}^{12}+M_{zz}^{21}+M_{xx}^{12}+M_{xx}^{21})/4$ and $\gamma = (2/(\Delta N)^2)(M_{zz}^{11}+M_{zz}^{22}+M_{xx}^{12}+M_{xx}^{21}-M_{xx}^{11}-M_{xx}^{22}-M_{zz}^{12}-M_{zz}^{21})$ is the anisotropy tensor. It is convenient to write Eq. (2.31) in this way because from Eqs. (2.22) and (2.23) we have that $\langle Sz\rangle = (\Delta N\cos\theta)/2$. This is a classical expectation value of a spin projection and a continuous function of θ and gives us appropriate bounds $|\langle Sz\rangle| \leq \Delta N/2$. The difference between the maximum energy orientation and the minimum energy orientation is given by

$$\begin{aligned}\Delta_{\theta=0}^{(2)}-\Delta_{\theta=\frac{\pi}{2}}^{(2)} &= A+\frac{\gamma}{2}\left[\frac{\Delta N\cos 0}{2}\right]^2 \\ &\quad -A-\frac{\gamma}{2}\left[\frac{\Delta N\cos\frac{\pi}{2}}{2}\right]^2 \\ &= \frac{\gamma}{2}\frac{(\Delta N)^2}{2} \end{aligned} \tag{2.32}$$

A positive γ corresponds to an easy plane (no barrier) and a negative γ corresponds to an easy axis with a barrier at $\langle Sz\rangle = 0$ and minimal at $\langle Sz\rangle = \pm\Delta N/2$, which is the interesting case to spin tunneling experiments. Therefore the second order energy shift can be written as

$$\Delta^{(2)} = A+\frac{\gamma}{2}\langle Sz\rangle^2 . \tag{2.33}$$

Once the anisotropy tensor has been diagonalized, the total energy shift, Eq. (2.17) can be rewritten as

$$\begin{aligned}\Delta^{(2)} &= \sum_{\sigma\sigma'}\sum_{ij} M_{ij}^{\sigma\sigma'} S_i^{\sigma\sigma'} S_i^{\sigma\sigma'} \\ &= M_{xx}S_x^2 + M_{yy}S_y^2 + M_{zz}S_z^2. \end{aligned} \tag{2.34}$$

Here one can write the Hamiltonian in terms of axial (D) and rhombic (E) parameters. In particular, for complexes with biaxial symmetry the Hamiltonian is represented as

$$H = DS_z^2 + E(S_x^2 - S_y^2), \tag{2.35}$$

where

$$D = M_{zz} - \frac{1}{2}\left(M_{xx} + M_{yy}\right) \tag{2.36}$$

$$E = \frac{1}{2}\left(M_{xx} - M_{yy}\right). \tag{2.37}$$

The magnetic anisotropy energies (MAEs) calculated in Paper IV (see Sec. 8) were carried out with a density functional theory code called NRLMOL (see Appendix C). This code calculates the MAEs by two methods: exact diagonalization and by using 2^{nd} order perturbation theory. In the exact method, the spin-orbit Hamiltonian for a quantization axis specified by θ and β parameters is first expressed in a basis constructed from all Khon-Sham (KS) orbitals in a given energy window with associated spinors expressed in the most general form (see Eqs. (2.20) and (2.21)). The total energy is then calculated by diagonalizing this Hamiltonian. This process is repeated for different values of both θ and β. Finally, the MAE is calculated from the difference between the highest and the lowest energies. On the other hand, in the perturbative method the spin-orbit interaction matrix elements that enter in the Eqs. (2.36) and (2.37), are calculated. Then, the Hamiltonian in Eq. (2.35) is solved in a spin basis set calculated from the excess of majority spins in the molecular system. For example, the excess of majority spins of the $\{Fe_4\}$ single-molecule magnet investigated in Paper IV was found to be 10. Therefore the spin of the molecule is $S = 10/2 = 5$. Using this spin, the magnetic anisotropy energies are calculated for three different values of the ratio E/D as shown Fig. 2.1.

3

Quantum Transport in Nanostructures

In Chapter 1 we showed that there exists a spin-electric coupling in triangular molecular magnets (TMMs). The strength of the coupling is determined by the induced dipole constant d. Coulomb-blockade transport experiments in the cotunneling regime can provide a direct way to determine the spin-electric coupling strength in TMMs. This is done in Paper V (see Sec. 9).

In Chapter 2 we studied the magnetic anisotropy energy (MAE) of a single-molecule magnet (SMM). In Paper IV , Sec. 8, we calculated the MAE of a $\{Fe_4\}$ SMM in a single-electron transistor geometry. Inelastic tunneling spectroscopy carried out in a three-terminal charge transport device through such a SMM has previously been reported [21]. In that report the authors detect the MAE (zero-field splitting) of charged states by means of cotunneling measurements.

Cotunneling spectroscopy has been used as a tool to identify magnetic and electronic properties in quantum systems such as few-electron quantum dots [49], carbon nanotube quantum dots [50, 51], metallic carbon nanotubes [52], and single-molecule junctions [53–55]. In order to perform energy spectroscopy of the quantum system, it is

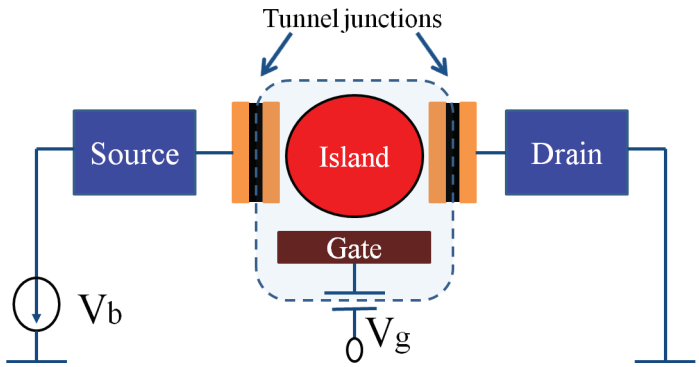

Figure 3.1: Schematic diagram of a single-electron transistor.

necessary to know exactly how the current changes when electrons go through it from lead to lead. This process depends on the allowed states involved in all possible transition channels between ground and excited states in the isolated molecule.

In this chapter we introduce a theoretical analysis of quantum transport in nanostructures based on model Hamiltonians. It is supported by a master-equation formalism [1] of quantum transport both in the sequential and cotunneling regime. First, we introduce the general background of transport. Then we define the sequential and cotunneling regimes. In Appendix B we show explicitly the derivation of the cotunneling rates using a renormalization scheme [56, 57].

3.1 Quantum Transport

Unlike transport in bulk systems, in the Coulomb blockade (CB) regime the interaction effects are dominant and control transport. Concepts like charge quantization and charging energy are the basis in this regime. CB occurs when an electron is captured in a nanostructure that is weakly coupled to conducting leads, provided that the tunnel conductance of the nanostructure is much less than the quantum of conductance

$$\mathcal{G} \ll \mathcal{G}_Q, \tag{3.1}$$

[1] In the weak tunneling regime, a master-equation description accounts for the large-scale features of the current-voltage characteristic of the single-electron transistor. *Ab*-initio approaches to quantum transport in a such regime are much more challenging and not completely developed. Some issues involved in this research are explained in the Paper IV (see Sec. 8).

where the conductance quantum $\mathcal{G}_Q = 2e^2/h$ is the quantized unit of the electrical conductance. CB physics is studied in systems known as single-electron transistors (SETs)), where electrons tunneling occur one at a time. A schematic diagram of a SET is shown in Fig. 3.1. SETs display fascinating transport features, such as Coulomb diamonds, Coulomb oscillations and Coulomb staircase [58, 59]. In a sequential tunneling regime, single-electron tunneling processes govern the CB. However, cooperative tunneling or co-tunneling processes, can become the dominant transport mechanism when single-electron processes are forbidden.

One important concept that one has to understand in CB is the charging energy, which is a classical effect due to charge discretization. Consider a small metallic island isolated from the rest of the world. The charge of this metallic island is defined as $Q = Ne$, where N is the number of excess electrons in the island and e is the electron charge. This charge produces an electric field around the island. The energy accumulated in this electric field can be expressed in terms of the island capacitance $E = Q^2/2C = (e^2/2C)N^2 \equiv E_C N^2$, where E_C is called the charging energy. Now, in order to add one more electron to the island, one has to pay an extra energy that is given by $E_C^{N+1} - E_C^N = 2(N+1)E_C$. The fact that the extra energy depends on the number of electrons, N, is an effect of the interaction. This energy cost should be provided by an external bias voltage or by a thermal fluctuation. If the extra energy is not enough, the electron tunneling is blocked and no current can flow. This phenomenon is known as Coulomb blockade [60].

Here we are interested in a SET where the central island is a magnetic molecule (see Fig. 3.2). The molecule is weakly coupled, through two tunnel junctions, to source and drain leads, which can be viewed as non-interacting systems. The electrical potential of the molecular magnet (MM) can be tuned by a third capacitively coupled electrode, a gate voltage. The only way for electrons to travel from one of the junctions to the other electrode is to tunnel through the MM. This process is discrete, therefore the electric charge that passes through the tunnel junction flows in multiples of e, the charge of a single electron. We assume the Coulomb interaction between electrons in the MM and those in the environment, to be determined by a single and constant capacitance $C = C_L + C_R + C_g$, where $C_{L/R}$ and C_g are the capacitances of the right/left lead and the gate electrode, respectively. Another assumption is that the single-particle spectrum is independent of these interactions.

Our Hamiltonian consists of three terms: $\mathcal{H}_{L/R}$ describing the reservoirs, $\mathcal{H}_{\text{mol}}$ for the MM and a $\mathcal{H}_{L/R}^T$ tunneling term that describes the coupling between the MM and the

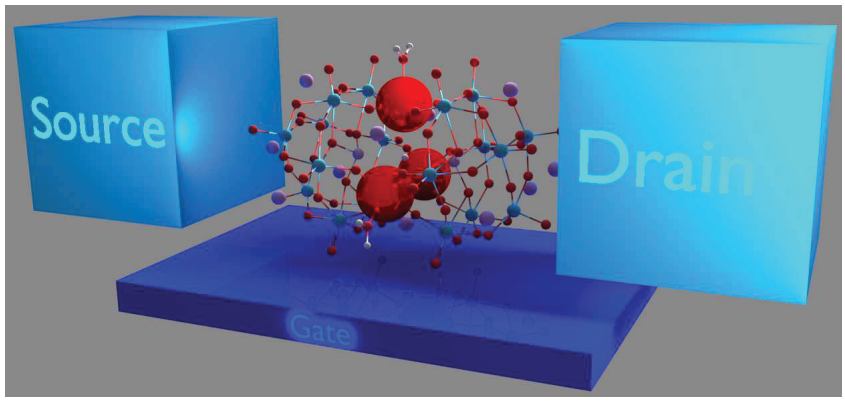

Figure 3.2: Schematic diagram of a molecule in a single-electron transistor (SET) device.

reservoirs:

$$\mathcal{H} = \mathcal{H}_{L/R} + \mathcal{H}_{\text{mol}} + \mathcal{H}^{T}_{L/R}\,, \tag{3.2}$$

where

$$\mathcal{H}_{L/R} = \sum_{k\alpha} \varepsilon^{L/R}_{k} a^{\dagger}_{L/Rk\alpha} a_{L/Rk\alpha} \tag{3.3}$$

describes free electrons in the left/right lead. Here, the operator $a^{\dagger}_{L/Rk\alpha}$ ($a_{L/Rk\alpha}$) creates (destroys) one electron with the wave vector k and spin α in the left/right lead, respectively, with energy $\varepsilon^{L/R}_{k}$. The tunnel junctions are represented by the tunneling Hamiltonian

$$\mathcal{H}^{T}_{L/R} = \sum_{km\alpha} \left(T^{L/R}_{km\alpha} a^{\dagger}_{L/Rk\alpha} c_{m\alpha} + \text{H.c.} \right), \tag{3.4}$$

where $T^{L/R}_{km\alpha}$ is the tunneling amplitude, $c^{\dagger}_{m\alpha}$ ($c_{m\alpha}$) creates (destroys) an electron in a single particle state with quantum numbers m and α inside the MM. The tunneling Hamiltonian $\mathcal{H}^{T}_{L/R}$ is treated as a perturbation to $\mathcal{H}_{\text{mol}}$ and $\mathcal{H}_{L/R}$.

The general form of the single-molecule magnet Hamiltonian is given by

$$\mathcal{H}_{\text{mol}} \quad = \mathcal{H}_0 + \mathcal{H}_{\text{U}} + \mathcal{H}_t + \mathcal{H}_{soi} + \mathcal{H}_{\text{EF}} \tag{3.5}$$

where

$$\mathcal{H}_0 = \sum_j \sum_\alpha \left(\epsilon_j - V_g\right) c^{\dagger}_{j\alpha} c_{j\alpha}, \tag{3.6}$$

with V_g the bias voltage. $\mathcal{H}_{\text{U}} = U \sum_j n_{j\uparrow} n_{j\downarrow}$ where U is the on-site Coulomb repulsion parameter and $n_{j\alpha} = c^{\dagger}_{j\alpha} c_{j\alpha}$ the number operator. $\mathcal{H}_t = t \sum_j \sum_\alpha c^{\dagger}_{j\alpha} c_{j+1\alpha} + \text{H.c.}$ is the

hopping Hamiltonian with t the hopping parameter. $\mathcal{H}_{\rm EF} = \mathcal{H}^1_{d-\varepsilon} + \mathcal{H}^0_{d-\varepsilon}$ is the electric field Hamiltonian defined in Eqs. (1.41) and (1.44) and $\mathcal{H}_{\rm SOI}$ the spin-orbit Hamiltonian defined in Eq. (1.45).

We divide the methods in two main parts. First, we obtain the transition rates and steady-state probabilities in both sequential tunneling regimes. Second, the transition rates for the cotunneling regime in the second-order perturbation theory are obtained and introduced into the current and conductance equations of the entire system.

3.2 Coulomb Blockade Regime, Sequential Tunneling

In the Coulomb blockade regime the coupling between leads and molecule is weak. Therefore some conditions have to be present. Tunneling rates Γ should be much smaller than the typical energy scales of the isolated molecule, $\hbar\Gamma \ll k_B T \ll E_c, \zeta_s$, where ζ_s is the s-th single particle level in the molecule. Also, the temperature should be smaller than the charging energy, $k_B T \ll E_c, \zeta_s$. The time between two tunneling events is the longest time scale in the regime, $\Delta t \gg \tau_\phi$, where τ_ϕ is the electron phase coherence. This guarantees that once the electron tunnels in, after long enough time it looses its phase coherence before it tunnels out. Therefore the charge state can be treated classically, and non-superposition of charge states is allowed. Only one-electron transitions occur in the system. These transitions are characterized by means of electron transfers and defined by rates Γ, where i, j are the initial and final system states involved in the electron transfer. The system is described by stationary non-equilibrium populations $\mathcal{P}_i$ of the state i. These occupation probabilities can be obtained from the master equation

$$\frac{d}{dt}\mathcal{P}_i = \sum_{j(j\neq i)} \left(\Gamma_{ij}\mathcal{P}_j - \Gamma_{ji}\mathcal{P}_i\right) \ , \tag{3.7}$$

where the first RHS term represents events where the electron tunnels into the state i from the state j, while the second RHS term represents events where the electron tunnels out from the state i into the state j. These probabilities obey the normalization condition

$$\sum_i \mathcal{P}_i = 1 \ . \tag{3.8}$$

In the steady state, the probability is time-indipendent $d\mathcal{P}_i/dt = 0$, therefore Eq. (3.7) can be written as

$$0 = \frac{d}{dt}\mathcal{P}_i = \sum_{j(j\neq i)} \left(\Gamma_{ij}\mathcal{P}_j - \Gamma_{ji}\mathcal{P}_i\right) \ . \tag{3.9}$$

In order to calculate the transition rates that enter into the master equation, we treat the tunneling Hamiltonian $\mathcal{H}^T$, Eq. (3.4), as a perturbation and use it in Fermi's golden Rule. Thus the transition from the system state i to the system state j through the left/right lead is given by

$$\Gamma_{i\to j}^{L/R} = \frac{2\pi}{\hbar}\sum_{i,j}\left|\left\langle j\left|H_{L/R}^{T}\right|i\right\rangle\right|^2 W_i\delta(E_j - E_i)\ , \tag{3.10}$$

where W_i is the thermal distribution function, and $E_j - E_i$ gives the energy conservation. The states $|i\rangle$ and $|j\rangle$ are the unperturbed system states and are defined as a product of the molecule and lead states $|i\rangle = |i_{mol}\rangle \otimes |i_l\rangle \otimes |i_r\rangle$. Transition rates depend on if an electron is leaving or entering into the nanostructure through the left or the right lead. Inserting the tunneling Hamiltonian Eq. (3.4) into the Fermi's golden Rule, Eq. (3.10), the transition rates can be defined as [58, 61]

$$\Gamma_{i\to j}^{L/R,-} = \gamma_{ji}^{L/R,-}\left[1 - f_{L/R}(E)\right]\ , \tag{3.11}$$

$$\Gamma_{i\to j}^{L/R,+} = \gamma_{ji}^{L/R,+}\left[f_{L/R}(E)\right]\ , \tag{3.12}$$

where

$$\gamma_{ji}^{L/R,-} \;=\; \Gamma^{L/R}\sum_{m,\alpha}\left|\langle j\left|c_{m,\alpha}\right|i\rangle\right|^2 \tag{3.13}$$

and

$$\gamma_{ji}^{L/R,+} \;=\; \Gamma^{L/R}\sum_{m,\alpha}\left|\left\langle j\left|\, c_{m,\alpha}^{\dagger}\right|i\right\rangle\right|^2 \tag{3.14}$$

are the transition matrix elements between the j and i states; $E = E_j - E_i$ is the energy difference between many-electron states, and $f_{L/R}(E) = \left[e^{(E-\mu_{L/R})/k_BT} + 1\right]^{-1}$ is the Fermi function. Here the combination between the tunneling amplitudes $T_{m,\alpha}^{L/R}$ and the left/right lead density of states $D_{L/R}(i_{L/R})$ is considered constant: $\Gamma^{L/R} = (2\pi/\hbar)\left|T_{m,\alpha}^{L/R}\right|^2 D_{L/R}(i_{L/R}) = (2\pi/\hbar)\left|T^{L/R}\right|^2 D_{L/R}(i_{L/R})$. The full transition matrix in the master equation, Eq. (3.7), is the sum of all contributions of electrons tunneling out or into the molecule, Eqs. (3.11) and (3.12):

$$\Gamma_{ij} = \Gamma_{ij}^{L,+} + \Gamma_{ij}^{R,+} + \Gamma_{ij}^{L,-} + \Gamma_{ij}^{R,-}\ . \tag{3.15}$$

The stationary rate equation, Eq. (3.9), is a system of linear equations and has to be solved numerically for a system of n many-electron states that are taken into account. We

can rewrite it as a matrix equation

$$0 = \sum_{j}^{n} \Lambda_{ij} \mathcal{P}_j, \tag{3.16}$$

where

$$\Lambda_{ij} = \Gamma_{ij} - \delta_{ij} \sum_{k=1}^{n} \Gamma_{kj}. \tag{3.17}$$

There must exist a physical solution to Eq. (3.18). Therefore we replace the first line of this equation by the normalization condition, Eq. (3.8), fixing $\Lambda_{1j} = 1$. Thus we can write

$$\delta_{1i} = \sum_{j}^{n} \Lambda_{ij} \mathcal{P}_j \tag{3.18}$$

instead of Eq. (3.18). Because of the low temperatures in the Coulomb regime, there are transition rates that are exponentially small. This leads to numerical problems where it is difficult to distinguish them from zero. Then some of the states do not contribute, and one has to devise an appropriate truncation method.

Finally, a current flowing through the left lead coming into the molecule must be equal to the current flowing through the right lead right lead coming out from the molecule. Knowing the occupation probabilities, Eq. (3.9), the current through the system is defined as [62]

$$I \equiv I^{L/R} = (-/+)e \sum_{i,j(j\neq i)} \mathcal{P}_j \left(\Gamma_{ij}^{L/R,-} - \Gamma_{ij}^{L/R,+} \right), \tag{3.19}$$

3.3 Cotunneling Regime

So far we have studied the regime where tunnel events are incoherent. The time between two tunnel events is long enough to guarantee that the electron tunneling in looses its coherence before it tunnels out. In this regime the leading contribution to transport through the molecule is the sequential tunneling. When this is forbidden, the current vanishes in the first-order perturbation theory and Coulomb blockade occurs. However, there are events in which two electron processes come into play. An electron is transfered from the left lead to right lead in two successive coherent tunneling events through the nanostructure via intermediate virtual states. The time that the electron spends on the molecule is much shorter than the time it needs to tunnel sequentially. During this short time, the

energy cost represented by the charging energy E_C, which blocks sequential tunneling, does not need to be paid. Such processes are called co-operative or cotunneling events. In this regime, higher order processes play a significant role. Cotunneling can be either elastic or inelastic. In the former the energies of the initial and final state are the same, while in the latter the energies are different. The energy difference is provided by a finite bias voltage. Signatures for these processes have also been observed in single-molecule junctions [20, 42, 43]. Beyond the Coulomb blockade regime, the tunneling Hamiltonian must be replaced by the T-matrix, which is given by

$$T = \mathcal{H}^T + \mathcal{H}^T \frac{1}{E_j - \mathcal{H}_0 + i\eta} T, \tag{3.20}$$

where E_j is the energy of the initial state $|j\rangle |n\rangle$. Here $|j\rangle$ refers to the equilibrium state on the left and the right lead and $|n\rangle$ is the initial molecular state, $\eta = 0+$ is a positive infinitesimal quantity and $\mathcal{H}_0 = \mathcal{H}_{mol} + \mathcal{H}_{L/R}$. To the fourth-order, the transition rates from state $|j\rangle |n\rangle$ to $|j'\rangle |n'\rangle$ with an electron tunneling from lead α to the lead α' is given by

$$\begin{aligned} \Gamma_{\alpha\alpha'}^{nj;n'j'} &= \frac{2\pi}{\hbar} \left| \langle j'| \langle n'| \mathcal{H}^T \frac{1}{E_{jn} - \mathcal{H}_0 + i\eta} \mathcal{H}^T |n\rangle |j\rangle \right|^2 \\ &\quad \times \delta(E_{j'n'} - E_{jn}) \,, \end{aligned} \tag{3.21}$$

where $E_{j'n'}$ and E_{jn} are the energies of the final and initial states, respectively. Here $|j'\rangle |n'\rangle = a^\dagger_{\alpha'\mathbf{k}'\sigma'} a_{\alpha\mathbf{k}\sigma} |j\rangle |n'\rangle$. Inserting the tunneling Hamiltonian, Eq. (3.4), in the last equation and after some algebra (see Appendix **??**) one can get the expression for the transition rates for processes from lead α till lead α' and from the molecular state $|n\rangle$ to the state $|n'\rangle$:

$$\begin{aligned} \Gamma_{\alpha\alpha'}^{n;n'} &= \sum_{\sigma\sigma'} \gamma_\alpha^\sigma \gamma_{\alpha'}^{\sigma'} \int d\varepsilon f(\varepsilon - \mu_\alpha) \left(1 - f(\varepsilon + \varepsilon_n - \varepsilon_{n'} - \mu_{\alpha'})\right) \\ &\quad \times \left| \sum_{n''} \left\{ \frac{A^{\sigma *}_{n''n'} A^{\sigma'}_{n''n}}{\varepsilon - \varepsilon_{n'} + \varepsilon_{n''} + i\eta} + \frac{A^{\sigma'}_{n'n''} A^{\sigma *}_{nn''}}{\varepsilon + \varepsilon_n - \varepsilon_{n''} + i\eta} \right\} \right|^2 , \end{aligned} \tag{3.22}$$

where σ is the electron spin, $f(\varepsilon)$ is the Fermi distribution function, μ_α is the chemical potential in the lead α, $\mu_L - \mu_R = -eV/2$, $|n''\rangle$ is a virtual state, $A^{\sigma'}_{ij} = \langle i| c_{\sigma'} |j\rangle$ and $A^{\sigma *}_{ij} = \langle j| c^\dagger_\sigma |i\rangle$. Here γ^σ_α is the tunneling amplitude. Here n and n' are states with the same number of particles. We have not taken into account processes charging the electron number by ± 2 [63, 64]. These transition rates cannot be evaluated directly because of the second-order poles from the energy denominators. A regularization scheme

has been carried out to solve these divergences and obtain the cotunneling rates [56, 57]. Here it is important to mention that these divergences occurring in the T-matrix approach are intrinsic to the method rather than to the physical problem. The fourth-order Bloch-Redfield quantum master equation (BR) and the real-time diagrammatic technique (RT) approaches to quantum transport have been developed to avoid any divergences and therefore no *ad hoc* regularization to cotunneling is required [65, 66]. However, the T-matrix approach agrees with these two approaches and gives good reasonable results deep inside the Coulomb blockade region. We expect to catch all the relevant physics for our system with the T-matrix approach. After the regularization scheme is implemented, we get the tunneling rates defined as (see Appendix B.2)

$$\begin{aligned}\Gamma^{n;n'}_{\alpha\alpha'} &= \sum_{\sigma\sigma'}\gamma^{\sigma}_{\alpha}\gamma^{\sigma'}_{\alpha'}\Bigg[\sum_{k}\left(A^2 J(E_1,E_2,\varepsilon_{ak})+B^2 J(E_1,E_2,\varepsilon_{bk})\right)\\ &\quad +2\sum_{q}\sum_{k\neq q}A_kA_q I(E_1,E_2,\varepsilon_{ak},\varepsilon_{aq})\sum_{q}\sum_{k\neq q}B_kB_q I(E_1,E_2,\varepsilon_{bk},\varepsilon_{bq})+\\ &\quad 2\sum_{q}\sum_{k}A_kB_q I(E_1,E_2,\varepsilon_{ak},\varepsilon_{bq})\Bigg] \end{aligned} \tag{3.23}$$

where $A_k = A^{\sigma *}_{kn'}A^{\sigma'}_{kn}$, $B_k = A^{\sigma'}_{n'k}A^{\sigma *}_{nk}$, $\varepsilon_{ak} = \varepsilon_{n'} - \varepsilon_k$, $\varepsilon_{bk} = \varepsilon_k - \varepsilon_n$, $E_1 = \mu_\alpha$ and $E_2 = \mu_{\alpha'} + \varepsilon_{n'} - \varepsilon_n$. Here I and J are integrals that come out after the regularization scheme and are defined in Eqs. (B.5) and (B.6), respectively, in Appendix B.

The complete master equation including both sequential and cotunneling contributions reads

$$\begin{aligned}\frac{d}{dt}\mathcal{P}_i &= \sum_{j(j\neq i)}\left(\Gamma_{ij}\mathcal{P}_j-\Gamma_{ji}\mathcal{P}_i\right)\\ &\quad +\sum_{\alpha\alpha' j}\left(\Gamma^{ji}_{\alpha\alpha'}\mathcal{P}_j-\Gamma^{ij}_{\alpha\alpha'}\mathcal{P}_i\right)\,,\end{aligned} \tag{3.24}$$

and the current through the system is now given by

$$\begin{aligned}I &\equiv I^{L/R} = (-/+)e\sum_{i,j(j\neq i)}\mathcal{P}_j\left(\Gamma^{L/R,-}_{ij}-\Gamma^{L/R,+}_{ij}\right)\\ &\quad +(-/+)e\sum_{i,j(j\neq i)}\mathcal{P}_j\left(\Gamma^{ji}_{LR/RL}-\Gamma^{ij}_{RL/LR}\right).\end{aligned} \tag{3.25}$$

4

Summary and outlook for future work

The main purpose of this thesis has been to investigate the control of magnetic properties of molecular magnets (MM) by means of electric fields. We have focused on two electric control mechanisms. The first mechanism is the so-called spin-electric coupling in spin frustrated antiferromagnetic MMs. The second mechanism deals with the manipulation of the magnetic anisotropy of a single-molecule magnet by adding or subtracting an electron via an external electric field.

Spin-electric coupling can be found in spin frustrated MMs. This coupling is mediated by the spin-induced dipole moment d. By symmetry properties it is possible to determine whether or not a molecule has an intrinsic dipole moment. Nevertheless, the actual d value cannot be determined by symmetry. It has to be calculated by ab-initio methods or extracted from experiments. In Paper I we focused on a $\{Cu_3\}$ MM. We studied its electronic and magnetic properties using ab-initio methods. Our main finding was the strength of the spin-electric coupling. We calculated $d = 3.38 \times 10^{-33}$C·m (0.001 Debye). The molecule response to an applied electric field shows that this spin-electric coupling mechanism is of potential interest for the use of these MMs in quantum information processing

as fast switching devices.

The ground-state manifold of the triangular $\{Cu_3\}$ MM can be split by the spin-orbit interaction (SOI) via the Dzyaloshinskii-Moriya interaction (DMI). In Paper II we calculated this splitting. We employed a Hubbard-model approach to express the DMI constant D in terms of the microscopic Hubbard-model parameters, such as the effective hopping integral between magnetic sites t, the on-site repulsion energy U, and the strength of the SOI λ_{SOI}. We then carried out an approximated method to extract these parameters from first-principles methods. We found a small splitting for the $\{Cu_3\}$ MM, which is consistent with experimental results.

In Paper III we investigated the spin-electric coupling in several triangular MMs and discussed the underlying mechanism leading to an enhanced coupling, which can be used as a convenient guide to synthesize MMs that can respond more efficiently to an external electric field. We investigated the dependence of spin-electric coupling on types of magnetic atoms, distances between magnetic centers and the role of the exchange path between magnetic atoms. We also studied a fifteen magnetic center MM called $\{V_{15}\}$. We described a method for constructing the chiral degenerate ground state of this molecule. A generalization of the spin-electric coupling in such a molecule is also reported in this paper. We found that, among the MMs we investigated, the $\{V_3\}$ MM has the strongest spin-electric parameter $d = 3.02 \times 10{-}31$C·m=0.09 Debye.

In Paper IV we investigated a single-molecule magnet (SMM) called $\{Fe_4\}$. We studied theoretically the properties of this SMM attached to metallic leads in a single-electron transistor geometry. We found that the spin ordering and the magnetic anisotropy of such molecule remain stable in the presence of metallic leads. We also calculated the variation in the magnetic anisotropy for charged states for both the isolated molecule and the molecule attached to the leads. We found that an external electric potential, modeling a gate voltage, can be used to manipulate the charge on the molecule-leads system and therefore the magnetic properties of the spintronics device.

Coulomb-blockade transport experiments in the cotunneling regime can provide a direct way to determine the spin-electric coupling strength in triangular MMs. In Paper V we calculated the spin-electric splitting of the ground state of a triangular MM. We found that this splitting can be detected in the inelastic cotunneling conductance measurements. The theoretical analysis, based on a one-band Hubbard model, was supported by master-equation calculations of quantum transport both in the sequential and the cotunneling regime. We employed the Hubbard-model parameters calculated in Paper II.

We also found a consistency between the d parameter calculated in this paper and the d calculated in Paper I by first-principles methods.

Many questions have been raised through our research. Several lines of investigation started with the thesis can be further pursued. Here we mention some possible directions for future work.

Firstly, the work on spin-electric coupling in spin frustrated MMs requires further investigation. The appearance of a dipole moment in triangular molecular magnets can be understood from a Hubbard model. It can be viewed as a microscopic charge redistribution that appears when one of the three spins, initially all up or down, in the triangular MM is flipped to form a 1/2-spin frustrated system. This redistribution is given in terms of the ratio of the Hubbard parameters t/U. Although the one-band Hubbard model that we have implemented in the calculation of this ratio and the Dzyaloshinskii-Moriya parameter, D, have been sufficient to capture the underlying physical picture, a multi-orbital Hubbard model [67] would provide a more accurate description. A more detailed ab-initio strategy to extract the parameters involved in the calculation of the spin-electric coupling can be investigated. With this more sophisticated approach, there is the hope of addressing and answering such questions as: "How do the non-magnetic atoms mediating the superexchange between magnetic atoms affect the d value? How does the spatial separation between magnetic ions influence the spin-electric coupling?"

The spin electric coupling investigated for triangular MMs also exists, albeit in a more subtle form, in other odd spin rings without inversion symmetry, such as pentagon antiferromagnetic rings. In this case, however, the presence of the spin-orbit interaction is crucial for the effect. Although it is expected that the spin-electric coupling should be smaller in this case, a systematic study would be worthwhile.

Secondly, in Paper IV we studied the magnetic properties of a single-molecule magnet in a single-electron transistor geometry. In Paper V we investigated quantum transport in a triangular molecular magnet. One line of research is to build up a formalism that combines generalized rate equations for quantum transport with a microscopic first-principles description of interesting molecular magnets [68]. Many research articles, reviews, and books dealing with molecular nanomagnetism, density functional theory (DFT), and Coulomb blockade transport have appeared, but research covering the different aspects of their interplay is lacking.

Establishing a connection between DFT and Coulomb blockade is certainly a very challenging task. This research would develop theories and methods to describe the cou-

pling between charges and quantum spins in electronic devices containing a few magnetic atoms or molecules weakly coupled to the leads where charging and electronic correlations play a crucial role. Studies would focus on the effect of the spin and orbit degrees of freedom on the tunneling spectroscopy in MMs. These investigations would contribute to the development of DFT procedures to calculate the matrix elements that enter in the tunneling and cotunneling rates in quantum transport. This research would thereby contribute to the development of a new class of spintronics devices such as molecular spin-transistors.

Part III

APPENDICES

A

Group Theory

A.1 Symmetry

Definition

Symmetry operation: transformation that changes the geometrical configuration of an object but leaves it indistinguishable from the initial configuration. The symmetry of a molecule can be determined by a set of such transformations that bring the molecule into self-coincidence. Every possible symmetry operation can be reduced to one of the following three operations or a combination of them:

- rotation by a defined angle around some axis;
- mirror reflection in a plane;
- parallel transport (translation).

Symmetry Axis

n-th order symmetry axis C_n: When an object is brought into self-coincidence after a rotation operation $\hat{C}_n$ of $2\pi/n$ angle around some axis, this axis is called an *n*th order symmetry axis and is denoted by C_n. A m successive rotation is also a symmetry operation and is denoted as $\hat{C}_n^m$. We can see that $\hat{C}_n^n = \hat{E}$ where $\hat{E}$ is the identity operation that leaves the object unchanged. Thus a C_n axis leads to the existence of a definite number of axis $C_{n/p}$, where p is a divisor of n.

Reflection Operation

A σ mirror reflection in the xy plane is the operation $\hat{\sigma}$ that brings the object $P(x_0, y_0, z_0)$ into $P'(x_0, y_0, -z_0)$. If a molecule under this operation is brought into self-coincidence, the molecule is said to posses a symmetry plane. A successive reflection operation brings a molecule back to its initial configuration, $\hat{\sigma}^2 = \hat{E}$, $\hat{\sigma}^3 = \hat{\sigma}$, etc.

Improper Rotation

Improper Rotation: combination of two symmetry operations, namely, a rotation $\hat{C}(\varphi)$ about the axis C through an angle φ and a reflection $\hat{\sigma}$ in a plane perpendicular to the axis. Assume a point $P(x_0, y_0, z_0)$. Apply an improper operation on P such that the final point is $P''(x_0, y_0', z_0')$. First make a rotation $\hat{C}(\varphi)P(x_0, y_0, z_0) = P'(x_0, y_0', z_0)$, now a reflection $\hat{\sigma}P'(x_0, y_0', z_0) = P''(x_0, y_0', z_0')$. The improper operation through an angle φ is denoted by $\hat{S}(\varphi)$. An improper rotation through an angle $2\pi/n$ is denoted by $\hat{S}_n$. A successive improper rotation can be written as $\hat{S}_n^m = \underbrace{\hat{C}_n\hat{\sigma}\ldots\hat{C}_n\hat{\sigma}}_{m} = \underbrace{\hat{C}_n\ldots\hat{C}_n}_{m}\cdot\underbrace{\hat{\sigma}\ldots\hat{\sigma}}_{m} = \hat{C}_n^m\hat{\sigma}^m$.

A very important and particular case of an improper rotation is the *inversion symmetry operation* $\hat{S}_2 = \hat{I}$, which brings a point $P(x_0, y_0, z_0)$ into the point $P(-x_0, -y_0, -z_0)$.

Definition of a Group

A *group* is defined as a set of elements satisfying the following four requirements:

- **Closure** Given any two elements of the group $\hat{X}$ and $\hat{Y}$, there is a third element $\hat{Z} = \hat{X}\hat{Y}$ that belongs to the set. This operation is called multiplication. Here it is essential to clarify that the term *multiplication* is a general term and does not

Axes	Directions
$3C_4$	$C_4(x), C_4(y), C_4(z)$
$4C_3$	$C_3(xyz), C_3(\overline{x}yz), C_3(x\overline{y}z), C_3(xy\overline{z})$
$6C_2$	$C_2(xy), C_2(yz), C_2(zx), C_2(\overline{x}y), C_2(\overline{y}z), C_2(\overline{z}x)$

Table A.1: Symmetry axes of the octahedral complex (see Fig. A.1). Here x, y, z are the positive and $\overline{x}$, $\overline{y}$, $\overline{z}$ are the negative directions of the coordinate axes.

necessarily mean an algebraic "multiplication". It can be an addition, division, translation, rotation, etc.

- **Identity element** The set contains an $\hat{E}$ element called identity element such that $\hat{E}\hat{X} = \hat{X}\hat{E}$ for any $\hat{E}$ element in the group.

- **Associativity** For all elements $\hat{X}$, $\hat{Y}$ and $\hat{Z}$ in the set, there is a rule of combination such that $\hat{X}(\hat{Y}\hat{Z}) = (\hat{X}\hat{Y})\hat{Z}$.

- **Inverse element** For each element $\hat{X}$ in the set, there exists an inverse element $\hat{X}^{-1} = \hat{Y}$ such that $\hat{X}\hat{Y} = \hat{Y}\hat{X} = \hat{E}$.

Equivalent Symmetry Elements

Suppose we have three symmetry elements A, B and C. Let A conjugates to B and C: $\hat{X}A = B$, $\hat{Y}A = C$, where $\hat{X}$ and $\hat{Y}$ are group operations. Now let the operation $\hat{Z} = \hat{Y}\hat{X}^{-1}$ from the same group transforms B into C: $\hat{Z}B = \hat{Y}\hat{X^{-1}}B = \hat{Y}A = C$. Thus all three elements A, B and C conjugate with each other. Mutually conjugated symmetry elements are called equivalent. Some examples are shown in Table A.1 for an octahedral complex (see Fig. A.1).

Classes

Suppose $\hat{A}$, $\hat{B}$ and $\hat{C}$ are three operations of a symmetry group. If there exists a $\hat{C}$ such that $\hat{A} = \hat{C}\hat{B}\hat{C}^{-1}$ then the operation $\hat{A}$ is said to be conjugate to $\hat{B}$. The complete collection of mutually conjugate group operations are called classes. For instance consider the following group $\mathbf{C}_{4\mu}$ of operations: $\hat{E}$, $\hat{C}_4$, $\hat{C}_4^2 = \hat{C}_2$, $\hat{C}_4^3$, $2\hat{\sigma}_{\mathrm{v}}$, $2\hat{\sigma}_{\mathrm{d}}$. Let us start with

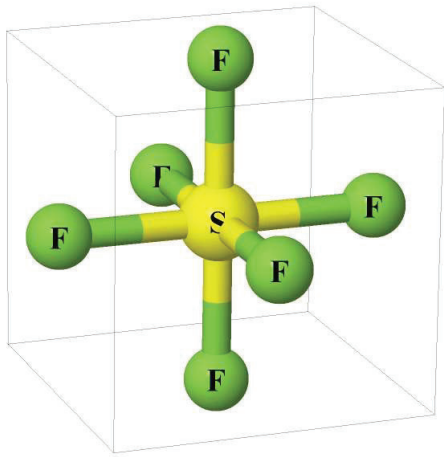

Figure A.1: Octahedral complex. Sulfur hexafluoride molecule.

the element $\hat{C}_4$:

$$\begin{aligned}
\hat{E}\hat{C}_4\hat{E}^{-1} &= \hat{C}_4, \\
\hat{C}_4\hat{C}_4\hat{C}_4^{-1} &= \hat{4}\hat{C}_4\hat{C}_4^3 = \hat{C}_4, \\
\hat{C}_2\hat{C}_4\hat{C}_2^{-1} &= \hat{C}_4, \\
\hat{C}_4^3\hat{C}_4(\hat{C}_4^3)^{-1} &= \hat{C}_4, \\
\hat{\sigma}_{\mathrm{v}}\hat{C}_4\hat{\sigma}_{\mathrm{v}}^{-1} &= \hat{\sigma}_{\mathrm{v}}\hat{C}_4\hat{\sigma}_{\mathrm{v}} = \hat{\sigma}_{\mathrm{v}}\hat{\sigma}_{\mathrm{d}}' = \hat{C}_4^3, \\
\hat{\sigma}_{\mathrm{v}}'\hat{C}_4(\hat{\sigma}_{\mathrm{v}}')^{-1} &= \hat{C}_4^3, \\
\hat{\sigma}_{\mathrm{d}}\hat{C}_4\hat{\sigma}_{\mathrm{v}}^{-1} &= \hat{C}_4^3, \\
\hat{\sigma}_{\mathrm{d}}'\hat{C}_4(\hat{\sigma}_{\mathrm{d}}')^{-1} &= \hat{C}_4^3.
\end{aligned}$$

These results can be found in a table form as shown in Table A.2.

A.2 Point Groups

Molecules can be classified by their symmetry operations. The collection of symmetry elements present in a molecule forms a group, commonly called point group. All the symmetry elements such as points, lines and planes, will intersect at a single point. Some of these point groups are:

	$\hat{E}$	$\hat{C}_4$	$\hat{C}_2$	$\hat{C}_4^3$	$\hat{\sigma}_\mathrm{v}$	$\hat{\sigma}'_\mathrm{v}$	$\hat{\sigma}_\mathrm{d}$	$\hat{\sigma}'_\mathrm{d}$
$\hat{E}$	$\hat{E}$	$\hat{C}_4$	$\hat{C}_2$	$\hat{C}_4^3$	$\hat{\sigma}_\mathrm{v}$	$\hat{\sigma}'_\mathrm{v}$	$\hat{\sigma}_\mathrm{d}$	$\hat{\sigma}'_\mathrm{d}$
$\hat{C}_4$	$\hat{C}_4$	$\hat{C}_2$	$\hat{C}_4^3$	$\hat{E}$	$\hat{\sigma}'_\mathrm{d}$	$\hat{\sigma}_\mathrm{d}$	$\hat{\sigma}_\mathrm{v}$	$\hat{\sigma}'_\mathrm{v}$
$\hat{C}_2$	$\hat{C}_2$	$\hat{C}_4^3$	$\hat{E}$	$\hat{C}_4$	$\hat{\sigma}'_\mathrm{v}$	$\hat{\sigma}_\mathrm{v}$	$\hat{\sigma}'_\mathrm{d}$	$\hat{\sigma}_\mathrm{d}$
$\hat{C}_4^3$	$\hat{C}_4^3$	$\hat{E}$	$\hat{C}_4$	$\hat{C}_2$	$\hat{\sigma}_\mathrm{d}$	$\hat{\sigma}'_\mathrm{d}$	$\hat{\sigma}'_\mathrm{v}$	$\hat{\sigma}_\mathrm{v}$
$\hat{\sigma}_\mathrm{v}$	$\hat{\sigma}_\mathrm{v}$	$\hat{\sigma}_\mathrm{d}$	$\hat{\sigma}'_\mathrm{v}$	$\hat{\sigma}'_\mathrm{d}$	$\hat{E}$	$\hat{C}_2$	$\hat{C}_4$	$\hat{C}_4^3$
$\hat{\sigma}'_\mathrm{v}$	$\hat{\sigma}'_\mathrm{v}$	$\hat{\sigma}'_\mathrm{d}$	$\hat{\sigma}_\mathrm{d}$	$\hat{\sigma}_\mathrm{v}$	$\hat{C}_4^3$	$\hat{E}$	$\hat{C}_2$	$\hat{C}_4$
$\hat{\sigma}_\mathrm{d}$	$\hat{\sigma}_\mathrm{d}$	$\hat{\sigma}_\mathrm{v}$	$\hat{\sigma}'_\mathrm{d}$	$\hat{\sigma}'_\mathrm{v}$	$\hat{C}_4$	$\hat{C}_4^3$	$\hat{E}$	$\hat{C}_2$
$\hat{\sigma}'_\mathrm{d}$	$\hat{\sigma}'_\mathrm{d}$	$\hat{\sigma}'_\mathrm{v}$	$\hat{\sigma}_\mathrm{v}$	$\hat{\sigma}_\mathrm{d}$	$\hat{C}_2$	$\hat{C}_4$	$\hat{C}_4^3$	$\hat{E}$

Table A.2: Multiplication table for the $\mathbf{C}_{4\mathrm{v}}$ group.

- **The rotational group $\mathbf{C}_n$**: it consists of rotations $\hat{C}_n^m$ about the *n*th order C_n axis.
  - $\mathbf{C}_1$: It contains only the identity operation $\hat{E}$.
  - $\mathbf{C}_2$: Two operations $\hat{C}_2$ and $\hat{E}$.
  - $\mathbf{C}_3$: Three operations $\hat{C}_3$, $\hat{C}_3^2$ and $\hat{E}$.
  - $\mathbf{C}_4$: Four operations $\hat{C}_4$, $\hat{C}_4^2$, $\hat{C}_4^3$ and $\hat{C}_4^4 = \hat{E}$.
  - $\mathbf{C}_6$: Six operations $\hat{C}_6$, $\hat{C}_6^2$, $\hat{C}_6^3$, $\hat{C}_6^4$, $\hat{C}_6^5$ and $\hat{C}_4^6 = \hat{E}$.
- **Rotoflection group $\mathbf{S}_{2n}$**: it consists of rotoflection transformations S_{2n}. Each operation over these groups constitutes a class.
  - $\mathbf{S}_2$: Two operations: $\hat{I}$ and $\hat{E}$.
  - $\mathbf{S}_4$: Four operations: $\hat{C}_2$, $\hat{S}_4$, $\hat{S}_4^3$ and $\hat{E}$.
  - $\mathbf{S}_4$: Six operations: $\hat{C}_3$, $\hat{C}_3^2$, $\hat{I}$, $\hat{C}_3^2\hat{\sigma}_h \equiv \hat{S}_6^{-1}$, $\hat{S}_6$ and $\hat{E}$.
- **Group $\mathbf{C}_{n\mathbf{h}}$**: It consists of rotations $\hat{C}_n^m$, reflections $\hat{\sigma}_\mathrm{h}$ and their products.
  - $\mathbf{C}_{1\mathrm{h}}$: Two operations: $\hat{C}_1 = \hat{E}$ and $\hat{\sigma}_\mathrm{h}$, and is denoted by $\mathbf{C}_3$.
  - $\mathbf{C}_{2\mathrm{h}}$: It consists of the operations: $\hat{E}$, $\hat{C}_2$, $\hat{\sigma}_\mathrm{h}$ and $\hat{\sigma}_\mathrm{h}\hat{C}_2 = \hat{I}$.
  - $\mathbf{C}_{3\mathrm{h}}$: Six operations: $\hat{E}$, $\hat{C}_3$, $\hat{C}_3^3$, $\hat{\sigma}_\mathrm{h}$, $\hat{S}_3$ and $\hat{S}_3^5$.
  - $\mathbf{C}_{4\mathrm{h}}$: Eight operations: $\hat{E}$, $\hat{C}_4$, $\hat{C}_2 = \hat{C}_4^2$, $\hat{C}_4^3$, $\hat{I}$, $\hat{S}_4^3$, $\hat{\sigma}_\mathrm{h}$ and $\hat{S}_4$.
- **Group $\mathbf{C}_{n\mathbf{v}}$**: It consists of a C_n axis and a vertical plane σ_v.

  - $\mathbf{C}_{2\mathrm{v}}$: Four operations: $\hat{E}$, $\hat{C}_2$, $\hat{\sigma}_{\mathrm{v}}$ and $\hat{\sigma}'_{\mathrm{v}}$.
  - $\mathbf{C}_{3\mathrm{v}}$: Six operations: $\hat{E}$, $\hat{C}_3$, $\hat{C}_3^2$, $\hat{\sigma}_{\mathrm{v}}$, $\hat{\sigma}'_{\mathrm{v}}$ and $\hat{\sigma}''_{\mathrm{v}}$.

- **Dihedral Groups $\mathbf{D}_n$**: It consists of a C_n axis and n horizontal C_2 axes intersecting at angles π/n.
  - $\mathbf{D}_2$: Four operations: $\hat{E}$, $\hat{C}_2$, $\hat{C}'_2$ and $\hat{C}''_2$.
  - $\mathbf{D}_3$: Eight operations, five classes: $\hat{E}$, $2\hat{C}_4$, $\hat{C}_4^2$, $2\hat{C}''_2$, and $2\hat{C}''_2$.

- **Dihedral Groups $\mathbf{D}_{n\mathbf{h}}$**: It consists of a D_n group plus an additional horizontal plane.
  - $\mathbf{D}_{2\mathrm{h}}$: Eight classes: $\hat{E}$, $\hat{C}_2(x)$, $\hat{C}_2(y)$, $\hat{C}_2(z)$, $\hat{\sigma}_{\mathrm{h}}$, $\hat{I}$, $\hat{\sigma}_{\mathrm{v}}(xz)$ and $\hat{\sigma}_{\mathrm{v}}(yz)$.
  - $\mathbf{D}_{3\mathrm{h}}$: Six classes: $\hat{E}$, $2\hat{C}_3$, $2\hat{S}_3$, $3\hat{C}'_2$, $\hat{\sigma}_{\mathrm{h}}$ and $3\hat{\sigma}_{\mathrm{v}}$.
  - $\mathbf{D}_{4\mathrm{h}}$: Eight classes: $\hat{E}$, $2\hat{C}_4$, $\hat{C}_4^2$, $2\hat{C}'_2$, $2\hat{C}''_2$, $\hat{\sigma}_{\mathrm{h}}$, $2\hat{\sigma}_{\mathrm{v}}$, $2\hat{\sigma}_{\mathrm{d}}$, $\hat{S}_4$ and $\hat{I}$.

- **Dihedral Groups $\mathbf{D}_{n\mathbf{d}}$**: It consists of a D_n group plus an additional vertical diagonal plane to the axis of D_n.
  - $\mathbf{D}_{2\mathrm{d}}$: Five classes: $\hat{E}$, $\hat{C}_2$, $2\hat{S}_4$, $2\hat{C}'_2$ and $2\hat{\sigma}_{\mathrm{d}}$.
  - $\mathbf{D}_{3\mathrm{d}}$: Six classes: $\hat{E}$, $2\hat{S}_6$, $2\hat{C}_3$, $\hat{I}$, $3\hat{C}'_2$ and $3\hat{\sigma}_{\mathrm{d}}$.

- **Cubic Groups T, $\mathbf{T_d}$, $\mathbf{T_h}$, O, $\mathbf{O_h}$**: Cubic groups include some of the symmetry operations of a cube. The groups **T, $\mathbf{T_d}$, $\mathbf{T_h}$** are called tetrahedral, while **O, $\mathbf{O_h}$** are octahedral.
  - $\mathbf{T}$: Four classes: $\hat{E}$, $4\hat{C}_3$, $4\hat{C}_3^2$ and $3\hat{C}_2$.
  - $\mathbf{T}_{\mathrm{h}}$ is the group product $\mathbf{T}\times\ \mathbf{C}_i$.
  - $\mathbf{T}_{\mathrm{d}}$ Five classes: $\hat{E}$, $8\hat{C}_3$, $6\hat{S}_4$, $3\hat{C}_2$ and $6\hat{\sigma}_{\mathrm{d}}$.
  - $\mathbf{O}$: Six classes: $\hat{E}$, $8\hat{C}_3$, $6\hat{C}_2$, $6\hat{C}_4$ and $3\hat{C}_4^2$.
  - $\mathbf{O}_{\mathrm{h}}$: Ten classes: $\hat{E}$, $8\hat{C}_3$, $6\hat{C}_2$, $6\hat{C}_4$, $3\hat{C}'_2$, $\hat{I}$, $6\hat{S}_4$, $8\hat{S}_6$, $3\hat{\sigma}_{\mathrm{h}}$ and $6\hat{\sigma}_{\mathrm{d}}$.

A.3 Group Representation

Each symmetry operation has its own matrix representation. Here we will give some examples of this matrices.

Matrix Form of Geometrical Representation

Let us consider $\mathbf{r}$ the position vector of a point $\mathbf{P}$ on the xy-plane. The point $\mathbf{P}$ can be written, in the Cartesian coordinates, as

$$\mathbf{P} = x\mathbf{i} + y\mathbf{j} \, ,$$

where $\mathbf{i}$ and $\mathbf{j}$ are unit vectors. The matrix representation of a counterclockwise rotation through an angle θ about the origin of the Cartesian coordinate system can be written as:

$$\mathbf{D}(\theta) = \begin{bmatrix} \cos\theta & -\sin\theta \\ \sin\theta & \cos\theta \end{bmatrix} \, .$$

Let us make a double rotation. First, we rotate a vector $\mathbf{r}_1 = x_1\mathbf{i} + y_1\mathbf{j}$ through an angle θ. The new vector $\mathbf{r}_2 = x_2\mathbf{i} + y_2\mathbf{j}$ is given by:

$$\begin{bmatrix} x_2 \\ y_2 \end{bmatrix} = \mathbf{D}(\theta) \begin{bmatrix} x_1 \\ y_1 \end{bmatrix} \, .$$

Second, we rotate $\mathbf{r}_2$ through an angle φ. Thus the new $\mathbf{r}_3$ vector is given by:

$$\begin{bmatrix} x_3 \\ y_3 \end{bmatrix} = \mathbf{D}(\varphi) \begin{bmatrix} x_2 \\ y_2 \end{bmatrix} = \mathbf{D}(\varphi)\mathbf{D}(\theta) \begin{bmatrix} x_1 \\ y_1 \end{bmatrix} = \mathbf{D}(\varphi + \theta) \begin{bmatrix} x_1 \\ y_1 \end{bmatrix} \, .$$

The matrices $\mathbf{D}(\theta)$, $\mathbf{D}(\varphi)$ and $\mathbf{D}(\theta + \varphi)$ correspond to the rotation operation $\hat{C}(\theta)$, $\hat{C}(\varphi)$ and $\hat{C}(\theta + \varphi)$, respectively. Multiplication of rotation matrices follow the same rule than multiplication of rotation operators. As a generalized rule, we can say: the product of geometrical operators

$$\hat{C}_n \ldots \hat{C}_2 \hat{C}_1 = \hat{Q}$$

can be obtained by multiplication of the matrices representing each operator

$$\mathbf{D}(\hat{R}_n) \ldots \mathbf{D}(\hat{R}_2)\mathbf{D}(\hat{R}_1) = \mathbf{D}(\hat{Q}).$$

Each geometrical operation is represented by a matrix, while a set of operations is represented by a set of matrices with the same multiplication table.

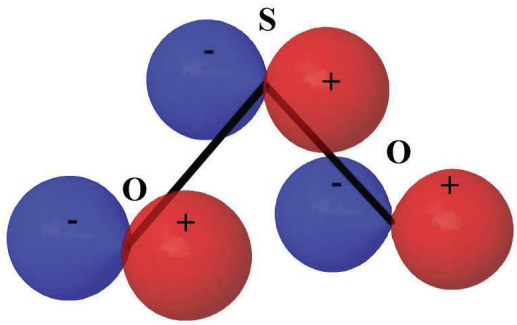

Figure A.2: SO_2 molecule with p orbitals on each atom.

Representation and Characters

Let us take the $\mathbf{C}_{2v}$molecule SO_2 with the orbital p_x on each atom (see Fig. A.2). The matrix representation of the group $\mathbf{C}_{2v}$ can be written as:

$$\begin{aligned} \mathbf{D}(\hat{E}) &= \begin{bmatrix} 1 & 0 & 0 \\ 0 & 1 & 0 \\ 0 & 0 & 1 \end{bmatrix}; \qquad \mathbf{D}(\hat{C}_2) = \begin{bmatrix} -1 & 0 & 0 \\ 0 & 0 & -1 \\ 0 & -1 & 0 \end{bmatrix}; \\ \mathbf{D}(\hat{\sigma}_v) &= \begin{bmatrix} 1 & 0 & 0 \\ 0 & 0 & 1 \\ 0 & 1 & 0 \end{bmatrix}; \qquad \mathbf{D}(\hat{\sigma}'_v) = \begin{bmatrix} -1 & 0 & 0 \\ 0 & -1 & 0 \\ 0 & 0 & -1 \end{bmatrix}. \end{aligned} \tag{A.1}$$

The corresponding multiplication table is given by:

$\mathbf{C}_{2h}$	$\hat{E}$	$\hat{C}_2$	$\hat{\sigma}_h$	$\hat{I}$
$\hat{E}$	$\hat{E}$	$\hat{C}_2$	$\hat{\sigma}_h$	$\hat{I}$
$\hat{C}_2$	$\hat{C}_2$	$\hat{E}$	$\hat{I}$	$\hat{\sigma}_h$
$\hat{\sigma}_h$	$\hat{\sigma}_h$	$\hat{I}$	$\hat{E}$	$\hat{C}_2$
$\hat{I}$	$\hat{I}$	$\hat{\sigma}_h$	$\hat{C}_2$	$\hat{E}$

The set of matrices representing all operations of a group is called matrix representation. The fact that a group can be written in a matrix representation tells us that there is a link between symbolic manipulation of operations and algebraic manipulation of numbers. The character χ of an operation or matrix A is the sum of its diagonal terms:

$$\chi(A) = \sum_i A_{ii}.$$

Irreducible Representation

If we have looked at the matrix representation of the $\mathbf{C}_{2h}$ group, Eq. (A.1), we would noted that they are block-diagonal form:

$$\mathbf{D} = \begin{pmatrix} (\bullet) & 0 & 0 \\ 0 & (\bullet) & (\bullet) \\ 0 & (\bullet) & (\bullet) \end{pmatrix}.$$

This matrix representation shows us that the symmetry operations do not mix one of the basis set with the others. Assume that the basis set for the $\mathbf{C}_{2h}$ group is ψ_a, ψ_b, ψ_c. Thus ψ_a itself is a basis set for the one-dimensional representation

$$\mathbf{D}(\hat{E}) = 1, \qquad \mathbf{D}(\hat{C}_2) = -1, \qquad \mathbf{D}(\hat{\sigma}_v) = 1, \qquad \mathbf{D}(\hat{\sigma}'_v) = -1, \tag{A.2}$$

which we shall call $\Gamma^{(1)}$. The other two basis functions are the basis of a two-dimensional representation $\Gamma^{(2)}$:

$$\begin{aligned} \mathbf{D}(\hat{E}) &= \begin{bmatrix} 1 & 0 \\ 0 & 1 \end{bmatrix}; \qquad \mathbf{D}(\hat{C}_2) = \begin{bmatrix} 0 & -1 \\ -1 & 0 \end{bmatrix}; \\ \mathbf{D}(\hat{\sigma}_v) &= \begin{bmatrix} 0 & 1 \\ 1 & 0 \end{bmatrix}; \qquad \mathbf{D}(\hat{\sigma}'_v) = \begin{bmatrix} -1 & 0 \\ 0 & -1 \end{bmatrix}. \end{aligned} \tag{A.3}$$

Thus the three-dimensional representation, $\Gamma^{(3)}$, has been **reduced** to the direct sum of a one-dimensional representation $\Gamma^{(1)}$ spanned by ψ_a, and a two-dimensional representation $\Gamma^{(2)}$, spanned by (ψ_b, ψ_c):

$$\Gamma^{(3)} = \Gamma^{(1)} + \Gamma^{(2)}.$$

The one-dimensional representation cannot be reduced any further, and is called an **irreducible representation**. Now, for the two-dimensional representation, we consider the linear combination $\psi_1 = \psi_b + \psi_c$ and $\psi_2 = \psi_b - \psi_c$. After some algebra we can see that, in the new basis set (ψ_1, ψ_2), Eqs. (A.3) can be written as:

$$\begin{aligned} \mathbf{D}(\hat{E}) &= \begin{bmatrix} 1 & 0 \\ 0 & 1 \end{bmatrix}; \qquad \mathbf{D}(\hat{C}_2) = \begin{bmatrix} -1 & 0 \\ 0 & 1 \end{bmatrix}; \\ \mathbf{D}(\hat{\sigma}_v) &= \begin{bmatrix} 1 & 0 \\ 0 & -1 \end{bmatrix}; \qquad \mathbf{D}(\hat{\sigma}'_v) = \begin{bmatrix} -1 & 0 \\ 0 & -1 \end{bmatrix}. \end{aligned} \tag{A.4}$$

$\mathbf{C}_{2v}$	$\hat{E}$	$\hat{C}_2$	$\hat{\sigma}_v$	$\hat{\sigma}'_v$	$f^{(\Gamma)}$	$f^{(\Gamma)}$
A_1	1	1	1	1	z	z^2, x^2, y^2
A_2	1	1	-1	-1		xy
B_1	1	-1	1	-1	x	zx
B_2	1	-1	-1	1	y	yz
I		II			III	IV

Table A.3: Character table of the $\mathbf{C}_{2v}$ group.

In this new representation all matrices are block-diagonal. Therefore any group operation does not mix the new basis set. Again we have reduced the $\Gamma^{(2)}$ to the sum of two one-dimensional representations. Thus $\psi_1 = \psi_b + \psi_c$ spans

$$\mathbf{D}(\hat{E}) = 1, \quad \mathbf{D}(\hat{C}_2) = -1, \quad \mathbf{D}(\hat{\sigma}_v) = 1, \quad \mathbf{D}(\hat{\sigma}'_v) = -1,$$

which is the same one-dimensional representation, Eq. (A.2), that we found for ψ_a and ψ_2

$$\mathbf{D}(\hat{E}) = 1, \quad \mathbf{D}(\hat{C}_2) = 1, \quad \mathbf{D}(\hat{\sigma}_v) = -1, \quad \mathbf{D}(\hat{\sigma}'_v) = -1,$$

which is a different one dimensional representation that we denote as $\Gamma^{(1)'}$. Thus we have found two irreducible representations of the $\mathbf{C}_{2v}$ group, Table A.3. The two representations are labeled B_1 and A_2, respectively. Labels A and B are used to denote one-dimensional representation. A is used if the character under the principal rotation is +1 while B if it is -1. E and T labels are used for two-dimensional and three-dimensional representation, respectively. Subscripts are used to distinguish if there is more than one irreducible representation of the same type.

Properties of Irreducible Representations

Here we formulate some properties of the irreducible representation of point groups. There is a detailed mathematical proof behind these properties. However we will write them without any proof [33]:

1. The number of inequivalent irreducible representations of a point group is equal to the number of classes in the group.

2. The sum of the squares of the dimensions of inequivalent irreducible representa-

tions is equal to the order of the group:

$$g_1^2 + g_1^2 + \cdots + g_r^2 = g,$$

where $g_1, g_2, \ldots, g_r$ are the dimensions of the irreducible representations, r is the number of classes and g is the order of the group.

3. The group characters of matrices belonging to operations in the same class are the same in any representation, reducible or irreducible.

4. Orthogonality of different representations.

$$\sum_{\hat{R}} \chi^{(\Gamma_1)}(\hat{R})\chi^{(\Gamma_2)}(\hat{R}) = 0 \quad \text{for} \quad \Gamma_1 \neq \Gamma_2.$$

5. The sum of squared characters in each of the irreducible representations is equal to the order of the group.

$$\sum_{\hat{R}} \left[\chi^{(\Gamma)}(\hat{R})\right]^2 = g$$

where Γ numbers the irreducible representation and the summation is over all the group operations

Character Table

For each point group there is a complete set of symmetry operations listed as a matrix known as Character table[1]. For instance, let us study the character table of the $\mathbf{C}_{3v}$ group given in Table A.3. In the upper-left corner the symmetry group is given (point group label). Next to it, on top, there are the symmetry operations of the group divided into classes ($\hat{E}, \hat{C}_2, \hat{\sigma}_v, \hat{\sigma}'_v$). The number of columns is equal to the number of classes. The left-hand column I (one-dimensional representation: A_1,A_2,B_1,B_2), contains the symbols of the irreducible representation Γ, symmetry representation labels. The next four columns, labeled as II, give the character of each representation for each symmetry operation. More formally, these columns tell us the basic type of behavior that orbitals may show when subjected to the symmetry operations of the group, +1 indicates that the orbital is unchanged and -1 indicates that it changes sign. Columns III and IV give us the simplest basis functions $f^{(\gamma)}$ (x,y,z,xy,yz,zx,x^2,y^2,z^2) of the irreducible representation. The function z is said to to be transformed according to the representation A_1, while x

[1] A character is a number that indicates the effect of an operation in a given representation

$\mathbf{D}_{3h}$	$\hat{E}$	$2\hat{C}_3$	$3\hat{C}_2$	$\hat{\sigma}_h$	$2\hat{S}_3$	$3\hat{\sigma}_v$		
$A_1^{'}$	1	1	1	1	1	1		x^2+y^2,z^2
$A_2^{'}$	1	1	-1	1	1	-1	R_z	
$E^{'}$	2	-1	0	2	-1	0	(x,y)	(x^2-y^2,xy)
$A_1^{''}$	1	1	1	-1	-1	-1		
$A_2^{''}$	1	1	-1	-1	-1	1	z	
$E^{''}$	2	-1	0	-2	1	0	(R_x,R_y)	xz,yz

Table A.4: Character table of the $\mathbf{D}_{3h}$ point group.

and y are transformed over the representation B_1 and B_2, respectively. The character of the identity operation $\hat{E}$ tells us the degeneracy of the orbital. Because there are not characters greater than 1 in the column headed $\hat{E}$ in C_{2v}, Table A.3, then there can be no doubly or triply degenerate orbitals in a C_{2v} molecule.

D_{3h} is an important point group in our work. Let us take a glance at the Table A.4. We can see that a D_{3h} molecule has doubly degeneracy. For the rows labeled $E^{'}$ and $E^{''}$, the characters are the sum of characters of individual orbitals in the basis. Thus a 0 means that a member of the doubly degenerate pair remains unchanged under a symmetry operation while the other member changes sign, $\chi = 1 - 1 = 0$.

A.4 Vanishing Integrals

The character tables (sec. A.3) provide a quick and convenient way of judging whether an overlap integral is necessarily zero. Let us consider the overlap integral

$$I = \int f_1 f_2 \, \mathrm{d}\tau \tag{A.5}$$

where f_1 might be an atomic orbital φ on one atom and f_2 an atomic orbital ψ on another atom. If we knew that the integral I is zero, we would say that there is not molecular orbital resulting from the overlap (φ, ψ).

The integral is an scalar value. Therefore it is independent of the coordinate system, it does not changes under any symmetry transformation of the molecule. Thus any operation brings the trivial identity transformation $I \rightarrow I$. Now, because the volume element $\mathrm{d}\tau$ is different than zero and invariant under any transformation, it follows that I is nonzero only if the integrand $f_1 f_2$ is invariant under any symmetry operation of the molecular

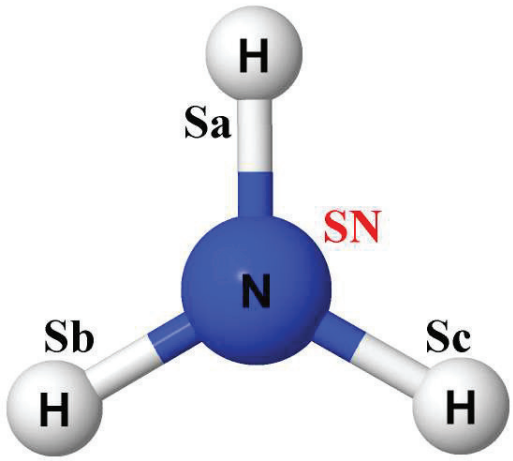

Figure A.3: NH_3 molecule.

point group. If the integrand changes its sign under a symmetry operation, the integral I would be necessarily zero, because its positive part will cancel its negative part. Therefore the only nonzero contribution comes from integrands for which the characters of the symmetry operations are all equal to +1. Thus, in order for I to be nonzero, the integrand $f_1 f_2$ must span the symmetry species A_1.

Group theory provides a procedure to determine the symmetry species of the product $f_1 f_2$, and hence to know if it really spans the symmetry species A_1. The character table of the product $f_1 f_2$ can be obtained by multiplication of the characters from the character tables of the functions f_1 and f_2 corresponding to a certain symmetry operator. Here we show this procedure [69]:

1. Decide on the symmetry species of the individual functions f_1 and f_2 by reference of the character table, and write their characters in two rows in the same order as in the table below.

2. Multiply the numbers in each column, writing the results in the same order.

3. Inspect the row produced, and see if it can be expressed as a sum of characters from each column of the group. The integral must be zero if this sum does not contain A_1.

For instance, we consider the molecule NH_3 shown in Fig. A.3. We let $f_1 = s_N$ be

an orbital of the N atom and f_2 be a linear combination of three hydrogen atom orbitals, $f_2 = s_H = s_a + s_b + s_c$. Each of the orbitals spans A_1 species:

	$\hat{E}$	$2\hat{C}_3$	$3\hat{\sigma}_v$
f_1	1	1	1
f_2	1	1	1
$f_1 f_2$	1	1	1

From the table we can see that the product $f_1 f_2$ spans A_1. Therefore the integral I, in this case, is not necessarily equal to zero. Thus the functions s_N and s_H may have nonzero overlap and bonding and antibonding molecular orbitals can be formed from linear combinations of s_N and s_H. The procedure of finding the irreducible representation of the product of two representations f_1 and f_2 can be written as a direct product of irreducible representations $\Gamma_1 \times \Gamma_2$. For our example above, it can be written as $A_1 \times A_1 = A_1$. Now consider the functions $f_1 = s_N$ and $f_2 = S_{bc} = s_b - s_c$. In this case s_N spans A_1 and s_{bc} spans E. Thus the product table can be written as:

	$\hat{E}$	$2\hat{C}_3$	$3\hat{\sigma}_v$
f_1	1	1	1
f_2	2	-1	0
$f_1 f_2$	2	-1	0

We can see that the product $f_1 f_2$ spans E instead of A_1. Therefore the integral is equal to zero and no bonding is allow between the orbitals s_N and s_{ab}. We can write this product as: $A_1 \times$ E = E. A shortcut for products such as $f_1 f_2$ is: if f_1 and f_2 are basis of irreducible representations and have the same symmetry species, then their overlap may be nonzero and may form bonding and antibonding combinations. If they have different symmetry species, their overlap must vanish.

The relation between the symmetry species of the atomic orbitals and their product, in general, is not as simple as in the previous example. In some cases, the product of functions f_1 and f_2 spans a sum of irreducible representations. Let us take as an example the point group $\mathbf{C}_{2v}$. When we multiply $f_1 f_2$ we could find the characters 2, 0, 0, -2, which is the sum of characters for A_2 and B_1. We write this product as $A_2 \times B_1 = A_2 + B_1$, which is called decomposition of a direct product. Now, because the sum does not include the species A_1, we conclude that the overlap integral is zero. Group theory provides a simple recipe to find the symmetry species of the irreducible representations [69]:

1. Write down a table with columns headed by the symmetry operations of the group.

2. In the first row write down the characters of the symmetry species we want to analyze.

3. In the second row, write down the characters of the irreducible representation Γ we are interested in.

4. Multiply the two rows together, add the products together, and divide by the order of the group.

Let us take the following example: imagine that we found the characters $f_1 f_2 \rightarrow 8$, -2, -6, 4 in the point group $\mathbf{C}_{2v}$. To find if A_1 does occur in the product with characters 8, -2, -6, 4 in $\mathbf{C}_{2v}$ and know if there may be overlap or not, we draw up the following table:

	$\hat{E}$	$\hat{C}_{2v}$	$\hat{\sigma}_v$	$\hat{\sigma}'_v$	sum	/order
$f_1 f_2$	8	-2	-6	4		
A_1	1	1	1	1		
	8	-2	-6	4	4	$1A_1$
A_2	1	1	-1	-1		
	8	-2	6	-4	8	$2A_2$
B_2	1	-1	-1	1		
	8	2	6	4	20	$5B_2$

Therefore, the product $f_1 f_2$ spans A_1+$2A_2$+$5B_2$ and because we found a species A_1, the overlap integral may be nonzero.

Another kind of interesting integrals in quantum mechanics are of the form:

$$I = \int f_1 f_2 f_3 \, \mathrm{d}\tau$$

where, for instance, f_1 and f_3 could be two basis functions and f_2 an operator. The rule for I to be nonzero is that the product $f_1 f_2 f_3$ must span A_1 or at least contain one component that spans A_1. Let us take as example the transition dipole moment, $\mathbf{r}$, for the H_2O. We want to calculate whether an electron in an orbital that spans A_1 can make a transition to an orbital that spans B_1. H_2O is a $\mathbf{C}_{2v}$ molecule. Checking this point group, one can see that the components of the dipole moment, namely x, y and z, span B_1,B_2 and A_1, respectively. Thus, the multiplication table for each component of the dipole moment is given by:

	x-component				y-component				z-component			
	$\hat{E}$	$\hat{C}_2$	$\hat{\sigma}_\mathrm{v}$	$\hat{\sigma}'_\mathrm{v}$	$\hat{E}$	$\hat{C}_2$	$\hat{\sigma}_\mathrm{v}$	$\hat{\sigma}'_\mathrm{v}$	$\hat{E}$	$\hat{C}_2$	$\hat{\sigma}_\mathrm{v}$	$\hat{\sigma}'_\mathrm{v}$
$f_1(\mathrm{B}_1)$	1	-1	1	-1	1	-1	1	-1	1	-1	1	-1
$f_2(x,y,z)$	1	-1	1	-1	1	-1	-1	1	1	1	1	1
$f_3(\mathrm{A}_1)$	1	1	1	1	1	1	1	1	1	1	1	1
$f_1 f_2 f_3$	1	1	1	1	1	1	-1	-1	1	-1	1	-1
spans	A_1				A_2				B_1			

We can see that the only component that spans A_1 is x. Therefore the x electric dipole transition is allowed and x-polarization of the radiation can be absorbed, or emitted in this transition.

A.5 Symmetry Adapted Orbitals

In this section we show how to find the symmetry adapted states for the $D_{3\mathrm{h}}$ point group. We recall the character table for this group, Table A.4. Every reducible representation (Γ^R) can be written as a linear combination of irreducible representations (Γ^{IR}) of a point group:

$$\Gamma^R = \sum_{IR} n_{IR}\Gamma^{IR} \,, \tag{A.6}$$

where n_{IR} is the number of times a particular irreducible representation occurs. Now we use the reduction formula to find n_{IR}:

$$n_{IR} = \frac{1}{h}\sum_Q k \cdot \chi^{IR}(Q) \cdot \chi^R(Q) \,,$$

where h is the number of operations in the group, Q a particular symmetry operation, k is the number of operations of Q, $\chi^{IR}(Q)$ the character of the irreducible representation under Q, and $\chi^R(Q)$ the character of the reducible representation under Q. For the irreducible representation A'_1 we have:

$$\begin{aligned}
n_{IR} &= \frac{1}{h}\sum_Q k \cdot \chi^{IR}(Q) \cdot \chi^R(Q) \\
n_{\mathrm{A}'_1} &= \frac{1}{12}\sum_Q k \cdot \chi^{\mathrm{A}'_1}(Q) \cdot \chi^R(Q) \\
n_{\mathrm{A}'_1} &= \frac{1}{12}\Big(1 \cdot \chi^{\mathrm{A}'_1}(\hat{E}) \cdot \chi^R(\hat{E}) + 2 \cdot \chi^{\mathrm{A}'_1}(\hat{C}_3) \cdot \chi^R(\hat{C}_3) + 3 \cdot \chi^{\mathrm{A}'_1}(\hat{C}_2) \cdot \chi^R(\hat{C}_2) + \\
&\quad 1 \cdot \chi^{\mathrm{A}'_1}(\hat{\sigma}_\mathrm{h}) \cdot \chi^R(\hat{\sigma}_\mathrm{h}) + 2 \cdot \chi^{\mathrm{A}'_1}(\hat{S}_3) \cdot \chi^R(\hat{S}_3) + 3 \cdot \chi^{\mathrm{A}'_1}(\hat{\sigma}_\mathrm{v}) \cdot \chi^R(\hat{\sigma}_\mathrm{v})\Big)
\end{aligned}$$

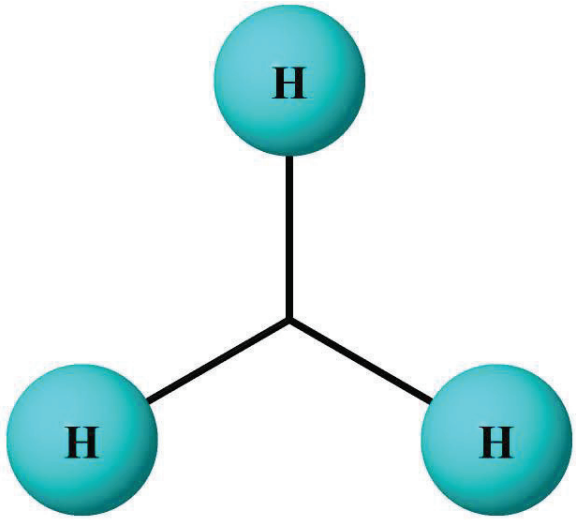

Figure A.4: H_3 molecule.

As an example we study the H_3 molecule shown in Fig. A.4. A reducible representation is found by determining how all the basis functions transform under each symmetry operation. We take a look at the bond between orbitals and imagine it as a displacement vector. If the displacement vector changes its phase we add +1, otherwise -1. Therefore, for H_3, under $\hat{E}$ all the 3 orbitals do not move $\rightarrow 3\hat{E}$. Under $\hat{C}_3$ none of the bonds are in their original position, $\rightarrow 0\hat{C}_3$. Under $\hat{C}_2$ only the bond on the axis is in its original position, $\rightarrow 1\hat{C}_3$. Under $\hat{\sigma}_\mathrm{h}$ the molecule remains in its original position, $\rightarrow 3\hat{\sigma}_\mathrm{h}$. Under $\hat{S}_3$ none of the bonds are in their original position, $\rightarrow 0\hat{S}_3$. Under $\hat{\sigma}_\mathrm{v}$ only the bond on the axis is in its original position, $\rightarrow 1\hat{\sigma}_\mathrm{v}$. The information obtained is given in the following table:

$D_{3\mathrm{h}}(\mathrm{H}_3)$	$\hat{E}$	$2\hat{C}_3$	$3\hat{C}_2$	$\hat{\sigma}_\mathrm{v}$	$2\hat{S}_3$	$3\hat{\sigma}_\mathrm{v}$
$\Gamma(\mathrm{H}_3)$	3	0	1	3	0	1

Now we combined this table with the character table of $D_{3\mathrm{h}}$ for the irreducible representation A_1':

$D_{3\mathrm{h}}(\mathrm{H}_3)$	$\hat{E}$	$2\hat{C}_3$	$3\hat{C}_2$	$\hat{\sigma}_\mathrm{v}$	$2\hat{S}_3$	$3\hat{\sigma}_\mathrm{v}$
A_1'	1	1	1	1	1	1
$\Gamma(\mathrm{H}_3)$	3	0	1	3	0	1

Therefore, for $n_{\mathrm{A}_1'}$ we have

$$\begin{aligned} n_{\mathrm{A}_1'} &= \frac{1}{12}\left(1\cdot 1\cdot 3+2\cdot 1\cdot 0+3\cdot 1\cdot 1+1\cdot 1\cdot 3+2\cdot 1\cdot 0+3\cdot 1\cdot 1\right) \\ &= \frac{1}{12}\left(3+0+3+3+0+3\right)=\frac{1}{12}\left(12\right)=1 \end{aligned}$$

Working out the symmetry irreducible representations of $D_{3\mathrm{h}}$ point group we have:

$$\begin{aligned} n_{\mathrm{A}_2'} &= \frac{1}{12}\left(1\cdot 1\cdot 3+2\cdot 1\cdot 0+3\cdot -1\cdot 1+1\cdot 1\cdot 3+2\cdot 1\cdot 0+3\cdot -1\cdot 1\right) \\ &= \frac{1}{12}\left(3+0-3+3+0-3\right)=\frac{1}{12}\left(0\right)=0 \\ n_{\mathrm{E}'} &= \frac{1}{12}\left(1\cdot 2\cdot 3+2\cdot -1\cdot 0+3\cdot 0\cdot 1+1\cdot 2\cdot 3+2\cdot -1\cdot 0+3\cdot 0\cdot 1\right) \\ &= \frac{1}{12}\left(6+0+0+6+0+0\right)=\frac{1}{12}\left(12\right)=1 \\ n_{\mathrm{A}_1''} &= \frac{1}{12}\left(1\cdot 1\cdot 3+2\cdot 1\cdot 0+3\cdot 1\cdot 1+1\cdot -1\cdot 3+2\cdot -1\cdot 0+3\cdot -1\cdot 1\right) \\ &= \frac{1}{12}\left(3+0+3-3+0-3\right)=\frac{1}{12}\left(0\right)=0 \\ n_{\mathrm{A}_2''} &= \frac{1}{12}\left(1\cdot 1\cdot 3+2\cdot 1\cdot 0+3\cdot -1\cdot 1+1\cdot -1\cdot 3+2\cdot -1\cdot 0+3\cdot 1\cdot 1\right) \\ &= \frac{1}{12}\left(3+0-3-3+0+3\right)=\frac{1}{12}\left(0\right)=0 \\ n_{\mathrm{E}''} &= \frac{1}{12}\left(1\cdot 2\cdot 3+2\cdot -1\cdot 0+3\cdot 0\cdot 1+1\cdot -2\cdot 3+2\cdot 1\cdot 0+3\cdot 0\cdot 1\right) \\ &= \frac{1}{12}\left(6+0+0-6+0+0\right)=\frac{1}{12}\left(0\right)=0 \end{aligned}$$

Inserting this result in Eq. (A.6), we have

$$\begin{aligned} \Gamma^R &= \sum_{IR} n_{IR}\Gamma^{IR} \\ \Gamma^R &= n_{\mathrm{A}_1'}\mathrm{A}_1'+n_{\mathrm{A}_2'}\mathrm{A}_2'+n_{E'}E'+n_{\mathrm{A}_1''}\mathrm{A}_1''+n_{\mathrm{A}_2''}\mathrm{A}_2''+n_{E''}E'' \\ \Gamma^R &= \mathrm{A}_1'+E' \end{aligned}$$

A.6 The Projector Operator

Now that we have determined the symmetry adapted orbitals, $\{\psi_{\mathrm{A}_1'},\psi_{\mathrm{E}'_{(1)}},\psi_{\mathrm{E}'_{(2)}}\}$, we will study the contribution from each orbital. This means that we are going to find the C

coefficients in the following equation,

$$\begin{aligned}
\psi_{\mathrm{A}_1'} &= C_1^{\mathrm{A}_1'}\phi_{H3_1} + C_2^{\mathrm{A}_1'}\phi_{H3_2} + C_3^{\mathrm{A}_1'}\phi_{H3_3} \\
\psi_{\mathrm{E}'_{(1)}} &= C_1^{\mathrm{E}'_{(1)}}\phi_{H3_1} + C_2^{\mathrm{E}'_{(1)}}\phi_{H3_2} + C_3^{\mathrm{E}'_{(1)}}\phi_{H3_3} \\
\psi_{\mathrm{E}'_{(2)}} &= C_1^{\mathrm{E}'_{(2)}}\phi_{H3_1} + C_2^{\mathrm{E}'_{(2)}}\phi_{H3_2} + C_3^{\mathrm{E}'_{(2)}}\phi_{H3_3} \ .
\end{aligned}$$

These C coefficients are the size of the atomic orbital contributions to the molecular orbitals and can be found by the projector operator:

$$P_\Gamma[\psi] = \frac{1}{h}\sum_Q \chi^{IR}(Q)\cdot Q[\psi] \tag{A.7}$$

where h is the number of operations in the group; Q is a particular symmetry operation; $[\psi]$ operates on an orbital function and $\chi^{IR}(Q)$ is the character of the irreducible representation under the symmetry operation Q. The reduction formula gives numbers n_{IR} while the projector operator gives a function.

As example we will show the effect of the projector operator acting on the molecule H_3 (Fig. A.4). First make an extended projection table with all the symmetry operations. Then identify the effect of each operation on a specific orbital $Q[\psi]$, for example s_1.

$D_{3\mathrm{h}}(\mathrm{H}_3)$	$\hat{E}$	$\hat{C}_3^1$	$\hat{C}_3^2$	$\hat{C}_2$	$\hat{C}_2'$	$\hat{C}_2''$	$\hat{\sigma}_\mathrm{v}$	$\hat{S}_3^1$	$\hat{S}_3^{-1}$	$\hat{\sigma}_\mathrm{v}$	$\hat{\sigma}_\mathrm{v}'$	$\hat{\sigma}_\mathrm{v}''$
$Q[s_1]$	s_1	s_2	s_3	s_1	s_3	s_2	s_1	s_2	s_3	s_1	s_2	s_3

Now choose an irreducible representation and calculate the product $\chi^{\mathrm{A}_1'}(Q)\cdot Q[\psi]$

$D_{3\mathrm{h}}(\mathrm{H}_3)$	$\hat{E}$	$\hat{C}_3^1$	$\hat{C}_3^2$	$\hat{C}_2$	$\hat{C}_2'$	$\hat{C}_2''$	$\hat{\sigma}_\mathrm{v}$	$\hat{S}_3^1$	$\hat{S}_3^{-1}$	$\hat{\sigma}_\mathrm{v}$	$\hat{\sigma}_\mathrm{v}'$	$\hat{\sigma}_\mathrm{v}''$
$Q[s_1]$	s_1	s_2	s_3	s_1	s_3	s_2	s_1	s_2	s_3	s_1	s_3	s_2
A_1'	1	1	1	1	1	1	1	1	1	1	1	1
$\chi^{\mathrm{A}_1'}(Q)\cdot Q[s_1]$	s_1	s_2	s_3	s_1	s_3	s_2	s_1	s_2	s_3	s_1	s_3	s_2

Therefore from Eq. (A.7), we have

$$\begin{aligned}
P_{\mathrm{A}_1'}[s_1] &= \frac{1}{h}\sum_Q \chi^{\mathrm{A}_1'}(Q)\cdot Q[s_1] \\
&= \frac{1}{12}\left(s_1+s_2+s_3+s_1+s_3+s_2+s_1+s_2+s_3+s_1+s_3+s_2\right) \\
&= \frac{1}{12}\left(4s_1+4s_2+4s_3\right) \\
&= \frac{1}{3}\left(s_1+s_2+s_3\right)
\end{aligned}$$

Thus, finally we have found the H3 wavefunction that transforms as A_1'. Each atomic orbital contributes in the same way to the wave function.

A.7 Symmetry Adapted Orbitals for Cyclic π Systems

An effective tool used for the investigation of electronic structure in quantum chemistry is the molecular orbital method. Unlike crystal field theory and hybrid orbital theory, in which there are restrictions like the approximation of point like, structureless ligands and pair bondings [33], the molecular orbital method takes into account the electronic structure of all atoms in the molecule. In this approximation molecular orbitals are constructed as a linear combination of atomic orbitals (LCAO):

$$\Psi = c_1\phi_1 + c_2\phi_2 + \cdots + c_n\phi_n \ ,$$

where ϕ_l are the atomic orbitals, c_n are the unknown coefficients and n is the number of atoms. Here we study the cyclic π system H_3. We will construct the LCAO molecular orbital for this molecule. Here we introduce the system to $\mathbf{C}_3$ instead of $\mathbf{D}_{3h}$. The character table for the $\mathbf{C}_3$ point group is given by:

$\mathbf{C}_3$	$\hat{E}$	$\hat{C}_3$	$\hat{C}_3^2$	$f^{(\Gamma)}$
A	1	1	1	z, R_z
E(ε,ε^*)	2	-1	-1	$x, y; R_x, R_y$
ε	1	ω	ω^*	$x+iy; R_x+iR_y$
ε^*	1	ω^*	ω	$x-iy; R_x-iR_y$

where all the irreducible representations are one-dimensional. A is totally symmetric and ω represents a complex number:

$$\omega = e^{2\pi i/3} = \cos\frac{2\pi}{3} + i\sin\frac{2\pi}{3} \ .$$

Let us apply the projector operator (Eq. (A.7)) to the s_1 basis set:

$\mathbf{C}_3(\mathrm{H}_3)$	$\hat{E}$	$\hat{C}_3^1$	$\hat{C}_3^2$
$Q[s_1]$	s_1	s_2	s_3
A	1	1	1
$\chi^{\mathrm{A}}(Q)\cdot Q[s_1]$	s_1	s_2	s_3
$Q[s_1]$	s_1	s_2	s_3
ε	1	ω	ω^*
$\chi^{\varepsilon}(Q)\cdot Q[s_1]$	s_1	ωs_2	$\omega^* s_3$
$Q[s_1]$	s_1	s_2	s_3
ε^*	1	ω^*	ω
$\chi^{\varepsilon^*}(Q)\cdot Q[s_1]$	s_1	$\omega^* s_2$	ωs_3

After normalizing, we find

$$\begin{aligned}
\Psi(A) &= \frac{1}{\sqrt{3}}(s_1+s_2+s_3)\\
\Psi(\varepsilon) &= \frac{1}{\sqrt{3}}(s_1+\omega s_2+\omega^* s_3)\\
\Psi(\varepsilon^*) &= \frac{1}{\sqrt{3}}(s_1+\omega^* s_2+\omega s_3)
\end{aligned}$$

$\Psi(\varepsilon)$ and $\Psi(\varepsilon^*)$ are the basis of one two-fold degenerate level. From the character table we can see that these functions transform as $x+iy$ and $x-iy$, respectively. Therefore it is convenient to introduce the real x and y basis of the two-dimensional representation E as:

$$\begin{aligned}
\Psi(Ex) &= \frac{1}{\sqrt{2}}(\Psi(\varepsilon)+\Psi(\varepsilon^*)) = \frac{1}{\sqrt{6}}(2s_1-s_2-s_3),\\
\Psi(Ey) &= -i\frac{1}{\sqrt{2}}(\Psi(\varepsilon)-\Psi(\varepsilon^*)) = \frac{1}{\sqrt{2}}(s_2-s_3)
\end{aligned}$$

Now, we can go back to the initial group $\mathbf{D}_{3\mathrm{h}}$. We can notice that the $\Psi(\mathbf{C}_3)$ is transformed in the $\mathbf{D}_{3\mathrm{h}}$ point group according to the representation A_1' while $\Psi(Ex)$ and $\Psi(Ey)$ correspond to the representation E' in the $\mathbf{D}_{3\mathrm{h}}$ point group.

B

Cotunneling Rates

B.1 Explicit derivation of Eq. (3.22)

Here we demostrate how to obtain the Eq. (3.22) we study the transition rates up to four order in the tunneling Hamiltonian. The transition rate from state $|j\rangle|n\rangle$ to $|j'\rangle|n'\rangle$ with one electron tunneling from lead α to the lead α' is given by

$$\Gamma_{\alpha\alpha'}^{nj;n'j'} = \frac{2\pi}{\hbar}\left|\langle j'|\langle n'|\mathscr{H}^T\frac{1}{E_{jn}-\mathscr{H}_0+i\eta}\mathscr{H}^T|n\rangle|j\rangle\right|^2\delta(E_{j'n'}-E_{jn})\,,$$

where $E_{j'n'}$ and E_{jn} are the energies of the final and initial states, respectively. $\mathscr{H}_T = \sum_{\alpha=L,R} t_\alpha \sum_{\mathbf{k}\sigma}\left(a_{\alpha\mathbf{k}\sigma}^\dagger c_\sigma + c_\sigma^\dagger a_{\alpha\mathbf{k}\sigma}\right)$ is the tunneling Hamiltonian Eq. (3.4) with $T_{km\alpha}^{L/R} = t_\alpha$. $\mathscr{H}_0 = \mathscr{H}_{mol} + \mathscr{H}_{leads}$ and η is a positive infinitesimal number. Here $|j'\rangle|n'\rangle = a_{\alpha'\mathbf{k}'\sigma'}^\dagger a_{\alpha\mathbf{k}\sigma}|j\rangle|n'\rangle$. $|j\rangle$ ($|n\rangle$) refers to the equilibrium state of the left and right Fermi sea (molecule). The total cotunneling rates for transitions that involve virtual transitions

between two n, n'-occupied molecule states are then given by

$$
\begin{aligned}
\Gamma^{nj;n'j'}_{\alpha\alpha'} &= \frac{2\pi}{\hbar}\sum_{\mathbf{k}\mathbf{k}'\sigma\sigma'}\Bigg|\langle j|\langle n'|a^\dagger_{\alpha\mathbf{k}\sigma}a_{\alpha'\mathbf{k}'\sigma'}\sum_{\alpha'''}t^*_{\alpha'''}\sum_{\mathbf{k}'''\sigma'''}\left(a^\dagger_{\alpha'''\mathbf{k}'''\sigma'''}c_{\sigma'''}+c^\dagger_{\sigma'''}a_{\alpha'''\mathbf{k}'''\sigma'''}\right)\\
&\quad\times\frac{1}{E_{jn}-\mathscr{H}_0+i\eta}\sum_{\alpha''}t_{\alpha''}\sum_{\mathbf{k}''\sigma''}\left(a^\dagger_{\alpha''\mathbf{k}''\sigma''}c_{\sigma''}+c^\dagger_{\sigma''}a_{\alpha''\mathbf{k}''\sigma''}\right)|n\rangle|j\rangle\Bigg|^2\\
&\quad\times\delta(E_{j'n'}-E_{jn})\\
&= \frac{2\pi}{\hbar}\sum_{\mathbf{k}\mathbf{k}'\sigma\sigma'}\Bigg|\langle j|\langle n'|a^\dagger_{\alpha\mathbf{k}\sigma}a_{\alpha'\mathbf{k}'\sigma'}\sum_{\alpha'''\mathbf{k}'''\sigma'''}\sum_{\alpha''\mathbf{k}''\sigma''}t^*_{\alpha'''}t_{\alpha''}\\
&\quad\times\Bigg(\underbrace{a^\dagger_{\alpha'''\mathbf{k}'''\sigma'''}c_{\sigma'''}\frac{1}{E_{jn}-\mathscr{H}_0+i\eta}a^\dagger_{\alpha''\mathbf{k}''\sigma''}c_{\sigma''}}_{=0,\ n\text{-2 states}}\\
&\quad+a^\dagger_{\alpha'''\mathbf{k}'''\sigma'''}c_{\sigma'''}\frac{1}{E_{jn}-\mathscr{H}_0+i\eta}c^\dagger_{\sigma''}a_{\alpha''\mathbf{k}''\sigma''}\\
&\quad+c^\dagger_{\sigma'''}a_{\alpha'''\mathbf{k}'''\sigma'''}\frac{1}{E_{jn}-\mathscr{H}_0+i\eta}a^\dagger_{\alpha''\mathbf{k}''\sigma''}c_{\sigma''}\\
&\quad\underbrace{+c^\dagger_{\sigma'''}a_{\alpha'''\mathbf{k}'''\sigma'''}\frac{1}{E_{jn}-\mathscr{H}_0+i\eta}c^\dagger_{\sigma''}a_{\alpha''\mathbf{k}''\sigma''}}_{=0,\ n\text{+2 states}}\Bigg)\\
&\quad\times|n\rangle|j\rangle\Big|^2\,\delta(E_{j'n'}-E_{jn})
\end{aligned}
$$

$$
\begin{aligned}
\Gamma^{nj;n'j'}_{\alpha\alpha'} &= \frac{2\pi}{\hbar}\sum_{\mathbf{k}\mathbf{k}'\sigma\sigma'}\Big|\langle j|\langle n'|\, a^\dagger_{\alpha\mathbf{k}\sigma}a_{\alpha'\mathbf{k}'\sigma'}\sum_{\alpha'''\mathbf{k}'''\sigma'''}\sum_{\alpha''\mathbf{k}''\sigma''}t^*_{\alpha'''}t_{\alpha''} \\
&\quad\times\Big\{c^\dagger_{\sigma'''}a_{\alpha'''\mathbf{k}'''\sigma'''}\,\frac{1}{E_{jn}-\mathscr{H}_0+i\eta}a^\dagger_{\alpha''\mathbf{k}''\sigma''}c_{\sigma''} \\
&\quad+a^\dagger_{\alpha'''\mathbf{k}'''\sigma'''}c_{\sigma'''}\frac{1}{E_{jn}-\mathscr{H}_0+i\eta}c^\dagger_{\sigma''}a_{\alpha''\mathbf{k}''\sigma''}\Big\}\,|n\rangle\,|j\rangle\Big|^2\,\delta(E_{j'n'}-E_{jn}) \\
&= \frac{2\pi}{\hbar}\sum_{\mathbf{k}\mathbf{k}'\sigma\sigma'}\Big|\sum_{\alpha'''\mathbf{k}'''\sigma'''}\sum_{\alpha''\mathbf{k}''\sigma''}t^*_{\alpha'''}t_{\alpha''}\Big\{ \\
&\quad\langle j|\langle n'|\, a^\dagger_{\alpha\mathbf{k}\sigma}a_{\alpha'\mathbf{k}'\sigma'}c^\dagger_{\sigma'''}a_{\alpha'''\mathbf{k}'''\sigma'''}\frac{1}{E_{jn}-\mathscr{H}_0+i\eta}a^\dagger_{\alpha''\mathbf{k}''\sigma''}c_{\sigma''}\,|n\rangle\,|j\rangle \\
&\quad+\langle j|\langle n'|\, a^\dagger_{\alpha\mathbf{k}\sigma}a_{\alpha'\mathbf{k}'\sigma'}a^\dagger_{\alpha'''\mathbf{k}'''\sigma'''}c_{\sigma'''}\frac{1}{E_{jn}-\mathscr{H}_0+i\eta}c^\dagger_{\sigma''}a_{\alpha''\mathbf{k}''\sigma''}\,|n\rangle\,|j\rangle\Big\}\Big|^2 \\
&\quad\times\delta(E_{j'n'}-E_{jn}) \qquad\qquad (B.1)
\end{aligned}
$$

Here n and n' are states with the same number of particles. Now we take a look at the numerator terms

$$
\begin{aligned}
\langle j|\, a^\dagger_{\alpha\mathbf{k}\sigma}a_{\alpha'\mathbf{k}'\sigma'}a_{\alpha'''\mathbf{k}'''\sigma'''}a^\dagger_{\alpha''\mathbf{k}''\sigma''}\,|j\rangle &= -\langle j|\, a^\dagger_{\alpha\mathbf{k}\sigma}a_{\alpha'''\mathbf{k}'''\sigma'''}a_{\alpha'\mathbf{k}'\sigma'}a^\dagger_{\alpha''\mathbf{k}''\sigma''}\,|j\rangle \\
&= -f\left(\varepsilon-\mu_\alpha\right)\delta_{\alpha\alpha'''}\delta_{\mathbf{k}\mathbf{k}'''}\delta_{\sigma\sigma'''} \\
&\quad\times\left(1-f\left(\varepsilon+\varepsilon_n-\varepsilon_{n'}-\mu_{\alpha'}\right)\right)\delta_{\alpha'\alpha''}\delta_{\mathbf{k}'\mathbf{k}''}\delta_{\sigma'\sigma''}
\end{aligned}
$$

and

$$
\begin{aligned}
\langle j|\, a^\dagger_{\alpha\mathbf{k}\sigma}a_{\alpha'\mathbf{k}'\sigma'}a^\dagger_{\alpha'''\mathbf{k}'''\sigma'''}a_{\alpha''\mathbf{k}''\sigma''}\,|j\rangle &= \langle j|\, a^\dagger_{\alpha\mathbf{k}\sigma}a_{\alpha'\mathbf{k}'\sigma'} \\
&\times\left(\cancelto{0}{\delta_{\alpha'''\alpha''}\delta_{\mathbf{k}'''\mathbf{k}''}\delta_{\sigma'''\sigma''}}-a_{\alpha''\mathbf{k}''\sigma''}a^\dagger_{\alpha'''\mathbf{k}'''\sigma'''}\right)|j\rangle \\
&= -\langle j|\, a^\dagger_{\alpha\mathbf{k}\sigma}a_{\alpha'\mathbf{k}'\sigma'}a_{\alpha''\mathbf{k}''\sigma''}a^\dagger_{\alpha'''\mathbf{k}'''\sigma'''}\,|j\rangle \\
&= \langle j|\, a^\dagger_{\alpha\mathbf{k}\sigma}a_{\alpha''\mathbf{k}''\sigma''}\,|j\rangle\,\langle j|\, a_{\alpha'\mathbf{k}'\sigma'}a^\dagger_{\alpha'''\mathbf{k}'''\sigma'''}\,|j\rangle \\
&= f\left(\varepsilon-\mu_\alpha\right)\delta_{\alpha\alpha''}\delta_{\mathbf{k}\mathbf{k}''}\delta_{\sigma\sigma''} \\
&\quad\left(1-f\left(\varepsilon+\varepsilon_n-\varepsilon_{n'}-\mu_{\alpha'}\right)\right)\delta_{\alpha'\alpha'''}\delta_{\mathbf{k}'\mathbf{k}'''}\delta_{\sigma'\sigma'''}
\end{aligned}
$$

Here we have used a Taylor series expansion on the operator $1/(E_{jn}-H_0) = (1/E_{jn})\sum_{l=0}^{\infty}(H_0/E_{jn})^l$.

Taking into account the last delta rules, we have

$$\begin{aligned}\langle n'|\, c^{\dagger}_{\sigma'''} c_{\sigma''}\, |n\rangle &= \sum_{n''} \langle n'|\, c^{\dagger}_{\sigma}\, |n''\rangle \langle n''|\, c_{\sigma'}\, |n\rangle = \sum_{n''} (\langle n''|\, c_{\sigma}\, |n'\rangle)^{\dagger} \langle n''|\, c_{\sigma'}\, |n\rangle \\ &= \sum_{n''} A^{\sigma *}_{n'' n'} A^{\sigma'}_{n'' n}\end{aligned}$$

and

$$\begin{aligned}\langle n'|\, c_{\sigma'} c^{\dagger}_{\sigma}\, |n\rangle &= \sum_{n''} \langle n'|\, c_{\sigma'}\, |n''\rangle \langle n''|\, c^{\dagger}_{\sigma}\, |n\rangle = \sum_{n''} \langle n'|\, c_{\sigma'}\, |n''\rangle (\langle n|\, c_{\sigma}\, |n''\rangle)^{\dagger} \\ &= \sum_{n''} A^{\sigma'}_{n' n''} A^{\sigma *}_{n n''}\end{aligned}$$

where $A^{\sigma'}_{n' n''} = \langle n'|\, c_{\sigma'}\, |n''\rangle$ and $A^{\sigma *}_{n n''} = \langle n''|\, c^{\dagger}_{\sigma}\, |n\rangle$. Here n'' represents an intermediate state.

Thus Eq. (B.1) becomes

$$\begin{aligned}\Gamma^{nj;n'j'}_{\alpha\alpha'} = \frac{2\pi}{\hbar} \sum_{\mathbf{k}\mathbf{k}'\sigma\sigma'} \Bigg| \sum_{\alpha'''\mathbf{k}'''\sigma'''} \sum_{\alpha''\mathbf{k}''\sigma''} t^{*}_{\alpha'''} t_{\alpha''} \Big\{ \\ - \langle j|\, \langle n'|\, a^{\dagger}_{\alpha\mathbf{k}\sigma} a_{\alpha'\mathbf{k}'\sigma'} a_{\alpha'''\mathbf{k}'''\sigma'''} c^{\dagger}_{\sigma'''} \frac{1}{\varepsilon_{n'} - \varepsilon_{n''} - \varepsilon + i\eta} c_{\sigma''}\, |n\rangle\, a^{\dagger}_{\alpha''\mathbf{k}''\sigma''}\, |j\rangle \\ + \langle j|\, \langle n'|\, a^{\dagger}_{\alpha\mathbf{k}\sigma} a_{\alpha'\mathbf{k}'\sigma'} a^{\dagger}_{\alpha'''\mathbf{k}'''\sigma'''} c_{\sigma'''} \frac{1}{\varepsilon_{n} - \varepsilon_{n''} + \varepsilon + i\eta} c^{\dagger}_{\sigma''}\, |n\rangle\, a_{\alpha''\mathbf{k}''\sigma''}\, |j\rangle \Big\} \Bigg|^2 \\ \times \delta(E_{j'n'} - E_{jn}) \qquad \text{(B.2)}\end{aligned}$$

$$\begin{aligned}\Gamma^{n;n'}_{\alpha\alpha'} = 2\,|t_{\alpha}|^2\,|t_{\alpha'}|^2 \sum_{\sigma\sigma'} \nu_{\alpha}(\sigma)\nu_{\alpha'}(\sigma') \int \mathrm{d}\varepsilon f(\varepsilon - \mu_{\alpha}) \left(1 - f\left(\varepsilon + \varepsilon_{n} - \varepsilon_{n'} - \mu_{\alpha'}\right)\right) \\ \times \left| \sum_{n''} \left\{ \frac{A^{\sigma *}_{n'' n'} A^{\sigma'}_{n'' n}}{\varepsilon - \varepsilon_{n'} + \varepsilon_{n''} + i\eta} + \frac{A^{\sigma'}_{n' n''} A^{\sigma *}_{n n''}}{\varepsilon + \varepsilon_{n} - \varepsilon_{n''} + i\eta} \right\} \right|^2 \qquad \text{(B.3)}\end{aligned}$$

$$\begin{aligned}\Gamma^{n;n'}_{\alpha\alpha'} = \sum_{\sigma\sigma'} \gamma^{\sigma}_{\alpha} \gamma^{\sigma'}_{\alpha'} \int \mathrm{d}\varepsilon f(\varepsilon - \mu_{\alpha}) \left(1 - f\left(\varepsilon + \varepsilon_{n} - \varepsilon_{n'} - \mu_{\alpha'}\right)\right) \\ \times \underbrace{\left| \sum_{n''} \left\{ \frac{A^{\sigma *}_{n'' n'} A^{\sigma'}_{n'' n}}{\varepsilon - \varepsilon_{n'} + \varepsilon_{n''} + i\eta} + \frac{A^{\sigma'}_{n' n''} A^{\sigma *}_{n n''}}{\varepsilon + \varepsilon_{n} - \varepsilon_{n''} + i\eta} \right\} \right|^2}_{Q} \qquad \text{(B.4)}\end{aligned}$$

B.2 Explicit derivation of Eq. (3.23)

From Eq. (B.4) we have

$$
\begin{aligned}
Q &= \left| \sum_{n''} \left\{ \frac{A^{\sigma *}_{n'' n'} A^{\sigma'}_{n'' n}}{\varepsilon - \varepsilon_{n'} + \varepsilon_{n''} + i\eta} + \frac{A^{\sigma'}_{n' n''} A^{\sigma *}_{n n''}}{\varepsilon + \varepsilon_{n} - \varepsilon_{n''} + i\eta} \right\} \right|^2 \\
&= \left(\frac{A^{\sigma' *}_{1n} A^{\sigma}_{1n'}}{\varepsilon - \varepsilon_{n'} + \varepsilon_1 - i\eta} + \frac{A^{\sigma}_{n1} A^{\sigma' *}_{n'1}}{\varepsilon + \varepsilon_{n} - \varepsilon_1 - i\eta} + \frac{A^{\sigma' *}_{2n} A^{\sigma}_{2n'}}{\varepsilon - \varepsilon_{n'} + \varepsilon_2 - i\eta} + \frac{A^{\sigma}_{n2} A^{\sigma' *}_{n'2}}{\varepsilon + \varepsilon_{n} - \varepsilon_2 - i\eta} \right. \\
&\quad \left. + \frac{A^{\sigma' *}_{3n} A^{\sigma}_{3n'}}{\varepsilon - \varepsilon_{n'} + \varepsilon_{n''} - i\eta} + \frac{A^{\sigma}_{n3} A^{\sigma' *}_{n'3}}{\varepsilon + \varepsilon_{n} - \varepsilon_3 - i\eta} \right) \\
&\quad \times \left(\frac{A^{\sigma *}_{1n'} A^{\sigma'}_{1n}}{\varepsilon - \varepsilon_{n'} + \varepsilon_1 + i\eta} + \frac{A^{\sigma'}_{n'1} A^{\sigma *}_{n1}}{\varepsilon + \varepsilon_{n} - \varepsilon_1 + i\eta} + \frac{A^{\sigma *}_{2n'} A^{\sigma'}_{2n}}{\varepsilon - \varepsilon_{n'} + \varepsilon_2 + i\eta} + \frac{A^{\sigma'}_{n'2} A^{\sigma *}_{n2}}{\varepsilon + \varepsilon_{n} - \varepsilon_2 + i\eta} \right. \\
&\quad \left. + \frac{A^{\sigma *}_{3n'} A^{\sigma'}_{3n}}{\varepsilon - \varepsilon_{n'} + \varepsilon_{n''} + i\eta} + \frac{A^{\sigma'}_{n'3} A^{\sigma *}_{n3}}{\varepsilon + \varepsilon_{n} - \varepsilon_3 + i\eta} \right)
\end{aligned}
$$

$$
\begin{aligned}
Q &= \sum_k \left(\frac{(A^{\sigma *}_{kn'} A^{\sigma'}_{kn})^2}{(\varepsilon - \varepsilon_{n'} + \varepsilon_k)^2 + \eta^2} + \frac{(A^{\sigma'}_{n'k} A^{\sigma *}_{nk})^2}{(\varepsilon + \varepsilon_{n} - \varepsilon_k)^2 + \eta^2} \right) \\
&\quad + 2\mathfrak{Re} \sum_q \sum_{k<q} \left(\frac{A^{\sigma *}_{qn'} A^{\sigma'}_{qn}}{\varepsilon - \varepsilon_{n'} + \varepsilon_q + i\eta} \frac{A^{\sigma *}_{kn'} A^{\sigma'}_{kn}}{\varepsilon - \varepsilon_{n'} + \varepsilon_k - i\eta} \right. \\
&\quad \left. + \frac{A^{\sigma'}_{n'q} A^{\sigma *}_{nq}}{\varepsilon + \varepsilon_{n} - \varepsilon_q + i\eta} \frac{A^{\sigma'}_{n'k} A^{\sigma *}_{nk}}{\varepsilon + \varepsilon_{n} - \varepsilon_k - i\eta} \right) \\
&\quad + 2\mathfrak{Re} \sum_q \sum_{k} \left(\frac{A^{\sigma *}_{kn'} A^{\sigma'}_{kn}}{\varepsilon - \varepsilon_{n'} + \varepsilon_q - i\eta} \frac{A^{\sigma'}_{n'k} A^{\sigma *}_{nk}}{\varepsilon + \varepsilon_{n} - \varepsilon_k - i\eta} \right)
\end{aligned}
$$

Thus Eq. (3.22) becomes

$$\begin{aligned}
\Gamma^{n;n'}_{\alpha\alpha'} &= \sum_{\sigma\sigma'}\gamma^{\sigma}_{\alpha}\gamma^{\sigma'}_{\alpha'}\int \mathrm{d}\varepsilon f\left(\varepsilon-\mu_{\alpha}\right)\left(1-f\left(\varepsilon+\varepsilon_{n}-\varepsilon_{n'}-\mu_{\alpha'}\right)\right)\\
&\quad\times\left|\sum_{n''}\left\{\frac{A^{\sigma*}_{n''n'}A^{\sigma'}_{n''n}}{\varepsilon-\varepsilon_{n'}+\varepsilon_{n''}+i\eta}+\frac{A^{\sigma'}_{n'n''}A^{\sigma*}_{nn''}}{\varepsilon+\varepsilon_{n}-\varepsilon_{n''}+i\eta}\right\}\right|^{2}\\
&= \sum_{\sigma\sigma'}\gamma^{\sigma}_{\alpha}\gamma^{\sigma'}_{\alpha'}\int \mathrm{d}\varepsilon f\left(\varepsilon-\mu_{\alpha}\right)\left(1-f\left(\varepsilon+\varepsilon_{n}-\varepsilon_{n'}-\mu_{\alpha'}\right)\right)\\
&\quad\times\left[\sum_{k}\left(\frac{(A^{\sigma*}_{kn'}A^{\sigma'}_{kn})^{2}}{(\varepsilon-\varepsilon_{n'}+\varepsilon_{k})^{2}+\eta^{2}}+\frac{(A^{\sigma'}_{n'k}A^{\sigma*}_{nk})^{2}}{(\varepsilon+\varepsilon_{n}-\varepsilon_{k})^{2}+\eta^{2}}\right)\right.\\
&\quad+2\mathfrak{Re}\sum_{q}\sum_{k<q}\left(\frac{A^{\sigma*}_{qn'}A^{\sigma'}_{qn}}{\varepsilon-\varepsilon_{n'}+\varepsilon_{q}+i\eta}\frac{A^{\sigma*}_{kn'}A^{\sigma'}_{kn}}{\varepsilon-\varepsilon_{n'}+\varepsilon_{k}-i\eta}\right.\\
&\quad\left.+\frac{A^{\sigma'}_{n'q}A^{\sigma*}_{nq}}{\varepsilon+\varepsilon_{n}-\varepsilon_{q}+i\eta}\frac{A^{\sigma'}_{n'k}A^{\sigma*}_{nk}}{\varepsilon+\varepsilon_{n}-\varepsilon_{k}-i\eta}\right)\\
&\quad\left.+\,2\mathfrak{Re}\sum_{q}\sum_{k}\left(\frac{A^{\sigma*}_{kn'}A^{\sigma'}_{kn}}{\varepsilon-\varepsilon_{n'}+\varepsilon_{q}-i\eta}\frac{A^{\sigma'}_{n'k}A^{\sigma*}_{nk}}{\varepsilon+\varepsilon_{n}-\varepsilon_{k}-i\eta}\right)\right]
\end{aligned}$$

$$\begin{aligned}
\Gamma^{n;n'}_{\alpha\alpha'} &= \sum_{\sigma\sigma'}\gamma^{\sigma}_{\alpha}\gamma^{\sigma'}_{\alpha'}\int \mathrm{d}\varepsilon f\left(\varepsilon-E_{1}\right)\left(1-f\left(\varepsilon-E_{2}\right)\right)\\
&\quad\times\left[\sum_{k}\frac{A^{2}}{(\varepsilon-\varepsilon_{ak})^{2}+\eta^{2}}\right. \qquad \text{(Integral type J)}\\
&\quad+\sum_{k}\frac{B^{2}}{(\varepsilon-\varepsilon_{bk})^{2}+\eta^{2}} \qquad \text{(Integral type J)}\\
&\quad+2\mathfrak{Re}\sum_{q}\sum_{k<q}\frac{A_{k}}{\varepsilon-\varepsilon_{ak}+i\eta}\frac{A_{q}}{\varepsilon-\varepsilon_{aq}-i\eta} \qquad \text{(Integral type I)}\\
&\quad+2\mathfrak{Re}\sum_{q}\sum_{k<q}\frac{B_{k}}{\varepsilon-\varepsilon_{bk}+i\eta}\frac{B_{q}}{\varepsilon-\varepsilon_{bq}-i\eta} \qquad \text{(Integral type I)}\\
&\quad\left.+\,2\mathfrak{Re}\sum_{q}\sum_{k}\frac{A_{k}}{\varepsilon-\varepsilon_{ak}+i\eta}\frac{B_{q}}{\varepsilon-\varepsilon_{bq}-i\eta}\right] \qquad \text{(Integral type I)}
\end{aligned}$$

where $A_k = A^{\sigma*}_{kn'}A^{\sigma'}_{kn}$, $B_k = A^{\sigma'}_{n'k}A^{\sigma*}_{nk}$, $\varepsilon_{ak} = \varepsilon_{n'} - \varepsilon_k$, $\varepsilon_{bk} = \varepsilon_k - \varepsilon_n$, $E_1 = \mu_\alpha$ and $E_2 = \mu_{\alpha'} + \varepsilon_{n'} - \varepsilon_n$

Integral type I

$$\begin{aligned} I(E_1,E_2,\varepsilon_1,\varepsilon_2) &= \mathfrak{Re}\int \mathrm{d}\varepsilon f(\varepsilon-E_1)\left[1-f(\varepsilon-E_2)\right]\frac{1}{\varepsilon-\varepsilon_1-i\gamma}\frac{1}{\varepsilon-\varepsilon_2+i\gamma} \\ &= \frac{n_B(E_2-E_1)}{\varepsilon_1-\varepsilon_2}\mathfrak{Re}\left\{\psi\left(\frac{1}{2}+\frac{i\beta}{2\pi}\left[E_2-\varepsilon_1\right]\right)-\psi\left(\frac{1}{2}-\frac{i\beta}{2\pi}\left[E_2-\varepsilon_2\right]\right)\right. \\ &\quad \left.-\psi\left(\frac{1}{2}+\frac{i\beta}{2\pi}\left[E_1-\varepsilon_1\right]\right)+\psi\left(\frac{1}{2}-\frac{i\beta}{2\pi}\left[E_1-\varepsilon_2\right]\right)\right\} \end{aligned} \tag{B.5}$$

Here ψ is the digamma function, n_B is the Bose function and $\beta = 1/k_BT$.

Integral type J

$$\begin{aligned} J(E_1,E_2,\varepsilon_1) &= \int \mathrm{d}\varepsilon f(\varepsilon-E_1)\left[1-f(\varepsilon-E_2)\right]\frac{1}{(\varepsilon-\varepsilon_1)^2+\eta^2} \\ &= \frac{\beta}{2\pi}n_B(E_2-E_1) \\ &\quad \times\mathfrak{Im}\left\{\psi'\left(\frac{1}{2}+\frac{i\beta}{2\pi}\left[E_2-\varepsilon_1\right]\right)-\psi'\left(\frac{1}{2}+\frac{i\beta}{2\pi}\left[E_1-\varepsilon_1\right]\right)\right\} \end{aligned} \tag{B.6}$$

Thus Eq. (B.5) becomes

$$\begin{aligned} \Gamma^{n;n'}_{\alpha\alpha'} &= \sum_{\sigma\sigma'}\gamma^{\sigma}_{\alpha}\gamma^{\sigma'}_{\alpha'}\left[\sum_k\left(A^2J(E_1,E_2,\varepsilon_{ak})+B^2J(E_1,E_2,\varepsilon_{bk})\right)\right. \\ &\quad +2\sum_q\sum_{k\neq q}\left(A_kA_qI(E_1,E_2,\varepsilon_{ak},\varepsilon_{aq})+B_kB_qI(E_1,E_2,\varepsilon_{bk},\varepsilon_{bq})\right) \\ &\quad \left.+\,2\sum_q\sum_k A_kB_qI(E_1,E_2,\varepsilon_{ak},\varepsilon_{bq})\right] \end{aligned} \tag{B.7}$$

C

Introduction to Density Functional Theory

C.1 Density Functional Theory

In simple words, density functional theory (DFT) is the most successful quantum mechanical method used in physics and chemistry to obtain an approximate solution to the Schrödinger equation of a many-body system such as atoms, molecules, clusters, periodic systems, etc. The core spirit of DFT resides in that the problem of solving the $3N$ spatial Schrödinger's many-particle wavefunction, where N is the number of particles, is reduced to the solution of an electron density functional, which contains only 3 spatial variables. Thus, instead of dealing with the huge amount of $3N$ variables, one only has to deal with 3 variables, which makes it far easier to handle. This reduction is mediated by the idea that there is a one-to-one unique relationship between the electron density and the exact ground state (GS) wavefunction. In the formulation given by Kohn, Hohenberg, and Sham in the 1960's, the real system is described by an effective one-body system [70, 71]. DFT is used to calculate magnetic and electronic properties of molecules, materials and defects, the binding energy of molecules, and relativistic effects in heavy elements and in

atomic nuclei and many other systems. Here we introduce the basic concepts underlying density functional theory, but before doing that, it is useful to mention the most important ideas behind DFT:

- In DFT we apply the Born-Oppenheimer approximation, which means that we treat the nuclei classically and only consider the electrons moving in electrostatic potential of fixed nuclei.
- The multi-electron wavefunction contains much more information than we really need, and therefore we only look for the electron density.
- The GS of a system always minimizes the expectation value of the Hamiltonian; consequently we only look at the total GS energy and charge density.
- There is still one contribution to the total energy that cannot be expressed in terms of the known quantities. This energy term, which models the exchange and correlation energy of the electrons, has to be approximated by educated guessing.

Here we outline the basic principles of DFT, and point out the extensions that must be taken into account in spin DFT (SDFT) [72–77]. One simple form of the independent Schrödinger equation is

$$H\Psi = E\Psi, \tag{C.1}$$

where H is the Hamiltonian operator, and Ψ is a set of solutions of the Hamiltonian. Each of these solutions, Ψ_n, has an associated eigenvalue E_n. The form of the Hamiltonian depends on the system. Some of the well-known and exactly solved examples are the particle in a box or a harmonic oscillator. In the case of many interacting electrons, *i.e.* a many-body problem, this equation is much more complicated. In this case the Schrödinger equation becomes

$$\begin{aligned}\left[\sum_i^N \left(-\frac{\hbar^2\nabla_i^2}{2m}\right) + \sum_i^N v(\mathbf{r}_i) + \sum_{i<j} U(\mathbf{r}_i,\mathbf{r}_j)\right]\Psi(\mathbf{r}_1,\mathbf{r}_2\ldots,\mathbf{r}_N) &= E\Psi(\mathbf{r}_1,\mathbf{r}_2\ldots,\mathbf{r}_N)\\ \left[\hat{T}+\hat{V}+\hat{U}\right]\Psi(\mathbf{r}_1,\mathbf{r}_2\ldots,\mathbf{r}_N) &= E\Psi(\mathbf{r}_1,\mathbf{r}_2\ldots,\mathbf{r}_N),\end{aligned} \tag{C.2}$$

where m is the electron mass, and N is the number of electrons, $v(\mathbf{r})$ is a potential acting on the electrons, $U(\mathbf{r}_i,\mathbf{r}_j)$ is the electron-electron interaction. The three terms in brackets

in this equation define, in order, the kinetic energy operator

$$\hat{T} = -\frac{\hbar^2}{2m}\sum_i \nabla_i^2, \tag{C.3}$$

and the interaction energy between each electron and the collection of atomic nuclei

$$\hat{V} = \sum_i v(\mathbf{r}_i) = \sum_{ik} \frac{Z_k e}{|\mathbf{r}_i - \mathbf{R}_k|}, \tag{C.4}$$

where the sum over k k extends over all nuclei in the system, each at the position $\mathbf{R}_k$. Finally, there is the interaction energy between different electrons

$$\hat{U} = \sum_{i<j} U(\mathbf{r}_i, \mathbf{r}_j) = \sum_{i<j} \frac{q^2}{|\mathbf{r}_i - \mathbf{r}_j|}. \tag{C.5}$$

In Eq. (C.2), Ψ is the electronic wavefunction, which is a function of the three spatial coordinates of each of the N electrons[1]. If we were interested, let us say, in a $\{Cu_3\}$ molecular magnet (see Sec. I), the full wavefunction would be a 3147-dimensional function (3 dimensions for each of the 1049 electrons)[2]. This shows us why solving the Schrödinger equation is a difficult task. The terms $\hat{T}$ and $\hat{U}$ are universal, while $\hat{V}$ is system-dependent.

It is useful to stop for a moment and think about the wavefunction and its utility. The wavefunction cannot be directly observed in experiments. The quantity that, in principle, can be measured is the probability that N electrons could be at a particular set of coordinates, $\mathbf{r}_1, \cdots, \mathbf{r}_N$. This probability is defined as

$$\Psi^*(\mathbf{r}_1, \cdots, \mathbf{r}_N)\Psi^*(\mathbf{r}_1, \cdots, \mathbf{r}_N), \tag{C.6}$$

where the asterisk indicates a complex conjugate. Another important remark is that in a real experiment, for the system measured it is not important which electron in the material is labeled i or j. This means that the probability is the quantity of physical interest. An important observable close to the probability is the density of electrons at a particular

[1] Here we have neglected the electron spin.

[2] A simple estimate of the computational complexity involved in solving the Schrödinger equation for this molecule is to imagine a real representation of Ψ on a mesh, in which each coordinate is discretized by using, let us say, only 10 mesh points. For 1049 electrons, Ψ becomes a function of $3 \times 1049 = 3147$ coordinates, and 10^{3147} values are required to describe Ψ on the mesh. The density $n(\mathbf{r})$ is a function of three coordinates, and requires only 10^3 values on the same mesh. Thus, the many-body wave function requires $10^{3147}/10^3 = 10^{3144}$ times more storage space than the density.

position in space, $n(\mathbf{r})$, which is written in terms of the individual electron wavefunctions as

$$n(\mathbf{r}) = N \int d^3r_2 \int d^3r_3 \ldots \int d^3r_N \Psi^*(\mathbf{r}, \mathbf{r}_2 \ldots, \mathbf{r}_N)\Psi(\mathbf{r}, \mathbf{r}_2 \ldots, \mathbf{r}_N). \tag{C.7}$$

Having said that, we can now state why DFT is such a great theory. It provides a systematic way to map a many-body problem with $\hat{U}$, into a single-particle problem without $\hat{U}$. DFT recognizes that in Coulomb systems, $\hat{T}$ and $\hat{U}$ are universal and only $\hat{V}$ differs between them. This is done when DFT lifts the status of the density $n(\mathbf{r})$ from being an observable to the rank of being a key variable, on which the calculation of all other observables can be based.

As its name says, DFT is a theory based on functionals. Here we introduce some useful mathematical definitions[3]:

- *Functional:* A functional is a rule for going from a function to a number. Let us define the function $f(x) = x^2 + x + 1$ and the functional $F[f] = \int_0^1 f(x)\, dx$. So, the functional $F[f]$ is a rule for going from f to the number $F[f] = 11/6$.

- *Functional derivative:* This tells us how the value of the functional changes if the function $f(x)$ is changed at the point x. It can be defined as

$$dF = \int_a^b dx \left.\frac{\delta F}{\delta f(x)}\right|_{f^0(x)} \delta f(x), \tag{C.8}$$

  where $f^0(x)$ is the particular function $f(x)$ that is the starting point for the infinitesimal change $\delta f(x)$. Here $\frac{\delta F}{\delta f(x)}$ is the functional derivative. For example, take the functional $F[f] = \int_0^1 f(x)^2\, dx$. To calculate the functional derivative, we calculate the change dF that is due to an infinitesimal change δf:

$$\begin{aligned} F[f + \delta f] &= \int_0^1 [f(x) + \delta f(x)]^2\, dx \\ &= \int_0^1 \left[f(x)^2 + 2f(x)\delta f(x) + \cancel{(\delta f(x))^2}^{\,0} \right] dx \\ &= F[f] + \int_0^1 2f(x)\delta f(x)\, dx. \end{aligned}$$

[3]These definitions are not defined in a rigorously mathematical formalism, but rather they are defined in a very simple way.

Thus, the infinitesimal change in F is

$$dF = F[f + \delta f] - F[f] \quad = \quad \int_0^1 2f(x)\delta f(x)\, dx.$$

Comparing it with Eq. (C.8) we have that the functional derivative corresponds to

$$\frac{\delta F}{\delta f(x)} \quad = \quad 2f(x).$$

The heart of the density functional theory resides in the Hohenberg-Kohn (HK) theorems. The first theorem states:

> *The ground-state energy from the Schrödinger equation is a unique functional of the electron density.*

This theorem tells us about the one-to-one mapping between the GS wavefunction and the GS electron density. It is possible to calculate the GS wavefunction $\Psi_0(\mathbf{r}_1, \mathbf{r}_2, \ldots, \mathbf{r}_N)$ provided the GS electron density n_0 (Eq. (C.7)). The GS electron density determines all properties of the GS, including the energy and wavefunction. Although the first HK theorem tells us about the existence of an electron density functional that could solve the Schrödinger equation , unfortunately it does not say anything about what this wonderful functional is.

The second HK theorem states

> *The density that minimizes the total energy is the exact ground-state density.*

If we knew the exact form of the functional, we would be able to vary it and find the energy from the functional is minimized. This is done in practice with approximate forms of the functional, not with the "true" functional.

A useful way to write down the HK energy functional is in terms of the wavefunctions, Eq. (C.7),

$$E[\Psi_i] = E_{\text{known}}[\Psi_i] + E_{\text{XC}}[\Psi_i], \tag{C.9}$$

where we have split the energy functional in two parts, namely, a known part $E_{\text{known}}[\Psi_i]$ and everything else $E_{\text{XC}}[\Psi_i]$. The known part includes four contributions

$$E_{\text{known}}[\Psi_i] = \frac{h^2}{m}\sum_i \int \Psi_i^* \nabla^2 \Psi_i \, d^3r + \int V(\mathbf{r}) n(\mathbf{r}) \, d^3r + \frac{e^2}{2} \iint \frac{n(\mathbf{r}) n(\mathbf{r}')}{|\mathbf{r}-\mathbf{r}'|} \, d^3r \, d^3r' + E_{\text{ion}}, \tag{C.10}$$

where the terms on the right-hand side of the equation correspond to the electron kinetic energies, the Coulomb interaction between electrons and the nuclei, the Coulomb interactions between pairs of electrons and the Coulomb interactions between pairs of nuclei. The other energy term, $E_{\text{XC}}[\Psi_i]$, is the exchange-correlation functional, and includes all the quantum effects that are not included in the known energy. Once one has the correct exchange-correlation functional, the next step is to find minimum energy solutions of the total energy functional. Kohn and Sham showed that the right electron density can be expressed in a way that involves solving a set of equations in which each equation only involves a single electron. In other words, in the Kohn-Sham (KS) approach, a fictitious non-interacting system is constructed, in such a way, that its density is the same as that of the interacting electrons. Therefore, the task is changed from finding the universal HK functional to finding the fictitious system of non-interacting electrons which has the same density as the "real" one with the interacting electrons.

The KS equations have the form

$$\left[\frac{h^2}{2m}\nabla^2 + V(\mathbf{r}) + V_H(\mathbf{r}) + V_{\text{XC}}(\mathbf{r})\right] \Psi_i(\mathbf{r}) = \varepsilon_i \Psi_i(\mathbf{r}), \tag{C.11}$$

where V is the interaction between an electron and the collection of atomic nuclei, and $V_H(\mathbf{r})$ is the Hartree (or Coulomb) potential[4],

$$V_H(\mathbf{r}) = e^2 \int \frac{n(\mathbf{r}')}{|\mathbf{r}-\mathbf{r}'|} \, d^3r'. \tag{C.12}$$

Finally, V_{XC} is the functional derivative of the exchange-correlation energy

$$V_{\text{XC}}(\mathbf{r}) = \frac{\delta E_{\text{XC}}(\mathbf{r}')}{\delta n(\mathbf{r})}. \tag{C.13}$$

Here we are now facing a problem about what to do first. There are four tasks to do, but they are in a circle. There is neither a beginning nor an end. To solve the KS equations, we need to define the Hartree potential. To define the Hartree potential we need to know

[4]This potential describes the Coulomb repulsion between the electron being considered in one of the KS equations and the total electron density defined by all electrons in the problem.

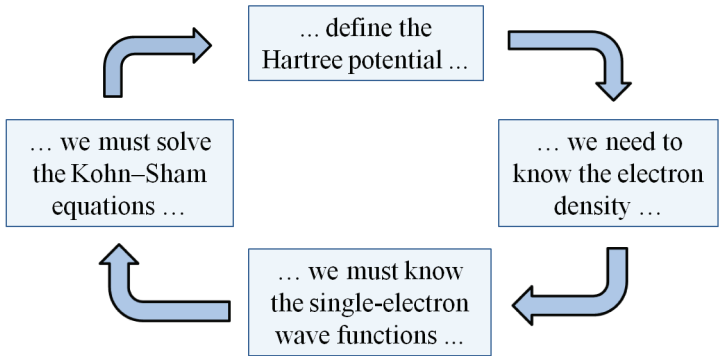

Figure C.1: Endless loop in solving the KS equations.

the electron density. To find the electron density, we must know the single-electron wave functions. To know the wavefunctions, we must solve the KS equations, and so on; (see Fig. C.1). In order to break this cycle we use an iterative algorithm:

1. Define (guess) an initial, trial electron density, $n(\mathbf{r})$.

2. Solve the KS equations defined using the electron density defined in step one to find the single-particle wavefunctions, $\Psi_i(\mathbf{r})$.

3. Calculate the electron density defined by the KS single-particle wavefunctions from step 2 ($n_{\text{KS}}(\mathbf{r})$ as in Eq. (C.7)).

4. Now, compare the calculated electron density from step two, $n_{\text{KS}}(\mathbf{r})$, with the trial electron density used in solving the KS equations in step one, $n(\mathbf{r})$. If $n(\mathbf{r}) = n_{\text{KS}}(\mathbf{r})$, then this is the ground-state electron density, but if $n(\mathbf{r}) \neq n_{\text{KS}}(\mathbf{r})$ then the trial electron density $n(\mathbf{r})$ must be adjusted in some way and one has to start over from step 2. Once these two densities are the same, it can be used to calculate the total energy.

Fig. C.2 shows a schematic flowchart of the self-consistent loop for solving the KS equations. Here we have omitted several important details about this self-consistent procedure, such as, the tolerance of the self-consistent condition, and how to define the initial density, but these details are beyond the scope of this introduction.

So far, we have seen that we could solve the many-body Schrödinger equation to find the ground-state energy. Thanks to the HK theorems we know that we can find the

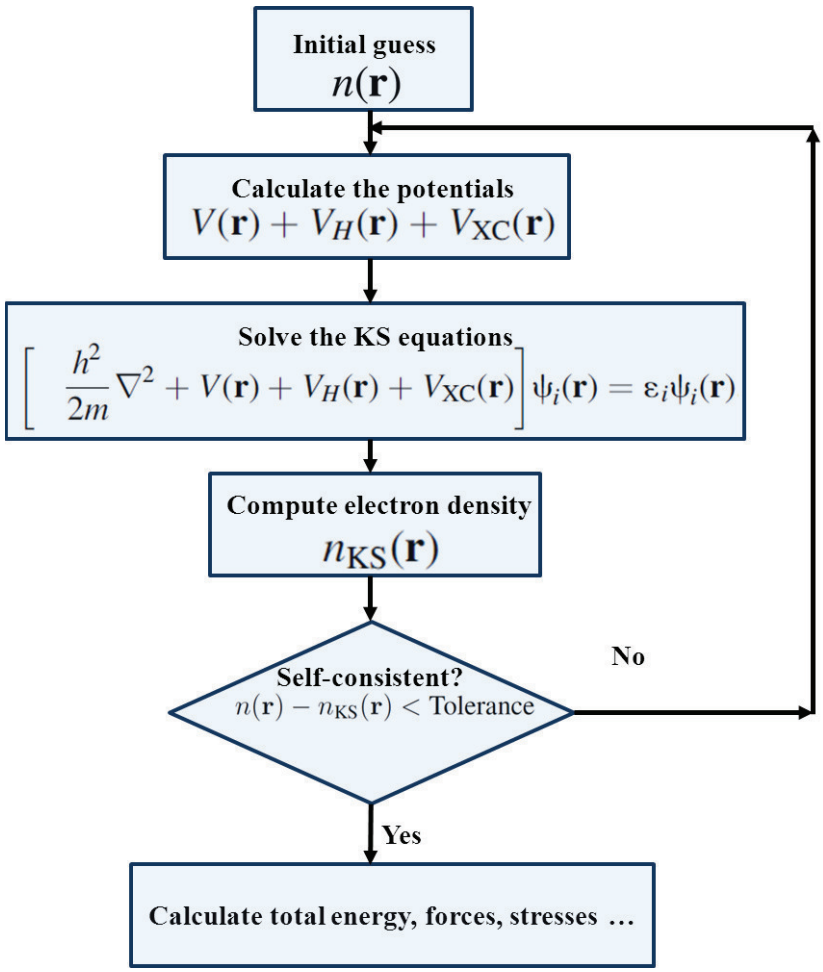

Figure C.2: Schematic representation of the self-consistent loop for solving the KS equations.

ground state of a many-body system minimizing the energy of a energy functional. Kohn and Sham have shown us a way to achieve this by means of a self-consistent solution of a set of single-particle equations. There is, however, a huge complication in this simple and beautiful scheme; in order to solve the KS equations, one has to define the exchange-correlation functional $E_{\rm XC}[\Psi_i]$. This is not an easy task; in fact, the true form of this exchange-correlation functional that will solve the true many-body Schrödinger equation is simply not known. Fortunately, as in many physics problems, it turns out that there is one case where this functional can be defined exactly: the uniform electron gas. In this case the density is uniform in all space, $n(\mathbf{r})$ =constant. To solve the KS equations using the uniform electron gas, we define the exchange-correlation potential as

$$V_{\rm XC}(\mathbf{r}) = V_{\rm XC}^{\text{electron gas}}[n(\mathbf{r})].$$

In this approximation we use the local density to model the exchange-correlation potential. This is called the local density approximation (LDA). Although the LDA gives us a way to define the KS equations, we must remember that this is not the true exchange-correlation functional. Since we are not solving the true Schrödinger equation t There are more functionals that are implemented in DFT calculations. A well-known functional beyond LDA uses the local electron density and its local gradient, it is called the generalized gradient approximation (GGA). Although the GGA includes more physical information than the LDA, sometimes it is not more accurate. There are many distinct GGA functionals out there. The most widely used are the Perdew-Wnag functional (PW91) and the Perdew-Burke-Ernzerhof functional (PBE).

We now introduce the spin density functional theory (SDFT) as a generalization of the DFT. In order to find the ground-state total energy E and spin densities $n_\uparrow(\mathbf{r})$, $n_\downarrow(\mathbf{r})$ for a collection of N electrons interacting with one another and with an external potential $V(\mathbf{r})$, we use the self-consistent solution of a fictitious one-electron Schrödinger equation , the spin Kohn-Sham equation:

$$\left[\frac{h^2}{2m}\nabla^2 + V([n];\mathbf{r}) + V_H([n];\mathbf{r}) + V_{\rm XC}^{\sigma}([n_\uparrow, n_\downarrow];\mathbf{r})\right]\Psi_{\alpha\sigma}(\mathbf{r}) = \varepsilon_{\alpha\sigma}\Psi_{\alpha\sigma}(\mathbf{r}), \quad \text{(C.14)}$$

with

$$n_\sigma(\mathbf{r}) = \sum_\alpha \theta(\mu - \varepsilon_{\alpha\sigma}) + |\Psi_{\alpha\sigma}(\mathbf{r})|^2, \quad \text{(C.15)}$$

$$n(\mathbf{r}) = n_\uparrow(\mathbf{r}) + n_\downarrow(\mathbf{r}), \quad \text{(C.16)}$$

$$\int d^3r\, n(\mathbf{r}) = N. \quad \text{(C.17)}$$

Here $\sigma = \uparrow$ or $\downarrow$ is the z-component of the spin, and α stands for the remaining one-electron quantum numbers. The step function in Eq. (C.15) guarantees that all KS spin orbitals with $\varepsilon_{\alpha\sigma} < \mu$ are singly-occupied, and those with $\varepsilon_{\alpha\sigma} < \mu$ are empty. The exchange-correlation potential is defined as

$$V_{\rm XC}^{\sigma}(\mathbf{r}) = \frac{\delta E}{\delta n_{\sigma}(\mathbf{r})}. \tag{C.18}$$

In the local spin density approximation (LSDA), the exchange-correlation energy functional is approximated as

$$E_{\rm XC}^{\rm LSDA}[n_{\uparrow}, n_{\downarrow}] = \int d^3r\, n(\mathbf{r}) \varepsilon_{\rm XC}(n_{\uparrow}(\mathbf{r}), n_{\downarrow}(\mathbf{r})), \tag{C.19}$$

where $\varepsilon_{\rm XC}(n_{\uparrow}(\mathbf{r}), n_{\downarrow}(\mathbf{r}))$ is the exchange-correlation energy per particle for an electron gas of uniform spin densities $n_{\uparrow}(\mathbf{r})$ and $n_{\downarrow}(\mathbf{r})$. In the GGA approximation, the spin exchange-correlation energy functional is a function of the densities and their gradient

$$E_{\rm XC}^{\rm GGA}[n_{\uparrow}, n_{\downarrow}] = \int d^3r\, f(n_{\uparrow}(\mathbf{r}), n_{\downarrow}(\mathbf{r}), \nabla n_{\uparrow}(\mathbf{r}), \nabla n_{\downarrow}(\mathbf{r})). \tag{C.20}$$

C.2 NRLMOL

Having discussed the main ideas behind DFT, we present the implementation of DFT used in this work: the Naval Research Laboratory Molecular Orbital Library (NRLMOL) computer code. It was developed by M. Pederson and co-workers and is freely available for non-profit use [78–86]. NRLMOL is based on the Kohn-Sham formulation of DFT and solves Kohn-Sham equations by expressing the Kohn-Sham orbitals as a linear combination of Gaussian orbitals. Very large basis sets, based on a nonlinear optimization procedure described in Ref. [84], have been used. As discussed in Ref. [84], this procedure simultaneously optimizes the contraction coefficients and the Gaussian-decay parameters by first performing atomic self-consistent field (SCF) calculations, using a single-Gaussian basis, and then using the conjugate-gradient method in conjunction with gradients of the energy with respect to the decay parameters to minimize the total atomic energy. A key feature of this optimization scheme is that it identifies a scaling law (proven in Ref. [84]) showing that the shortest-range Gaussian should scale as $Z^{10/3}$ to ensure that there is no basis-set superposition error. The basis sets are available upon request. The exchange-correlation functionals that can be used in NRLMOL are:

- LDA exchange-correlation functionals: VWN, CA, Perdew-Zunger 81, RPA, Wigner Interpolation Functional, Kohn-Sham exchange only and Gunnarsson-Lundquist.
- GGA functionals: PW91 and PBE.

The NRLMOL capability covers full or partial structure optimization, calculations of harmonic vibrational frequencies, infra-red spectra, Raman spectra, polarizability, density of states, joint density of states, vibrational polarizability, etc, and has been applied successfully to calculate the electronic and magnetic properties of several molecular magnets [32, 38, 47, 87–100]. In addition, NRLMOL uses the point group symmetry of molecules in an efficient manner, and practically any point group can be used. The default basis set of the NRLMOL has been specifically optimized for the Perdew- Burke-Ernzerhof exchange-correlation functional within the generalized gradient approximation and is much larger than the default basis sets used in other codes. One important feature of NRLMOL is its very efficient parallelization that allows for calculations of more than a hundred atoms at the all-electron level, which has been important in the case of the molecular magnets discussed in this thesis. Fig. C.3 shows a simplified flowchart that describes the standard tasks which are used in NRLMOL in order to solve self-consistently the Kohn-Sham equations [101]. In order to set up the mesh, NRLMOL divides the space into three different types of regions: atomic spheres, interstitial parallelepipeds and excluded cube regions. First of all, NRLMOL determines the locations and charges of the linear combination of Gaussian functions centered at the atomic sites. Once these are determined, the program uses a previously generated basis set. This previous basis set has been obtained by performing a self-consistent LDA calculation of the spherical unpolarized atom where the total energy of the atom was converged to within 10 meV. Second of all, for each isolated atom, the self-consistent potential is numerically determined and a least-square representation of it is generated. These potentials are expanded as a sum of bare spherical Gaussians or as a sum of Gaussian-screened $1/r$ potentials. Given the basis sets and the Gaussian-representation of the atomic potentials, it is possible to obtain very good insight into the class of multicenter integrands that need to be integrated, and this information is used to generate a numerical variational integration mesh that allows determining precisely the integrals required for the calculation of secular matrices, total energies and derivatives. Once the variational mesh is defined, the calculation starts. For the initial guess of the wavefunctions, one has to rely on the least-square fit representation of overlapping atomic potentials to determine a starting Hamiltonian. Once the wavefunctions are determined, by solution of Poisson's equation, it is possible to calculate the

potential due to these wavefunctions. Further, the Coulomb potential due to the electrons and the nuclei, as well as the exchange-correlation energy density and potentials, are required. The exchange-correlation term requires the evaluation of spin densities and the first and second derivatives of the spin densities for the GGA. The solution of the KS equation for that potential determines the new wavefunctions. The equations are then solved self-consistently by iterating until the total energy is converged to a 10^{-5} Hartree. Once self-consistency is achieved, the forces acting on each atom are determined from the Hellmann-Feynman-Pulay theorem. After obtaining all the forces acting on all the atoms, a conjugate-gradient method can be used to determine a new set of atomic coordinates. Once a new set of atomic coordinates is determined, we find that the wavefunction expansion coefficients provide the best starting point for a calculation on this geometry. Once an equilibrium geometry and the KS wavefunctions are determined there are many physical observables that could be calculated.

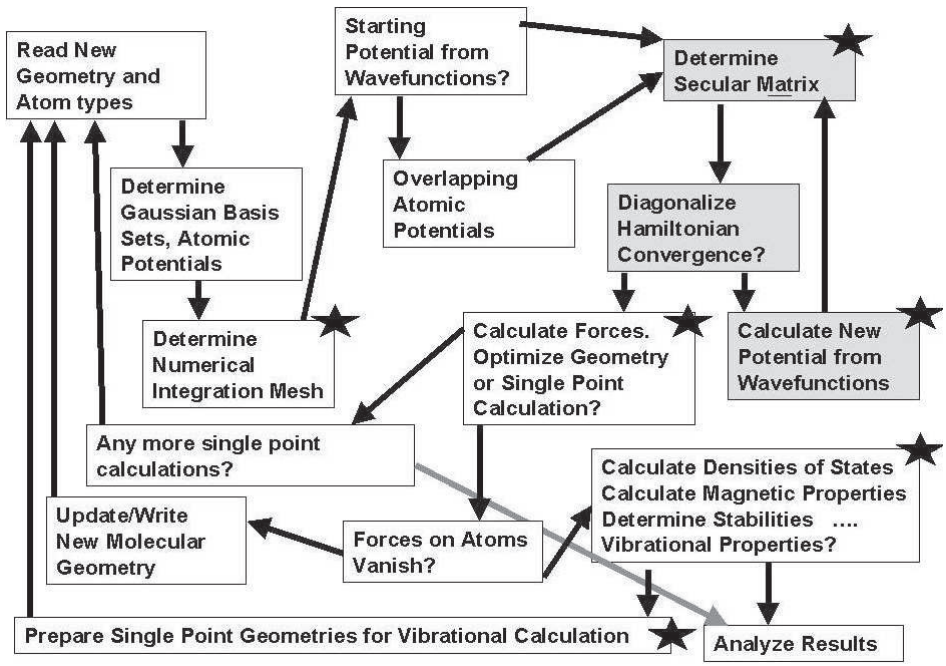

Figure C.3: Flow chart of parallel version of NRLMOL. The gray area represents the iterative part of the self-consistency cycle which is the computationally intensive part of the problem. The stars on the boxes represent the tasks which are massively parallelized. Reprinted with permission of John Wiley & Sons.

Bibliography

[1] M. N. Baibich, J. M. Broto, A. Fert, F. N. Van Dau, F. Petroff, P. Etienne, G. Creuzet, A. Friederich, and J. Chazelas, Phys. Rev. Lett. **61**, 2472 (1988).

[2] G. Binasch, P. GrÃijnberg, F. Saurenbach, and W. Zinn, Phys. Rev. B **39**, 4828 (1989).

[3] H. Zabel, Superlattices and Microstructures **46**, 541 (2009).

[4] F. Pulizzi, Nat Mater **11**, 367 (2012).

[5] A. R. Rocha, V. M. Garcia-Suarez, S. W. Bailey, C. J. Lambert, J. Ferrer, and S. Sanvito, Nat. Mater. **4**, 335 (2005).

[6] C. Schneider, B. Zhao, R. Kozhuharova, S. Groudeva-Zotova, T. MÃijhl, M. Ritschel, I. MÃűnch, H. Vinzelberg, D. Elefant, A. Graff, A. Leonhardt, and J. Fink, Diamond and Related Materials **13**, 215 (2004).

[7] S. Sanvito and A. Rocha, Journal of Computational and Theoretical Nanoscience **3**, 624 (2006).

[8] L. Bogani and W. Wernsdorfer, Nat. Mater. **7**, 179 (2008).

[9] S. Sanvito, Nat Phys **6**, 562 (2010).

[10] S. Sanvito, Chem. Soc. Rev. **40**, 3336 (2011).

[11] S. Jiang, K. GoÃ§, C. Cervetti, and L. Bogani, **55**, 867 (2012).

[12] J. Mater. Chem. **19**, 1670 (2009).

[13] D. Gatteschi, R. Sessoli, and J. Villain, *Molecular Nanomagnets* (Oxford University Press, Oxford, 2006).

[14] J. R. Friedman, M. P. Sarachik, J. Tejada, and R. Ziolo, Phys. Rev. Lett. **76**, 3830 (1996).

[15] L. Thomas, F. Lionti, R. Ballou, D. Gatteschi, R. Sessoli, and B. Barbara, Nature **383**, 145 (1996).

[16] W. Wernsdorfer and R. Sessoli, Science **284**, 133 (1999).

[17] A. Ardavan, O. Rival, J. J. L. Morton, S. J. Blundell, A. M. Tyryshkin, G. A. Timco, and R. E. P. Winpenny, Phys. Rev. Lett. **98**, 057201 (2007).

[18] M. Trif, F. Troiani, D. Stepanenko, and D. Loss, Phys. Rev. Lett. **101**, 217201 (2008).

[19] M. Trif, F. Troiani, D. Stepanenko, and D. Loss, Phys. Rev. B **82**, 045429 (2010).

[20] E. A. Osorio, K. Moth-Poulsen, H. S. J. van der Zant, J. Paaske, P. Hedegård, K. F. J. Bendix, and T. Bjørnholm, Nanolett. **10**, 105 (2010).

[21] A. S. Zyazin, J. W. G. van den Berg, E. A. Osorio, H. S. J. van der Zant, N. P. Konstantinidis, M. Leijnse, M. R. Wegewijs, F. May, W. Hofstetter, C. Danieli, and A. Cornia, Nano Letters **10**, 3307 (2010).

[22] A. S. Zyazin, H. S. van der Zant, M. R. Wegewijs, and A. Cornia, Synthetic Metals **161**, 591 (2011).

[23] J. Hu and R. Wu, Phys. Rev. Lett. **110**, 097202 (2013).

[24] U. Kortz, N. K. Al-Kassem, M. G. Savelieff, N. A. Al Kadi, and M. Sadakane, Inorg. Chem. **40**, 4742 (2001).

[25] T. Yamase, E. Ishikawa, K. Fukaya, H. Nojiri, T. Taniguchi, and T. Atake, Inorg. Chem. **43**, 8150 (2004).

[26] P. A. Angaridis, P. Baran, R. BocÌŇa, F. Cervantes-Lee, W. Haase, G. Mezei, R. G. Raptis, and R. Werner, Inorg. Chem. **41**, 2219 (2002).

[27] D. Gatteschi, L. Pardi, A. L. Barra, A. Muller, and J. Doring, Nature **354**, 463 (1991).

[28] S. Accorsi, A.-L. Barra, A. Caneschi, G. Chastanet, A. Cornia, A. C. Fabretti, D. Gatteschi, C. MortalÃš, E. Olivieri, F. Parenti, P. Rosa, R. Sessoli, L. Sorace, W. Wernsdorfer, and L. Zobbi, J. Am. Chem. Soc. **128**, 4742 (2006).

[29] K.-Y. Choi, Y. H. Matsuda, H. Nojiri, U. Kortz, F. Hussain, A. C. Stowe, C. Ramsey, and N. S. Dalal, Phys. Rev. Lett. **96**, 107202 (2006).

[30] S. Carretta, P. Santini, G. Amoretti, M. Affronte, A. Ghirri, I. Sheikin, S. Piligkos, G. Timco, and R. E. P. Winpenny, Phys. Rev. B **72**, 060403 (2005).

[31] J. Luzon, K. Bernot, I. J. Hewitt, C. E. Anson, A. K. Powell, and R. Sessoli, Phys. Rev. Lett. **100**, 247205 (2008).

[32] M. F. Islam, J. F. Nossa, C. M. Canali, and M. Pederson, Phys. Rev. B **82**, 155446 (2010).

[33] S. T. Boris, *Group Theory in Chemistry and Spectroscopy.* (Dover publications, INC, ADDRESS, 2006).

[34] J. Friedel, P. Lenglart, and G. Leman, J. Phys. Chem. Solids. **25**, 781 (1964).

[35] T. A. Kaplan, Z. Phys. B - Condensed Matter **49**, 313 (1983).

[36] N. E. Bonesteel, T. M. Rice, and F. C. Zhang, Phys. Rev. Lett. **68**, 2684 (1992).

[37] T. Moriya, Phys. Rev. **120**, 91 (1960).

[38] J. F. Nossa, M. F. Islam, C. M. Canali, and M. R. Pederson, Phys. Rev. B **85**, 085427 (2012).

[39] E. Fradkin, *Field Theories of condensed matter systems* (Addison Wesley, Addison wesley, 1991).

[40] M. R. Pederson and S. N. Khanna, Phys. Rev. B **60**, 9566 (1999).

[41] A. R. Rocha, V. M. Garcia-Suarez, S. Bailey, C. Lambert, J. Ferrer, and S. Sanvito, Phys. Rev. B **73**, 085414 (2006).

[42] M.-H. Jo, J. E. Grose, K. Baheti, M. M. Deshmukh, J. J. Sokol, E. M. Rumberger, D. N. Hendrickson, J. R. Long, H. Park, and D. C. Ralph, Nano Lett. **6**, 2014 (2006).

[43] H. B. Heersche, Z. de Groot, J. A. Folk, H. S. J. van der Zant, C. Romeike, M. R. Wegewijs, L. Zobbi, D. Barreca, E. Tondello, and A. Cornia, Phys. Rev. Lett. **96**, 206801 (2006).

[44] M. N. Leuenberger and D. Loss, Nature **410**, 789 (2001).

[45] J. Lehmann, A. Gaita-Arino, E. Coronado, and D. Loss, Nat Nano **2**, 312 (2007).

[46] M. R. Pederson and S. N. Khanna, Phys. Rev. B **60**, 9566 (1999).

[47] J. Kortus, M. R. Pederson, T. Baruah, N. Bernstein, and C. S. Hellberg, Polyhedron **22**, 1871 (2003).

[48] A. V. Postnikov, J. Kortus, and M. R. Pederson, Phys. Stat. Sol. (b) **243**, 2533 (2006).

[49] R. Schleser, T. Ihn, E. Ruh, K. Ensslin, M. Tews, D. Pfannkuche, D. C. Driscoll, and A. C. Gossard, Phys. Rev. Lett. **94**, 206805 (2005).

[50] J. V. Holm, H. I. Jørgensen, K. Grove-Rasmussen, J. Paaske, K. Flensberg, and P. E. Lindelof, Phys. Rev. B **77**, 161406 (2008).

[51] J. Paaske, A. Rosch, P. Wolfle, N. Mason, C. M. Marcus, and J. Nygard, Nat Phys **2**, 460 (2006).

[52] S. Sapmaz, P. Jarillo-Herrero, J. Kong, C. Dekker, L. P. Kouwenhoven, and H. S. J. van der Zant, Phys. Rev. B **71**, 153402 (2005).

[53] N. Roch, S. Florens, V. Bouchiat, W. Wernsdorfer, and F. Balestro, Nature **453**, 633 (2008).

[54] J. J. Parks, A. R. Champagne, G. R. Hutchison, S. Flores-Torres, H. D. Abruña, and D. C. Ralph, Phys. Rev. Lett. **99**, 026601 (2007).

[55] E. A. Osorio, K. O'Neill, M. Wegewijs, N. Stuhr-Hansen, J. Paaske, T. BjÃÿrnholm, and H. S. J. van der Zant, Nano Lett. **7**, 3336 (2007).

[56] M. Turek and K. A. Matveev, Phys. Rev. B **65**, 115332 (2002).

[57] J. Koch, F. von Oppen, Y. Oreg, and E. Sela, Phys. Rev. B **70**, 195107 (2004).

[58] H. Bruus and K. Flensberg, *Many body quantum theory in condensed matter physics* (Oxford Graduate Texts, ADDRESS, 2004).

[59] Y. V. Nazarov and Y. M. Blander, *Quantum Transport Introduction to Nanoscience* (Cambridge University Press, ADDRESS, 2009).

[60] M. Kastner, Annalen der Physik **9**, 885 (2000).

[61] M. Tews, Annalen der Physik **13**, 249 (2004).

[62] D. Weinmann, W. HÃd'usler, and B. Kramer, Phys. Rev. Lett. **74**, 984 (1995).

[63] J. Koch, M. E. Raikh, and F. von Oppen, Phys. Rev. Lett. **96**, 056803 (2006).

[64] M. Leijnse, M. R. Wegewijs, and M. H. Hettler, Phys. Rev. Lett. **103**, 156803 (2009).

[65] M. Leijnse and M. R. Wegewijs, Phys. Rev. B **78**, 235424 (2008).

[66] S. Koller, M. Grifoni, M. Leijnse, and M. R. Wegewijs, Phys. Rev. B **82**, 235307 (2010).

[67] J. Yoon and E. I. Solomon, Coordination Chemistry Reviews **251**, 379 (2007).

[68] L. Michalak, C. M. Canali, M. R. Pederson, M. Paulsson, and V. G. Benza, Phys. Rev. Lett. **104**, 017202 (2010).

[69] P. Atkins and J. de Paula, *Physical Chemistry.* (W. H. Freeman and Company, New York, ADDRESS, 2006).

[70] P. Hohenberg and W. Kohn, Phys. Rev. **136**, B864 (1964).

[71] W. Kohn and L. J. Sham, Phys. Rev. **140**, A1133 (1965).

[72] U. von Barth, Phys. Scripta. **T109**, 9 (2004).

[73] U. von Barth, J. Phys. C **5**, 1629 (1972).

[74] K. Capelle, Brazilian Journal of Physics **36**, 1318 (2006).

[75] K. Capelle, arXiv:cond-mat/0211443 (2006).

[76] C. Fiolhais, F. Nogueira, and M. Marques, *A Primer in Density Functional Theory.* (Springer-Verlag Berlin Heidelberg, ADDRESS, 2003).

[77] D. Sholl and J. Steckel, *Density Functional Theory: A Practical Introduction* (John Wiley & Sons, Inc., Hoboken, New Jersey, ADDRESS, 2009).

[78] M. R. Pederson and C. C. Lin, Phys. Rev. B **35**, 2273 (1987).

[79] M. R. Pederson and K. A. Jackson, Phys. Rev. B **41**, 7453 (1990).

[80] K. Jackson and M. R. Pederson, Phys. Rev. B **42**, 3276 (1990).

[81] M. R. Pederson and K. A. Jackson, Phys. Rev. B **43**, 7312 (1991).

[82] M. R. Pederson, B. M. Klein, and J. Q. Broughton, Phys. Rev. B **38**, 3825 (1988).

[83] D. Porezag and M. R. Pederson, Phys. Rev. B **54**, 7830 (1996).

[84] D. Porezag and M. R. Pederson, Phys. Rev. A **60**, 2840 (1999).

[85] A. Briley, M. R. Pederson, K. A. Jackson, D. C. Patton, and D. V. Porezag, Phys. Rev. B **58**, 1786 (1998).

[86] A. A. Quong, M. R. Pederson, and J. L. Feldman, Solid State Communications **87**, 535 (1993).

[87] Naval Research Laboratory Molecular Orbital Library (NRLMOL), http://quantum.utep.edu/nrlmol/nrlmol.html.

[88] J. Kortus, C. S. Hellberg, and M. R. Pederson, Phys. Rev. Lett. **86**, 3400 (2001).

[89] M. R. Pederson and S. N. Khanna, Phys. Rev. B **59**, R693 (1999).

[90] M. Pederson and S. Khanna, Chemical Physics Letters **307**, 253 (1999).

[91] M. R. Pederson, D. V. Porezag, J. Kortus, and S. N. Khanna, J. Appl. Phys. **87**, 5487 (2000).

[92] J. Kortus and M. R. Pederson, Phys. Rev. B **62**, 5755 (2000).

[93] J. Kortus, M. Pederson, C. Hellberg, and S. Khanna, Eur. Phys. J. D **16**, 177 (2001).

[94] M. R. Pederson, J. Kortus, and S. N. Khanna, J. Appl. Phys. **91**, 7149 (2002).

[95] J. Kortus, T. Baruah, M. R. Pederson, C. Ashman, and S. N. Khanna, Appl. Phys. Lett. **80**, 4193 (2002).

[96] P. Bobadova-Parvanova, K. A. Jackson, S. Srinivas, and M. Horoi, Phys. Rev. B **66**, 195402 (2002).

[97] M. R. Pederson, N. Bernstein, and J. Kortus, Phys. Rev. Lett. **89**, 097202 (2002).

[98] J. Kortus, T. Baruah, N. Bernstein, and M. R. Pederson, Phys. Rev. B **66**, 092403 (2002).

[99] T. Baruah and M. R. Pederson, Chemical Physics Letters **360**, 144 (2002).

[100] T. Baruah and M. R. Pederson, Int. J. Quantum Chem. **93**, 324 (2003).

[101] M. Pederson, D. Porezag, J. Kortus, and D. Patton, physica status solidi (b) **217**, 197 (2000).

Part IV

Papers

5

First-principles study of spin-electric coupling in a Cu3 single molecular magnet

PHYSICAL REVIEW B **82**, 155446 (2010)

First-principles study of spin-electric coupling in a $\{Cu_3\}$ single molecular magnet

M. Fhokrul Islam, Javier F. Nossa, and Carlo M. Canali
School of Computer Science, Physics and Mathematics, Linnaeus University, Kalmar, Sweden

Mark Pederson
Naval Research Laboratory, Code 6390, Washington, DC 20375-5345, USA
(Received 5 August 2010; published 26 October 2010)

We report on a study of the electronic and magnetic properties of the triangular antiferromagnetic $\{Cu_3\}$ single-molecule magnet, based on spin-density-functional theory. Our calculations show that the low-energy magnetic properties are correctly described by an effective three-site spin $s=1/2$ Heisenberg model, with an antiferromagnetic exchange coupling $J\approx 5$ meV. The ground-state manifold of the model is composed of two degenerate spin $S=1/2$ doublets of opposite chirality. Due to lack of inversion symmetry in the molecule these two states are coupled by an external electric field, even when spin-orbit interaction is absent. The spin-electric coupling can be viewed as originating from a modified exchange constant δJ induced by the electric field. We find that the calculated transition rate between the chiral states yields an effective electric dipole moment $d=3.38\times 10^{-33}$ C m$\approx e10^{-4}a$, where a is the Cu separation. For external electric fields $\varepsilon\approx 10^8$ V/m this value corresponds to a Rabi time $\tau\approx 1$ ns and to a δJ on the order of a few μeV.

DOI: 10.1103/PhysRevB.82.155446 PACS number(s): 75.50.Xx, 75.75.−c

I. INTRODUCTION

Single-molecule magnets (SMMs) have been intensively studied in the last two decades (for a review see Ref. 1). At low temperature these remarkable molecules behave in part like bulk magnets thanks to their very long magnetization relaxation time. At the same time SMMs are genuine quantum systems. They display a variety of nontrivial quantum effects such as the quantum tunneling of the magnetization,[2,3] Berry phase interference,[4] and quantum spin coherence.[5] Due to their double nature, SMMs are ideal systems to investigate decoherence and the interplay between classical and quantum behavior.[5]

From the point of view of applications, interest in SMMs has been in part spurred by the possibility that these structures could represent the ultimate molecular-scale limit for magnetic units in high-density magnetic storage materials. More recently SMMs have been recognized as promising building blocks in molecular spintronics, the emerging field combining spintronics and molecular electronics.[6–11] In particular, thanks to their long spin coherence time,[5] SMMs are good candidates to realize spintronic devices that maintain, control and exploit quantum coherence of individual spin states. These devices could find important applications in the field of quantum information processing.[12,13]

One key issue in using SMMs in molecular spintronics and quantum information processing is the ability of switching efficiently between their different magnetic states. The conventional way of manipulating magnetic states is by applying an external magnetic field. However, this approach has significant drawbacks when it comes to controlling magnetic states at the molecular level. Quantum manipulation of SMM requires application of an external field at a very small spatial and temporal scale. It is, however, very difficult to achieve such a small scale manipulation using standard electron-spin control techniques such as electron spin resonance driven by ac magnetic field.[5]

One promising alternative to achieve control of magnetic states at the molecular level is to use an electric field instead. Typically, by using scanning tunnel microscope (STM) tips, for example, it is possible to apply strong time-dependent electric fields in subnanoregions, with time scales of 1 ns.[14,15] Clearly since electric fields do not couple directly to spins, it is essential to find efficient mechanisms for spin-electric coupling as well as real SMMs where this mechanism can be at play. In principle, an electric field can interact with spins indirectly via the spin-orbit interaction. However, since the strength of the coupling scales like the volume of the system (More specifically, it is the ratio of the spin-orbit interaction strength to the single-particle energy mean-level spacing that is proportional to the volume of the system. If we view a molecular magnet as an ultra-small quantum dot, the relative strength of the spin-orbit interaction should scale accordingly and one expects that the effective spin-electric coupling should be very small. Although we believe that this statement is reasonable, a microscopic study of the spin-electric coupling via spin-orbit interaction has not been done yet.) this mechanism is not the most efficient one for manipulating SMMs.

Recently, it has been proposed[16] that in some molecular antiferromagnets lacking inversion symmetry, such as the triangular antiferromagnetic $\{Cu_3\}$ and other odd-spin rings, an electric field can efficiently couple spin states through a combination of exchange and chiralilty of the spin-manifold ground state.[16] The $\{Cu_3\}$ molecule while large,[17,18] reduces to a simple model composed of three identical spin $s=1/2$ Cu cations coupled by an antiferromagnetic (Heisenberg) exchange integration. Its ground state consists of two total-spin $S=1/2$ doublets of opposite spin chirality, degenerate in the absence of spin-orbit interaction. According to an analysis based on group theory,[16,19] due to the lack of inversion symmetry, an electric field can couple states of opposite chirality through the dipole operator, even when spin-orbit interaction is absent. This opens up the possibility of using this two-level system of chiral states as components of qbits in quantum computation. In the presence of an additional small dc magnetic field that mixes the spin states, the electric field-

induced transitions can also result in spin flips.

An intuitive picture of this coupling is the following. Since a spin $S=1/2$ triangular antiferromagnet is frustrated, there exist three energetically degenerate antiferromagnetic spin configurations for $S_z=1/2$ and three for $S_z=-1/2$. Both eigenstates of the chiral operator, with a given value of S_z, are appropriate, equally weighted, linear combinations of these three frustrated spin configurations. Each of these three configurations, if prepared, would have a dipole moment with the same magnitude that points from the antiparallel sites to the midpoint between the two parallel sites. While the net dipole moment of the two chiral eigenstates is zero, the dipole transition matrix element between them is not and it is simply related to the magnitude of the permanent dipole moment of the energetically degenerate frustrated configurations.

In practice the relevance of this spin-electric mechanism depends on the coupling strength of the chiral states by the electric field, i.e., on the value of the dipole moment of the frustrated spin configurations. Theoretically this is an issue that only a microscopic calculation for the specific molecule can address. The main objective of this work is to calculate the strength of this coupling for the $\{Cu_3\}$ molecule using *ab initio* methods. Our approach is based on spin-density-functional theory (SDFT), implemented in the NRLMOL codes, which has been very successful in describing the electronics and magnetic properties of Mn_{12} acetate and other SMMs.[20–23] Recently SDFT implemented in NRLMOL has been used in a first-principles study of quantum transport in a Mn_{12} single-electron transistor.[24]

Our results show that indeed the crucial electric-dipole moment is not negligible in $\{Cu_3\}$ and it would correspond to characteristic Rabi times of 1 ns in the presence of typical electric fields generated by STM tips. As originally suggested in Ref. 16, the spin-electric coupling can be interpreted as due to a modified exchange interaction brought about by the electric field. Although here we only address the specific case of $\{Cu_3\}$, our paper introduces a methodology that can be followed in a systematic study of other SMMs without inversion symmetry.

The paper is organized as follows. In Sec. II we discuss the electronic and magnetic properties of triangular $\{Cu_3\}$ molecule based on *ab initio* calculations and show that the low-energy quantum properties of the molecule can be described by an effective three-spin $s=1/2$ Heisenberg model with antiferromagnetic coupling. In Sec. II B we review the underlying mechanism of spin-electric coupling in $\{Cu_3\}$ antiferromagnet, based on the effective spin Hamiltonian. The first-principles computation of the spin-electric coupling and electric dipole moment of $\{Cu_3\}$ is presented in Sec. IV. In Sec. IV B we discuss the effect of the electric field on the exchange coupling. Finally we present the summary of our work in Sec. V.

II. ELECTRONIC AND MAGNETIC PROPERTIES OF $\{Cu_3\}$

A. Microscopic description of the molecule

The $\{Cu_3\}$ molecule that we are interested in has chemical composition $Na_{12}[Cu_3(AsW_9O_{33})_2 \cdot 3H_2O] \cdot 32H_2O$.[17] This molecule has been studied experimentally by different groups.[17,18] The three Cu^{2+} cations form an equilateral triangle and, as we show below, are the sites of three identical $s=1/2$ quantum spins. The frontier electrons on each of these sites have primarily d character. The bridging atoms consist of predominantly paired electrons and are only polarized to the degree that the same-spin states hybridize with the unpaired d electrons on the Cu sites. Due to the localized nature of transition-metal $3d$ states, direct exchange stabilization due to parallel neighboring states is expected to be exponentially small. Therefore, unless the frontier d electrons are spatially orthogonal by symmetry to the d electrons on other sites, *antiferromagnetic ordering* between electrons on a pair of neighboring Cu atoms is energetically preferred due to the increase in the system's kinetic energy, induced by orthogonality constraints, when neighboring states are parallel.

Our calculated antiferromagnetic coupling parameter is in general accord with what would be expected from the Goodenough-Kanamori rules.[25–27] These rules were originally developed, using perturbative arguments, to predict the sign of magnetic coupling between two cations that are coupled through anions and they apply situations such as this $\{Cu_3\}$ system where a localized Heitler-London picture is a good approach to representing the magnetic orbitals. However, they were really derived for situations where next-neighbor cation ions are coupled through a single anion. The $\{Cu_3\}$ system has significantly more complicated bridging between cations and the Cu atoms are third, rather than second, nearest neighbors. For the case of two cations coupled via an anion, the Goodenough-Kanamori rules state that the coupling between two magnetic ions with half-occupied orbitals is almost always antiferromagnetic unless there is a 90° angle between the bridging anion and the two cations. While the term kinetic exchange has been introduced for this type of phenomena, a recent analysis[28] has shown that some of the assumptions about kinetic exchange always leading to antiferromagnetic behavior can be incorrect for special cases. However, the kinetic energy of the system is found to increase when the unpaired orbitals on different states are placed in parallel spin states.

Although the spin model of three exchange-coupled spin 1/2 is quite useful to understand the magnetic properties of the $\{Cu_3\}$ SMM, all the other atoms in the molecule are essential for its geometrical stability and for the resulting superexchange interaction among the spins at the Cu sites. A proper *ab initio* description of the molecule must therefore include to a certain extent all these atoms.

Building a suitable model of the molecule is a considerable challenge since the model molecule should preserve the essential physics. We have constructed the molecule by preserving the D_{3h} symmetry of the polyanionic part of the molecule as observed in the experiment.[17,18] Three of the twelve Na atoms of the molecule are placed at the belt region of the molecule. These three are the most important of all the Na atoms for the stability of the belt region of the molecule. There is some uncertainty in the position of the Na atoms but we have placed eight of the remaining nine Na atoms in a way to preserve the D_{3h} symmetry. The last Na atom is replaced by a H atom and is placed at the center of the mol-

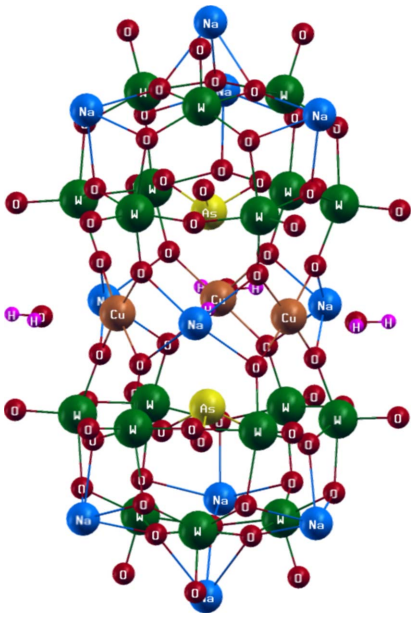

FIG. 1. (Color online) Model of the $\{Cu_3\}$ molecule with chemical composition $Na_{11}H[Cu_3(AsW_9O_{33})_2 \cdot 3H_2O]$ used in this work. Xcrysden visualization tool (Ref. 29) is used for this figure.

ecule to maintain the charge neutrality of the valance electrons. The model of the molecule used in this calculation is shown in Fig. 1.

We have relaxed the geometry using the *ab initio* package NRLMOL (Refs. 30 and 31) that uses a Gaussian basis set to solve the Kohn-Sham equations using Perdew-Burke-Ernzerhof generalized gradient approximation.[32] All-electron calculations are performed for all elements of the molecule except for tungsten, for which we have used pseudo potentials. The relaxation is first performed by setting the net total spin of the molecule to $S=3/2$ and then by changing the net spin to 1/2. Self-consistency is reached when the total energy is converged to 10^{-6} Hartree or less.

The density of states of the molecule is shown in Fig. 2. The highest occupied molecular orbital-lowest unoccupied molecular orbital (HOMO-LUMO) gap for the majority spin is calculated to be about 0.78 eV and that for minority spin is about 0.58 eV. Although in our calculations we have used an equilateral arrangement of the three Cu atoms, it is found experimentally that the $\{Cu_3\}$ molecule in the ground state is slightly distorted into an isosceles triangle.[17] Since the calculated HOMO-LUMO gap for the equilateral configuration is relatively large, the distortion is likely to be due to magnetic exchange rather than to the Jahn-Teller effect.

One important result of our calculations, after the geometry relaxation have been implemented, is that the ground state of the system is antiferromagnetic, with a net total spin of 1/2 in accordance with experiment.[33] The ground-state

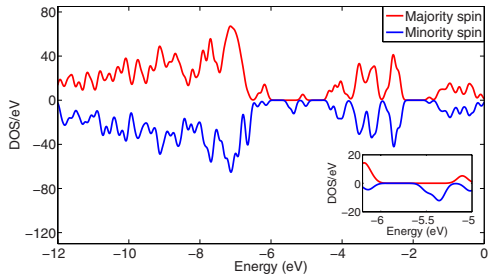

FIG. 2. (Color online) Density of states of $\{Cu_3\}$ molecule. HOMO-LUMO gaps for majority and minority spins are shown in the inset.

energy is lower by about 8.4 meV relative to spin $S=3/2$ configuration. This allows us to assign an exchange constant $J \approx 5$ meV to the three-site Heisenberg spin model mentioned above (see also next section).

The calculated magnetization density of the relaxed molecule shows the presence of three electron-spin magnetic moments $\mu_i \approx 0.55\mu_B$, $i=1,2,3$, essentially localized at the three Cu atom sites. Note that the orbital moments are quenched. These results confirm that the low-energy properties of the $\{Cu_3\}$ molecule can be approximately described by an effective spin Hamiltonian of three spins $s=1/2$ localized at the Cu sites.

The exchange coupling between two Cu atoms is indirect and follows a superexchange path[18] along Cu-O-W-O-W-O-Cu as shown in Fig. 3—see the yellow line connecting the atoms. To understand this coupling mechanism we focus on one of the three CuO_5 complexes of the molecule (shown inside the circle in Fig. 3). Because of the square-pyramidal C_{4v} point-group symmetry of this complex, the d_{xy}, d_{xz}, and d_{yz} states of Cu have lower energies compared to the $d_{x^2-y^2}$ and d_{z^2} states. Moreover, our calculation shows that the axial Cu-O distance (2.35 A) in each unit is larger than the four

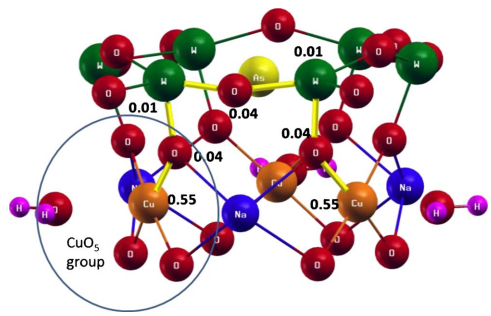

FIG. 3. (Color online) Superexchange coupling between two Cu atoms. The yellow line connecting two Cu atoms through three O and two W atoms shows the path along which spin coupling between Cu atoms is mediated. The numbers near the atoms are the magnetic moment (in units of μ_B) of the atoms along the exchange path.

equatorial Cu-O distances (1.93 A). Thus the energy of d_{z^2} state is lower than $d_{x^2-y^2}$ state and the unpaired d electron of the Cu^{2+} ion resides in $d_{x^2-y^2}$ state that is directed along the equatorial Cu-O vectors. Therefore, the exchange coupling between two Cu atoms involves three O atoms and two W atoms.

The magnetic moment calculations of the atoms of $\{Cu_3\}$ molecule also support the superexchange path. The magnetic moments at the O and W atoms on this path is much smaller than at the Cu sites but still two order of magnitude larger than at atoms not belonging to this path.

B. Effective spin Hamiltonian description

Based on the results of the *ab initio* calculations, the low-energy properties of the $\{Cu_3\}$ molecule can be described by the following quantum spin Hamiltonian:

$$H_0 = \sum_{i=1}^{3} J_{i,i+1}\mathbf{s}_i \cdot \mathbf{s}_{i+1} + \sum_{i=1}^{3} \mathbf{D}_{i,i+1} \cdot \mathbf{s}_i \times \mathbf{s}_{i+1}, \tag{1}$$

where J is the exchange parameter, $\mathbf{D}$ is the Dzyaloshinskii vector and $\mathbf{s}_i$ are three spins-1/2, located at the Cu sites. The first term in the Hamiltonian is an isotropic Heisenberg model. The geometry-relaxation and electronic-structure calculations showed that the Cu atoms form an equilateral triangle with a very small intrinsic deformation. Since the atomic environment around each of the the three Cu-Cu bonds is the same, we take the three exchange constants $J_{i,i+1}$ to be the same value, J. On the basis of the splitting between the ferromagnetic and antiferromagnetic configurations discussed in the previous section, J is positive and $\simeq 5$ meV. The second term in Eq. (1) is the anisotropic Dzyaloshinskii-Moriya (DM) exchange interaction originating from spin-orbit interaction. Its strength $|\mathbf{D}_{i,i+1}|$ is at least one order of magnitude smaller than the isotropic exchange constant J, and we will disregard it for the moment.

The ground state of Eq. (1) is total spin $S=1/2$ manifold, which can be constructed in terms of six degenerate spin configurations, three associated with $S_z=+1/2$ and the other three associated with $S_z=-1/2$. Figure 4 shows the three possible spin configurations associated with $S_z=+1/2$. The total-spin $S=3/2$ four-dimensional subspace has an energy of order J above the ground-state manifold.

Within the $S=1/2$ ground-state manifold, we can construct two degenerate, linearly independent doublets. Specifically the two $S_z=+1/2$ states [shown in Fig. 4(b)] are

$$\left|E_+,+\frac{1}{2}\right\rangle = \frac{1}{\sqrt{3}}[\Psi_{\downarrow\uparrow\uparrow} + \omega\Psi_{\uparrow\downarrow\uparrow} + \omega^2\Psi_{\uparrow\uparrow\downarrow}],$$

$$\left|E_-,+\frac{1}{2}\right\rangle = \frac{1}{\sqrt{3}}[\Psi_{\downarrow\uparrow\uparrow} + \omega^2\Psi_{\uparrow\downarrow\uparrow} + \omega\Psi_{\uparrow\uparrow\downarrow}] \tag{2}$$

while the $S_z=-1/2$ states are

$$\left|E_+,-\frac{1}{2}\right\rangle = \frac{1}{\sqrt{3}}[\Psi_{\uparrow\downarrow\downarrow} + \omega\Psi_{\downarrow\uparrow\downarrow} + \omega^2\Psi_{\downarrow\uparrow\uparrow}],$$

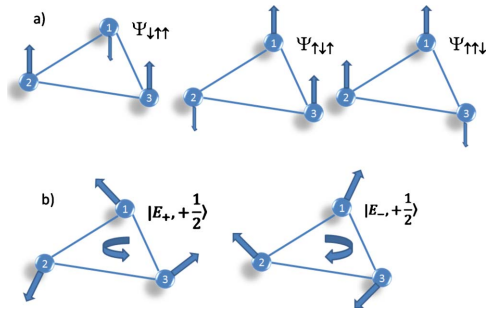

FIG. 4. (Color online) (a) The three spin configurations of the molecule associated with total spin projection $S_z=+1/2$. (b) The two chiral states formed from a) with chirality +1 and −1, respectively.

$$\left|E_-,-\frac{1}{2}\right\rangle = \frac{1}{\sqrt{3}}[\Psi_{\uparrow\downarrow\downarrow} + \omega^2\Psi_{\downarrow\uparrow\downarrow} + \omega\Psi_{\downarrow\downarrow\uparrow}], \tag{3}$$

where $\omega = e^{i2\pi/3}$. The quantum numbers E_+ and E_- specify the so called handness or chirality of the states $|E_\pm, M\rangle$, which are eigenstates of the chirality operator

$$C_z = \frac{4}{\sqrt{3}}\mathbf{s}_1 \cdot \mathbf{s}_2 \times \mathbf{s}_3 \tag{4}$$

with eigenvalues ± 1, respectively. It is useful to introduce also the other two components of the chiral vector operator

$$C_x = -\frac{2}{3}(\mathbf{s}_1 \cdot \mathbf{s}_2 - 2\mathbf{s}_2 \cdot \mathbf{s}_3 + \mathbf{s}_3 \cdot \mathbf{s}_1), \tag{5}$$

$$C_y = \frac{2}{\sqrt{3}}(\mathbf{s}_1 \cdot \mathbf{s}_2 - \mathbf{s}_3 \cdot \mathbf{s}_1), \tag{6}$$

and the ladder operators $C_\pm \equiv C_x \pm iC_y$. Note that $[C_l, C_m] = i2\epsilon_{lmn}C_n$ and $[C_l, S_m] = 0$. Here ϵ_{lmn} is the Levi-Civita symbol. The ladder operators reverse the chirality of the states: $C_\pm|E_\mp, M\rangle = |E_\pm, M\rangle$. They also have the property that $C_\pm|E_\pm, M\rangle = 0$. Thus $\mathbf{C}$ behaves exactly like the operator $\mathbf{S}$ (for $S=1/2$) in chiral space.

In the microscopic description of the molecule implemented within density functional theory via the NRLMOL code, the chiral states defined in Eqs. (2) and (3) have to be understood as being composed both of a spin and an orbital part.

We conclude this section with an observation of the DM interaction. As shown in Ref. 16, the DM interaction within the $S=1/2$ ground-state manifold takes the simple form $H_{DM} = \Delta_{SO}C_zS_z$, where Δ_{SO} is the effective spin orbit coupling constant. Thus equal-spin states of opposite chirality are split by $2\Delta_{SO}$.

III. SPIN-ELECTRIC EFFECT IN {Cu_3}

A. Absence of inversion symmetry and coupling of ground-state chiral states

The triangular spin-1/2 antiferromagnet {Cu_3} belongs to the class of antiferromagnetic rings with an odd number of half-integer spins.[34,35] In these systems, the lack of inversion symmetry of the molecule as a whole implies that the ground state is a four-dimensional manifold, whose basis states $|E_\pm, S_z = \pm 1/2\rangle$ are characterized by the spin projection $S_z = \pm 1/2$ and by the chirality $C_z = \pm 1$ (which we also label as $E_\pm$). In contrast, antiferromagnetic rings with an even number of spins have nondegenerate $S=0$ singlet ground state. According to the original proposal in Refs. 16 and 19, in odd-spin rings the two states of opposite chirality $|E_\pm, S_z = M\rangle$ can be coupled linearly by an external electric field, even in the absence of spin-orbit interaction. In order for electric coupling to be nonzero, other criteria must be satisfied.[19] First of all, permanent electric dipoles $\mathbf{d}_{ij}$ must be present on the bridges that mediate the coupling of spin $\mathbf{s}_i$ and $\mathbf{s}_j$. A necessary (although not sufficient) condition for this is that the superexchange bridge that magnetically couples $\mathbf{s}_i$ and $\mathbf{s}_j$ lacks a center of inversion symmetry. Even when local dipole moments are present on individual bridges, the resulting final spin-electric coupling between chiral states depends in a nontrivial way on the overall symmetry of the molecule. The best way to settle this issue is to carry out a systematic symmetry analysis based on group theory. It turns out that in triangular spin-1/2 antiferromagnets the coupling is nonzero. On the other hand in pentagon spin 1/2 antiferromagnets, the coupling vanishes, unless spin-orbit interaction is included.[19]

We focus now on the spin-electric coupling of chiral states in {Cu_3}. In the presence of an external electric field $\boldsymbol{\varepsilon}$, The Hamiltonian acquires the additional electric-dipole term $H_\varepsilon = \Sigma_i e\mathbf{r}_i \cdot \boldsymbol{\varepsilon} = e\mathbf{R}\cdot\boldsymbol{\varepsilon}$, where e is the electron charge and $\mathbf{r}_i$ is the coordinate of the i_{th} electron.

In the subspace of spin projection $S_z = 1/2$ of the ground-state manifold, which is invariant under the application of the operator H_ε, the perturbed Hamiltonian $H_0 + H_\varepsilon$ can be expressed in the basis of the chiral states as

$$H = H_0 + H_\varepsilon = \begin{vmatrix} \left\langle E_+,+\frac{1}{2}\right| H_0 \left|E_+,+\frac{1}{2}\right\rangle & \left\langle E_+,+\frac{1}{2}\right| H_\varepsilon \left|E_-,+\frac{1}{2}\right\rangle \\ \left\langle E_-,+\frac{1}{2}\right| H_\varepsilon \left|E_+,+\frac{1}{2}\right\rangle & \left\langle E_-,+\frac{1}{2}\right| H_0 \left|E_-,+\frac{1}{2}\right\rangle \end{vmatrix}, \tag{7}$$

A similar expression holds for the $S_z = -1/2$ subspace. The eigenvalues of H are

$$E^\pm_{1/2}(\boldsymbol{\varepsilon}) = E^\pm_{1/2}(0) \pm |\mathbf{d}\cdot\boldsymbol{\varepsilon}|, \tag{8}$$

with $E^\pm_{1/2}(0) = \langle E_\pm, +\frac{1}{2}|H_0|E_\pm, +\frac{1}{2}\rangle$, and the corresponding eigenstates

$$|\chi^\pm_{1/2}(\boldsymbol{\varepsilon})\rangle = \frac{1}{\sqrt{2}}\left(\left|E_+,+\frac{1}{2}\right\rangle \pm \frac{|\mathbf{d}\cdot\boldsymbol{\varepsilon}|}{\mathbf{d}\cdot\boldsymbol{\varepsilon}}\left|E_-,+\frac{1}{2}\right\rangle\right). \tag{9}$$

Here we have introduced the electric dipole matrix element $\mathbf{d}$, which couples states of opposite chirality (but with the same spin projection)

$$\mathbf{d} = \left\langle E_+,+\frac{1}{2}\right| e\mathbf{R} \left|E_-,+\frac{1}{2}\right\rangle. \tag{10}$$

For the specific example of {Cu_3} molecule only the matrix elements of X and Y components of $\mathbf{R}$ are nonzero and

$$\left\langle E_+,+\frac{1}{2}\right| eX \left|E_-,+\frac{1}{2}\right\rangle = i\left\langle E_+,+\frac{1}{2}\right| eY \left|E_-,+\frac{1}{2}\right\rangle = \frac{d}{\sqrt{2}}, \tag{11}$$

where $d \equiv |\mathbf{d}|$.

The matrix element in Eq. (10) is the key quantity in the spin-electric coupling mechanism. Substituting the expressions for the chiral states from Eqs. (2) and using the orthogonality of spin states we obtain

$$\mathbf{d} = \frac{1}{3}(\langle\Psi_{\downarrow\uparrow\uparrow}|e\mathbf{R}|\Psi_{\downarrow\uparrow\uparrow}\rangle + \omega\langle\Psi_{\uparrow\downarrow\uparrow}|e\mathbf{R}|\Psi_{\uparrow\downarrow\uparrow}\rangle + \omega^2\langle\Psi_{\uparrow\uparrow\downarrow}|e\mathbf{R}|\Psi_{\uparrow\uparrow\downarrow}\rangle). \tag{12}$$

Evaluating the dipole matrix element between two states of opposite chirality is therefore equivalent to calculating the dipole moment of each of the three spin configurations. This matrix element determines the strength of spin-electric coupling and we are primarily interested in calculating this quantity by *ab initio* methods.

Finally, note that all the matrix elements of the electric dipole operator $e\mathbf{R}$ are identically zero in the $S=3/2$ subspace. This is obvious since $\langle\Psi_{\uparrow\uparrow\uparrow}|e\mathbf{R}|\Psi_{\uparrow\uparrow\uparrow}\rangle$ and $\frac{1}{3}(\langle\Psi_{\downarrow\uparrow\uparrow}|e\mathbf{R}|\Psi_{\downarrow\uparrow\uparrow}\rangle + \langle\Psi_{\uparrow\downarrow\uparrow}|e\mathbf{R}|\Psi_{\uparrow\downarrow\uparrow}\rangle + \langle\Psi_{\uparrow\uparrow\downarrow}|e\mathbf{R}|\Psi_{\uparrow\uparrow\downarrow}\rangle)$ are both zero by symmetry. We will confirm this result by direct *ab initio* calculations.

B. Effective spin Hamiltonian description

The effect of the electric field on the the low-energy spectrum of {Cu_3} can be recast in the form of the effective spin model introduced in Sec. II B. Since the electric dipole operator has nonzero matrix elements only in the ground-state manifold, where it couples states with equal spin components and opposite chirality, we expect that the spin-electric Hamiltonian H_ε can be rewritten as a linear combination of the ladder operators $C_\pm$. By comparing the matrix elements of H_ε given in Eqs. (10) and (11) with the action of $C_\pm$ on the chiral states, one can show that[19]

$$H^{\text{eff}}_\varepsilon = \frac{d}{\sqrt{2}}\boldsymbol{\varepsilon}'\cdot\mathbf{C}_\parallel, \tag{13}$$

where $\boldsymbol{\varepsilon}' = R_z(\phi)(7\pi/6 - 2\theta)\boldsymbol{\varepsilon}$, with $R(\phi)$ being the matrix representing a rotation by an angle ϕ around the z axis, and θ being the angle between the in-plane component $\boldsymbol{\varepsilon}_\parallel$ of the electric field and the bond $\mathbf{s}_1$-$\mathbf{s}_2$. By using Eqs. (5) and (6) we

can now rewrite $\mathbf{C}_{\|}=(C_x,C_y)$ in term of spin-operators $\mathbf{s}_i$ and we obtain[19]

$$H_{\varepsilon}^{\text{eff}}=\sum_{i}^{3}\delta J_{ii+1}(\boldsymbol{\varepsilon})\mathbf{s}_i\cdot\mathbf{s}_j, \tag{14}$$

where the modified exchange parameters take the form[19]

$$\delta J_{ii+1}(\boldsymbol{\varepsilon})=\frac{4d}{3\sqrt{2}}|\boldsymbol{\varepsilon}_{\|}|\cos\left(\frac{2\pi}{3}i+\theta\right). \tag{15}$$

This expression of the effective electric-dipole Hamiltonian suggests a transparent physical interpretation of the spin-electric couping mechanism.[16,19] An external electric field changes the charge distribution of the $\{Cu_3\}$ molecule which, in turn, changes the exchange interaction between neighboring atoms. Since the modified exchange interaction does not commute with H_0, it can cause transitions between chiral states within the ground-state manifold.

In Eq. (15), $\boldsymbol{\varepsilon}_{\|}$ is the projection of electric field on the Cu_3 plane (in our case $\boldsymbol{\varepsilon}_{\|}=\boldsymbol{\varepsilon}$), i=1 and $\theta=30°$ is the angle between $\boldsymbol{\varepsilon}$ and the line joining Cu_1 and Cu_2. Finally, note that Eqs. (14) and (15) provide an estimate of the dependence of the ground-state energy as function of the electric field. Since in the absence of spin-orbit coupling the electric-dipole Hamiltonian has zero matrix elements in the $S=3/2$ subspace, Eq. (15) gives us an estimate of the dependence of the exchange constant J (proportional to the splitting between the $S=1/2$ ground state and $S=3/2$ excited state) on $\boldsymbol{\varepsilon}$.

IV. *AB INITIO* EVALUATION OF THE SPIN-ELECTRIC COUPLING

A. Calculation of the electric dipole moment

To construct the chiral states of the full $\{Cu_3\}$ molecule, we have calculated the ground state of the molecule for different spin configurations, as shown in Fig. 4. Although there are two doublets of chiral states for the triangular arrangement of three spin 1/2 atoms, in this calculation we have used only one doublet associated with the spin projection +1/2 since we are interested in coupling between states of opposite chirality with the same spin projection.

To study the spin-electric effect we have applied an external field along the perpendicular bisectors between positions 2 and 3 of the Cu_3 triangle shown in Fig. 5, and have calculated the corresponding ground-state energy self-consistently for different spin configurations. We have kept the direction of the field relative to coordinate axes fixed, and have changed the orientation of the spins at the Cu atoms to generate the three possible spin configurations of the $\{Cu_3\}$ molecule.

Our calculations show that $\{Cu_3\}$ molecule in the spin $S_z=3/2$ state does not have any permanent electric-dipole moment. On the other hand each of the three frustrated spin $S_z=1/2$ configurations have a small permanent (i.e, zero-field) dipole moment, as expected from the general discussion of Sec. III. The three moments have all the same magnitude but their directions are along the perpendicular bisector of Cu_3 triangle and between two Cu atoms with parallel spin alignments. The relative orientations of these moments along with components are shown in Fig. 6. The fact that the $S_z=3/2$ state does not have permanent dipole moment whereas $S_z=1/2$ states do, suggests that the dipole moments are solely due to spin effects.

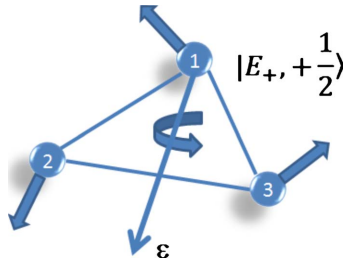

FIG. 5. (Color online) The direction of the applied electric fields used in this calculation.

In the presence of an electric field the energies of the $\{Cu_3\}$ molecule are slightly lower when field is between two Cu atoms with parallel spins than for the other two spin configurations, where the field is between two Cu atoms with antiparallel spin alignments. This difference in energy is due to the direction of permanent moment relative to the induced moment. We have calculated the permanent dipole moment of the ground-state spin configuration by fitting the dependence of energy of one of the $S_z=1/2$ spin configurations with external field, as shown in Fig. 7. The calculated values of the permanent dipole moment and polarizability of $\{Cu_3\}$ molecule are $p=4.77\times10^{-33}$ C m and $\alpha=1.025\times10^{-38}$ C m^2/V, respectively. Although there is no experimental value of polarizability available for $\{Cu_3\}$, polarizabilities within DFT calculations are generally accurate to 1–3 %.

The value p extracted from this fitting is consistent with the direct calculation of the electric dipole moment of the three spin configurations at zero field, implemented in the NRLMOL. To calculate the matrix element $\mathbf{d}$ given in Eq. (12), we substitute the components of the moments for the different spin configurations of Fig. 6,

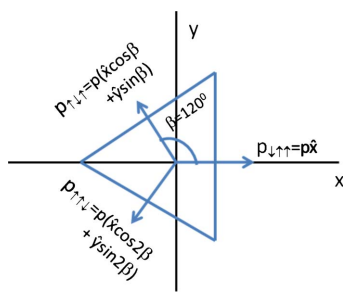

FIG. 6. (Color online) Dipole moments of three spin configurations and their relative angles. $\mathbf{p}_{\downarrow\uparrow\uparrow}=\langle\Psi_{\downarrow\uparrow\uparrow}|e\mathbf{R}|\Psi_{\downarrow\uparrow\uparrow}\rangle$, $\mathbf{p}_{\uparrow\downarrow\uparrow}=\langle\Psi_{\uparrow\downarrow\uparrow}|e\mathbf{R}|\Psi_{\uparrow\downarrow\uparrow}\rangle$, and $\mathbf{p}_{\uparrow\uparrow\downarrow}=\langle\Psi_{\uparrow\uparrow\downarrow}|e\mathbf{R}|\Psi_{\uparrow\uparrow\downarrow}\rangle$ are the moments corresponding to the spin configurations of Fig. 4(a).

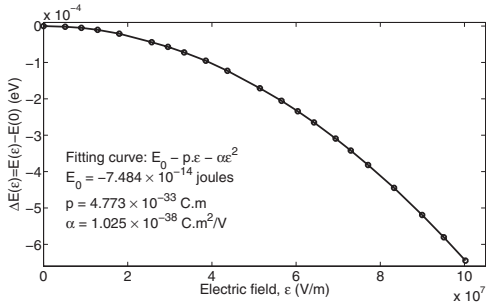

FIG. 7. Electric field dependence of the energy for one of the three spin $S_z=1/2$ spin configurations. The plot for the other two configurations is very similar and the fitting yields essentially the same values of p and α.

$$\mathbf{d} = \frac{1}{3}p[(1+\omega\cos\beta+\omega^2\cos 2\beta)\hat{\mathbf{x}}+(\omega\sin\beta + \omega^2\sin 2\beta)\hat{\mathbf{y}}] = \frac{p}{2}(\hat{\mathbf{x}}+i\hat{\mathbf{y}}). \tag{16}$$

The magnitude of the dipole coupling in $\{Cu_3\}$ molecule is, therefore

$$d = \frac{p}{\sqrt{2}} = 3.38\times 10^{-33}\ \text{C m}. \tag{17}$$

The efficiency of the $\{Cu_3\}$ molecule as a switching device depends on how fast an electric field can generate transitions from one chiral state to the other. The characteristic (Rabi) time for transitions between the two chiral states is given by

$$\tau = \frac{h}{|\mathbf{d}\cdot\boldsymbol{\varepsilon}|}. \tag{18}$$

Here, h is Planck constant, $\mathbf{d}$ is the dipole matrix element between states of different chirality given by Eq. (17), and $\boldsymbol{\varepsilon}$ is the external electric field. Figure 8 shows the dependence of the Rabi time on external field, with the maximum value

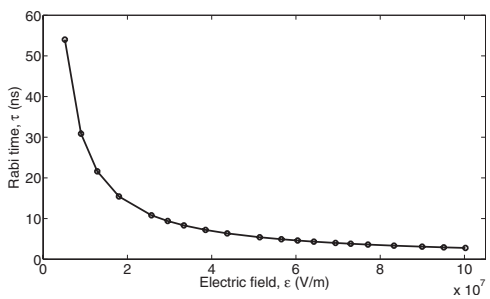

FIG. 8. Electric field dependence of the Rabi time for quantum transitions between the two ground state.

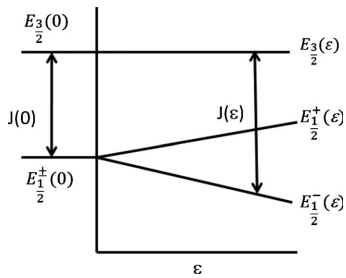

FIG. 9. Schematic electric-field dependence of the energies of the $S=1/2$ chiral states and spin $S=3/2$ excited state, and the exchange energy J defined in Eq. (19).

of ≈ 50 ns for a field $\varepsilon \simeq 5\times 10^6$ V/m. For larger fields on the order of $\simeq 10^8$ V/m, easily attainable in the vicinity of a STM tip, the Rabi time is on the order of 1 ns, which is considered to be a relatively fast control-time in quantum information processing.

B. Modification of the exchange coupling in an electric field

To calculate the dependence of the exchange coupling J on the electric field, we need to determine how the spin $S=1/2$ ground state and the spin $S=3/2$ excited state depend on the field. We define the exchange energy $J(\boldsymbol{\varepsilon})$ as the difference

$$J(\boldsymbol{\varepsilon}) = E_{3/2}(\boldsymbol{\varepsilon}) - E^{-}_{1/2}(\boldsymbol{\varepsilon}), \tag{19}$$

where $E_{1/2}(\boldsymbol{\varepsilon})$ and $E_{3/2}(\boldsymbol{\varepsilon})$ are the energies of the $S=1/2$ ground state and of the spin $S=3/2$ excited state, respectively, in the presence of an electric field.

Based on on our discussion of Sec. III A [see Eq. (8)], the energy of the $S=1/2$ chiral ground-state manifold and the $S=3/2$ excited state vs ε are shown schematically in Fig. 9, where we have disregarded the quadratic dependence of both $E_{3/2}$ and $E_{1/2}$ on the field due to the induced electric dipole moment.

The calculation of the electric-field-modified exchange parameter using first-principles methods is not completely straightforward since the SDFT calculations done within NRLMOL allow us to calculate the energy of a given spin configuration whereas the (chiral) ground state is a linear combination of three possible spin configurations. However, we can get an estimate of the dependence of J on $\boldsymbol{\varepsilon}$ by approximating

$$E^{-}_{1/2}(\varepsilon) \approx \alpha_1^2\langle\Psi_{\downarrow\uparrow\uparrow}|H_{\mathrm{DFT}}(\boldsymbol{\varepsilon})|\Psi_{\downarrow\uparrow\uparrow}\rangle + \alpha_2^2\langle\Psi_{\uparrow\downarrow\uparrow}|H_{\mathrm{DFT}}(\boldsymbol{\varepsilon})|\Psi_{\uparrow\downarrow\uparrow}\rangle + \alpha_3^2\langle\Psi_{\uparrow\uparrow\downarrow}|H_{\mathrm{DFT}}(\boldsymbol{\varepsilon})|\Psi_{\uparrow\uparrow\downarrow}\rangle = \alpha_1^2 E_{\downarrow\uparrow\uparrow} + \alpha_2^2 E_{\uparrow\downarrow\uparrow} + \alpha_3^2 E_{\uparrow\uparrow\downarrow}.$$

The coefficients $\alpha' s$ can be obtained by expanding $|\chi^{-}_{1/2}(\boldsymbol{\varepsilon})\rangle$ in Eq. (9) in terms of the spin configurations, which leads to

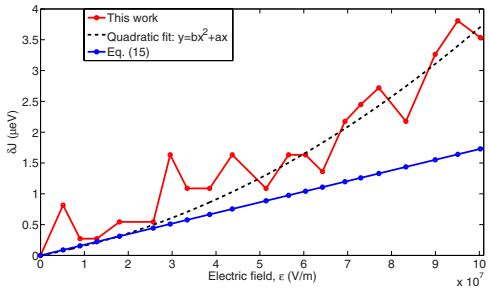

FIG. 10. (Color online) Electric-field dependence of the variation in the exchange energy $\delta J(\varepsilon) \equiv J(\varepsilon) - J(0)$ induced by the field. The red curve (fluctuating) is the first-principles result obtained by evaluating Eq. (22) and the dashed black curve is the quadratic fit of $\delta J(\varepsilon)$. The blue curve (straight line) is a plot of Eq. (15) with the numerical value of d extracted from the first-principles calculations.

$$|\chi_{1/2}^{-}(\boldsymbol{\varepsilon})\rangle = \frac{1}{\sqrt{6}}[(1-r)\Psi_{\downarrow\uparrow\uparrow} + (\omega - \omega^2 r)\Psi_{\uparrow\downarrow\uparrow} + (\omega^2 - \omega r)\Psi_{\uparrow\uparrow\downarrow}] = \alpha_1\Psi_{\downarrow\uparrow\uparrow} + \alpha_2\Psi_{\uparrow\downarrow\uparrow} + \alpha_3\Psi_{\uparrow\uparrow\downarrow}, \tag{20}$$

where $r = \frac{|\mathbf{d}\cdot\boldsymbol{\varepsilon}|}{\mathbf{d}\cdot\boldsymbol{\varepsilon}} = \frac{1}{\sqrt{2}}(1-i)$, for the given choice of the electric field direction.

Therefore,

$$E_{1/2}^{-}(\boldsymbol{\varepsilon}) \approx \frac{1}{6}\left[(2-\sqrt{2})E_{\downarrow\uparrow\uparrow} + \left(2 + \frac{1-\sqrt{3}}{\sqrt{2}}\right)E_{\uparrow\downarrow\uparrow} + \left(2 + \frac{1+\sqrt{3}}{\sqrt{2}}\right)E_{\uparrow\uparrow\downarrow}\right]. \tag{21}$$

The energies $E_{\uparrow\downarrow\uparrow}$ and $E_{\uparrow\uparrow\downarrow}$ are the same because of symmetry. Since the difference between $E_{\downarrow\uparrow\uparrow}$ and $E_{\uparrow\downarrow\uparrow}$ is very small and near the accuracy limit of our calculations, we further approximate $E_{\downarrow\uparrow\uparrow} \approx E_{\uparrow\downarrow\uparrow}$.

The exchange parameter J becomes

$$J(\boldsymbol{\varepsilon}) \approx E_{\uparrow\uparrow\uparrow}(\boldsymbol{\varepsilon}) - E_{\downarrow\uparrow\uparrow}(\boldsymbol{\varepsilon}), \tag{22}$$

with $E_{\uparrow\uparrow\uparrow}(\boldsymbol{\varepsilon}) \equiv E_{3/2}(\boldsymbol{\varepsilon})$.

In Fig. 10 we plot the electric field-induced variation in the exchange energy $\delta J(\varepsilon) \equiv J(\varepsilon) - J(0)$ vs ε. The result for δJ obtained by evaluating Eq. (22) with SDFT is shown by the red curve. For this part of the calculations the convergence criterion has been increased up to 10^{-8} Hartree. We can see that the dependence of J on electric field is quite small, and δJ is in the microelectron volt range for electric fields $\varepsilon = (1-10) \times 10^7$ V/m. These energies are not far form the accuracy limit of our numerical calculations, which is the reason of the fluctuations seen in the plot. Nevertheless the overall trend is an increase in $\delta J(\varepsilon)$ with ε, which is approximately linear at low fields. Note that the SDFT evaluations of $E_{\uparrow\uparrow\uparrow}(\varepsilon)$ and $E_{\downarrow\uparrow\uparrow}(\varepsilon)$ contain a quadratic contribution in ε but this nearly cancels at small fields when computing δJ, and it becomes appreciable only at $\varepsilon \geq 5 \times 10^7$ V/m.

The blue line in Fig. 10 shows the dependence of δJ on $\boldsymbol{\varepsilon}$ given by the prefactor of the cosine function in Eq. (15), which was derived within the spin Hamiltonian formalism. When plotting Eq. (15) we have used the value of d extracted from our first-principles calculations. Comparing the two curves, we note that, apart form the fluctuations in the numerical result mentioned above, the theoretical and numerical values for δJ are consistent, and both procedures predict an overall increase in δJ with electric field. The quadratic behavior of δJ observed at higher electric fields is due to the slight difference in polarizabilities of $S = 1/2$ and $S = 3/2$ spin configurations.

The electric field dependence of the exchange constant in this work is calculated for one direction of electric field only, between the Cu atoms at sites 2 and 3, as shown in Fig. 5. Although in principle the angular dependence of the exchange constant on the electric field direction can be calculated using our method, given the smallness of δJ (close to the limiting accuracy of our DFT calculations) and the ensuing fluctuations in the calculated values (see Fig. 10), it is in practice hard to extract this dependence unambiguously.

V. SUMMARY

In this paper we have carried out a first-principles study of the spin-electric coupling in single-molecule magnets (SMMs) without inversion symmetry. Specifically, we have analyzed the clear-cut case of the $\{Cu_3\}$ triangular antiferromagnet where because of spin frustration, the ground state consists of two generate spin 1/2 doublets of opposite chirality. Theory predicts[16,19] that an electric field can couple these states, even when spin-orbit interaction is absent. The main goal of our work has been to compute how strong this coupling is.

Our calculations of the electronic structure of the $\{Cu_3\}$ molecule show that the spin magnetic moments are localized at the three Cu atom sites of the molecule. The magnetic properties of the molecule are correctly described by a triangular spin $s = 1/2$ Heisenberg antiferromagnet, with an exchange coupling J on the order of 5 meV that separates the energies of the spin-$S = 1/2$ ground-state many-fold and the spin-$S = 3/2$ excited states. In agreement with theoretical predictions,[16,19] we find that an electric field couples the two ground-state doublets of opposite chirality, even when spin-orbit interaction is absent. For electric fields that are not too large ($\varepsilon \geq 5 \times 10^7$ V/m.), the strength of the coupling is linear in the field and proportional to the permanent electric dipole moment d of the three frustrated spin configurations. The calculations yield a value of $d \approx 4 \times 10^{-33}$ C m $\approx e10^{-4}a$ for $\{Cu_3\}$, where a is the Cu atom separation. Corresponding Rabi times for electric field-induced transitions between chiral states can be as short as 1 ns, for electric fields on the order of 10^8 V/m, which are easily produced by a nearby STM tip. Thus this spin-electric coupling mechanism is of potential interest for the use of single-molecule magnets in quantum information processing as fast switching devices.

Our calculations also indicate that the presence of an external electric field modifies the exchange constant J. Typi-

cally the electric field increases J, although the energy scale of this change is in the microelectron volt range for typical STM-generated electric fields. Thus for this specific antiferromagnetic SMM, the electric field cannot trigger directly a level crossing between magnetic states with different total spin, as suggested recently for other SMMs.[36,37]

This work shows that a microscopic investigation of the spin-electric coupling using the NRLMOL first-principles code is feasible, and can systematically implemented for a large class of SMMs which lack inversion symmetry. In this paper we have disregarded the effect of spin-orbit interaction and external magnetic field. The spin-orbit interaction strength is small compared to the exchange coupling J. In the case of $\{Cu_3\}$ it simply introduces a small splitting between the chiral states but is not expected to influence significantly the spin-electric coupling. However, in other antiferromagnetic rings with an odd number of spins spin-orbit interaction is essential for the very existence of the coupling mechanism.[19] Work to include both spin-orbit interactions and an external magnetic field is in progress. Together with the group-theory analysis presented in Ref. 19, these studies will be a considerable help in guiding future experiments and selecting the most promising SMMs for applications in quantum information processing and nanospintronics.

ACKNOWLEDGMENTS

We would like to thank Daniel Loss for introducing us to this problem and for several useful discussions. This work was supported by the Faculty of Natural Sciences at Linnaeus University and the Swedish Research Council under Grant No. 621-2007-5019.

[1] D. Gatteschi, R. Sessoli, and J. Villain, *Molecular Nanomagnets* (Oxford University Press, Oxford, 2006).
[2] J. R. Friedman, M. P. Sarachik, J. Tejada, and R. Ziolo, Phys. Rev. Lett. **76**, 3830 (1996).
[3] L. Thomas, F. Lionti, R. Ballou, D. Gatteschi, R. Sessoli, and B. Barbara, Nature (London) **383**, 145 (1996).
[4] W. Wernsdorfer and R. Sessoli, Science **284**, 133 (1999).
[5] A. Ardavan, O. Rival, J. J. L. Morton, S. J. Blundell, A. M. Tyryshkin, G. A. Timco, and R. E. P. Winpenny, Phys. Rev. Lett. **98**, 057201 (2007).
[6] A. R. Rocha, V. M. Garcia-Suarez, S. W. Bailey, C. J. Lambert, J. Ferrer, and S. Sanvito, Nature Mater. **4**, 335 (2005).
[7] S. Sanvito and A. R. Rocha, J. Comput. Theor. Nanosci. **3**, 624 (2006).
[8] A. R. Rocha, V. M. Garcia-Suarez, S. Bailey, C. Lambert, J. Ferrer, and S. Sanvito, Phys. Rev. B **73**, 085414 (2006).
[9] M. H. Jo, J. E. Grose, K. Baheti, M. M. Deshmukh, J. J. Sokol, E. M. Rumberger, D. N. Hendrickson, J. R. Long, H. Park, and D. C. Ralph, Nano Lett. **6**, 2014 (2006).
[10] H. B. Heersche, Z. de Groot, J. A. Folk, H. S. J. van der Zant, C. Romeike, M. R. Wegewijs, L. Zobbi, D. Barreca, E. Tondello, and A. Cornia, Phys. Rev. Lett. **96**, 206801 (2006).
[11] L. Bogani and W. Wernsdorfer, Nature Mater. **7**, 179 (2008).
[12] M. N. Leuenberger and D. Loss, Nature (London) **410**, 789 (2001).
[13] J. Lehmann, A. Gaita-Arino, E. Coronado, and D. Loss, Nat. Nanotechnol. **2**, 312 (2007).
[14] C. F. Hirjibehedin, C. P. Lutz, and A. J. Heinrich, Science **312**, 1021 (2006).
[15] A. C. Bleszynski-Jayich, L. E. Fröberg, M. T. Björk, H. J. Trodahl, L. Samuelson, and R. M. Westervelt, Phys. Rev. B **77**, 245327 (2008).
[16] M. Trif, F. Troiani, D. Stepanenko, and D. Loss, Phys. Rev. Lett. **101**, 217201 (2008).
[17] U. Kortz, N. K. Al-Kassem, M. G. Savelieff, N. A. Al Kadi, and M. Sadakane, Inorg. Chem. **40**, 4742 (2001).
[18] K.-Y. Choi, Y. H. Matsuda, H. Nojiri, U. Kortz, F. Hussain, A. C. Stowe, C. Ramsey, and N. S. Dalal, Phys. Rev. Lett. **96**, 107202 (2006).
[19] M. Trif, F. Troiani, D. Stepanenko, and D. Loss, Phys. Rev. B **82**, 045429 (2010).
[20] M. R. Pederson and S. N. Khanna, Phys. Rev. B **60**, 9566 (1999).
[21] M. Pederson, D. Porezag, J. Kortus, and D. Patton, Phys. Status Solidi B **217**, 197 (2000).
[22] J. Kortus, M. R. Pederson, T. Baruah, N. Bernstein, and C. S. Hellberg, Polyhedron **22**, 1871 (2003).
[23] A. V. Postnikov, J. Kortus, and M. R. Pederson, NEWSLETTER 61 of the ψ_k-Network 2004, http://psi-k.dl.ac.uk/newsletters/News_61/Highlight_61.pdf
[24] Ł. Michalak, C. M. Canali, M. R. Pederson, M. Paulsson, and V. G. Benza, Phys. Rev. Lett. **104**, 017202 (2010).
[25] J. Kanamori, J. Phys. Chem. Solids **10**, 87 (1959).
[26] J. B. Goodenough, Phys. Rev. **100**, 564 (1955).
[27] J. B. Goodenough, J. Phys. Chem. Solids **6**, 287 (1958).
[28] H. Weihe and H. U. Gudel, Inorg. Chem. **36**, 3632 (1997).
[29] A. Kokalj, J. Mol. Graphics Modell. **17**, 176 (1999).
[30] M. R. Pederson and K. A. Jackson, Phys. Rev. B **41**, 7453 (1990).
[31] K. Jackson and M. R. Pederson, Phys. Rev. B **42**, 3276 (1990).
[32] J. P. Perdew, K. Burke, and M. Ernzerhof, Phys. Rev. Lett. **77**, 3865 (1996).
[33] A. Stowe, S. Nellutla, N. Dalal, and U. Kortz, Eur. J. Inorg. Chem. **2004**, 3792 (2004).
[34] S. Carretta, P. Santini, G. Amoretti, M. Affronte, A. Ghirri, I. Sheikin, S. Piligkos, G. Timco, and R. E. P. Winpenny, Phys. Rev. B **72**, 060403 (2005).
[35] J. Luzon, K. Bernot, I. J. Hewitt, C. E. Anson, A. K. Powell, and R. Sessoli, Phys. Rev. Lett. **100**, 247205 (2008).
[36] N. Baadji, M. Piacenza, T. Tugsuz, F. D. Sala, G. Maruccio, and S. Sanvito, Nature Mater. **8**, 813 (2009).
[37] E. A. Osorio, K. Moth-Poulsen, H. S. J. van der Zant, J. Paaske, P. Hedegård, K. F. J. Bendix, and T. Bjørnholm, Nano Lett. **10**, 105 (2010).

6

First-principles studies of spin-orbit and Dzyaloshinskii-Moriya interactions in the Cu3 single-molecule magnet

First-principles studies of spin-orbit and Dzyaloshinskii-Moriya interactions in the $\{Cu_3\}$ single-molecule magnet

J. F. Nossa, M. F. Islam, and C. M. Canali
School of Computer Science, Physics and Mathematics, Linnaeus University, SE-39182 Kalmar, Sweden

M. R. Pederson
US Department of Energy SC22.1, Washington DC 20585-1290

(Received 13 November 2011; published 22 February 2012)

Frustrated triangular molecule magnets such as $\{Cu_3\}$ are characterized by two degenerate $S = 1/2$ ground states with opposite chirality. Recently, it has been proposed theoretically [M. Trif *et al*., Phys. Rev. Lett. **101**, 217201 (2008)] and verified by *ab initio* calculations [M. F. Islam *et al*., Phys. Rev. B **82**, 155446 (2010)] that an external electric field can efficiently couple these two chiral spin states, even in the absence of spin-orbit interaction (SOI). The SOI is, nevertheless, important since it introduces a splitting in the ground-state manifold via the Dzyaloshinskii-Moriya (DM) interaction. In this paper, we present a theoretical study of the effect of the SOI on the chiral states within spin-density functional theory. We employ a recently introduced Hubbard-model approach to elucidate the connection between the SOI and the Dzyaloshinskii-Moriya interaction. This allows us to express the Dzyaloshinskii-Moriya interaction constant D in terms of the microscopic Hubbard-model parameters, which we calculate from first principles. The small splitting that we find for the $\{Cu_3\}$ chiral state energies ($\Delta \approx 0.02$ meV) is consistent with experimental results. The one-band Hubbard-model approach adopted and analyzed here also yields a better estimate of the isotropic exchange constant than the ones obtained by comparing total energies of different spin configurations. The method used here for calculating the DM interaction unmasks its simple fundamental origin, which is the off-diagonal spin-orbit interaction between the generally multireference vacuum state and single-electron excitations out of those states.

DOI: 10.1103/PhysRevB.85.085427 PACS number(s): 75.50.Xx, 75.75.−c, 75.70.Tj

I. INTRODUCTION

In the last 20 years, single-molecule magnets (SMMs) have been widely studied both for their fundamental physical properties[1] and for possible applications in magnetic storage and quantum information.[2,3] Unlike traditional bulk magnetic materials, molecular magnetic materials can be magnetized in a magnetic field without any interaction between the individual molecules. This magnetization is a property of the molecules themselves. The magnetization occurs because of the large ground-state (GS) spin and the large easy-axis magnetic anisotropy barrier separating the spin-up and spin-down states. In principle, it is possible to store and manipulate information in one SMM. Furthermore, the two quantum states representing the two possible spin orientations can be used to build a quantum qubit. Whether used as classical magnetic storage units or as quantum coherent elements, the crucial requirement in both cases is the ability to control and manipulate the magnetic states of the SMM in an efficient way. Manipulation by magnetic fields is straightforward but, in practice, cannot be realized with molecular-size spatial resolution and at fast temporal scales. Unlike magnetic fields, electric fields are easily produced, quickly switched, and can be applied locally at the nanoscale and molecular scale. Therefore, manipulation of the properties of SMMs by external electric fields is an attractive and promising alternative.[4]

Although electric fields do not directly couple to spins, electric manipulation of the spin states is possible indirectly via spin-orbit coupling. This requires the presence of a strong spin-orbit coupling such that the electric field can effectively flip the spin states by acting on the orbital part of the spin orbitals. When SMMs are involved, this is not the most efficient mechanism, since the relative strength of spin-orbit interaction scales like the volume of the molecule.

Recently, a different mechanism of spin-electric coupling in antiferromagnetic (AFM) SMMs, characterized by a lack of inversion symmetry and spin frustration, has been proposed.[4] The best example of such a system is a triangular spin $s = 1/2$ ring with AFM coupling, realized, for example, in the $\{Cu_3\}$ SMM. The low-energy physics of this system can be described by a three-site spin $s = 1/2$ Heisenberg Hamiltonian whose ground-state manifold is composed of two degenerate (total) spin $S = 1/2$ doublets, with wave functions represented by

$$\left|\chi_{\pm}, S_z = +\frac{1}{2}\right\rangle = \frac{1}{\sqrt{3}}(|\downarrow\uparrow\uparrow\rangle + \epsilon_{\pm}|\uparrow\downarrow\uparrow\rangle + \epsilon_{\mp}|\uparrow\uparrow\downarrow\rangle), \tag{1}$$

$$\left|\chi_{\pm}, S_z = -\frac{1}{2}\right\rangle = \frac{1}{\sqrt{3}}(|\uparrow\downarrow\downarrow\rangle + \epsilon_{\pm}|\downarrow\uparrow\downarrow\rangle + \epsilon_{\mp}|\downarrow\downarrow\uparrow\rangle), \tag{2}$$

where the many-body states $|\sigma_1\sigma_2\sigma_3\rangle$ are products of spin-orbital states, $\sigma_i = (\uparrow, \downarrow)$, $i = 1,2,3$, localized on the three magnetic ions of the molecules, and $\epsilon_{\pm} = \exp(\pm 2\pi i/3)$. The four states $|\chi_{\pm}, S_z = \pm 1/2\rangle$ in Eqs. (1) and (2) are labeled by the eigenvalues $S_z = \pm 1/2$ of the z component of the total spin, and by the chirality quantum number $\chi_{\pm} = \pm 1$, that is, the eigenvalues of the chiral operator,

$$C_z = \frac{4}{\sqrt{3}}\mathbf{s}_1 \cdot \mathbf{s}_2 \times \mathbf{s}_3, \tag{3}$$

where $\mathbf{s}_i$ (i =1,2,3) is the spin of the ith atom.

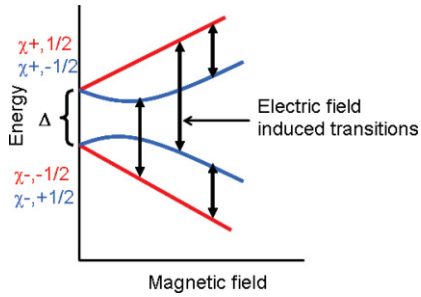

FIG. 1. (Color online) Schematic diagram of electric-field-induced transitions between states of different chirality belonging to the spin $S = 1/2$ ground-state manifold of a triangular antiferromagnet. Δ represents zero-field splitting of the chiral states due to Dzyaloshinskii-Moriya interaction.

An electric field couples to the SMM through $e\mathbf{E}\cdot\mathbf{R}$, where e is the electron charge and $\mathbf{R} = \sum_{i=1}^{3}\mathbf{r}_i$, with r_i being the coordinates of the ith electron. The two spin-orbital states $|\chi_{\pm}, S_z\rangle$, characterized by opposite chirality and equal spin projection, form the basis of a two-dimensional E' irreducible representation of D_{3h}. General group theory arguments then guarantee that the matrix elements $e\langle\chi_{+1}, S_z|X_-|\chi_{-1}, S_z\rangle = e\langle\chi_{-1}, S_z|X_+|\chi_{+1}, S_z\rangle = 2id \neq 0$, where $X_{\pm} \equiv \pm X + iY$ are the in-plane components of $\mathbf{R}$, which also transform as the two-dimensional irreducible representation E'. Here, d is a real number that is referred to as spin-electric dipole coupling. It follows that due to these nonzero matrix elements, an electric field can cause transitions between two ground-state wave functions of opposite chirality, but with the same S_z.

The observation of such electric-field-induced transitions from one chiral state to another requires that the degeneracies between these states be lifted. The anisotropic Dzyaloshinskii-Moriya (DM) interaction plays a crucial role in that it provides one possible mechanism that lifts the degeneracies between states of different chirality without mixing them, as shown in Fig. 1. More generally, the presence of the DM interaction provides a mechanism to control the size of quantum entanglement in magnetic trimers as a function of the temperature and external magnetic field.[5] Experimentally, the DM-induced splitting in $\{Cu_3\}$ is estimated to be small (approximately 0.5 K).[6]

Recently,[7] we have investigated the details of the electronic properties of the $\{Cu_3\}$ SMM, which has the chemical composition $Na[Cu_3(AsW_9O_{33})\cdot 3H_2O]\cdot 32H_2O$. It has been shown experimentally that the ground state of this molecule has AFM order with $J \approx 5$K.[6] This molecule is one of the most promising triangular spin-1/2 molecules where the spin-electric effect can be realized. In particular, we introduced a scheme to evaluate the strength of spin-electric dipole coupling d using *ab initio* methods. However, the value of the anisotropic DM exchange constant interaction, which is responsible for the ground-state zero-field splitting, has not yet been calculated. The purpose of this work is to calculate this splitting by *ab initio* methods. In order to achieve this goal, we analyze the microscopic origin of the DM interaction via a Hubbard-model approach in the presence of spin-orbit integration, which is the correct minimal model to describe both spin and charge fluctuations of these strongly correlated electron systems. At half filling and in the large Hubbard U limit, spin-dependent virtual hopping processes, induced by the spin-orbit interaction, give rise to an anisotropic exchange interaction.[8] There is a close analogy with the isotropic Heisenberg exchange interaction obtained in second-order perturbation theory in the spin-independent hopping perturbation. In addition to elucidating the physical mechanism leading to the anisotropic DM exchange interaction, this approach provides a very convenient prescription of how to extract the DM exchange constant from first-principles calculations, which we have carried out for $\{Cu_3\}$.

This paper is organized as follows. In Sec. II A, we discuss the general properties of the DM interaction. The Hubbard-model approach for calculating the DM vector, adopted in this work, is discussed in Sec. II B. In Sec. III, we discuss details of extracting Hubbard-model parameters from our *ab initio* calculations. In Sec. III D, we discuss other methods that are usually employed for calculating the DM vector. Finally, in Sec. IV, we present a summary of our work.

II. THE DZYALOSHINSKII-MORIYA INTERACTION IN FRUSTRATED ANTIFERROMAGNETIC SPIN RINGS

A. General properties of the DM interaction

The Dzyaloshinskii-Moriya (DM) interaction is an anisotropic exchange interaction resulting from the interplay of the Coulomb interaction and the spin-orbit coupling in systems of low crystal symmetry. The DM interaction is an important effect for many magnetic systems and plays a crucial role in determining the zero-field splitting of energy levels. An anisotropic exchange interaction of the form

$$\mathbf{D}_{12}\cdot\mathbf{S}_1\times\mathbf{S}_2, \tag{4}$$

which is linear in the spin-orbit interaction, was put forward by Dzyaloshinskii on the basis of symmetry considerations.[9] Here, D_{12} is the DM vector between two localized spins, S_1 and S_2. Later, Moriya[10,11] provided a mechanism for this interaction by extending Anderson's theory of superexchange[12] to include the effect of spin-orbit coupling. Let us consider for simplicity two "magnetic ions" located at sites $\mathbf{R}$ and $\mathbf{R}'$, each occupied by a single electron in the ground state. Second-order perturbation theory in the hopping Hamiltonian H_t coupling the two sites gives rise to an isotropic AFM interaction with exchange constant $J = 2t^2_{\mathbf{RR}'}/U$, where $t_{\mathbf{RR}'}$ is a spin-independent hopping integral and U is the energy required to transfer an electron from $\mathbf{R}$ to $\mathbf{R}'$. When spin-orbit interaction H_{SOI} is included, similar second-order processes can generate an anisotropic exchange interaction in the form of Eq. (4), with $D \sim t_{\mathbf{RR}'}b_{\mathbf{RR}'}/U$ where $b_{\mathbf{RR}'}$ is an SOI-induced spin-dependent hopping integral. To the lowest order, $b_{\mathbf{RR}'}$ is just the matrix elements of the H_{SOI} between two orbitals localized at $\mathbf{R}$ and $\mathbf{R}'$. This is the dominant contribution to D. In the case in which, at each site, more than one orbital $|\mathbf{R},\mu\rangle$, $\mu = 1,2,\ldots$, plays a role, higher-order terms such as $b_{\mathbf{RR}'} = t_{\mathbf{RR}'}\langle\mathbf{R},\mu|H_{\mathrm{SOI}}|\mathbf{R}',\mu'\rangle/\Delta E_{\mu,\mu'}$ are possible, making the corresponding D effectively a third-order coupling in the

perturbations H_t and $H_{\rm SOI}$. It turns out that $D \simeq (\Delta g/g)$, where g is the free-electron gyromagnetic ratio and Δg is the deviation from g induced by the SOI.[11]

As shown by Moriya, other terms linear in the SOI contribute to the anisotropic exchange of the form of Eq. (4). The second most important contribution is also a second-order term resulting from the SOI and *direct* interatomic exchange interaction $J^{\rm ex}(\mathbf{R},\mathbf{R}')$. In AFM crystals, this term is $J^{\rm ex}(\mathbf{R},\mathbf{R}')/J$ times smaller than the second-order contribution proportional to $t_{\mathbf{RR}'}b_{\mathbf{RR}'}$. Finally, third-order contributions to D include the hopping terms twice and the intra-atomic exchange constant J_0. They are J_0/U smaller than second-order terms.

The DM exchange vector $\mathbf{D}$ vanishes when the symmetry of the crystal is high. This is the case, for example, when the center of inversion of the system is located halfway between the two magnetic ions in a unit cell. In low-dimensional crystals where $D \neq 0$, the anisotropic exchange is typically the most important anisotropic contribution between spins. The DM interaction favors noncollinear spin configurations, with typical canted spins. As such, it determines the spin arrangements and it is responsible for the weak ferromagnetism observed in some predominantly AFM crystals, such as α-Fe_2O_2. The tendency toward canted spin configurations is most easily seen by minimizing the energy in Eq. (4) for two classical spins, when the DM vector $\mathbf{D}$ is, for example, perpendicular to the line joining the two ions. From Eq. (4), we can see that the minimum energy corresponds to a spin configuration where both spins are perpendicular to each other and to the direction of $\mathbf{D}$. Similar conclusions can be obtained by analyzing the same system quantum mechanically. The DM interactions are also responsible for the proposed noncollinear spin configurations in magnetic clusters engineered by scanning tunneling microscopy (STM) techniques on insulating surfaces.[13,14]

B. The DM interaction for antiferromagnetic spin rings within the one-band Hubbard-model approach

In this section, we specialize the previous discussion to the case of an AFM spin triangle, and show how the DM interaction can be derived microscopically from a Hubbard model at half filling, in the presence of spin-orbit interaction.

As mentioned in Sec. I, the low-energy magnetic properties of $\{Cu_3\}$ are well described by an isotropic AFM Heisenberg model,

$$H_{\rm H} = \sum_{\langle i,j\rangle} J_{ij}\mathbf{s}_i \cdot \mathbf{s}_j, \quad J_{ij} > 0, \tag{5}$$

where $\mathbf{s}_i$ are spin vector operators of magnitude $s_i = 1/2$, predominately localized at the three Cu sites. Here, i and j stand for atomic indices. If the small distortion from a perfect equilateral arrangement of the three Cu atoms is neglected, then the three exchange constants are the same, $J_{ij} = J$. Density functional theory (DFT) calculations[7] find $J \approx 3.7$ meV. The GS manifold comprises two spin $S = 1/2$ doublets, which can be represented by the two chiral states given in Eqs. (1) and (2), or any two orthogonal linear combination of these. The spin $S = 3/2$ excited-state multiplet is separated by the GS by an energy of order J.

It is well known that the AFM Heisenberg model represents an effective low-energy spin model that can be derived from an underlying Hubbard model at half filling in the large t/U limit. The choice of the best minimal model capturing the essential microscopic features of the electronic system is often a complex task, particularly when the exchange interaction between the magnetic ions is mediated via several paths involving nonmagnetic ions, as in the case of $\{Cu_3\}$. We will neglect these complications and assume that an effective one-band Hubbard model suffices for this purpose. We will see that our first-principles calculations corroborate this choice, showing that one localized orbital at each magnetic ion indeed is enough to describe the low-energy physics of the system. We will comment later on the possibility of considering a more complex Hubbard model to describe the nonmagnetic bridges between Cu atoms, as well as the need to include more than one orbital at the Cu sites.

The second quantized one-band Hubbard Hamiltonian reads

$$H_U = -t\sum_{i,j}\sum_{\alpha}\{c^\dagger_{i\alpha}c_{j\alpha} + \text{H.c.}\} + \frac{1}{2}U\sum_i n_{i\uparrow}n_{i\downarrow}, \tag{6}$$

where $c^\dagger_{i\alpha}$ ($c^\dagger_{i\alpha}$) creates (destroys) an electron with spin α at site i, and $n_{i\alpha} = c^\dagger_{i\alpha}c_{i\alpha}$ is the particle-number operator. More precisely, the index i labels a Wannier function localized at site i. The first term represents the kinetic energy, characterized by a spin-independent hopping parameter t, which is the same for all pairs of sites due to the C_3 symmetry of the $\{Cu_3\}$ molecule magnet. The second term is an on-site repulsion energy of strength U, which has an effect only when two electrons of opposite spins reside on the same site. It is the on-site repulsion energy.

The spin-orbit interaction in the Hubbard model is described by adding the following spin-dependent hopping term:[8,15–17]

$$H_{\rm SOI} = \sum_{i,j}\sum_{\alpha,\beta}\left\{c^\dagger_{i\alpha}\left(i\frac{\mathbf{P}_{ij}}{2}\cdot\boldsymbol{\sigma}_{\alpha\beta}\right)c_{j\beta} + \text{H.c.}\right\}, \tag{7}$$

where σ is the vector of the three Pauli matrices. Here, the vector $\mathbf{P}_{ij}$ is proportional to the matrix element of $\nabla V \times \mathbf{p}$ between the orbital parts of the Wannier functions at sites i and j; V is the one-electron potential and $\mathbf{p}$ is the momentum operator. Clearly, the spin-orbit term has the form of a spin-dependent hopping, which is added to the usual spin-independent hopping proportional to t. This form of the spin-orbit interaction is a special case of Moriya's hopping terms[11] in the limit that all but one orbital energy is taken to infinity,[16] and it is consistent with our choice of a one-band Hubbard model.

In contrast to the spin-independent hopping term, the spin-depending hopping parameters are related by both the full symmetry of the molecule and the *local symmetry* of localized orbitals.[8] Now, because of the σ_v symmetry, $\mathbf{P}_{ij} = P\mathbf{e}_z$. The final expression of the Hubbard model, including the spin-orbit

interaction, is

$$H_{U+\mathrm{SOI}} = \sum_{i,\alpha}\{c^{\dagger}_{i\alpha}(-t + i\lambda_{\mathrm{SOI}}\alpha)c_{i+1\alpha} + \mathrm{H.c.}\} + \frac{1}{2}U\sum_{i} n_{i\uparrow}\, n_{i\downarrow}, \tag{8}$$

where $\lambda_{\mathrm{SOI}} \equiv P/2 = \mathbf{P}_{ij}/2 \cdot \mathbf{e}_z$ is the spin-orbit parameter.

We want to treat the two hopping terms perturbatively on the same footing by doing an expansion around the atomic limit $t/U,\ \lambda_{\mathrm{SOI}}/U \to 0$. In many molecular magnets, $t \gg \lambda_{\mathrm{SOI}}$. This turns out to be the case also for $\{Cu_3\}$. In other molecules, the two hopping parameters are of the same order of magnitude.

We are interested in the half-filling regime. We know that second-order perturbation theory in t results in an AFM isotropic exchange term that splits the spin degeneracy of the low-energy sector of the Hubbard model, defined by the singly occupied states. This action can be represented with an effective spin Hamiltonian, i.e., the isotropic Heisenberg model, with exchange constant $J = 4t^2/|U|$.[18] Similarly, Loss *et al.* showed that another second-order term proportional to $t\lambda_{\mathrm{SOI}}/U$ generates an anisotropic exchange term that can be identified with the DM interaction.[8] They write approximate adapted many-body states to first order in the perturbation $|t|,\lambda_{\mathrm{SOI}} \ll U$, corresponding to singly occupied states. In particular, there are two independent doublets,

$$\left|\psi^{1\alpha}_{E^{\prime}_{\pm}}\right\rangle = \frac{1}{\sqrt{3}}(|\downarrow\uparrow\uparrow\rangle + \epsilon_{\pm}|\uparrow\downarrow\uparrow\rangle + \epsilon_{\mp}|\uparrow\uparrow\downarrow\rangle) \tag{9}$$

and

$$\left|\psi^{1\alpha}_{E^{\prime}_{\pm}}\right\rangle = \frac{1}{\sqrt{3}}(|\uparrow\downarrow\downarrow\rangle + \epsilon_{\pm}|\downarrow\uparrow\downarrow\rangle + \epsilon_{\mp}|\downarrow\downarrow\uparrow\rangle), \tag{10}$$

with $\epsilon_{\pm} = \exp(\pm 2\pi i/3)$. These are states with $S = 1/2$ and $S_z = \pm 1/2$. These states are formally identical to the chiral states given in Eqs. (1) and (2). Now, each of the terms appearing in these equations is a single Slater determinant obtained by three creation operators acting on the vacuum, e.g.,

$$|\uparrow\uparrow\downarrow\rangle \equiv c^{\dagger}_{1\uparrow}c^{\dagger}_{2\uparrow}c^{\dagger}_{3\downarrow}|0\rangle. \tag{11}$$

The states $|\psi^{1\alpha}_{E^{\prime}_{\pm}}\rangle$ and $|\psi^{1\alpha}_{E^{\prime}_{-}}\rangle$ are eigenstates of the Hubbard Hamiltonian when $t = \lambda_{\mathrm{SOI}} = 0$. The tunneling and SOI mix the singly occupied and doubly occupied states. The first-order correction is obtained by mixing in doubly occupied states,

$$\left|\Phi^{1\alpha}_{E^{\prime}_{\pm}}\right\rangle \equiv \left|\psi^{1\alpha}_{E^{\prime}_{\pm}}\right\rangle + \frac{(\epsilon_{-} - 1)(t \pm \alpha\lambda_{\mathrm{SOI}})}{\sqrt{2}U}\left|\psi^{2\alpha}_{E^{\prime}_{\pm}}\right\rangle + \frac{3\epsilon_{+}(t \pm \alpha\lambda_{\mathrm{SOI}})}{\sqrt{2}U}\left|\psi^{2\alpha}_{E^{\prime\prime}_{\pm}}\right\rangle, \tag{12}$$

where

$$\left|\psi^{2\alpha}_{E^{\prime}_{\pm}}\right\rangle = \frac{1}{\sqrt{6}}\sum_{i=1}^{3}\epsilon^{i-1}_{1,2}\left(\left|\psi^{\alpha}_{i1}\right\rangle + \left|\psi^{\alpha}_{i2}\right\rangle\right) \tag{13}$$

and

$$\left|\psi^{2\alpha}_{E^{\prime\prime}_{\pm}}\right\rangle = \frac{1}{\sqrt{6}}\sum_{i=1}^{3}\epsilon^{i-1}_{1,2}\left(\left|\psi^{\alpha}_{i1}\right\rangle - \left|\psi^{\alpha}_{i2}\right\rangle\right), \tag{14}$$

with $|\psi^{\alpha}_{ij}\rangle = c^{\dagger}_{i\uparrow}c^{\dagger}_{i\downarrow}c^{\dagger}_{j\alpha}|0\rangle$ $(i = 1,2,3$ and $j \neq i)$ representing the doubly occupied sites.

The next step is to take the expectation value of the spin-orbit part of Eq. (8) in these approximated states. The result is[8]

$$\left\langle\Phi^{1\alpha}_{E^{\prime}_{\pm}}\middle|H_{\mathrm{SOI}}\middle|\Phi^{1\alpha}_{E^{\prime}_{\pm}}\right\rangle = \pm\frac{5\sqrt{3}\lambda_{\mathrm{SOI}}t}{2U}\mathrm{sgn}(\alpha). \tag{15}$$

Note that the off-diagonal matrix elements of H_{SOI} vanish; in other words, the SOI splits but does not mix the chiral states.

In the small $t/U,\ \lambda_{\mathrm{SOI}}/U$ limit, we can resort to a spin-only description of the low-energy physics of the system. The ground-state manifold [corresponding to the states of Eq. (12)] is given by the two chiral spin states of Eqs. (1) and (2).

The anisotropic DM spin-exchange Hamiltonian in D_{3h} symmetry is given by[8]

$$H_{\mathrm{DM}} = \frac{iD_z}{2}\sum_{1}^{3}(s^{i}_{+}\, s^{i+1}_{-} - s^{i}_{-}\, s^{i+1}_{+}). \tag{16}$$

Now, for a molecular magnet with D_{3h} symmetry, the spin-orbit interaction acting in the $S = 1/2$ subspace can be reduced to the effective form[4]

$$H_{\mathrm{SOI}} = \Delta_{\mathrm{SOI}}C_zS_z, \tag{17}$$

where Δ_{SOI} is the effective SOI coupling constant and $S_z = s_{1z} + s_{2z} + s_{3z}$ is the z component of the total spin S. By using Eq. (3), one can see that with the identification $D_z = (1/\sqrt{3})\Delta_{\mathrm{SOI}}$, this form of the spin-orbit interaction reduces to H_{DM} given in Eq. (16).

The DM interaction expressed in this form clearly shows that it splits but does not mix the two chiral states.[19] The splitting is exactly proportional to D_z and, via Eq. (15) in the low-energy regime, we can make the identification[4]

$$D_z = \frac{5\lambda_{\mathrm{SOI}}t}{U}. \tag{18}$$

This Hubbard-model analysis suggests an avenue to extract the DM parameters from an *ab initio* calculation. Only three parameters are needed, namely, the spin-orbit interaction λ_{SOI}, the hopping parameter t, and the on-site repulsion energy U.

Before carrying out this procedure, it is useful to comment on possible generalizations of the Hubbard model considered here and their implications for the DM exchange interaction. One obvious generalization is to consider a multiband model, where at each magnetic site i, besides the GS orbital g_i consider so far, there are one or more excited states e_i. If this is the case, other contributions to the DM interaction already considered by Moriya and mentioned in Sec. II A are possible. In an interesting set of papers, Yoon and Solomon considered explicitly these terms in the study of a class of trinuclear Cu complexes (see, for example, the review paper [20], and references therein). Their expression for the DM (antisymmetric) exchange parameter is, as in our case, first order in the SOI. It involves the product of the matrix element of the SOI between the GS and an excited state at the same magnetic site, $\langle g_i|H_{\mathrm{SOI}}|e_i\rangle$, times the two-electron (super)exchange interaction $J^{e_ig_j}_{g_ig_j}$ between two different magnetic sites, i,j. These terms could possibly be relevant in a multiorbital Hubbard model, particularly in

the case of strong (super)exchange pathways involving the same GS orbitals. As we will see in the following section, for the specific $\{Cu_3\}$ molecular magnet considered here, a one-band Hubbard model seems to capture the salient magnetic properties of the system. Therefore we will focus on this model and neglect the DM contributions arising from the many-orbital case. [21]

Finally, one could also consider the more complicated situation where the magnetic sites are connected by ligand bridges. A generalized Hubbard model describing this situation was already considered in Ref. 4, where a corresponding expression of the DM exchange was derived. Again, these are all possible improvements of the one-band, all-magnetic-site model. Our strategy, however, is to carry out an *ab initio* study of the DM interaction based on the simplest relevant model and see how well it can capture the underlying physics.

C. Semiclassical analysis of the DM interaction in frustrated spin systems

The quantum mechanical frustration present in an AFM spin triangle and the DM interaction both tend to favor noncollinear spin configurations. It is instructive to study their interplay in a semiclassical approach, where noncollinearity is a more intuitive concept.

The *classical* Heisenberg model with an energy functional given by Eq. (5) has two degenerate "ground states," given by the two noncollinear spin configurations shown in Fig. 2. Classically, these two states are the best way to bypass the frustration present for any collinear spin configuration in a triangular antiferromagnet. Quantum mechanically, the two noncollinear spin configurations can be represented by the states

$$|\psi_{\mathrm{nc}\pm}\rangle = [(\alpha_1|\uparrow\rangle_1 + \beta_1|\downarrow\rangle_1) \otimes (\alpha_2|\uparrow\rangle_2 + \beta_2|\downarrow\rangle_2) \otimes (\alpha_3|\uparrow\rangle_3 + \beta_3|\downarrow\rangle_3)], \tag{19}$$

where $\alpha = \cos(\theta/2)$ and $\beta = \exp\{i\phi\}\sin(\theta/2)$. Here, θ is the elevation angle and ϕ is the azimuth angle. The three spinors, $(\alpha_i|\uparrow\rangle_i + \beta_i|\downarrow\rangle_i)$, $i = 1,2,3$, are three spin-1/2 coherent states defined by the three noncollinear directions obtained by rotating consecutively by the angle $\pm 240^\circ$ (see Fig. 2). Anticlockwise rotations (by -240°) define a left-handed helical state [Fig. 2(a)]; clockwise rotations (by $+240^\circ$) define a right-hand helical state [Fig. 2(b)].

In contrast to the true GS given in Eqs. (1) and (2), the noncollinear states defined in Eq. (19) are neither eigenstates of the quantum Hamiltonian given by Eq. (5) nor of $\mathbf{S}^2$ and S_z. The expectation value of the Hamiltonian H_H at these states is defined by

$$\langle\psi_{\mathrm{nc}\pm}|H_{\mathrm{H}}|\psi_{\mathrm{nc}\pm}\rangle = 3J/4. \tag{20}$$

The fact that the energy of the collinear states is higher than the energy of the chiral states by $3J/8$ is not surprising, since the noncollinear states defined in Eq. (19) are a mixture of $S = 1/2$ and $S = 3/2$ components.

When rewritten in terms of the electronic states for the corresponding Hubbard model at half filling in the small t/U limit, the noncollinear spin-coherent states defined in Eq. (19) can be considered to be the "best" energy states given by a single Slater determinant (note that the chiral states cannot be written as a single Slater determinant).

It is now interesting to examine the effect of the DM interaction on these states. A straightforward calculation shows that for the DM interaction of Eq. (16), where only the z component of $\mathbf{D}$ is nonzero,

$$\langle\psi_{\mathrm{nc}\pm}|H_{\mathrm{DM}}|\psi_{\mathrm{nc}\pm}\rangle = \pm\frac{3}{4}\frac{\sqrt{3}}{2}D_z. \tag{21}$$

Therefore, as for the GS manifold of the exact eigenstates, the DM interaction *splits* but does *not couple* the two noncollinear states. The DM parameter D_z is, by Eq. (21), related to the DM interaction-induced energy gap between the two noncollinear states,

$$\Delta E_{\mathrm{nc}} = \langle\psi_{\mathrm{nc}+}|H_{\mathrm{DM}}|\psi_{\mathrm{nc}+}\rangle - \langle\psi_{\mathrm{nc}-}|H_{\mathrm{DM}}|\psi_{\mathrm{nc}-}\rangle = \frac{3\sqrt{3}}{4}D_z. \tag{22}$$

This result suggests a way of extracting the DM vector parameter $\mathbf{D}$ similar in spirit to the method used to calculate the isotropic exchange parameter J by comparing the energy difference of states with ferromagnetic and AFM spin configurations, respectively. In the next section, we will see that this procedure can also be carried out by first-principles methods.

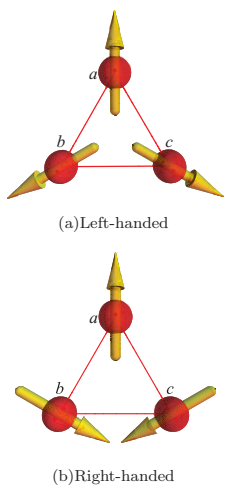

FIG. 2. (Color online) Noncollinear helical system of three Cu-atom spins. (a) Anticlockwise rotations (by -240°) define a left-handed helical state. (b) Clockwise rotations (by $+240^\circ$) define a right-hand helical state.

III. *AB INITIO* CALCULATION OF THE DM VECTOR

All of the calculations in this work are carried out by using the *ab initio* package NRLMOL,[22,23] which uses a Gaussian basis set to solve the Kohn-Sham equations within the Perdew-Burke-Ernzerhof (PBE) generalized gradient approximation (GGA).[24] The PBE-GGA calculations discussed here use the

TABLE I. Number of primitive Gaussians used for each type of atom, the minimum and maximum values of the exponents, and the number of contracted Gaussians. Here, α represents the range of the exponents for the primitive Gaussians.

Atom	Bare	Contracted functions			Maximum	Minimum
type	Gaussians	s	p	d	α	α
H	1	4	3	1	7.8×10^{3}	7.5×10^{-2}
W	6	4	2	3	1.5×10^{0}	3.6×10^{-2}
O	13	5	4	3	6.1×10^{6}	1.0×10^{-1}
Na	16	6	4	3	2.5×10^{7}	2.7×10^{-2}
Cu	20	7	5	4	4.8×10^{8}	5.0×10^{-2}
As	21	7	6	4	7.0×10^{8}	6.1×10^{-2}

massively parallel NRLMOL electronic structure code. The numerical methods are described in full in Ref. 25. Very large basis sets, based on a nonlinear optimization procedure described in Ref. 26, have been used. As discussed in Ref. 26, this procedure simultaneously optimizes the contraction coefficients and the Gaussian-decay parameters by first performing atomic self-consistent field (SCF) calculations, using single-basis Gaussians, and then using the conjugate-gradient method in conjunction with gradients of the energy with respect to the decay parameters to minimize the total atomic energy. A key feature of this optimization scheme is that it identified a scaling law (proven in Ref. 26) showing that the shortest-range Gaussian should scale as $Z^{10/3}$ to ensure that there is no basis-set superposition error. The basis sets are available upon request. Table I shows the number of Gaussians used in our calculations for each atom. For more computational details and the electronic properties of $\{Cu_3\}$, we refer the reader to our previous work.[7] In this molecule, the three Cu^{2+} cations form an equilateral triangle and are the sites of three identical $s = 1/2$ quantum spins. The electrons on each of the Cu atoms have primarily d character. Our calculations have shown that the low-energy magnetic properties are correctly described by an effective three-site spin $s = 1/2$ Heisenberg model, with an AFM exchange coupling, $J \approx 5$ meV.

A. Calculation of the hopping term t

As discussed in Sec. II B, the Hubbard-model approach is based on allowing the localized electrons to hop to their nearest-neighbor sites and, in the present case of the $\{Cu_3\}$ molecule, these localized electrons are d electrons. Therefore, for calculating hopping parameter t, the relevant states are those d electron states that lie close to the Fermi level. Let $|K,\alpha\rangle$ be the three relevant Kohn-Sham eigenstates calculated from NRLMOL. We can write them as a linear combination of the localized atomic orbitals, centered at the three Cu sites, $\{|\phi_a\rangle,|\phi_b\rangle,|\phi_c\rangle\} \otimes |\chi_\alpha\rangle$, with $\alpha = \uparrow, \downarrow$ for spin up and down, respectively:

$$|K,\alpha\rangle = \sum_i C^i_{K\alpha} |\phi_i\rangle|\chi_\alpha\rangle, \tag{23}$$

where $C^i_{K\alpha}$ is the weight of the localized $|\phi_i\rangle|\chi_\alpha\rangle$ wave function.

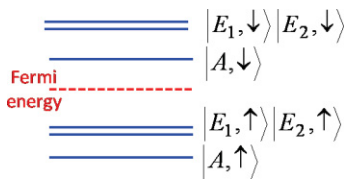

FIG. 3. (Color online) Schematic diagram of the Kohn-Sham energy levels around the Fermi level.

For the $|\uparrow\uparrow\uparrow\rangle$ spin configuration, in the absence of spin-orbit interaction, the relevant three levels around the Fermi level are doubly and singly degenerate. These levels are sketched in Fig. 3.

We obtain the level structure by diagonalizing the three-site Hamiltonian in the absence of the SOI,

$$H_0 = \varepsilon_0 \sum_i |\phi_i\rangle\langle\phi_i| - t \sum_{i\neq j} |\phi_i\rangle\langle\phi_j|, \tag{24}$$

where ε_0 is the on-site energy, t is the hopping term, and $i,j = a,b,c$ represent the copper sites. We get the eigenvalues $\varepsilon_0 + t$ and $\varepsilon_0 - 2t$ for the twofold and onefold degenerate states, respectively. The Kohn-Sham eigenvectors can be defined as a linear combination of the localized wave functions,

$$\begin{aligned} |E_1,\uparrow\rangle &= \frac{1}{\sqrt{2}}(|\phi_a\rangle - |\phi_b\rangle)|\uparrow\rangle, \\ |E_2,\uparrow\rangle &= \frac{1}{\sqrt{6}}(|\phi_a\rangle + |\phi_b\rangle - 2|\phi_c\rangle)|\uparrow\rangle, \\ |A,\uparrow\rangle &= \frac{1}{\sqrt{3}}(|\phi_a\rangle + |\phi_b\rangle + |\phi_c\rangle)|\uparrow\rangle. \end{aligned} \tag{25}$$

Now the localized states can be written in term of the Kohn-Sham functions,

$$\begin{aligned} |\phi_a\rangle|\uparrow\rangle &= \frac{|A,\uparrow\rangle}{\sqrt{3}} + \frac{|E_1,\uparrow\rangle}{\sqrt{2}} + \frac{|E_2,\uparrow\rangle}{\sqrt{6}}, \\ |\phi_b\rangle|\uparrow\rangle &= \frac{|A,\uparrow\rangle}{\sqrt{3}} - \frac{|E_1,\uparrow\rangle}{\sqrt{2}} + \frac{|E_2,\uparrow\rangle}{\sqrt{6}}, \\ |\phi_c\rangle|\uparrow\rangle &= \frac{|A,\uparrow\rangle}{\sqrt{3}} - 2\frac{|E_2,\uparrow\rangle}{\sqrt{6}}. \end{aligned} \tag{26}$$

Our calculations show that these states are primarily localized on the Cu atoms and have d character. We have obtained the Kohn-Sham eigenenergies for the onefold and twofold degenerate states,

$$\begin{aligned} \langle E_1,\uparrow|H_0|E_1,\uparrow\rangle &= \tfrac{1}{2}(\langle\phi_a| - \langle\phi_b|)H_0(|\phi_a\rangle - |\phi_b\rangle) = \varepsilon_0 + t, \\ \langle A,\uparrow|H_0|A,\uparrow\rangle &= \tfrac{1}{3}(\langle\phi_a| + \langle\phi_b| + \langle\phi_c|)H_0 \\ &\quad \times (|\phi_a\rangle + |\phi_b\rangle + |\phi_c\rangle) = \varepsilon_0 - 2t. \end{aligned} \tag{27}$$

From Eqs. (27), we can finally evaluate the value of the parameter t as

$$t = \tfrac{1}{3}(\langle E_1,\uparrow|H_0|E_1,\uparrow\rangle - \langle A,\uparrow|H_0|A,\uparrow\rangle) = 50.84 \text{ meV}. \tag{28}$$

B. Calculation of the spin-orbit interaction parameter λ_{SOI}

The standard spin-orbit interaction representation for spherical systems is given by

$$U_{so}(r,\mathbf{L},\mathbf{S}) = \frac{1}{2c^2}\mathbf{S}\cdot\mathbf{L}\frac{1}{r}\frac{d\Phi(r)}{dr}, \tag{29}$$

where r is the position, $\mathbf{L}$ is the angular momentum, $\mathbf{S}$ is the spin moment, c is the speed of light, and Φ is a spherically symmetric potential. The above equation is exact for spherical systems. For a multicenter system, a superposition of such terms needs to be considered. However, this approximation could miss nonspherical correlations that are important for anisotropic energies. Instead of using Eq. (29), a generalization of the spin-orbit interaction for nonspherical or multicenter systems is given by

$$U_{so}(\mathbf{r},\mathbf{p},\mathbf{S}) = -\frac{1}{2c^2}\mathbf{S}\cdot\mathbf{p}\times\nabla\Phi(\mathbf{r}), \tag{30}$$

where $\mathbf{p}$ is the momentum operator and a external electric field is given by $\mathbf{E} = -\nabla\Phi$.

Pederson *et al.* (see Ref. 27) have shown an exact simplified method for incorporating spin-orbit coupling into density functional calculations. In order to get the basis set for the spin-orbit coupling, the single-electron wave function can be expressed as

$$\psi_{is}(\mathbf{r}) = \sum_{j\alpha} C^{is}_{j\alpha} f_j(\mathbf{r})\chi_\alpha, \tag{31}$$

where $f_j(\mathbf{r})$ is a spatial basis function, χ_α is either a majority or minority spin spinor, and $C^{is}_{j\alpha}$ are determined by effectively diagonalizing the Hamiltonian matrix. In order to calculate the effect of the SOI [Eq. (30)], it is necessary to calculate matrix elements of the form

$$\begin{aligned} U_{j\alpha,k\alpha'} &= \langle f_j\chi_\alpha|U(\mathbf{r},\mathbf{p},\mathbf{S})|f_k\chi_{\alpha'}\rangle \\ &= \sum_x \frac{1}{i}\langle f_j|V_x|f_k\rangle\langle\chi_\alpha|S_x|\chi_{\alpha'}\rangle, \end{aligned} \tag{32}$$

where

$$\langle f_j|V_x|f_k\rangle = \frac{1}{2c^2}\left(\left\langle\frac{df_j}{dz}\middle|\Phi\middle|\frac{df_k}{dy}\right\rangle - \left\langle\frac{df_j}{dy}\middle|\Phi\middle|\frac{df_k}{dz}\right\rangle\right). \tag{33}$$

The matrix elements for V_y and V_z are obtained by cyclical permutations of x, y, and z in Eq. (33). This methodology for the SOI matrix gives several advantages, including that it does not require the determination of the electric field; it is specially ideal for basis functions constructed from Gaussian-type orbitals, Slater-type functions, and plane waves.

We are interested in the matrix elements in the localized basis set, given by Eq. (26),

$$\begin{aligned} &\langle\phi_i|\langle\chi_\uparrow|U_{so}|\phi_k\rangle|\chi_\uparrow\rangle \\ &= -\frac{1}{2c^2}\langle\phi_i|\mathbf{p}\times\nabla\Phi(\mathbf{r})|\phi_k\rangle\cdot\langle\chi_\uparrow|\mathbf{S}|\chi_\uparrow\rangle \\ &= \frac{1}{2i}\langle\phi_i|V_z|\phi_k\rangle = -\frac{i}{2}p^z_{ik} \equiv -i\lambda_{SOI}. \end{aligned} \tag{34}$$

We can write these matrix elements in the Kohn-Sham basis set as

$$\begin{aligned} \langle\phi_i|\langle\chi_\uparrow|U_{so}|\phi_k\rangle|\chi_\uparrow\rangle = \sum_{KK'} &\left(\tilde{C}^i_{K\uparrow}\right)^*\tilde{C}^i_{K'\uparrow} \\ &\times\langle K,\uparrow|U_{\rm SOI}|K',\uparrow\rangle. \end{aligned} \tag{35}$$

We have obtained the matrix elements for the spin-orbit interaction in the Kohn-Sham basis, $\{|E_1\rangle,|E_2\rangle,|A\rangle\}\otimes|\chi_\alpha\rangle$ [Eq. (35)], and used Eqs. (26) to obtain the matrix elements:

$$p^z = \begin{pmatrix} 0 & 0.85 & 0.85 \\ 0.85 & 0 & 0.85 \\ 0.85 & 0.85 & 0 \end{pmatrix}. \tag{36}$$

From Eq. (34), we have $\lambda_{\rm SOI} = p^z_{ik}/2 = 0.43$ meV.

C. Calculation of the Hubbard U and evaluation of D_z and J

The most common approach for the calculation of U involves the calculation of energy E of the molecule with N, $N+1$, and $N-1$ electron, and the extraction of U from the following equation:

$$\begin{aligned} U &= E(N+1) + E(N-1) - 2E(N) \\ &= [E(N+1) - E(N)] - [E(N) - E(N-1)] = A - I. \end{aligned} \tag{37}$$

In the above equation, A is (minus) the electron affinity[28] and I is the ionization energy. For systems that are not closed shell, such as those considered here, the U value is essentially the second derivative of energy with respect to the charge, and it is possible to determine U by calculating the energy as a function of the charge.

For the single-band Hubbard model corresponding to the $\{Cu_3\}$ molecule, we are interested in obtaining energies for the charge-transfer excitations involving the transfer of a localized d electron on one copper site to a localized d electron on another site. Specifically, we wish to know the energy of $|X\rangle = |\uparrow_a\downarrow_a\uparrow_c\rangle$ relative to $|\uparrow_a\downarrow_b\uparrow_c\rangle$. There are a total of 12 charge-transfer excitations that can be made with one site that is doubly occupied and one electron on one of the other sites. For the half-filled case of interest here, the energy difference depends upon the electron affinity of the state on site a, the ionization energy of the state on site b, and the residual long-range Coulomb interaction between the negatively charged electron added to site a and the positively charged hole that is left behind on site b. Since site b and site a are equivalent, it follows that we simply need to calculate U for any one of the copper sites in the half-filled case. A very rough estimate of the charge-transfer energy may be determined by calculating the PBE-GGA energy of the Cu atom with an electron configuration of $1s^2 2s^2 3s^2 4s^2 p^6 3p^6 3d^n$ with $n = 8$, 9, 10. Using $n = 9$ as the reference state, one finds a bare U value of 13.76 eV, which, after accounting for the particle-hole interaction $(27.2116/R_{Cu-Cu} = 2.95$ eV, where $R_{Cu-Cu} = 4.87$ Bohr is the distance between magnetic centers), is shifted to 10.8 eV.

In the $\{Cu_3\}$ molecule, we have chosen to calculate U quasianalytically by gradually adding (or subtracting) a small fraction of electronic charge δq to one of the half-filled Cu d

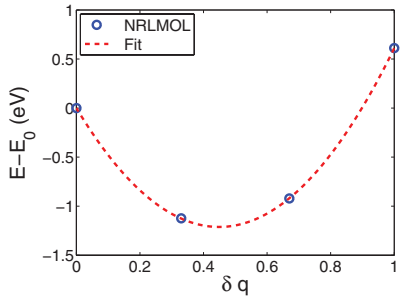

FIG. 4. (Color online) Dependence of the total energy on added fractional charge δq. The (blue) circle represent the results of NRLMOL calculations, and the dashed (red) line represents a quadratic fit.

states. The energy of the system as a function of δq is shown in Fig. 4, where we can see that it can be well reproduced by a quadratic fitting curve. The figure shows that upon adding a fractional charge to a localized orbital, the total energy initially decreases, since the orbital energy is negative. Eventually, however, the competing Coulomb repulsion takes over and the net change in total energy for adding one electron to a localized orbital is positive. In contrast, with one extra electron delocalized throughout the molecule, the total energy is usually smaller than the energy of the neutral molecule.

The difference in the energy of the system before and after adding a fraction of electronic charge δq is given by $\Delta E = U_{\text{eff}} = U\delta q^2 - e^2\delta q^2/R_{\text{Cu-Cu}}$, where $U = \partial^2 E(q)/\partial q^2$. We have calculated the effective parameter U_{eff} by setting $\delta q = 1$:

$$U_{\text{eff}} = \delta q^2\left[\frac{\partial^2 E(q)}{\partial q^2} - \frac{e^2}{R_{\text{Cu-Cu}}}\right] = 9.06 \text{ eV}, \qquad (38)$$

where $E(q) = E_0 + (U/2)(q - q_0)^2$, with E_0 being a constant.

1. Evaluation of D_z and J

Having calculated the parameters t, λ_{SO}, and U_{eff}, we are now able to use Eq. (18) and evaluate the Dzyaloshinskii-Moriya parameter D_z. We obtain

$$D_z = 5\frac{\lambda_{\text{SOI}} t}{U_{\text{eff}}} = 0.01 \text{ meV}. \qquad (39)$$

This value of D_z yields a small splitting of the chiral state, $\Delta \approx 0.02$ meV ≈ 0.3 K. Experimental estimates of the DM parameter find a splitting that is three to four times larger than this value. Considering the smallness of this energy, the uncertainty in the experimental measurements and the approximation in evaluating t, U, and λ_{SOI}, the two estimates are consistent with each other. A better agreement between theory and experiment could perhaps be provided by considering additional contributions to the DM interaction, as, for example, proposed by Solomon *et al.*[20] As we discussed earlier, these terms would be present in our formalism within a generalized multiband Hubbard model. Although these terms cannot be *a priori* disregarded and should be carefully evaluated, the success of the one-band Hubbard model in describing the low-energy magnetic properties of the system (see below) seems to suggest that they are less likely to resolve the discrepancy with experiment.

On the other hand, it is also possible that part of the discrepancy between theory and experiment is due to the fact that other mechanisms, different from the DM interaction, contribute to the splitting. In particular, Ref. 29 pointed out that small deformations of the triangular molecule can lift the chiral degeneracy and this contribution to the splitting could be even more important than the DM interaction. If this is indeed the case, then our results would imply that our method of computing the DM parameter is actually rather accurate.

From a computational point of view, it is interesting at this point to evaluate the isotropic exchange constant J from the Hubbard-model perturbative approach, which gives

$$J = 4t^2/U \approx 1 \text{ meV}. \qquad (40)$$

This estimate of J is considerably closer to the experimental value of 0.5 meV than the value of 3.7 meV obtained by computing the energy difference between states with ferromagnetic and AFM spin configurations.[7] This is again another indication that a one-band Hubbard model considered here might be the correct effective model to describe the $\{Cu_3\}$ molecular magnet.

D. Comparison with other methods

In a recent work, Takeda *et al.*[30] have used a noncollinear approach to estimate the DM interaction. Instead of the use of simple product functions, this work capitalizes on the use of generalized orbitals, which are composed of a linear combination of both spinors with different and variable spatial functions. By using such a representation, it is possible to develop single determinants, which are composed of a linear combination of the chiral spin-1/2 states and the nonchiral spin-3/2 states. For example, the states associated with the system depicted in Fig. 2(a) would be represented according to

$$\begin{aligned}|\psi_{nc\pm}\rangle &= |X_\pm^a X_\pm^b X_\pm^c\rangle \\ &= \frac{1}{2\sqrt{2}}[|\uparrow\uparrow\uparrow\rangle \pm i|\downarrow\uparrow\uparrow\rangle \mp (-1)^{1/6}|\uparrow\downarrow\uparrow\rangle \\ &\quad \mp (-1)^{5/6}|\uparrow\uparrow\downarrow\rangle \mp i|\downarrow\downarrow\downarrow\rangle - |\uparrow\downarrow\downarrow\rangle \\ &\quad + (-1)^{1/3}|\downarrow\uparrow\downarrow\rangle - (-1)^{2/3}|\downarrow\uparrow\downarrow\rangle], \qquad (41)\end{aligned}$$

where $X_+(\theta,\phi) = \cos(\theta/2)|\uparrow\rangle + \exp\{i\phi\}\sin(\theta/2)|\downarrow\rangle$ and $X_-(\theta,\phi) = \sin(\theta/2)|\uparrow\rangle - \exp\{i\phi\}\cos(\theta/2)|\downarrow\rangle$, with $\theta = \pi/2$ and $\phi = \pi/2, 7\pi/2, -\pi/2$. They further claim that $\Delta E_{\text{nc}} = 3\sqrt{3}/4D_z$ [see Eq. (22)] can be estimated by a perturbational treatment of the SOI as follows:

$$\Delta E_{\text{nc}} = \langle\psi_{\text{nc}+}|H_{\text{SOI}}|\psi_{\text{nc}+}\rangle - \langle\psi_{\text{nc}-}|H_{\text{SOI}}|\psi_{\text{nc}-}\rangle, \qquad (42)$$

where H_{SOI} is the one-electron spin-orbit interaction. These expectation values can be calculated by DFT.

It is clear from the expression given by Eq. (41) that the expectation value of the spin-orbit interaction for this and other states would be linear, so, without other considerations, one cannot extract an interaction that depends upon the excitations of interest to the Hubbard Hamiltonian. However, in analogy with the expansion of the many-electron wave function for molecular hydrogen in regions intermediate between the bond-

ing and separated-atom limit, a self-consistent optimization of such a starting determinant allows the spin orbitals to be intermediate between the doubly occupied and singly occupied representations. While the resulting noncollinear wave function is still a single Slater determinant in character, the expansion of the noncollinear state in terms of the Hubbard states would show a wave function comprised primarily of the 8×8 half-filled determinants, but would also contain small contributions of the ionic contributions which are shifted upward by U_{eff}. It is the small admixture of these states that allow Takeda *et al*. to extract both the exchange parameters and the DM interaction through the use of noncollinear representations. This approach could have advantages from an operational viewpoint since it effectively addresses the potential role of other excited states that are routinely excluded from the Hubbard Hamiltonian. However, the precise interactions, which ultimately mediate the appearance of the DM interaction, require additional analysis that is every bit as arduous as that presented here.

An alternative method to calculate the DM vector, based on Andersen's "local force theorem,"[31] was developed by Solovyev *et al*.[32] More recently, this method was utilized in conjunction with DFT to study the DM interaction between magnetic atoms inserted in different crystalline systems and surfaces.[14,33] Essentially, this method expresses the DM vector in terms of the Green's functions of the system, modified by the spin-orbit interaction. Although computationally sophisticated, the Green's function method is physically less transparent than the one adopted here, particularly for a finite system such as triangular SMM, where the crucial ingredients leading to the anisotropic DM exchange can be reduced to a few parameters that have a direct physical interpretation within the Hubbard model.

IV. CONCLUSIONS

We carried out a first-principles investigation of the zero-field splitting of the chiral ground states of a $\{Cu_3\}$ single-molecule magnet (SMM) caused by the Dzyaloshinskii-Moriya interaction. Our approach relies on the perturbative analysis of a Hubbard model, which includes spin-orbit interaction. In the large U limit, appropriate for $\{Cu_3\}$, it is possible to express the Dzyaloshinskii-Moriya constant in terms of the parameters that define the Hubbard model, such as the effective hopping integral between magnetic sites t, the on-site repulsion energy U, and the strength of the spin orbit λ_{SOI}. We then carried out an approximate method to extract the values of these parameters from our spin-density functional theory calculations of the SMM. The value of the Dzyaloshinskii-Moriya constant D that we found is of the order of 0.01 meV, which is a factor of 5 smaller than the value measured experimentally. Given the uncertainty of the experimental result and the fact that other effects might contribute to the zero-field spin splitting of the chiral states, our estimate should be considered consistent with experiment.

The method of computing the DM parameter by effectively extending Anderson's theory of superexchange to include spin-orbit interaction is very close to Moriya's original formulation of anisotropic exchange. It is interesting to note that if we use this approach to calculate the isotropic superexchange constant J of the Heisenberg model describing $\{Cu_3\}$, we obtain a value that is closer to the experimental result than the estimates based on total energy calculations of ferromagnetic vs AFM spin configurations. This seems to suggest that this approach is not only physically very intuitive, but it might also bear promise for good numerical accuracy.

While the methods discussed here provide physical insight into the nature of the DM interaction, we note that for future calculations, it would be desirable to consider excitations that are not normally included in the single-band Hubbard model. A multiband Hubbard model, where additional contributions to the DM interaction are present,[20] could in particular provide a better agreement between the theoretical and experimental values of the DM interaction parameter. For such an approach, it would be necessary to include methodologies that allow for the calculation of all excitations in such systems.

ACKNOWLEDGEMENT

This work was supported by the School of Computer Science, Physics and Mathematics at Linnaeus University, the Swedish Research Council under Grants No. 621-2007-5019 and No. 621-2010-3761, and the NordForsk research network No. 080134 "Nanospintronics: theory and simulations." We would like to thank D. Loss and D. Stepanenko for a very helpful explanation of their Hubbard-model approach to the DM interaction in molecular antiferromagnets. The early parts of this collaboration were supported in part by the NRL.

[1] D. Gatteschi, R. Sessoli, and J. Villain, *Molecular Nanomagnets* (Oxford University Press, Oxford, 2006).
[2] M. N. Leuenberger and D. Loss, Nature (London) **410**, 789 (2001).
[3] J. Lehmann, A. Gaita-Arino, E. Coronado, and D. Loss, Nature Nano **2**, 312 (2007).
[4] M. Trif, F. Troiani, D. Stepanenko, and D. Loss, Phys. Rev. Lett. **101**, 217201 (2008).
[5] J. M. Florez and P. Vargas, J. Magn. Magn. Mater. **324**, 83 (2012).
[6] K.-Y. Choi, Y. H. Matsuda, H. Nojiri, U. Kortz, F. Hussain, A. C. Stowe, C. Ramsey, and N. S. Dalal, Phys. Rev. Lett. **96**, 107202 (2006).
[7] M. F. Islam, J. F. Nossa, C. M. Canali, and M. Pederson, Phys. Rev. B **82**, 155446 (2010).
[8] M. Trif, F. Troiani, D. Stepanenko, and D. Loss, Phys. Rev. B **82**, 045429 (2010).
[9] I. Dzyaloshinskii, J. Phys. Chem. Solids **4**, 241 (1958).
[10] T. Moriya, Phys. Rev. Lett. **4**, 228 (1960).
[11] T. Moriya, Phys. Rev. **120**, 91 (1960).
[12] P. W. Anderson, Phys. Rev. **115**, 2 (1959).
[13] C. F. Hirjibehedin, C.-Y. Lin, A. F. Otte, M. Ternes, C. P. Lutz, B. A. Jones, and A. J. Heinrich, Science **317**, 1199 (2007).
[14] A. N. Rudenko, V. V. Mazurenko, V. I. Anisimov, and A. I. Lichtenstein, Phys. Rev. B **79**, 144418 (2009).

[15]J. Friedel, P. Lenglart, and G. Leman, J. Phys. Chem. Solids. **25**, 781 (1964).
[16]T. A. Kaplan, Z. Phys. B **49**, 313 (1983).
[17]N. E. Bonesteel, T. M. Rice, and F. C. Zhang, Phys. Rev. Lett. **68**, 2684 (1992).
[18]E. Fradkin, *Field Theories of Condensed Matter Systems* (Addison Wesley, Redwood City, 1991).
[19]Note also that the Hamiltonian in Eq. (16) does not mix the GS spin $S = 1/2$ manifold with the excited-state spin $S = 3/2$ multiplet, and leaves the latter unchanged.
[20]J. Yoon and E. J. Solomon, Coor. Chem. Rev. **251**, 379 (2006).
[21]The trinuclear Cu complexes considered in Ref. 20 have geometric and magnetic properties that differ considerably from the $\{Cu_3\}$ molecular magnet considered in this paper. For example, the typical distance between magnetic ions in Ref. 20 is twice as large. Yet the superexchange interaction is almost 10 times larger.
[22]M. R. Pederson and K. A. Jackson, Phys. Rev. B **41**, 7453 (1990).
[23]K. Jackson and M. R. Pederson, Phys. Rev. B **42**, 3276 (1990).
[24]J. P. Perdew, K. Burke, and M. Ernzerhof, Phys. Rev. Lett. **77**, 3865 (1996).
[25]M. Pederson, D. Porezag, J. Kortus, and D. Patton, Phys. Status Solidi B **217**, 197 (2000).
[26]D. Porezag and M. R. Pederson, Phys. Rev. A **60**, 2840 (1999).
[27]M. R. Pederson and S. N. Khanna, Phys. Rev. B **60**, 9566 (1999).
[28]Note that usually the electron affinity is defined as $[E(N) - E(N + 1)]$, where $E(N)$ is the energy of the neutral system.
[29]Y. Furukawa, Y. Nishisaka, K.-i. Kumagai, P. Kögerler, and F. Borsa, Phys. Rev. B **75**, 220402 (2007).
[30]R. Takeda, S. Yamanaka, M. Shoji, and K. Yamaguchi, Int. J. Quantum Chem. **107**, 1328 (2007).
[31]A. R. Machintosh and O. K. Andersen, in *Electrons at the Fermi Surface*, edited by M. Springford (Cambridge University Press, London, 1980), p. 149.
[32]I. Solovyev, N. Hamada, and K. Terakura, Phys. Rev. Lett. **76**, 4825 (1996).
[33]V. V. Mazurenko and V. I. Anisimov, Phys. Rev. B **71**, 184434 (2005).

7

Electric control of spin states on frustrated triangular molecular magnets

Electric control of spin states in frustrated triangular molecular magnets

J. F. Nossa,[1,2] M. Fhokrul Islam,[1] C. M. Canali,[1] and M. R. Pederson[3]

[1] *Department of Physics and Electrical Engineering, Linnaeus University, SE-39182 Kalmar, Sweden*

[2] *Solid State Physics/The Nanometer Structure Consortium, Lund University, Box 118, SE-221 00 Lund Sweden*

[3] *Office of Basic Energy Sciences, SC22.1, U.S. Department of Energy, 1000 Independence Ave. SW Washington, DC 20585-1290*

(Dated: August 5, 2013)

Frustrated triangular molecular magnets are a very important class of magnetic molecules. External electric fields can couple to the spin chirality of such molecules. The coupling exists even in the absence of spin-orbit interaction. Spin-electric coupling in these molecular magnets (MMs) represents a very efficient and fast way of manipulating the magnetic states of the MM. This manipulation can be achieved via a localized electric field generated, e.g., by a nearby Scanning Tunneling Microscope tip, with possible applications in quantum information processing. The efficiency of this coupling depends on the electric dipole moment between chiral states. In this paper we report on first-principles calculations of spin-electric coupling in several triangular molecules. We discuss the underlying mechanism leading to an enhanced coupling, which can be used as a convenient guide to synthesize MMs that can respond more efficiently to an external electric field.

I. INTRODUCTION

The ability to manipulate spins of a system by an external field is one of the central issues addressed in spintronics. Traditionally, magnetic fields are used for controlling magnetic states. But the efficient manipulation of spins by an external magnetic field at nanoscale level has significant drawbacks. The quantum manipulation of spins in this regime has to be performed at very small spatial ($\sim$ nm) and temporal ($\sim$1 ns) scales. This requires large magnetic fields and high spatial resolution, which is very difficult to achieve.

An alternative to the magnetic field is to apply an electric field for spin manipulation. However, since spin does not couple to the electric field directly, the electric manipulation of spins requires the presence of strong spin-orbit coupling. In a system with strong spin-orbit interaction (SOI) an electric field can modify orbitals which in turn can change the spin states since spin states are coupled to the orbitals through the SOI. The electric control of spins through spin-orbit coupling has been studied in magnetic semiconductors since spin-orbit coupling is stronger in such systems.[1] Multiferroic compounds are another class of systems where spin-electric coupling is intensely investigated because of their strong magnetoelectric effects.[2–4]

Since SOI scales with the size of the system, it is very weak in molecular magnets (MMs). Thus, electric control of the spins through SOI is inefficient and hence, alternative approaches are being investigated. It has recently been shown that electric control of magnetization is possible in some di-cobaltocene-based molecules.[5] However, in this work we focus on a different class of MMs, namely spin frustrated MMs with triangular symmetry where electric control of spin states can be achieved through the chirality of the system.[6,7] The lack of inversion symmetry in such systems allows the spins to couple with electric field to linear order.

The strength of the coupling between spin chiral states and external electric fields is a crucial quantity as it is responsible for the efficiency of this mechanism in these systems. Calculation of the coupling constant by *ab*-initio methods is a challenging task. We have developed a method for calculating the coupling strength and have previously applied to a $\{Cu_3\}$ MM.[8] However, it is not yet clear what kind of molecules have strong spin-electric coupling.

To address this issue, in this work, we have calculated spin-electric coupling in several triangular MMs. To investigate the dependence of spin-electric coupling on different types of magnetic atoms, distances between magnetic centers and exchange paths between magnetic atoms. We have chosen three different MMs: $K_{12}[(VO)_3(BiW_9O_{33})_2\cdot 29H_2O$[9] (hereafter $\{V_3\}$) and $\{Cu_3\}Cl_3N_6C_9H_9O$[10] (hereafter $\{Cu_3O\}$) triangular MMs, which have three magnetic centers. We also study a $K_6[V_{15}As_6O_{42}(H_2O)]8H_2O$ MM[11] (hereafter $\{V_{15}\}$) which has fifteen magnetic atoms.

The spin-electric coupling in triangular molecules is achieved through the chirality of the ground state of these molecules. Construction of the chiral ground states for $\{V_3\}$ and $\{Cu_3O\}$ MMs is rather simple as only three magnetic centers are involved. On the other hand, the construction of chiral states for the

$\{V_{15}\}$ MM requires some generalization as it involves fifteen magnetic centers. In this work we also describe a method for constructing the chiral states of the $\{V_{15}\}$ molecule and the calculation of spin-electric coupling in generalized chiral states.

The organization of this paper is as follows. In section II we describe the mechanism of spin-electric coupling in frustrated anti-ferromagnetically ordered MMs with D_{3h} symmetry. In section III we discuss the electronic structures of the three molecules we have investigated in this work and finally in section IV we discuss the results of our calculations.

II. SPIN-ELECTRIC COUPLING VIA CHIRAL STATES

The lower energy regime of a spin frustrated triangular molecular magnet (MM) is composed of two two-fold degenerate chiral states. Based on a spin model and symmetry properties of the triangular molecule, one can demonstrate that electric fields can couple states of opposite chirality but with the same spin through the spin induced dipole moment.[6,7]

The strength of the spin-electric dipole coupling constant, d, determines the effectiveness of the manipulation of the spin states by electric fields. A precise estimate of this strength constant cannot be obtained analytically and has to be determined by *ab*-initio calculations or through experiments.

In this section we first describe the generalization of chiral states in a MM of fifteen magnetic centers called $\{V_{15}\}$ MM (see Fig. 1). Chiral states have usually been well defined for a three-site triangular MM such a $\{Cu_3\}$.[8] We then derive an expression for the spin-electric coupling in the generalized $\{V_{15}\}$ MM chiral states.

The unique cluster anion $\{V_{15}\}^{13}$ contains fifteen V^{IV} ions (S_i=1/2). It exhibits layers of different magnetization. There are two hexagon layers sandwiching a triangular central belt layer. The isotropic Heisenberg exchange Hamiltonian for the $\{V_{15}\}$ MM can be written as

$$H_{\rm H} = \sum_{\langle i,j\rangle}^{15} J_{ij}\mathbf{s}_i \cdot \mathbf{s}_j \ , \quad J_{ij} > 0 \ , \tag{1}$$

where J_{ij} is the Heisenberg exchange parameter between the spins $\mathbf{s}_i$ and $\mathbf{s}_j$.

The the size of the Hilbert space for this molecule is $2^{15} = 32768$. To obtain all the spin states of the system one needs to diagonalize the Hamiltonian in this large basis set. To study the spin-electric coupling in $\{V_{15}\}$, we need to focus only on the $S_z = 1/2$ ground state subspace. Since total spin projection S_z of the system commutes with the Hamiltonian, we can express it in block diagonal form and work only in the $S_z = 1/2$ subspace.

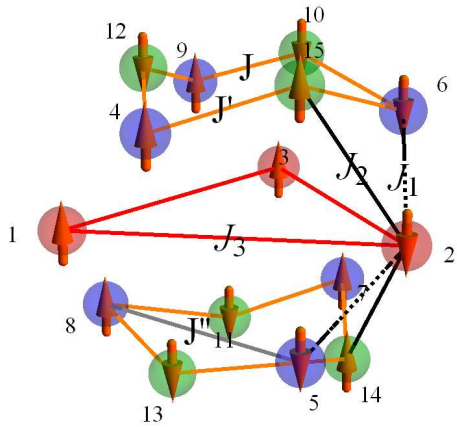

FIG. 1. (Color online) Spin structure of one of the ground state spin configurations of the $\{V_{15}\}$ molecular magnet (MM). There are six exchange parameters in this molecule, namely, J_1, J_2, J_3, J, J' and J''. These parameters have been calculated previously by *ab*-initio methods.[12]

By diagonalizing the Hamiltonian in the $S_z = 1/2$ subspace we obtain a two-fold degenerate ground state. It contains only 1200 different spin configurations that have spin projection zero on the hexagon layers of the molecule (see blue and green balls in Fig. 1). Only 1/3 of these spin configurations are associated with each of the three 1/2-spin triangular configurations at the central belt layer (see red balls in Fig. 1). In addition, for each of the three spin configurations of the central triangle only 64 hexagon spin configurations are related by C_3 symmetry. These last 192 spin states contribute about 99.9% to the total $S_z = 1/2$ ground state. The two real solutions of the ground state are:

$$\psi_1^R = \sum_{i=1}^{64}(a_{1i}\,|h_i duu\rangle + b_{1i}\,|h_i duu\rangle + c_{1i}\,|h_i duu\rangle)$$
$$\psi_2^R = \sum_{i=1}^{64}(a_{2i}\,|h_i duu\rangle + b_{2i}\,|h_i duu\rangle + c_{2i}\,|h_i duu\rangle) \tag{2}$$

where h_i's are different hexagon configurations for each spin arrangement of the central triangle $|duu\rangle$, $|udu\rangle$ and $|uud\rangle$. Here u and d stand for up and down

spin, respectively and a_{ji}, b_{ji}'s are real coefficients.

To construct the chiral operator for this system we note that the exchange parameters for different pairs shown in Fig. 1 are J=290.3, J'=222.7, J''=15.9, J_1=13.8, J_2=23.4 and J_3=0.55 meV[12]. Clearly, the exchange interaction between the pairs in the central triangle is much weaker compared to the exchange interaction between other pairs. Therefore, the low energy magnetic structure is determined by the three magnetic sites at the central triangle of the $\{V_{15}\}$ molecule. The chiral operator for this system can be defined only by these three sites as

$$C_z = \frac{4}{\sqrt{3}}\mathbf{s}_1 \cdot \mathbf{s}_2 \times \mathbf{s}_3 \ . \tag{3}$$

Since the chiral operator, C_z, defined in Eq. (3) commutes with the spin Hamiltonian in Eq. (1), they share common eigenstates. We have obtained the chiral states by diagonalizing the chiral operator in the basis of real ground states, Eq. (2), that gives,

$$\begin{aligned}\Psi_1 &= \psi_1^R + i\psi_2^R \\ \Psi_2 &= \psi_1^R - i\psi_2^R\end{aligned} \tag{4}$$

Substituting Eq. (2) in Eq. (4), and after some algebra we obtain,

$$\begin{aligned}\Psi_1 &= \sum_{i=1}^{64} a_i(|h_i duu\rangle + \omega\,|h_i' duu\rangle + \omega^2\,|h_i'' duu\rangle) \\ \Psi_2 &= \sum_{i=1}^{64} b_i(|h_i duu\rangle + \omega^2\,|h_i' duu\rangle + \omega\,|h_i'' duu\rangle)\end{aligned} \tag{5}$$

Here, $\omega = e^{\frac{i2\pi}{3}}$ and a_i,b_i are complex coefficients. Note that Ψ_1 and Ψ_2 are states of opposite chirality. An external electric field can couple these states through the induced dipole moment.

Alternatively, we can treat the effect of the chiral operator as a small perturbation and diagonalize the Hamiltonian,

$$H_{\rm H} = \sum_{\langle i,j\rangle}^{15} J_{ij}\mathbf{s}_i \cdot \mathbf{s}_j \ + \lambda C_z; \quad J_{ij} > 0 \ , \tag{6}$$

in the basis of 1200 spin configurations of $S_z = 1/2$ subspace and obtain the same chiral ground state as above.

Spin-electric coupling in the $\{V_{15}\}$ MM

An external electric field couples states of opposite chirality but same spin. Therefore, we are interested in calculating the matrix element

$$\left\langle \Psi_1 \left| e\vec{E}\cdot\vec{r} \right| \Psi_2 \right\rangle = e\vec{E}\cdot\langle\Psi_1|\,\vec{r}\,|\Psi_2\rangle = e\vec{E}\cdot\vec{d}\,. \tag{7}$$

Substituting Eq. (5) in Eq. (**??**), we obtain

$$\begin{aligned}\vec{d} &= \sum_{i=1}^{64} a_i^* b_i\,(\langle h_i duu\,|\vec{r}\,|\,h_i duu\rangle + \omega\,\langle h_i' udu\,|\vec{r}\,|\,h_i' udu\rangle \\ &\quad \omega^2\,\langle h_i'' uud\,|\vec{r}\,|\,h_i'' uud\rangle) \\ &= \sum_{i=1}^{64} a_i^* b_i(\vec{p}_i^{\,duu} + \omega\,\vec{p}_i^{\,udu} + \omega^2\vec{p}_i^{\,uud}) \\ &= \sum_{i=1}^{64} a_i^* b_i\,\vec{p}_i\end{aligned} \tag{8}$$

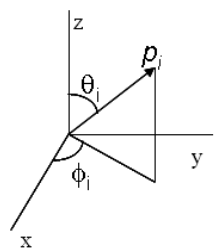

FIG. 2. Dipole moment of a spin configuration.

The magnitude of $\vec{p}_i^{\,duu}$, $\vec{p}_i^{\,udu}$ and $\vec{p}_i^{\,uud}$ are the same because of the C_3 symmetry. Thus, we can express $\vec{p}_i$ as (see Fig.2)

$$\begin{aligned}\vec{p}_i &= p_i[\sin\theta_i\cos\phi_i\widehat{x} + \sin\theta_i\sin\phi_i\widehat{y} \\ &\quad +\omega\sin\theta_i\cos(\phi_i+\alpha)\widehat{x} + \omega\sin\theta_i\sin(\phi_i+\alpha)\widehat{y} \\ &\quad +\omega^2\sin\theta_i\cos(\phi_i+2\alpha)\widehat{x} + \omega^2\sin\theta\sin(\phi+2\alpha)\widehat{y}] \\ &= p_i\sin\theta_i[\{\cos\phi_i + \omega\cos(\phi_i+\alpha) + \omega^2\cos(\phi_i+2\alpha)\} \\ &\quad \widehat{x} + \{\sin\phi_i + \omega\sin(\phi_i+\alpha) + \omega^2\sin(\phi_i+2\alpha)\}\widehat{y}] \\ &= \frac{3}{2}p_i\sin\theta_i[\{\cos\phi_i - i\sin\phi_i\}\widehat{x} + \{\sin\phi_i + i\cos\phi_i\}\widehat{y}].\end{aligned}$$

Therefore,

$$\begin{aligned}e\vec{E}\cdot\vec{d} &= \frac{3e}{2}\sum_{i=1}^{64} a_i^* b_i p_i\sin\theta_i[\{\cos\phi_i - i\sin\phi_i\}E_x \\ &\quad +\{\sin\phi_i + i\cos\phi_i\}E_y] \\ &= \frac{3}{2}eE\sum_{i=1}^{64} a_i^* b_i p_i\sin\theta_i[\{\cos\phi_i - i\sin\phi_i\} \\ &\quad +\{\sin\phi_i + i\cos\phi_i\}],\end{aligned}$$

where we have assumed $E_x = E_y$. The strength of the spin-electric coupling is then

$$|\overrightarrow{d}| = \frac{3}{2}\left|\sum_{i=1}^{64} a_i^* b_i p_i \sin\theta_i [\{\cos\phi_i + \sin\phi_i\} + i\{\cos\phi_i - \sin\phi_i\}]\right|. \quad (9)$$

For triangular MMs with three magnetic centers such as $\{Cu_3\}$, $\{V_3\}$ etc., only three spin configurations are involved and they contribute equally to the ground state. Thus, Eq. (9) reduces to[8]

$$d = \frac{p}{\sqrt{2}} \quad (10)$$

III. ELECTRONIC STRUCTURE OF TRIANGULAR MOLECULAR MAGNETS

In this work we have investigated three molecular magnets (MMs), namely, $\{V_3\}$, $\{Cu_3O\}$ and $\{V_{15}\}$. Here we present the electronic structure of these molecules. Our results show that a spin model of three exchange-coupled spin $s = 1/2$ is useful to understand the magnetic properties of triangular MMs. However, all the other atoms in the molecule are essential for its geometrical stability and for the resulting superexchange interaction among the spins at the magnetic sites. Therefore, for a proper *ab*-initio description of the molecule, these atoms must be included to a certain extent in the calculations.

Our theoretical studies were performed with the all-electron Gaussian-orbital-based NRLMOL (Refs. 14 and 15). All calculations employed Gaussian basis set to solve the Kohn-Sham equations using Perdew-Burke-Ernzerhof[16] (PBE) generalized gradient approximation (GGA) for the exchange-correlation potential. Full basis sets were used for all atoms except for tungsten, for which we have used pseudo potentials. Prior to geometry relaxation, an initial net total spin configuration for the triangular core were assigned to S=3/2. Self-consistency were reached when the total energy is converged to 10^{-6} Hartree or less. After optimization, the net spin were changed to S=1/2.

A. $\{V_3\}$

The model of $\{V_3\}$ MM used in this calculation consists of 104 atoms. The molecule has D_{3h} symmetry with three V^{4+} ions forming an equilateral triangle as shown in Fig. 3. The structure of the molecule is identical to that of $\{Cu_3\}$ MM[8] except that the distance between V ions in this case is 5.69 Å, which is larger than the separation between Cu ions in $\{Cu_3\}$ MM.

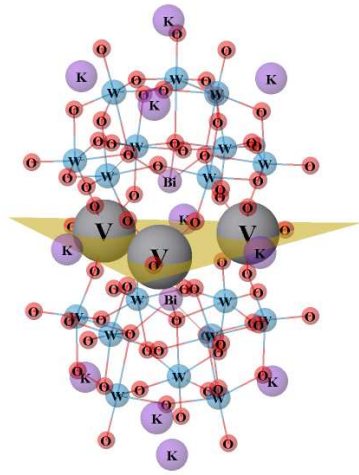

FIG. 3. (Color online) Ball and stick model of $\{V_3\}$ molecular magnet with chemical composition $K_{12}[(VO)_3(BiW_9O_{33})_2{\cdot}29H_2O$.[9]

The three V^{4+} ions are the sites of three identical s=1/2 quantum spins. The frontier electrons on each of these sites are primarily of d character. Fig. 4 shows the density of states (DOS) of $\{V_3\}$ MM where highest occupied molecular orbital (HOMO) and lowest unoccupied molecular orbital (LUMO) are dominated by V d electrons. The inset figure shows the DOS close to the HOMO-LUMO close to the Fermi energy. The energies of the minority spin highest occupied orbital (HOMO) and lowest unoccupied molecular orbital (LUMO) levels are found to be -4.16 and -4.03 eV, respectively, while the majority spin HOMO and LUMO levels are found to be -6.01 and -3.96 eV, respectively. The majority-minority and minority-majority spin flips gaps (0.20 and 1.97 eV, respectively) are both positive, which ensures that the system is stable with respect to the total magnetic moment. The ground state of the molecule is antiferromagnetic with total spin $S = 1/2$. The exchange constant, defined as proportional to the difference between the ground $S = 1/2$ energy, E_{duu}, and the first excited $S = 3/2$ energy, E_{uuu}, is $J = 2(E_{uuu} - E_{duu})/3 \approx 1.2$ meV.

The magnetic interactions among the magnetic ions in a molecule might be of the direct exchange or superexchange type. Interactions mediated through direct overlap of electronic orbitals are called direct exchange. The exchange interaction between d elec-

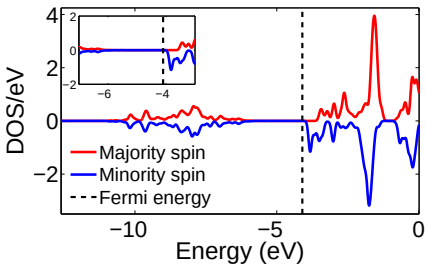

FIG. 4. Majority and minority density of states for the $\{V_3\}$ ring. Inset figure inset shows the density of states close to the HOMO-LUMO.

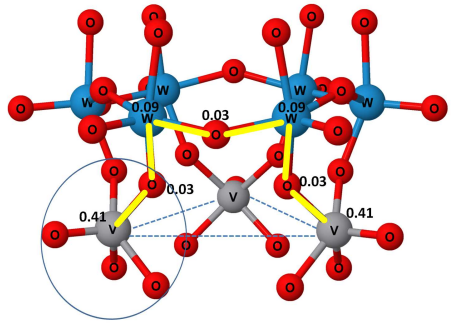

(a)

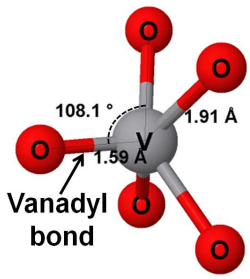

(b)

FIG. 5. (Color online) a) Superexchange coupling between two V atoms. The yellow line connecting two V atoms shows the superexchange path through three O and two W atoms. The numbers near the atoms are the magnetic moment (in units of μ_B) of the corresponding atoms along the superexchange path. Local VO_5 complex is marked by a blue circle. b) Local square-pyramid coordination polyhedra of a V^{4+} atom.

trons of two V in $\{V_3\}$ MM is mediated either by an intermediate oxygen ion, V-O-V, or by more complicated exchange paths involving other non-magnetic atoms such a V-O-W-O-W-O-V shown by yellow line in Fig. 5(a). Superexchange interaction through two or more non-magnetic ions is also called by some authors super-super-exchange.[17] We will, however, refer to it simply as superexchange.

Qualitative relationships for signs and values of spin exchange interactions, for simple systems, were first developed by Goodenough[18,19], and extended by Kanamori.[20] The strengths of the superexchange interactions can be estimated in terms of the angle sustained in the V-O-V bond and the symmetry properties of the vanadium d orbitals. Superexchange involving more non-magnetic ions, such a V-O-W-O-W-O-V path shown in Fig. 5(a), is far from being a trivial problem. So far there are no such qualitative rules for predicting the magnitude and sign of this interactions. In some cases a longer-path superexchange interaction through non-magnetic atoms can be even stronger than the direct superexchange interactions.[21]

In order to understand the magnetic properties and superexchange path of the $\{V_3\}$ MM we note that the local crystal field symmetry of V ions are of square-pyramidal as shown in Fig. 5(b). The vanadyl (VO^{2+}) bond, apex of the pyramid, is 1.59 Å, while the other, almost co-planar, V-O bonds are 1.91-1.94 Å. The d-orbitals of the V ion split into different energy levels under the influence of this crystal field. In the ground state of a V^{4+} ($3d^1$) ion in a pyramidal crystal field (distorted octahedral[22]) containing a vanadyl bond, the unbounded electron is placed in the d_{xy} orbital of t_{2g} subspace(see Fig. 6).

The energy gap Δ_1 between the non-degenerate orbital d_{xy} and the the first degenerated excited state, d_{yz} or d_{xz} orbitals, is much larger than k_BT.[23] The spatial location of the d_{xy} orbital is perpendicular to the vanadyl bond, see Fig. 5(b). The overlap between the d_{xy} orbitals of the V^{4+} and the surrounding equatorial p orbitals of the oxygen atoms is of π-type. The d-orbital energies are shown in Fig. 4. The dominant magnetic interactions take place through these equatorial atoms while the interaction with the apical oxygen atom is expected to be much weaker.

The magnitude and sign of the resulting magnetic superexchange interaction between V^{4+} ions is much more complicated than in the case of cuprates like Cu^{2+} compounds. In the later, the unbounded electron is placed in the $d_{x^2-y^2}$ orbital, which takes part in the σ-bond between copper and oxygen. Thus, the overlap and angle involved in the exchange path are

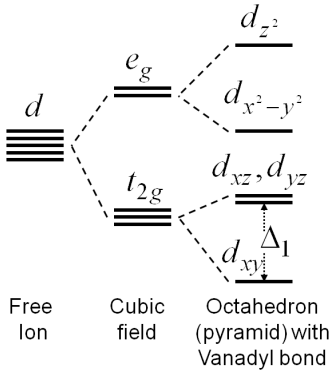

FIG. 6. Crystal field splitting of d-orbitals for the cubic field and octahedron symmetry.

clearly well defined. On the other hand, the π-bond between d_{xy} of V^{4+} and surrounding oxygen ions is less well defined because its overlap strongly depends of the relative orientations between the vanadium ion and the surrounding oxygen ions.

B. $\{Cu_3\}$O

The structure of the $\{Cu_3O\}$ molecular magnet (MM)(see Fig. 7) consists of a Cu equilateral triangular cluster with Cu^{4+}-Cu^{4+} separation of 3.29 Å, with one oxygen at the center of the molecule. The distance between a Cu atom and O atom is 1.9 Å.

The three cation Cu^{2+} atoms are the sites of three identical s=1/2 quantum spins. The frontier electrons on each of these sites are primarily of d character. The density of states is shown in Fig. 8. The energies of the minority spin HOMO and LUMO levels are found to be at -6.62 and -6.09 eV, respectively, while the majority spin HOMO and LUMO levels are found to be at -6.46 and -5.44 eV, respectively. As in the $\{V_3\}$ MM case, the majority-minority and minority-majority spin flips gaps (1.18 and 0.37 eV, respectively) are both positive, which ensures that the system is stable with respect to the total magnetic moment. The ground state of the molecule is antiferromagnetic with total spin $S = 1/2$. The energy difference $E_{S=3/2} - E_{S=1/2} \approx 14meV$ is in agreement with the experiment,[24] Thus, the exchange constant is $J \approx 9.3$ meV

The magnetic interactions in $\{Cu_3O\}$ is mediated along the superexchange path involving one oxygen atom is Cu-O-Cu. The Cu-Cu bond length is 3.29Å, Cu-O 1.9 Å, Cu-N 1.9 Å, angle Cu-O-Cu is 120° (See

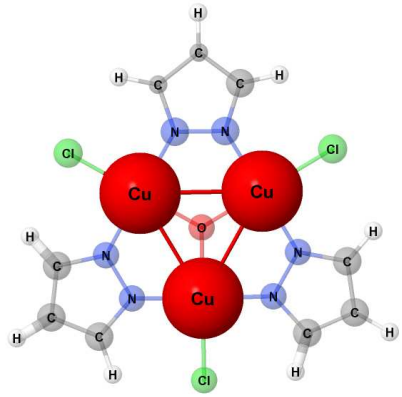

FIG. 7. (Color online) $\{Cu_3\}Cl_3N_6C_9H_9O^{10}$ molecular magnet (MM). Cu-Cu bond length is 3.29Å, Cu-O 1.9 Å, Cu-N 1.9 Å, angle Cu-O-Cu is 120°.

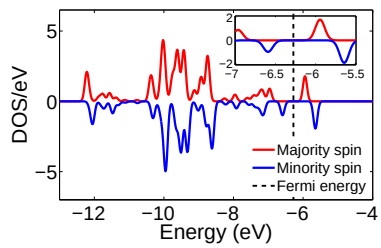

FIG. 8. Majority and minority density of states for the $\{Cu_3O\}$ molecular magnet (MM). Inset figure inset shows the density of states close to the HOMO-LUMO.

Fig. 7). The superexchange interaction depends both of the O bridging atom and Cu-O-Cu angle. It has been shown that manipulation of the Cu-O-Cu angle produces transitions from antiferromagnetic to ferromagnetic exchange.[25] It also has been demonstrated that the more flatted the $\{Cu_3O\}$ bridge, i.e., Cu-O-Cu angle $\approx 120°$, the stronger the magnetic interaction is.[24,26]

C. V_{15}

The chemical composition of the $\{V_{15}\}$ molecular magnet (MM), synthesized by Gatteschi *et al* Ref. 11, is $K_6[V_{15}As_6O_{42}(H_2O)]8H_2O$. It has 15 spin $s = 1/2$ transition metal atom V as shown in Fig. 9(a), which are the magnetic centers of the molecule.

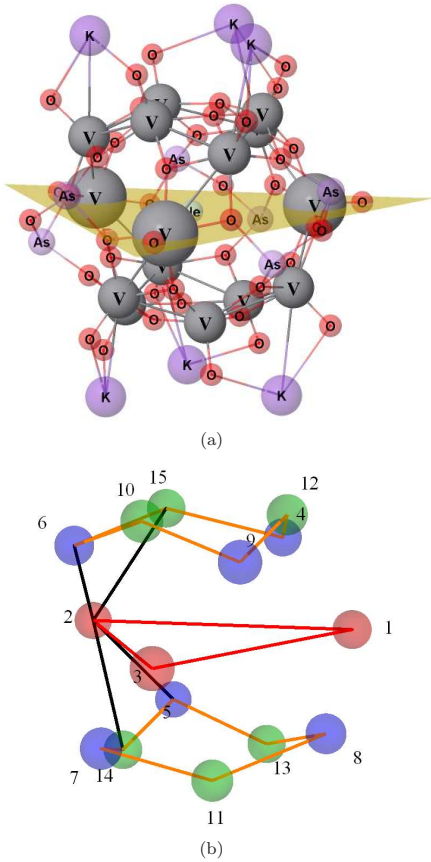

FIG. 9. (Color online) Spin structure of the $\{V_{15}\}$ molecular magnet (MM). Three V atoms are placed in a central triangle sandwiched by two distorted hexagons.

As shown in Fig. 9(b), $\{V_{15}\}$ MM has three V atoms at the central region forming an equilateral triangle (red balls). The rest of the 12 atoms form two hexagons, one above and one below the triangle. However, the hexagons are slightly distorted. Let us consider the upper hexagon. Three of the atoms (blue upper balls), lay down in a triangular plane slightly below the other three atoms of the hexagon (green upper balls). The same applies to the lower hexagon. $\{V_{15}\}$ MM does not have σ_h symmetry operation but the atoms in the upper hexagon are related to the corresponding atoms in the lower hexagon by S_3 symmetry. Thus, $\{V_{15}\}$ has D_3 symmetry.

Although $\{V_{15}\}$ has fifteen V atoms, it can be viewed as a combination of three pentanuclear subsystems. Each system consists of one V atom in the central belt and two pairs V-V from the upper and lower hexagons. For example, in Fig. 9(b), a subsystem consists of the balls numbered as 2, 5, 6, 14 and 15. The atoms of this pentanuclear subsystem are connected by a black line.

At low temperatures, the total magnetic moment of the ions on the hexagons are quenched due to the strong antiferromagnetic coupling between them. Thus, only the spin of the V in the central belt is active and it determines the spin of the whole subsystem. Therefore, the subsystem can be considered as an effective quasi-particle of spin $s = 1/2$ placed on the corner of a central triangle (ball number 2 for the subsystem connected by black lines). As a consequence, the entire molecule can be viewed as a an effective trinuclear system of spins $s = 1/2$.[13] This model of an effective three magnetic sites makes $\{V_{15}\}$ a perfect candidate for spin-electric coupling just as $\{Cu_3\}$, $\{V_3\}$ and $\{Cu_3O\}$ MMs.

Note that although the magnetic ions on the hexagons do not contribute to the magnetic moment of the molecule, they are involved in the superexchange path between subsystems. Similarly, the construction of the chiral ground states of this molecule, which is necessary for spin-electric coupling, involves all of them (see Sec. II).

IV. RESULTS AND DISCUSSION

The *ab*-initio calculations of exchange parameters and strength of spin-electric coupling for different triangular molecular magnets investigated in this work is summarized in Table I.

Mol	dis (Å)	J (meV)	d (a.u.)	Maj HL (eV)	Min HL (eV)
$\{Cu_3O\}$	3.29	9.3	9.78×10^{-3}	1.02	0.53
$\{Cu_3\}$	4.88	3.7	2.56×10^{-4}	0.72	0.69
$\{V_3\}$	5.70	1.3	3.56×10^{-2}	0.21	0.17
$\{V_{15}\}$	7.00	1	4.07×10^{-3}	1.12	1.11

TABLE I. Exchange constant J, dipole d, distance between magnetic centers *dis*, Majority HOMO-LUMO gap and minority HOMO-LUMO gap for several molecular magnets (MMs).

We can note from Table I that the exchange constants of these molecular magnets (MMs), as expected, decreases exponentially as the distance between the magnetic centers increases. Shorter superexchange path between Cu atoms in $\{Cu_3O\}$

results in strongest exchange coupling among the molecules investigated in this work.

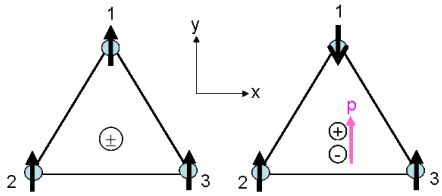

FIG. 10. Cartoon of the spin induced dipole moment in triangular molecular magnets.

The differences in spin-electric coupling between different molecules, as discussed in section II, depends on the *spin induced* dipole moments of the three spin configurations associated with $S_z = 1/2$. Their magnitudes are same due to symmetry. When the molecule is in the $S_z = 3/2$ configuration, the center of the positive and the negative charges coincide, resulting in zero dipole moment. On the other hand, if one of the spins is flipped, charges are redistributed which gives rise to a net displacement of positive and negative charge centers as shown in Fig. 10. Therefore, the average charge at a site may be different from 1.

We have carried out a calculation of the charge density of the *uuu* and *duu* spin configurations for the $\{Cu_3\}$, $\{V_3\}$ and $\{Cu_3O\}$ molecules (see Fig. 11). First, we calculated the *uuu* total charge density, $q(uuu)$. Then, we flipped one spin (Up to Down in Fig. 11) and calculated the *duu* total charge density, $q(duu)$. Finally, we calculated the difference

$$\delta q = q(uuu) - q(duu) \tag{11}$$

Our results show a charge redistribution when one spin is flipped. This leads to the appearance of a $spin - induced$ dipole moment. In Fig. 11 blue (red) color corresponds to excess (lack) of charge. From Fig. 11c) and d), we can see that for the $\{V_3\}$ MM there is much more concentration of blue regions, where excess of charge exists. This visible charge redistribution leads to a stronger dipole moment on $\{V_3\}$ MM. It is also interesting to notice that the colorful charge redistribution shows the superexchange path of the molecule (see yellow path in Fig. 5(a) and 11). Therefore, this simple model could be used to calculate superexchange paths and more importantly to predict which molecules have stronger spin-electric coupling.

The microscopic origin of charge redistribution and appearance of dipole moment in triangular 1/2-

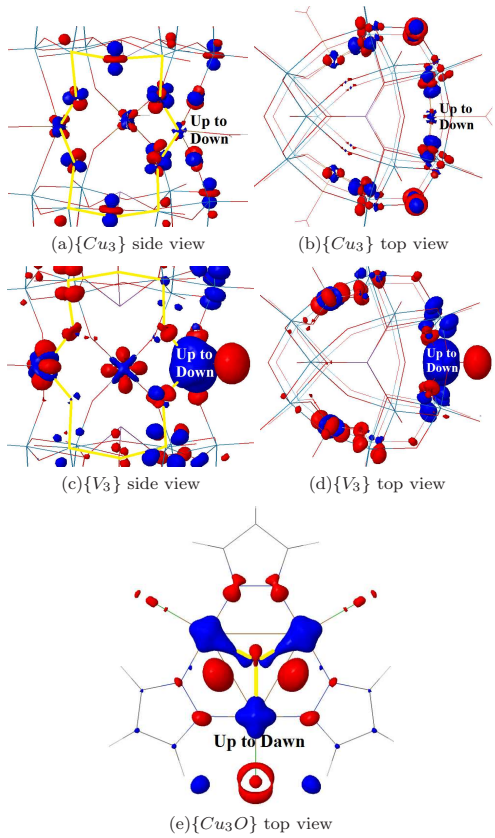

(a)$\{Cu_3\}$ side view (b)$\{Cu_3\}$ top view

(c)$\{V_3\}$ side view (d)$\{V_3\}$ top view

(e)$\{Cu_3O\}$ top view

FIG. 11. (Color online) Charge redistribution of the $\{Cu_3\}$, $\{Cu_3\}$ and triangular molecular magnets (MMs). Once one spin up from the *uuu* spin configuration is flipped, a charge redistribution occurs. Blue (red) color corresponds to excess (lack) of charge.

spin molecules can be understood from the Hubbard model. As shown by Bulaevskii *et al*[27] and Khomskii *et al*[28,29], the charge redistribution at a magnetic site i of a triangular molecule is related to the Hubbard model parameters by

$$\delta q_i = 8\left(\frac{t}{U}\right)^3 [\mathbf{S}_i\cdot(\mathbf{S}_{i+1}+\mathbf{S}_{i+2}) - 2\mathbf{S}_{i+1}\cdot\mathbf{S}_{i+2}] \tag{12}$$

where U is on-site interaction energy, t is the hopping parameter of the Hubbard model and $\mathbf{S}_i$ is the spin operator on site i. The *spin induced* dipole mo-

ment is given by

$$p_x = 12ea\left(\frac{t}{U}\right)^3 \mathbf{S}_1 \cdot (\mathbf{S}_2 - \mathbf{S}_3)$$
$$p_y = 4\sqrt{3}ea\left(\frac{t}{U}\right)^3 (\mathbf{S}_1 \cdot (\mathbf{S}_2 + \mathbf{S}_3) - 2\mathbf{S}_2 \cdot \mathbf{S}_3) \quad (13)$$

Clearly, the charge redistribution and thus, the *spin induced* dipole moment depend on the ratio, t/U. The result is consistent with the dipole coupling between two chiral states obtained by Trif *et al.*[30]

An approximate approach to extract these Hubbard model parameters by *ab*-initio methods is discussed in the appendix. Using this approach we have calculated the parameters $U_{\{Cu_3\}} = 9.06$ eV, $t_{\{Cu_3\}} = 50$ meV, $U_{\{V_3\}} = 1$ eV, $t_{\{V_3\}} = 53$ meV. The corresponding dipole coupling are $d_{\{Cu_3\}} = 3.48 \times 10^{-5}$ au and $d_{\{V_3\}} = 3.93 \times 10^{-3}$ au for $\{Cu_3\}$ and $\{V_3\}$ MMs, respectively. The coupling strength obtained from Hubbard model parameters is about one order of magnitude smaller than that obtained directly from *ab*-initio calculations. However, we note that the ratio of the coupling strengths is same in both cases. The difference in the strength is probably due to approximate nature of these calculations.

While we have not calculated coupling strength of $\{V_{15}\}$ MM from Hubburd model, our DFT calculations show that spin-electric coupling is weaker in $\{V_{15}\}$ compared to $\{V_3\}$. As shown in table I, the distance between V atoms in $\{V_{15}\}$ is larger compared to the same atoms in $\{V_3\}$, resulting in weaker hopping parameter, t. Since U parameter is not expected to be different, we can conclude from Eqs. 13 that coupling is weaker in $\{V_{15}\}$.

V. SUMMARY

In this work we have calculated the spin-electric coupling strength for different triangular molecular magnets (MMs), such as $\{Cu_3O\}$, $\{V_3\}$ and $\{V_{15}\}$ using first-principles method. Among these MMs, $\{V_3\}$ has the largest spin-electric coupling constant, d. Our results show that spin-electric coupling in $\{V_3\}$ is two order and in $\{V_{15}\}$ and $\{Cu_3O\}$ are one order of magnitude larger than $\{Cu_3\}$.

In these triangular systems an electric field can couple states of opposite chirality but of same spin. While construction of chiral states in $\{V_3\}$ and in $\{Cu_3O\}$ is rather straightforward as only three spin configurations are involve, the construction of chiral states in $\{V_{15}\}$ is more complicated due to fifteen magnetic centers present in this MM. In this work we have generalized the construction of chiral states for $\{V_{15}\}$ that has D_3 symmetry. We have calculated the effect of the chiral operator on these states and have also showed how the generalized chiral states are coupled by an external electric field.

We have carried out calculations of the charge redistribution in triangular MMs. This charge redistribution occurs when one spin is flipped in a triangular MM to form a total S=1/2 state. We have shown that a simple method of calculating the charge redistribution could lead to the determination of the superexchange path in such systems. This method also could be used as a fingerprint in the search of MMs with strong spin-electric coupling.

Appendix: Hubbard Model Parameters

Here we discuss the method employed to extract Hubbard model parameters from *ab*-initio calculations.[?]

1. Calculation of the Hubbard U

The most common approach for calculating U involves calculation of energy, E, of the molecule with N, $N+1$ and $N-1$ electron and extracting U from the equation below,

$$\begin{aligned} U &= E(N+1) + E(N-1) - 2E(N) \\ &= [E(N+1) - E(N)] - [E(N) - E(N-1)] \\ &= A - I \, . \end{aligned} \quad (A.1)$$

In the above equation A is (minus) the electron affinity[31] and I is the ionization energy. For systems that are not closed shell, such as those considered here, the U value is essentially the second derivative of energy with respect to charge and it is possible to determine U by calculating the energy as a function of charge.

For the single-band Hubbard-model corresponding to the the molecules studied here, we are interested in obtaining energies for the charge-transfer excitations involving the transfer of a localized d-electron on one ion site to a localized d-electron on another site. Specifically we wish to know the energy of $|X\rangle = |\uparrow_a\downarrow_a\uparrow_c\rangle$ relative to $|\uparrow_a\downarrow_b\uparrow_c\rangle$. There are a total of twelve charge-transfer excitations that can be made with one-site doubly occupied and one electron on one of the other sites. For the half-filled case of interest here, the energy difference depends upon the electron affinity of the state on site a, the ionization energy of the state on site b and the residual long-range coulomb interaction between the negatively charged electron added to site a and the positively charged hole that is left behind on site b. Since

site b and site a are equivalent, it follows that we simply need to calculate U for any one of the magnetic sites in the half filled case.

For the molecules investigated in this work, we have chosen to calculate U quasi-analytically by gradually adding (or subtracting) a small fraction of electronic charge δq to one of the half-filled magnetic d-states. The energy of the $\{V_3\}$ molecular magnet as a function of δq is shown in Fig. 12. We can see that it can be well reproduced by a quadratic fitting curve. The figure show that, upon adding a fractional charge to a localized orbital, the total energy initially decreases, since the orbital energy is negative. Eventually, however, the competing Coulomb repulsion takes over and the net change in total energy for adding one electron to a localized orbital is positive. In contrast, with one extra electron delocalized throughout the molecule the total energy is usually smaller than the energy of the neutral molecule.

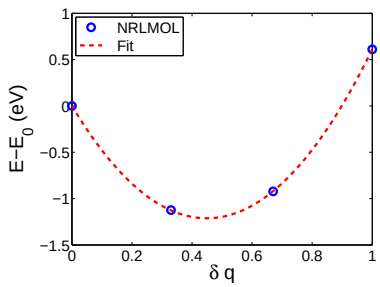

FIG. 12. Dependence of the total energy on added fractional charge δq for $\{V_3\}$ molecular magnet. The (blue) circle represent the results of NRLMOL calculations and the dashed (red) line represents a quadratic fit.

The difference in the energy of the system before and after adding a fraction of electronic charge δq is given by $\Delta E = U_{eff} = U\delta q^2 - e^2\delta q^2/R_{\text{Cu-Cu}}$, where $U = \partial^2 E(q)/\partial q^2$. We have calculated the effective parameter U_{eff} by setting $\delta q = 1$:

$$U_{eff} = \delta q^2 \left(\frac{\partial^2 E(q)}{\partial q^2} - \frac{e^2}{R_{\text{Cu-Cu}}} \right) \qquad \text{(A.2)}$$

where $E(q) = E_0 + (U/2)(q - q_0)^2$ with E_0 being a constant.

2. Calculation of t

The Hubbard model approach is based on allowing the localized electrons to hop to its nearest neighbor sites and in the present work these localized electrons are d electrons. Therefore, for calculating hopping parameter t, the relevant states are those d electron states that lie close to the Fermi level. Let $|K, \alpha\rangle$ be the three relevant Kohn-Sham eigenstates calculated from NRLMOL. We can write them as a linear combination of the localized atomic orbitals, centered at the three magnetic sites, $\{|\phi_a\rangle, |\phi_b\rangle, |\phi_c\rangle\} \otimes |\chi_\alpha\rangle$, with $\alpha = \uparrow, \downarrow$ for spin up and down, respectively:

$$|K, \alpha\rangle = \sum_i C^i_{K\alpha} |\phi_i\rangle |\chi_\alpha\rangle \ . \qquad \text{(A.3)}$$

where $C^i_{K\alpha}$ is the weight of the localized $|\phi_i\rangle |\chi_\alpha\rangle$ wavefunction.

For the $|\uparrow\uparrow\uparrow\rangle$ spin configuration the relevant three levels around the Fermi level are doubly and singly degenerate. These levels are sketched in Fig. 13

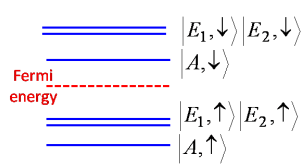

FIG. 13. Schematic diagram of the Kohn-Sham energy levels around the Fermi level

We obtain the level structure by diagonalizing the three-site Hamiltonian:

$$H_0 = \varepsilon_0 \sum_i |\phi_i\rangle \langle\phi_i| - t \sum_{i \neq j} |\phi_i\rangle \langle\phi_j| \ , \qquad \text{(A.4)}$$

where ε_0 is the on-site energy, t is the hopping term and $i, j = a, b, c$ represent the copper sites. We get the eigenvalues $\varepsilon_0 + t$ and $\varepsilon_0 - 2t$ for the two-fold and one-fold degenerate states, respectively. The Kohn-Sham eigenvectors can be defined as a linear combination of the localized wavefunctions,

$$\begin{aligned} |E_1, \uparrow\rangle &= \frac{1}{\sqrt{2}} \left(|\phi_a\rangle - |\phi_b\rangle \right) |\uparrow\rangle \ , \\ |E_2, \uparrow\rangle &= \frac{1}{\sqrt{6}} \left(|\phi_a\rangle + |\phi_b\rangle - 2\,|\phi_c\rangle \right) |\uparrow\rangle \ , \\ |A, \uparrow\rangle &= \frac{1}{\sqrt{3}} \left(|\phi_a\rangle + |\phi_b\rangle + |\phi_c\rangle \right) |\uparrow\rangle \ . \end{aligned} \qquad \text{(A.5)}$$

Now the localized states can be written in term of

the Kohn-Sham functions

$$
\begin{aligned}
|\phi_a\rangle\,|\uparrow\rangle &= \frac{|A,\uparrow\rangle}{\sqrt{3}} + \frac{|E_1,\uparrow\rangle}{\sqrt{2}} + \frac{|E_2,\uparrow\rangle}{\sqrt{6}}\,,\\
|\phi_b\rangle\,|\uparrow\rangle &= \frac{|A,\uparrow\rangle}{\sqrt{3}} - \frac{|E_1,\uparrow\rangle}{\sqrt{2}} + \frac{|E_2,\uparrow\rangle}{\sqrt{6}}\,,\\
|\phi_c\rangle\,|\uparrow\rangle &= \frac{|A,\uparrow\rangle}{\sqrt{3}} - 2\frac{|E_2,\uparrow\rangle}{\sqrt{6}}\,.
\end{aligned}
\tag{A.6}
$$

Our calculations showed that these states are primarily localized on the V and Cu atoms and have d character. We have obtained the Kohn-Sham eigenenergies for the one-fold and two-fold degenerate states

$$
\begin{aligned}
\langle E_1,\uparrow|\,H_0\,|E_1,\uparrow\rangle &= \frac{1}{2}\left(\langle\phi_a| - \langle\phi_b|\right) H_0 \left(|\phi_a\rangle - |\phi_b\rangle\right)\\
&= \varepsilon_0 + t\,,\\
\langle A,\uparrow|\,H_0\,|A,\uparrow\rangle &= \frac{1}{3}\left(\langle\phi_a| + \langle\phi_b| + \langle\phi_c|\right) H_0\\
&\quad \left(|\phi_a\rangle + |\phi_b\rangle + |\phi_c\rangle\right)\\
&= \varepsilon_0 - 2t\,.
\end{aligned}
\tag{A.7}
$$

From Eqs. (A.7) we can finally evaluate the value of the parameter t as:

$$
t = \frac{1}{3}\left(\langle E_1,\uparrow|\,H_0\,|E_1,\uparrow\rangle - \langle A,\uparrow|\,H_0\,|A,\uparrow\rangle\right). \tag{A.8}
$$

ACKNOWLEDGMENT

This work was supported by the School of Computer Science, Physics and Mathematics at Linnaeus University, the Swedish Research Council under Grants No: 621-2007-5019 and 621-2010-3761, and the NordForsk research network 080134 "Nanospintronics: theory and simulations".

[1] D. Chiba, M. Sawicki, Y. Nishitani, Y. Nakatani, F. Matsukura, and H. Ohno, Nature **455**, 515 (2008).
[2] W. Kleemann, Physics **2**, 105 (2009).
[3] D. Lebeugle, A. Mougin, M. Viret, D. Colson, and L. Ranno, Phys. Rev. Lett. **103**, 257601 (2009).
[4] K. T. Delaney, M. Mostovoy, and N. A. Spaldin, Phys. Rev. Lett. **102**, 157203 (2009).
[5] N. Baadji, M. Piacenza, T. Tugsuz, F. D. Sala, G. Maruccio, and S. Sanvito, Nat. Mater. **8**, 813 (2009).
[6] M. Trif, F. Troiani, D. Stepanenko, and D. Loss, Phys. Rev. Lett. **101**, 217201 (2008).
[7] M. Trif, F. Troiani, D. Stepanenko, and D. Loss, Phys. Rev. B **82**, 045429 (2010).
[8] M. F. Islam, J. F. Nossa, C. M. Canali, and M. Pederson, Phys. Rev. B **82**, 155446 (2010).
[9] T. Yamase, E. Ishikawa, K. Fukaya, H. Nojiri, T. Taniguchi, and T. Atake, Inorg. Chem. **43**, 8150 (2004).
[10] P. A. Angaridis, P. Baran, R. Boca, F. Cervantes-Lee, W. Haase, G. Mezei, R. G. Raptis, and R. Werner, Inorg. Chem. **41**, 2219 (2002).
[11] D. Gatteschi, L. Pardi, A. L. Barra, A. Muller, and J. Doring, Nature **354**, 463 (1991).
[12] J. Kortus, C. S. Hellberg, and M. R. Pederson, Phys. Rev. Lett. **86**, 3400 (2001).
[13] R. Winpenny, *Molecular Cluster Magnets* (World Scientific Publishing Co. Pte. Ltd., 2012).
[14] M. R. Pederson and K. A. Jackson, Phys. Rev. B **41**, 7453 (1990).
[15] K. Jackson and M. R. Pederson, Phys. Rev. B **42**, 3276 (1990).
[16] J. P. Perdew, K. Burke, and M. Ernzerhof, Phys. Rev. Lett. **77**, 3865 (1996).
[17] M.-H. Whangbo, H.-J. Koo, and D. Dai, *Special issue on The Impact of Theoretical Methods on Solid-State Chemistry*, Journal of Solid State Chemistry **176**, 417 (2003).
[18] J. B. Goodenough, Phys. Rev. **100**, 564 (1955).
[19] J. B. Goodenough, Journal of Physics and Chemistry of Solids **6**, 287 (1958).
[20] J. Kanamori, Journal of Physics and Chemistry of Solids **10**, 87 (1959).
[21] H.-J. Koo, M.-H. Whangbo, P. D. VerNooy, C. C. Torardi, and W. J. Marshall, *Inorganic Chemistry*, Inorg. Chem. **41**, 4664 (2002).
[22] M. Schindler, F. C. Hawthorne, and W. H. Baur, *Chemistry of Materials*, Chem. Mater. **12**, 1248 (2000).
[23] C. J. Ballhausen and H. B. Gray, *Inorganic Chemistry*, Inorg. Chem. **1**, 111 (1962).
[24] R. J. Butcher, C. J. O'Connor, and E. Sinn, *Inorganic Chemistry*, Inorg. Chem. **20**, 537 (1981).
[25] R. Boca, L. Dlh, G. Mezei, T. Ortiz-Prez, R. G. Raptis, and J. Telser, *Inorganic Chemistry*, Inorg. Chem. **42**, 5801 (2003).

[26] S. Ferrer, F. Lloret, E. Pardo, J. M. Clemente-Juan, M. Liu-Gonzlez, and S. Garca-Granda, *Inorganic Chemistry*, Inorg. Chem. **51**, 985 (2011).
[27] L. N. Bulaevskii, C. D. Batista, Mostovoy, M. V., and D. I. Khomskii, Phys. Rev. B **78**, 024402 (2008).
[28] D. Khomskii, J. Phys. Condens. Matter **22**, 164209 (2010).
[29] D. Khomskii, Nat. Commun. (2012), 10.1038/ncomms1904 (2012).
[30] M. Trif, F. Troiani, D. Stepanenko, and D. Loss, Phys. Rev. B **82**, 045429 (2010).
[31] Note that usually, the electron affinity is defined as $[E(N) - E(N+1)]$, where $E(N)$] is the energy of the neutral system.

8

Electric control of a Fe4 single-molecule magnet in a single-electron transistor

Electric control of a $\{Fe_4\}$ single-molecule magnet in a single-electron transistor

J. F. Nossa,[1,2] M. Fhokrul Islam,[1] C. M. Canali,[1] and M. R. Pederson[3]

[1] *Department of Physics and Electrical Engineering, Linnaeus University, SE-39182 Kalmar, Sweden*

[2] *Solid State Physics/The Nanometer Structure Consortium, Lund University, Box 118, SE-221 00 Lund Sweden*

[3] *Office of Basic Energy Sciences, SC22.1, U.S. Department of Energy, 1000 Independence Ave. SW Washington, DC 20585-1290*

(Dated: March 15, 2013)

Using first-principles methods we study theoretically the properties of an individual $\{Fe_4\}$ single-molecule magnet (SMM) attached to metallic leads in a single-electron transistor geometry. We show that the conductive leads do not affect the spin ordering and magnetic anisotropy of the neutral SMM. On the other hand, the leads have a strong effect on the anisotropy of the charged states of the molecule, which are probed in Coulomb blockade transport. Furthermore, we demonstrate that an external electric potential, modeling a gate electrode, can be used to manipulate the magnetic properties of the system. For a charged molecule, by localizing the extra charge with the gate voltage closer to the magnetic core, the anisotropy magnitude and spin ordering converges to the values found for the isolated $\{Fe_4\}$ SMM. We compare these findings with the results of recent quantum transport experiments in three-terminal devices.

I. INTRODUCTION

In recent years molecular spintronics has emerged as one of the most active areas of research within magnetism at the atomic scale.[1–6] Progress in the field is driven in part by advances in chemical design and synthesis, which allow the realization of interesting magnetic molecules with desired electronic and magnetic properties. A second essential feature of ongoing research is the improved ability of integrating individual magnetic molecules into solid-state nano-electronic devices.

Typically magnetic molecules have long spin-relaxation times, which can be utilized in high-density information storage. They are also usually characterized by a weak hyperfine interaction with the environment, resulting in long spin coherence times, which is an essential property for applications in quantum information processing. Single-molecule magnets (SMMs) are a special class of spin-ordered and/or magnetically active molecules characterized by a relatively high molecular spin and large magnetic anisotropy energy.[7] The latter lifts the spin degeneracy even at zero magnetic field, and favors one particular alignment of the spin, making the molecule a nanoscale magnet.

One of the goals of molecular spintronics is to address the magnetic states of individual magnetic molecules with electric fields and electric currents. In the last six years experimental efforts toward this goal have considered different classes of magnetic molecules and strategies to incorporate them into electric nano-circuits. A particularly interesting direction focuses on quantum transport in a single-electron transistor (SET), a three-terminal device where a SMM bridges the nanogap between two conducting nano-leads, and can further be electrically manipulated by the gate voltage of a third nearby electrode. In the regime of weak coupling to the leads, the electric charge on the central SMM is quantized and can be controlled by the external gate. When Coulomb blockade is lifted by either gate or bias voltages, transport occurs via tunneling of single electrons in and out of the SMM. Therefore a study of transport in this geometry can provide detailed information on the magnetic properties of individual SMMs, both when the molecule is neutral and when it is electrically charged.

Early SET experiments on SMMs[8,9] focused on the archetypal SMM $\{Mn_{12}\}$-acetate[7,10], characterized by the ground-state spin $S = 10$ and a large magnetic anisotropy barrier of approximately 50 K. Unfortunately these experiments and studies of self-assembled molecules on gold surfaces[11] have shown that the magnetic properties of $\{Mn_{12}\}$ complexes are extremely fragile and easily disrupted when the molecule is attached to metallic leads or surfaces.

More recently, another class of SMMs, namely the tetranuclear $\{Fe_4\}$ molecule, has emerged as a candidate in molecular spintronics that does not suffer the drawbacks of $\{Mn_{12}\}$. The properties of $\{Fe_4\}$ in its neutral state are well studied in the crystal phase[12,13], and include a molecular ground-state spin $S = 5$ and an intermediate magnetic anisotropy barrier ≈ 15 K. In contrast to what happens with $\{Mn_{12}\}$, these magnetic characteristics remain stable when the molecule is deposited on a gold surface.[14,15] Furthermore, its tripodal ligands

are shown to be advantageous for the preparation of single-molecule electronic devices. Indeed, recent three-terminal quantum transport experiments[16–18], with $\{Fe_4\}$ as the central island of a SET, show that this molecule behaves indeed as a nanoscale magnet, even when it is wired to metallic leads. The magnetic anisotropy is significantly affected by adding or subtracting single charges to the molecule[16], an operation that can be performed reversibly with the gate voltage. More refined techniques[18] allow the extraction of the magnetic anisotropy of the neutral and charged molecule from the transport measurements with unprecedented accuracy.

In this paper we carry out density functional theory (DFT) calculations to evaluate the magnetic properties of a $\{Fe_4\}$ connected to gold electrodes and under the effect of an external electric field representing a gate voltage. The geometry considered here is supposed to model the typical situation realized in current SET experiments, although some details might be different. The main aim of our work is to investigate theoretically how the spin ordering and the magnetic anisotropy of $\{Fe_4\}$ are affected by weak coupling to the leads, both when the molecule is in its neutral state and when a single charge is added to or subtracted from the device. A second important objective of the paper is a theoretical analysis of how these magnetic properties can be modified and controlled by means of an external electric potential representing a gate electrode.

Although a full-fledged first-principles study of quantum transport is beyond the scope of the present paper, as we explain below, we believe that our analysis of the charged states under the effect of an external electric field is useful to develop methods to compute the tunneling conductance within a master equation formalism. Ref. 19 introduced a DFT description of the neutral and charged states of an *isolated* $\{Mn_{12}\}$ SMM, which were then used in a master equation formalism for quantum transport. Here the coupling to the leads was treated with phenomenological tunneling amplitudes taken form experiment. In Ref. 20 charge transport was studied by means of a non-equilibrium Green's function approach, which included the presence of metallic leads in the regime of strong coupling. Transport calculations carried out in the same transport regime but based on microscopic tight-binding models have also been considered.[21] This approach has the drawback that charging effects, essential for the description of SET experiments, cannot be adequately incorporated.

In this sense the present paper is a further contribution to these early attempts to use first-principles methods based on DFT to investigate quantum transport in a SET with a SMM. We are aware that the use of DFT can be problematic when it comes to describing the electronic structure and Fermi level alignment of molecules coupled to external electrodes, particularly when charged states are involved. Assessing the limitations of DFT in this context is also a technical aim of the present paper. In this regard, we discuss potential uncertainties in the relative level alignment of the electrode and molecular states.

The main findings of our analysis are the following. The SMM $\{Fe_4\}$ in its neutral state is indeed quite robust against the presence of metallic leads: both spin ordering and magnetic anisotropy are essentially identical to the one of the isolated molecule. For the case of a charged molecule, the effect of the leads is more complex. Our calculations show that the extra charge tend to reside primarily on the ligands between molecule and metallic leads, and only minimally on the magnetic core. As a result the addition of electrons affects the magnetism of molecule (specifically the magnetic anisotropy) considerably less than when the molecule is isolated. We find that an external gate voltage can be used to localize the extra charge closer to the central magnetic core, and in this case the magnetic characteristics of the device converge to the ones of the isolated $\{Fe_4\}$ SMM.

The organization of this paper is as follows. In Sec. II we present an overview of the theoretical and computational approach employed in this work. The electronic and magnetic properties of different charge states of the isolated $\{Fe_4\}$ SMM is discussed in Sec. III. The effects of the metallic leads on the properties of the molecule are discussed in Sec. IV. In Sec. V we discuss how a confining electric potential affects the magnetic properties of the molecule. In Sec. VI we compare the results of our calculations with recent SET transport experiments. Finally in Sec. VII we summarize our results.

II. THEORETICAL BACKGROUND

A. Spin Hamiltonian and the giant-spin model

In a first approximation, the exchange interaction between the magnetic ions of a molecular magnet can be described by an isotropic Heisenberg model

$$H = \sum_{ij} J_{ij} \mathbf{s}_i \cdot \mathbf{s}_j \ , \tag{1}$$

where $\mathbf{s}_i$ is the spin of the magnetic ion i and the constants J_{ij} describe the super-exchange coupling

between ions i and j. Clearly, the validity of Eq. (1) relies crucially on the assumption that each magnetic ion is characterized by a well-defined quantum spin, localized at the ion position. There might be cases where the spin-polarization of the molecule is delocalized, where this assumption may break down. Such cases are especially probable when an excess tunneling electron is present. Once the exchange constants are known, the Hamiltonian can be diagonalized. Since H is a sum of scalars in spin space, it commutes with the total spin $\mathbf{S}$. Therefore the eigenvalues of $\mathbf{S}^2$ and S_z can be used to label the eigenstates of H.

In the case of single-molecule magnets, the ground state (GS) of Eq. (1) is characterized by a relatively large spin S, and it is separated by a fairly large energy $\Delta J \equiv \mathrm{Max}_{\{ij\}}\left[J_{ij}\right]$ from excited states with different total spins. Thus, at low energies $< \Delta J$ the magnetic molecule behaves effectively as an atom with a relatively large spin S, known as *'giant spin'*. The approximation of restricting to the lowest spin multiplet is known as *giant-spin model*. According to Eq. (1), each spin multiplet is degenerate. In the next section we will discuss how spin-orbit interaction lifts this degeneracy, splitting the $2S+1$ states of the GS multiplet.

Note that the ground-state spin S is not always the maximum value $S_{\max}$ allowed by Eq. (1). Due to the presence of antiferromagnetic components, the most common situation encountered in SMMs is an intermediate value $1 < S < S_{\max}$, which quasi-classically corresponds to a ferrimagnetic spin configuration. Below we will show how all the physical quantities entering in the spin Hamiltonian of Eq. (1) and the value of the giant spin S can be calculated within DFT.

B. Spin-orbit interaction and magnetic anisotropy barrier

Spin-orbit interaction introduces terms to Eq. (1) that break rotational invariance in spin space. Up to second-order perturbation theory, these terms, besides anisotropic corrections to the Heisenberg model, include the antisymmetric Dzyaloshinskii-Moriya spin exchange, and the single-ion magnetic anisotropy $H_{ia} = -\sum_i (\mathbf{d}_i \cdot \mathbf{s}_i)^2$. Because of these terms, the total spin is no longer a good quantum number. Within the giant-spin model of SMMs, where the isotropic exchange is the dominant magnetic interaction, the main effect of the spin-orbit interaction is to lift the spin degeneracy of the GS multiplet. To second-order perturbation theory, this can be described by the following anisotropy Hamiltonian for the giant spin operator $\mathbf{S} = (S_x, S_y, S_z)$

$$\mathcal{H} = DS_z^2 + E(S_x^2 - S_y^2)\,. \tag{2}$$

The parameters D and E specify the axial and transverse magnetic anisotropy, respectively. If $D < 0$ and $|D| >> |E|$, which are defining properties for SMMs, the system exhibits an easy axis in the z-direction. In the absence of magnetic field, and neglecting the small transverse anisotropy term, the GS of Eq. (2) is doubly degenerate and it corresponds to the eigenstates of S_z with eigenvalues $\pm S$. To go from the state $S_z = +S$ to the state $S_z = -S$ the system has to surmount a magnetic anisotropy energy barrier $\Delta E = |D|S^2$. In addition, transitions which change the axial quantum numbers require some type of carrier to balance the change in spin. When the transverse term is not negligible and S_z is not a good quantum number, we can still define an anisotropy barrier separating the two (degenerate) lowest energy levels as the energy difference between GS energy and the energy of the highest excited state. If $D > 0$ the systems has a quasi-easy plane perpendicular to the z-axis without energy barrier.

The anisotropy parameters D and E can be calculated within a self-consistent-field (SCF) one-particle theory (e.g. DFT or Hartree Fock), by including the contribution of the spin-orbit interaction. Here we summarize the main steps of the procedure originally introduced in Ref. 22. (For more recent reviews see Refs. 23 and 24.)

The starting point are the matrix elements of the spin-orbit interaction (SOI) operator

$$U(\mathbf{r}, \mathbf{p}, \mathbf{s}) = -\frac{1}{2c^2}\mathbf{s} \cdot \mathbf{p} \times \boldsymbol{\nabla}\Phi(\mathbf{r}) \tag{3}$$

($\mathbf{p}$ is the momentum operator; $\mathbf{s}$ is the electron spin operator; Φ is the Coulomb potential and c is the speed of light), taken with respect to the unperturbed single-particle spinor wave functions $|\psi_{k\sigma}\rangle = |\phi_{k\sigma}\rangle|\chi_\sigma\rangle$, which are solutions of the SCF-approximation Schrödinger equation

$$H|\psi_{k\sigma}\rangle = \epsilon_{k\sigma}|\psi_{k\sigma}\rangle \tag{4}$$

Here $\phi_{k\sigma}(\mathbf{r}) \equiv \langle \mathbf{r}||\phi_{k\sigma}\rangle$ is the orbital part of the wavefunction; the two-component spinors $|\chi_\sigma\rangle$, $\sigma = (1, 2)$ are the eigenstates of $\mathbf{s}\cdot\hat{\mathbf{n}}$, where the unit vector $\hat{\mathbf{n}} = \hat{\mathbf{n}}(\theta, \varphi)$ is an arbitrary quantization axis.

The matrix elements can be written as[22]

$$\begin{aligned} U_{k\sigma,k'\sigma'} &= \langle \psi_{k\sigma}\,|\, U(\mathbf{r}, \mathbf{p}, \mathbf{s})\,|\,\psi_{k'\sigma'}\rangle \\ &= -i\sum_i \langle \phi_{k\sigma}|\, V_i\,|\phi_{k'\sigma'}\rangle\, \langle \chi_\sigma|\, s_i\,|\chi_{\sigma'}\rangle\ , \end{aligned} \tag{5}$$

where the matrix elements of the operator $\mathbf{V} = (V_x, V_y, V_z)$ are defined as

$$\langle \phi_{k\sigma} | V_x | \phi_{k'\sigma'} \rangle = \frac{1}{2c^2} \left(\left\langle \frac{\partial \phi_{k\sigma}}{\partial z} \middle| \Phi \middle| \frac{\partial \phi_{k'\sigma'}}{\partial y} \right\rangle - \left\langle \frac{\partial \phi_{k\sigma}}{\partial y} \middle| \Phi \middle| \frac{\partial \phi_{k'\sigma'}}{\partial z} \right\rangle \right) \quad (6)$$

and cyclical. Note that Eq. (6) avoids the time-consuming calculation of the gradient of the Coulomb potential, replacing it with the calculation of the gradient of the basis functions in which $\phi(\mathbf{r})$ is expanded. The above representation of the spin-orbit interaction arises by an integration by parts of the matrix element defined in Eq. (6). It is similar to the form of spin-orbit interaction that comes out of the Dirac equation.

In the absence of an external magnetic field, the first-order perturbation-theory correction to the *total GS energy* cause by the SOI is zero because of time-reversal symmetry. The second-order correction is nonzero and can be written as

$$\Delta_2 = \sum_{\sigma\sigma'} \sum_{i,j} M_{ij}^{\sigma\sigma'} s_i^{\sigma\sigma'} s_j^{\sigma'\sigma} \,, \quad (7)$$

where

$$s_i^{\sigma\sigma'} \equiv \langle \chi_\sigma | s_i | \chi_{\sigma'} \rangle \,, \quad (8)$$

and

$$M_{ij}^{\sigma\sigma'} \equiv - \sum_{k=\mathrm{occ}} \sum_{k'=\mathrm{unocc}} \frac{\langle \phi_{k\sigma} | V_i | \phi_{k'\sigma'} \rangle \langle \phi_{k'\sigma'} | V_j | \phi_{k\sigma} \rangle}{\epsilon_{k\sigma} - \epsilon_{k'\sigma'}} \,, \quad (9)$$

where the sums over k and k' involve occupied and unoccupied states, respectively.

Eq. (7) is the central equation in the study of the magnetic anisotropy. Since the spin matrix elements $s_i^{\sigma\sigma'}$ depend on the orientation of the arbitrary axis of quantization $\hat{\mathbf{n}}$, so does also the total energy shift. This is precisely the origin of the magnetic anisotropy brought about by SOI.

We now consider the case of a closed-shell molecule, a system with a well defined HOMO-LUMO gap in order to avoid problems with partial occupancy, with ΔN excess of majority spin electrons.

We have the important relation

$$\langle \chi_1 | s_i | \chi_1 \rangle = - \langle \chi_2 | s_i | \chi_2 \rangle = \frac{\langle S_i \rangle}{\Delta N} \quad (10)$$

where $\langle S_i \rangle$ is the GS expectation value of the i^{th}-component of the total spin of the system for the given choice of the quantization axis. On the basis of our discussion of the giant-spin model, $\langle S_i \rangle$ can be re-interpreted as the expectation values of the components of the giant-spin operator $\mathbf{S}$ for the spin-coherent state $|S, \hat{\mathbf{n}}\rangle$ with $S = \Delta N/2$.

Using the resolution of the identity in spin space, $\sum_\sigma |\chi_\sigma\rangle \langle \chi_\sigma| = 1$, we can write

$$\begin{aligned} &\langle \chi_1 | s_i | \chi_2 \rangle \langle \chi_2 | s_j | \chi_1 \rangle = \\ &\langle \chi_1 | s_i s_j | \chi_1 \rangle - \langle \chi_1 | s_i | \chi_1 \rangle \langle \chi_1 | s_j | \chi_1 \rangle \\ &= \langle \chi_1 | s_i s_j | \chi_1 \rangle - \frac{\langle S_i \rangle \langle S_j \rangle}{(\Delta N)^2} \end{aligned} \quad (11)$$

and a similar expression for $\langle \chi_2 | s_i | \chi_1 \rangle \langle \chi_1 | s_j | \chi_2 \rangle$.

With the help of Eqs. (10), (11) and $\langle \chi_\sigma | (s_i)^2 | \chi_\sigma \rangle = 1/4$, Eq. (7) takes the form

$$\Delta_2 = \alpha + \sum_{ij} \gamma_{ij} \langle S_i \rangle \langle S_j \rangle \,, \quad (12)$$

where $\alpha = \sum_{ij} (M_{ii}^{12} + M_{ii}^{21})$ is a constant independent of the quantization axis. The anisotropy tensor γ_{ij} is given by

$$\gamma_{ij} = \frac{1}{(\Delta N)^2} \sum_{ij} (M_{ij}^{12} + M_{ij}^{22} - M_{ij}^{12} - M_{ij}^{21}) \quad (13)$$

The tensor γ_{ij} can now be diagonalized by a unitary transformation and Δ_2 becomes

$$\Delta_2 = \alpha + A(\langle S'_x \rangle)^2 + B(\langle S'_y \rangle)^2 + C(\langle S'_z \rangle)^2 \quad (14)$$

$$= \alpha + A \langle (S'_x)^2 \rangle + B \langle (S'_y)^2 \rangle + C \langle (S'_z)^2 \rangle \quad (15)$$

where A, B, C are the eigenvalues of γ_{ij} and the S'_i are the three spin components rotated along its three principal axis (Eq. (15) follows from Eq. (14) thanks to the properties of spin coherent states).

This expression for Δ_2 is exactly the expectation value $\langle S, \hat{\mathbf{n}} | \mathcal{H} | S, \hat{\mathbf{n}} \rangle$ of the quantum spin Hamiltonian

$$\mathcal{H} = \alpha + A(S'_x)^2 + B(S'_y)^2 + C(S'_z)^2 \,, \quad (16)$$

in the spin coherent state $|S, \hat{\mathbf{n}}\rangle$. Eq. (16) is equivalent to Eq. (2) up to an irrelevant constant.

The perturbative method described here works well for systems with a large HOMO-LUMO gap. However, for systems that have nearly degenerate and not fully occupied HOMO levels, which often is the case for charged molecules, the perturbative approach breaks down, since some of the energy denominators in Eq. (9) vanish. To avoid this problem the magnetic anisotropy can alternatively be calculated by an exact diagonalization method. In this approach, the solutions of the one-particle Schrödinger equation in the SCF approximation (which does not include SOI), are used to construct a finite matrix representation of the SOI,

which is then diagonalized exactly. The matrix is then diagonalized subject to the constraint that the resulting spin is aligned along a give choice of the quantization axis. The resulting single-particle solutions $\{\epsilon'_k, |\psi'_k\rangle = \sum_\sigma |\phi'_{k\sigma}\rangle|\chi_\sigma\rangle\}$ are used to compute the trace of the system as a function of direction of the quantization axis (or average direction of the magnetization). In Ref.[25], a discussion of the relationship between the second-order variation in the trace and the self-consistent second-order variation of total energy is presented.

Once one has obtained the trace as a function of axis of quantization, one can use relatively standard techniques to decompose the trace into a spherical harmonic representation and then determine the magnetic principal axes. Alternatively by choosing magnetic principal axes that are equivalent to those predicted from the second-order expressions, it is always possible to directly compare exact-diagonalization results with the second-order results. Using exact diagonalization, One can further extract parts of the fourth- and higher-order anisotropy terms as well. However, since self-consistency and other terms also affect the magnetic anisotropy at fourth-order and beyond, the exact diagonalization results are primarily used to determined whether the second-order results are expected to be stable and a good approximation to experiment. In cases where near degeneracies occur at the Fermi level, the second-order and exact-diagonalization results can be very different especially if the states near the Fermi level are coupled by the spin-orbit interaction. For such cases, a much more careful analysis of results is needed and it is reasonable to expect that some degree of self-consistency with non-collinear capabilities will be needed.

For electronic-structure methods, such as NRL-MOL, where the wavefunctions are expanded in terms of atom-centered localized basis functions the second-order perturbative method allows one to further analyze the anisotropy Hamiltonian on an atom-by-atom basis. By expanding the Kohn-Sham orbitals ($|\phi_{k\sigma}\rangle$) in Eq. (9) in terms of the atom-centered basis, the second-order expression (Eq. (7)) can be decomposed into a sum over four centers.[26] The super-diagonal terms (all center indices the same) can then be used to determine an anisotropy Hamiltonian associated with each atom. In Ref.[26], this decomposition has been used to verify the perpendicular hard-axis alignment model in the Co_4 easy-plane magnetic molecule. In Ref.[27], Baruah's method was used to demonstrate that essentially all of the magnetism in Mn_{12}-acetate was due to the outer eight S=2 crown Mn ions, and that the sum of the single-ion anisotropies was very close to the total anisotropy. Further the degree to which non-additivity occurred was explained by a canting of the atom projected anisotropy axes relative to the global anisotropy axis.

To complete the discussion about second-order anisotropy Hamiltonians, derived either perturbatively or via exact diagonalization, it is important to note a contribution to van Wullen and coworkers.[28,29]. Van Wullen noted that once a method is used to determine the spin-orbit energy as a function of axis of quantization that an additional quantum correction is needed to determine the parameter's D and E in the anisotropy Hamiltonian. For example, the $M_s = 0$ eigenstate is not aligned with an axis of quantization along the x-axis, the y-axis or any other axis. Therefore more care must be taken to determine D once the classical energy as a function of expectation value of $\mathbf{S}$ is known. Accounting for this correction changes the definition of D, as originally derived by Pederson and Khanna, by a factor of $(S+1/2)/S$. While this correction is small in the large S limit, it can be important for systems with lower spin.

C. Computational details

In this paper we use a self-consistent field approximation based on density-functional theory (DFT). A review of this approach in the study of molecular magnets can be found in Ref.[24]. Here we remind a few key features that are relevant for the present work.

In a DFT calculation of a magnetic molecule, we obtain the total energy of the system for specially prepared spin symmetry-breaking metastable states. In many cases these are ferrimagnetic spin configurations, suggested by experiment. The energies of these different metastable states can then be compared and the lowest-energy spin configuration determined. Alternatively, it is also possible to impose a fixed spin configuration, which in principle would not remain stable after convergence. In all these symmetry-breaking calculations the state with a given spin configuration is represented by a single Slater determinant of occupied single-particle states, constructed in terms of self-consistent Kohn-Sham eigenvectors. In the absence of SOI, the Kohn-Sham wavefunctions have a well-defined spin character, majority or minority spin. Therefore, the single Slater determinant, representing a given spin configuration, is an eigenstate of the component of the total spin $\mathbf{S}$ in the direction of the quantization axis $\hat{\mathbf{n}}$, which is the magnetization direction. In general this single Slater determinant is not an eigenstate

of $\mathbf{S}^2$, but in many cases it will have a large overlap with the eigenstate of $\mathbf{S}^2$ with S equal to the eigenvalue of $\mathbf{S}\cdot\hat{\mathbf{n}}$. The GS total spin S of the molecule (in the absence of SOI) is taken to be equal to one half of the excess of majority spin electrons, $S = \Delta N/2 = (N_{\rm maj} - N_{\rm min})/2$, for the metastable spin configuration with the lowest total energy. The spin magnetic moment of the system in units of the Bohr magneton $\mu_{\rm B}$ is then $\mu_S = \Delta N \mu_{\rm B} = 2S\mu_{\rm B}$. In the DFT study of SMMs the possible presence of fractional occupancy of some of the KS wavefunctions close to the Fermi energy might result in noninteger values of $N_{\rm maj} - N_{\rm min}$. Typically this happens when the HOMO-LUMO gap is very small or vanishing. We will encounter examples of this difficulty in the study of the charged states of $\{Fe_4\}$. The existence of this general problem was first discussed by Janak *et al*[30] in reference to near degeneracies between $3d$ and $4s$ electrons in neutral isolated atoms. In Ref.[31] a set of equations are derived which, while cumbersome to solve, allow one to variationally determine the electronic occupations that satisfy the conditions proposed by Janak in Ref.[30].

DFT can be used to extract the parameters defining the spin Hamiltonian that is supposed to describe the exchange interaction between the magnetic ions of the molecule. First of all DFT can be used to ascertain whether or not there is a localized spin at each magnetic ion, by calculating the total spin polarization inside a sphere centered about a given atom. For typical SMMs, including the one considered in this paper, while the magnetization density is not localized entirely on the magnetic ions, the assumption of a well-defined quantum spin often turns out to be quite reasonable. Once this is established, the calculation of the total energy for a few spin configurations permits the computation of the exchange constants of Eq. (1). We will see an example of this in the next section.

The DFT calculations discussed herein are performed with the Gaussian-orbital-based NRLMOL program.[32,33] All calculations employ the Perdew-Burke-Ernzerhof[34] (PBE) generalized-gradient approximation for the density functional. A large basis set is employed in which the exponents for the single Gaussians have been fully optimized for DFT calculations. The NRLMOL code employs a variational mesh for numerically precise integration and an analytic solution of Poisson's equation.

All-electron calculations are performed for all elements of the $\{Fe_4\}$ SMM except for the Au atoms that are used to construct the leads attached to the molecule, for which we have used pseudo potentials. All the electronic and magnetic properties are calculated using an optimized geometry.

III. ELECTRONIC AND MAGNETIC PROPERTIES OF ISOLATED $\{Fe_4\}$ SMM

The chemical composition of the molecule used in this work is $Fe_4C_{76}H_{132}O_{18}$.[35] The four Fe atoms in $\{Fe_4\}$ SMM form an equilateral triangle, as shown in Fig. 1. The molecule has idealized D_3 symmetry with the C_2 axis passing through the central atom and one of the peripheral atoms. Using first-principles methods we have calculated, in detail, the electronic and the magnetic properties of the $\{Fe_4\}$ SMM.

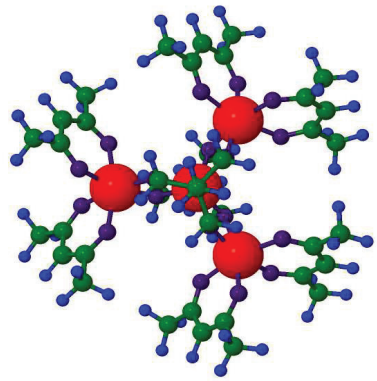

FIG. 1. (Color online) Ball-stick top view of an isolated $\{Fe_4\}$ SMM. Red, green, blue and purple balls correspond to iron, carbon, hydrogen and oxygen atoms, respectively

In the ground state, the central Fe atom is coupled anti-ferromagnetically with three peripheral atoms, whereas the three peripheral atoms are coupled ferromagnetically with each other, as shown in Fig. 2. Each of the four Fe atoms has spin $S_{Fe} = 5/2$, thus the total spin of the ground state is $S = 5$. The magnetic interactions between these atoms can be described by the Heisenberg spin Hamiltonian (Eq. (2)),

$$H = J(\mathbf{s}_1\cdot\mathbf{s}_2 + \mathbf{s}_1\cdot\mathbf{s}_3 + \mathbf{s}_1\cdot\mathbf{s}_4) + J'(\mathbf{s}_2\cdot\mathbf{s}_3 + \mathbf{s}_3\cdot\mathbf{s}_4 + \mathbf{s}_4\cdot\mathbf{s}_2)\,. \quad (17)$$

The two exchange parameters J and J' can be written in terms of the expectation values of the Hamiltonian of Eq. (17), for different spin config-

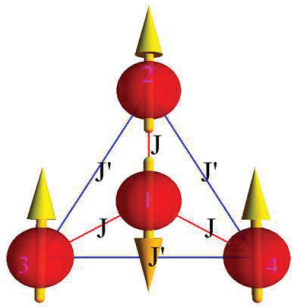

FIG. 2. Exchange interaction constants between four Fe atoms in $\{Fe_4\}$ SMM.

urations.

$$J = -\frac{2}{75}(E_{duuu} - E_{uuuu}) ,$$
$$J' = \frac{1}{75}(2E_{duuu} - 3E_{uudd} + E_{uuuu}) . \quad (18)$$

Here, E_{duuu}, E_{dduu} and E_{uuuu} are the energies of the molecule where the spin orientations at their respective atomic positions (1,2,3,4) are labeled as d = down or u = up. Using NRLMOL we have calculated the energies of different spin configuration and upon substitution in Eq. (17), we obtain $J = 9.94$ meV and $J' = 0.64$ meV. DFT calculations overestimates J and J' since estimated values from susceptibility measurements[36] are 2.62 meV and 0.14 meV, respectively. However, we note that the ratio of these two parameters agrees quite well for both theory and experiment. These values of the exchange constants ensure that the GS of the spin Hamiltonian Eq. (18) has indeed a total spin $S = 5/2$, well separated from excited states characterized by other values of S.

Using first-principles methods we have calculated the electronic and magnetic properties of $\{Fe_4\}$ SMM for the neutral ($Q = 0$) and two charged states, namely, the anion ($Q = -1$) and the cation ($Q = +1$). (We will refer to the value Q as the *extra charge* added to the system.) A summary of the results is shown in Table I. These results can be understood with the help of the structure of the single-particle energy levels around the Fermi level in the absence of SOI, plotted in Fig. 3 for the three charge states $Q = 0, \pm 1$.

The neutral molecule has a stable $S = 5/2$ GS, as anticipated. The HOMO-LUMO gap of the neutral isolated Fe_4 molecule is is about 0.85 eV, where both HOMO and LUMO levels are minority (down) spin

TABLE I. Properties of the isolated $\{Fe_4\}$ SMM for the three different charge states. *Note that the energy gap reported for the cation refers to the energy difference between the half-filled HOMO and empty LUMO. See Fig. 3(c).

Charge state	Spin magnetic moment $\mu_S(\mu_B)$	HOMO-LUMO energy gap (eV)	Anisotropy barrier (K)
Q=0	10.0	0.85	16.05
Q=+1	9.3	0.80*	53.42
Q=-1	9.0	0.06	1.88

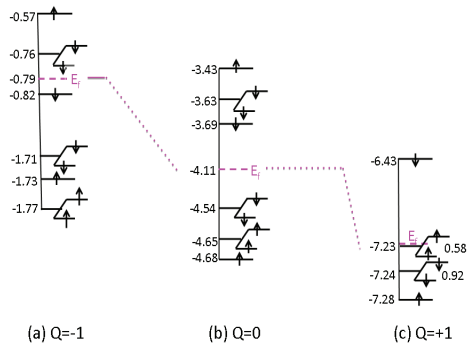

FIG. 3. Energy levels (eV) of different charge states of isolated the $\{Fe_4\}$ SMM without spin-orbit coupling. E_f represents the Fermi level. The numbers on the right of the HOMO and HOMO-1 levels in (c) are the fractional occupancies of the corresponding level.

states, see Fig. 3(b). Apart from a small swapping of two levels below the HOMO, the level structure for the $Q = -1$ charge state can be obtained from the the energy levels of the neutral system simply by filling the neutral LUMO with a spin-down electron, see Fig. 3(a). As a result the total spin of the anion is $S = 9/2$. Note also that the HOMO-LUMO gap of the anion is now reduced to 0.06 eV compared to the neutral molecule. The electronic states changes significantly for the $Q = +1$ charge (cation) state: the two doubly degenerate spin-up HOMO-1 and spin-down HOMO states of the neutral molecule swap place, see Fig. 3(c). Furthermore, since there is now one fewer electron, the new HOMO is now half-filled. This implies that the total spin of the cation is again reduced with respect to the neutral molecule by 1/2, that is, $S = 9/2$. The fractional occupancy of the HOMO plays important role in the enhancement of the magnetic anisotropy, discussed below. Our DFT calculations yield values of the total spin S in agreement with the level structure of Fig. 3. In particular for the charged states $Q = \pm 1$,

even when the initial spin configuration is set to be $S = 11/2$, the system converges eventually to the value $S = 9/2$.

For the neutral molecule, the magnetic anisotropy landscape is characterized by an easy axis in the direction perpendicular to the plane containing the four Fe atoms (the z-axis). As shown in Table I, we find that the anisotropy barrier for this case is about 16 K, which is in agreement with previous calculations[37] (In Ref[37], the authors have used two different $\{Fe_4\}$ complexes. The molecular symmetry for one of these complexes is C_2, whereas the the other one has D_3 symmetry. Our calculations agree well with the one that has D_3 symmetry.). Note that a well-defined energy gap between occupied and unoccupied states (regardless of the spin), ensures that the perturbative and exact calculation of the anisotropy coincide.

The magnetic anisotropy of the $Q = +1$ charge state has also uniaxial character in the z-direction, with a barrier of about 53 K, significantly larger than that obtained for the neutral molecule. On the other hand for the $Q = -1$ charge state the anisotropy is reduced to about 1.9 K, with an easy axis in the XY-plane of the Fe atoms. The large change in the anisotropy for the two charged states has a very different origin for the two cases and can be understood in the following way.

For the $Q = -1$ case, the small gap between the like-spin HOMO and LUMO states might at first suggest a breakdown of the perturbative treatment. In fact, these two states are coupled only minimally by SOI. The most important coupling occurs between the spin-down HOMO and the spin-up LUMO+1 states. The energy difference between these two states is ≈ 0.25 eV. This value and the corresponding energy denominator in Eq. (9) is large enough for perturbation theory to work (as a comparison with the exact approach clearly shows) and, at the same time, small enough for this individual transition to completely determine the main features of the anisotropy landscape. In particular, it turns out that this term in Eq. (9) favors an easy axis along a direction in the XY-plane of the Fe atoms. Since this magnetization direction is unfavorable for other terms in Eq. (9) (which prefer the z-direction), there are positive and negative contributions in the total energy difference for the two magnetization directions (calculated with Eq. (7)), which in the end lead to a reduced anisotropy barrier.

The large enhancement of the magnetic anisotropy barrier found for the $Q = +1$ state can also be understood with the help of single-particle energy diagram shown in Fig. 3(c). We observe that the half-filled doubly-degenerate spin-up HOMO level lies just above a (close-to-100%) filled doubly degenerate spin-down HOMO-1 level. The term involving transitions between these two occupied and unoccupied levels totally dominate Eq.(9). In fact, the smallness of the corresponding energy denominator (a few meV) renders the perturbative approach inadequate. This is a classical example of a quasi-degeneracy at the Fermi level, where the exact treatment of SOI is necessary. As it is often the case, the inclusion of SOI lifts the quasi-degeneracy for a particular direction of the magnetization, leading to a substantial decrease of the total energy for that direction and, consequently, to a large anisotropy energy barrier.

IV. $\{Fe_4\}$ SMM ATTACHED TO METALLIC LEADS

In this section we investigate how the electronic and magnetic properties of the $\{Fe_4\}$ SMM change when the molecule is attached to metallic leads, as in transport experiments. The system that we have in mind is a single-electron transistor device, where metallic nano-leads, separated by a nanogap created by either break junction or electric migration, are bridged by a molecule functionalized with convenient chemical ligands. In our theoretical modeling, we are forced to find a convenient finite representation of otherwise semi-infinite leads in the form of finite clusters. For the calculations reported in this paper we have chosen to model a metallic nano-lead with a finite cluster of 20 gold (^{79}Au) atoms, arranged in a special tetrahedral structure, which can be viewed as a fragment of the face-centered cubic lattice of bulk Au (see Fig. 4). This metal cluster, Au_{20}, has been previously investigated by by Li *et al.* in Ref. 38, where it was shown that 20 Au atoms arranged in this geometric configuration form a very stable system. Its very large HOMO-LUMO gap (1.77 eV) makes Au_{20} chemically very inert. What is also important is that its unique tetrahedral structure makes this cluster an ideal model for Au surfaces at the nanoscale. Our rational for using this cluster to model metal leads is that during the fabrication of the nanometer-spaced electrodes, via self-breaking by electro-migration for example, the ensuing Au nano-leads will relax into the most stable configuration which might be well described by tetrahedral Au_{20}. In a way, the tetrahedral Au_{20} is the best representation of bulk Au at the nanoscale.

Secondly, since ultimately we would like to investigate transport properties of this system in coulomb blockade regime, it is essential that coupling between the leads and molecule is weak.

After constructing the two leads in the form of

two Au_{20} clusters, we have connected the molecule via phenyl groups, as shown in Fig. 4. The functionalization of the ligands of $\{Fe_4\}$ SMM by means of phenyl groups is well-known and suitable to attach the molecule to Au surfaces[12,15].

A similar way of connecting the $\{Fe_4\}$ SMM to Au leads is employed in SET experiments in the Coulomb blockade regime[16–18], and it ensures that the electronic coupling between the molecule and electrodes is weak. To maintain proper bonding and ionic neutrality of the entire cluster we have further removed one hydrogen (H) atom from the molecule close to the contact point and have added it to the chain part of the cluster. We have considered two different ways of doing this. In the first case (hereafter called Type-1 lead) we have added the H atom to the sulfur (S) atom near the Au cluster. In the second case (hereafter called Type-2 lead) we have added H to the carbon (C) atom near the contact point as shown in Fig. 4. After connecting the leads with the molecule we have relaxed the entire system again. Typically we find that the system with Type-2 leads is more stable, that is, its energy is approximately 0.6 eV lower than the energy of the system with Type-1 leads. We will nevertheless report results for both cases unless otherwise specified.

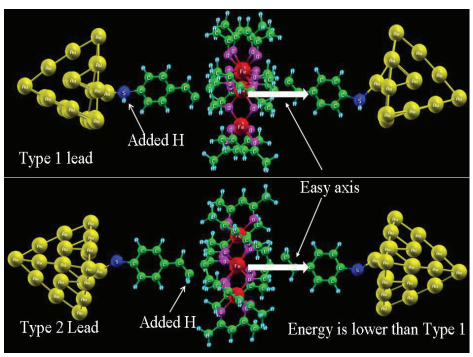

FIG. 4. $\{Fe_4\}$ SMM connected to Au_{20} leads. Two types of leads are used in these calculations. In Type-1 lead a H atom is added to the S atom near the gold lead (top figure). In Type-2 lead a H atom is added to a C atom in the phenyl group near the $\{Fe_4\}$ molecule (bottom figure).

A summary of the magnetic properties of the neutral molecule attached to A_{20} leads is shown in Table II. We can see that the combined molecule plus leads system maintains a sizable HOMO-LUMO gap of about 0.75 eV. The first important result is that coupling the leads does not cause a change of the spin of the molecule, which remains equal to the value of the isolated neutral $\{Fe_4\}$, $S = 5$. Secondly, the leads have a very small effect also on the magnetic anisotropy of the system: the magnetic anisotropy landscape has still an easy axis along the same z-direction (see white arrow in Fig. 4), with an energy barrier quite close to the 16 K of the isolated molecule.

TABLE II. Properties of neutral $\{Fe_4\}$ SMM attached to A_{20} leads, compared to the properties of the isolated molecule (first row). Type-1 and Type 2 (called in the paper also Type-1 lead and Type-2 lead) refer to the two different choices to place an Hydrogen atom to the ligand, See Fig. 4

	Spin magnetic moment $\mu_S(\mu_B)$	HOMO-LUMO gap (eV)	Anisotropy barrier (K)
$\{Fe_4\}$	10	0.85	16.05
$\{Fe_4\}$+Type 1	10	0.87	15.99
$\{Fe_4\}$+Type 2	10	0.57	15.47

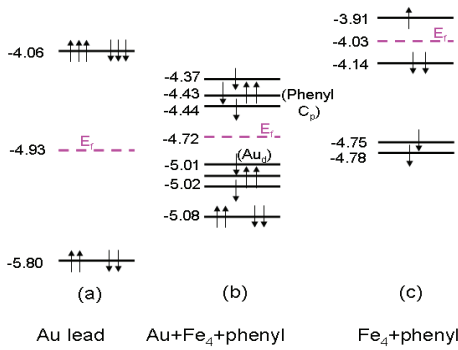

FIG. 5. Shifts in the energy levels (eV) of neutral $\{Fe_4\}$ SMM when connected to two Au_{20} leads (of Type-2). (a) Isolated Au lead (b) Leads+$\{Fe_4\}$+phenyl and (c) $\{Fe_4\}$+phenyl. The labels Au_d and Phenyl C_p in (b) indicate that the main contribution to those levels comes from d levels of the Au leads and p levels of C in the phenyl ligands respectively.

We can gain some insight about the robustness of the magnetic structure of $\{Fe_4\}$ SMM under the influence of metallic contacts by investigating the changes in the single-particle energy levels and level alignment and occurring when the leads are connected to the molecule. We have calculated separately the energy levels of the isolated Au lead(s) and the $\{Fe_4\}$ + phenyl group, along with the levels of the combined system [Au leads + $\{Fe_4\}$ + phenyl group]. The results are shown in Fig. 5. The states at and near the Fermi level of the two subsystems are dominated by the d-levels of Au atoms and the p lev-

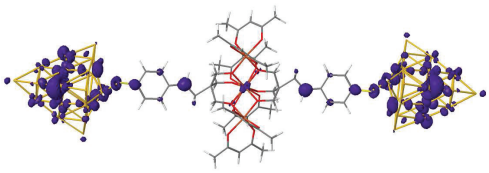

(a)Homo-neutral

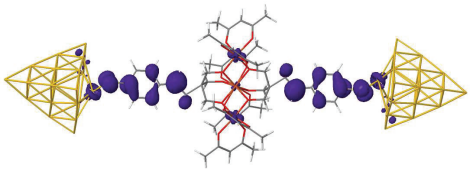

(b)Lumo-neutral

FIG. 6. HOMO and LUMO of the neutral molecule.

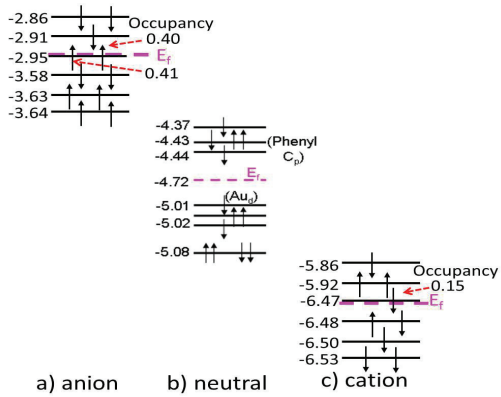

FIG. 7. Energy levels (eV) for the three charge states $Q = 0, \pm 1$ for the $\{Fe_4\}$ SMM connected to two Au_{20} leads (of Type-2). (a) Anion. (b) Neutral (same as in Fig. 5(b)). (c) Cation. The labels Au_d and Phenyl C_p in (b) indicate that the main contribution to those levels comes from d levels of the Au leads and p levels of C in the phenyl ligands respectively.

els of the C atoms of the phenyl group. Thus, when the two systems are combined, the charge transfer taking place to align the Fermi energies of the two subsystems is restricted only within the contact region, leaving the magnetic properties of the $\{Fe_4\}$ inner core unchanged. Fig. 5(b) shows that the energy levels of the combined system around at the Fermi level correspond primarily to states remote from the magnetic core. This is also supported by Fig. 6, where we plot the probability density for the HOMO and LUMO states of the $\{Fe_4\}$ + leads system. Both states have negligible contributions on Fe atoms or atoms immediately nearby to these. As we will see below, this implies that the magnetic properties will remain unchanged even when extra charge is added to (or subtracted form) the system.

Fig. 5(b) shows that both the non-degenerate spin-down HOMO and the non-degenerate spin-down LUMO of the neutral system lie quite close in energy to degenerate levels (occupied and non-occupied respectively). Therefore we can expect that subtle energy-level swaps may occur when one electron is added to or subtracted from the system. As it is evident from Fig. 7, this is exactly what the calculations show. For the case of leads of Type 2, the HOMO of the anion ($Q = -1$) is now a half-occupied doubly-degenerate spin-up level, lying very close to a non-degenerate spin-down LUMO. This leads to a GS spin $S = 11/2$, and to a spin magnetic moment close to $\mu_s = 11\mu_B$ (See Table III).[39] A similar situation occurs for the $Q = +1$ charge state, which has a GS spin $S = 11/2$. We find that this state is however almost degenerate with another state with $S = 9/2$. For leads of Type-1 (which are less stable), the spin configurations $S = 11/2$ and $S = 9/2$ are almost degenerate for both charged states, $Q = \pm 1$. Note that the spin magnetic moment of the Q= -1 charge state is now closer to $\mu_S = 9\mu_B$. The quasi-degeneracy of two different spin configurations is a situation where the assumption of the existence of a well-defined giant-spin model may not be entirely adequate.

TABLE III. Magnetic properties of the three charge states when the $\{Fe_4\}$ SMM is attached to Au leads as in Fig. 4.

Charge state	Spin magnetic moment $\mu_S(\mu_B)$		Anisotropy barrier (K)	
	Type 1	Type 2	Type 1	Type 2
Q=0	10.0	10.0	15.99	15.47
Q=+1	9.0	10.95	17.73	14.74
Q=-1	9.6	10.65	11.23	16.97

As shown in the Table III, in contrast to the case of the isolated $\{Fe_4\}$ SMM where the anisotropy of the charged states are significantly different from that of the neutral molecule, when the leads are attached to the molecule the anisotropy barrier of the charged states remains close to the value of the neutral system. We also note that magnetic properties of the charge states have some dependence on type of the lead attached to the molecule.

As anticipated above, an explanation of this be-

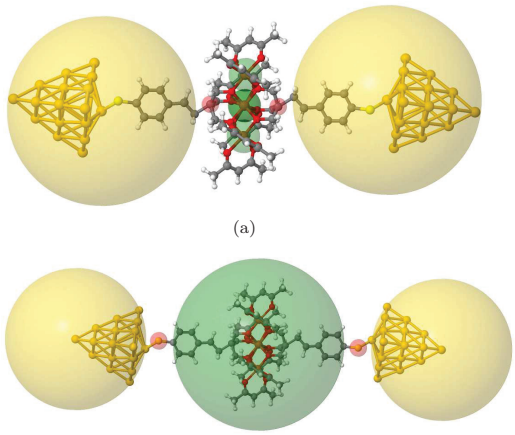

(a)

(b)

FIG. 8. (Color online) Evaluation of the fraction of extra charge for the anion state ($Q = -1$, one extra electron added) with respect to the neutral state, contained in different regions of the $\{Fe_4\}$ molecule plus leads and phenyl groups. In (a) each yellow sphere surrounding the lead and the phenyl group contains about 40% of an electron charge. In (b) each yellow sphere, surrounding only the Au lead, contains 21% of electron charge. Therefore, the amount of charge transferred to the leads is about 42% and to the phenyl groups is 38%. The rest of the extra charge $\approx 20\%$ is in the $\{Fe_4\}$ region.

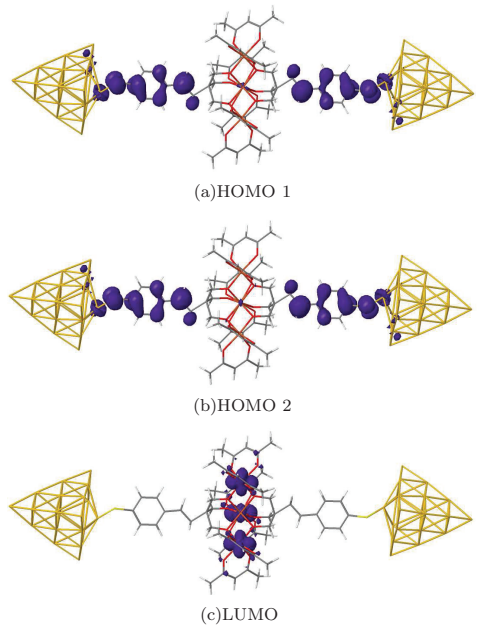

(a)HOMO 1

(b)HOMO 2

(c)LUMO

FIG. 9. The two quasi-degenerate HOMOs and the LUMO of the anion charge state. Approximately 20% of the HOMO wave functions reside on the Au leads, primarily on the interstitial space between Au atoms. See Fig. 8. This contribution is not visible on the scale of this plot.

havior is already suggested by the energy diagram of Fig. 5(b) and the plots of Fig. 6 demonstrating that both the HOMO and the LUMO of the neutral system are states predominately localized around the Au leads and within the phenyl group respectively. Therefore, we expect that when we add or remove an electron from the system it largely resides in the lead and phenyl group, leaving the magnetic states in $\{Fe_4\}$ molecule relatively unchanged. The easy axis, in all cases, points perpendicularly to the Fe_4 plane, as shown in Fig. 4, except for $Q = -1$ charge state of Type-1 lead, which is in the plane.

Further support to this picture is provided by calculating the real-space location of the extra charge when an electron is added or subtracted to the system. As an example, we consider here the case of the anion, where one electron is added to the system. Since part of this extra charge might end up in interstitial regions between atoms (this is the case for the extra charge on the Au leads), particular care must be taken in drawing conclusions based only on the atomic-position plot of the HOMO states, shown in Fig. 9, which might miss this contribution. To capture the interstitial contribution, we draw instead a large sphere enclosing a given region of the system. NRLMOL is able to calculate the extra charge contained globally in that region, including interstitial contribution. By repeating the same calculation with different spheres centered at different locations, we can eventually determine the amount of extra charge in different relevant parts of the system.

In Fig. 8(a) we consider a sphere (yellow color) containing both the lead and the phenyl group linker. We find that the amount of extra charge contained in this region is 40% of one electronic charge. The remaining 20% is located on atoms in the nearest surrounding of the $\{Fe_4\}$ core. In Fig. 8(b) the sphere encloses only the Au lead but no linker. For this case we find that each Au leads contains 21% of extra electronic charge. We conclude that when one electron is added to the system, a total of 42% of the extra charge resides on the leads, 38% on the ligands and only 20% is around the magnetic core of $\{Fe_4\}$. This 20% of added charge in not directly

on the Fe atoms and therefore does not change the magnetic properties of $\{Fe_4\}$ significantly.

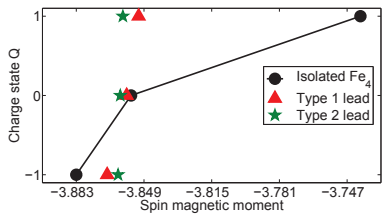

(a)Central Fe atom

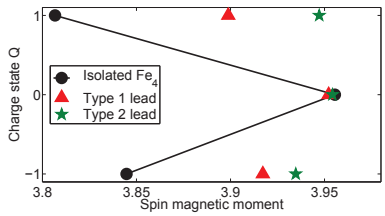

(b)Vertex Fe atoms

FIG. 10. Local magnetic moments of Fe atoms. The negative and the positive moments in the two figures imply that moments of central and vertex atoms are opposite to each other.

Further evidence of this important conclusion is provided by the comparison of the calculated local spin magnetic moments of the Fe atoms for the isolated $\{Fe_4\}$ molecule and for molecule-plus-lead system, for different charge states. The results are shown in Fig 10. We note from the figure that for the isolated molecule the magnetic moments change considerably for the charged states, whereas for molecule plus lead system, the corresponding change is very small. Clearly, when the molecule is attached to the Au leads, adding or removing one unit charge affects the magnetic states of the $\{Fe_4\}$ minimally, which is also why we do not see a large change in magnetic anisotropy for different charge states.

We conclude this section with a few comments on the important issues of the nature of the charged states and the character of the coupling molecule-leads, as evinced by the DFT calculations. Firstly, we have seen that when one electron is added or subtracted to the system $\{Fe_4\}$ + (finite) leads, the extra charge is predominantly localized on the ligands ($\approx$ 40%) and on the leads ($\approx$ 40%). If we could increase the size of the leads, a larger fraction of the extra charge would be likely to spread on the metallic leads. Therefore one could argue that the charged states $Q = \pm 1$ investigated above are not a fully adequate description of the charged states involved in the sequential tunneling processes taking place in a SET, where the additional charge should be essentially localized on the central island. Secondly, and partly connected to this issue, the non-zero amplitude of the LUMO wavefunction of the neutral system (which is quite close to the HOMO wavefunction of the anion) seems to indicate that the ligands considered here do not behave as tunnel barriers of a SET, but rather model an example of strong coupling between molecule and leads[40] Both these features could be due to limitations of the DFT approach considered here, which tends to over-delocalize any added charge. Such drawbacks can possibly be improved by more refined DFT treatments, involving, for example, self-inter corrections. While we believe that these refinements are important and should be further investigated, the goal and strategy of the present paper is to simulate with DFT a realistic example of SMM attached to leads, being aware of these limitations.

V. EFFECT OF AN EXTERNAL ELECTRIC POTENTIAL

In SET devices the charge of the central island weakly coupled to metallic electrodes can be varied experimentally one by one by applying an external electric field via a third gate electrode, which overcomes the charging energy e^2/C of the island. Here we investigate the effect of an external gate electrode, whose electric potential tends to confine the extra charge closer to the molecule. Note that in phenomenological studies of SETs based on model Hamiltonians, a gate voltage only shifts the energies of the isolated "quantum dot" without affecting its wavefunctions. As we show below, in our case the gate voltage can be used to localize a wavefunction closer to the molecule and modify its coupling to the leads. The resulting charged states should be a better representation of the states involved in tunneling transport in SET when Coulomb blockade is lifted.

We model the external potential by a simple Gaussian confining potential of the form

$$U = V_0 e^{-\alpha_x (x-x_0)^2 - \alpha_y (y-y_0)^2 - \alpha_z (z-z_0)^2}. \qquad (19)$$

Here V_0 is magnitude of the potential centered at (x_0,y_0,z_0), which in our case is the position of the central Fe atom of the $\{Fe_4\}$. The constants α's are the width of the potential along the corresponding directions and are chosen so that the potential drops

quickly at distances larger than $\{Fe_4\}$. The sign of V_0 determines whether the extra electron will be confined into or repelled from the $\{Fe_4\}$ molecule. Thus for the anion case a negative V_0 will attract the electron whereas for the cation case a positive V_0 will attract the "hole" inside the molecule.

We start by looking at the effect of the gate voltage on the anisotropy of the isolated $\{Fe_4\}$ SMM. We have first considered a gate voltage that depends only on the variable z. The resulting electric field points along the the z-axis, which is the easy axis of the molecule.

From Fig 11 we note that in the anion case a confining potential for the extra electron ($V_0 < 0$) reduces the anisotropy barrier; whereas repelling the extra charge away from the molecule increases the anisotropy. The neutral molecule displays an opposite behavior as a function of V_0. In both cases the the behavior of the anisotropy is close to a linear function of $V_0 < 0$. As expected, the variation of the barrier for the neutral molecule is limited, less than 10 % for the largest applied voltage. The cation is special. We have seen that at zero voltage, the system has a large anisotropy barrier (see Table I). due to a quasi-degeneracy at the Fermi level. The external potential lifts this degeneracy and the anisotropy barrier decreases sharply for both signs of V_0.

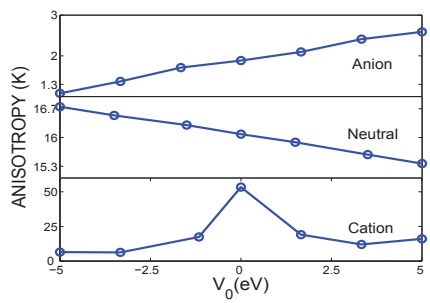

FIG. 11. Variation of the magnetic anisotropy barrier as a function of a confining potential V_0 applied along C_3 axis (perpendicular to the plane of the $\{Fe_4\}$ triangle) of an isolated $\{Fe_4\}$ SMM.

The confining potential that we have applied above does not break the C_3 symmetry of the system and hence the parameter E in Eq. (2), characterizing the transverse component of the magnetic anisotropy, is zero. However, the symmetry can be broken by applying an electric field along directions other than the easy axis. Table IV shows the effect of this broken symmetry on the anisotropy of the isolated $\{Fe_4\}$ SMM.

TABLE IV. The effects of confining potential on neutral $\{Fe_4\}$ SMM. Δ is the anisotropy barrier and D and E are the parameters of the Hamiltonian Eq. (2), all in units of K.

V_0 (eV)	α_x	α_y	α_z	ANISOTROPY		
				Δ (K)	D (K)	E (K)
0.0	0	0	0	16.06	-0.63	0.00
-5.0	0.01	0	0.01	17.00	-0.64	-0.03
-5.0	0.01	0	0	15.77	-0.60	-0.02

It is evident from Table IV that E is no longer zero if the electric field is applied along directions other than the easy axis. A non-zero E allows different eigenstates of z-component of the giant spin to mix with each other. a transverse component in principle can cause quantum tunneling of the molecule giant spin. Thus, this method can be used as electric control of magnetic properties. It can play a significant role in transport, for example by modifying spin selections rule and by opening alternative channels via quantum tunneling of the magnetization.

We now discuss the effect of the applied gate voltage when the $\{Fe_4\}$ molecule is attached to Au leads. In this case we have applied the field only along the easy axis of the molecule attached to the leads of Type 2, as shown in Fig. 4. We have seen in the previous section that since HOMO and LUMO states and states close in energy to these are primarily localized on the Au leads and phenyl linker, an added or removed electron leaves $\{Fe_4\}$ largely unaffected. But the presence of a confining potential ($V_0 < 0$ for electrons), applied only on $\{Fe_4\}$ part of the system, brings the states localized within $\{Fe_4\}$ SMM closer to LUMO levels. Thus, when an electron is added to the system, the fraction of this extra charge that goes inside the molecule increases as we increase the confining potential. Similarly, when an electron is subtracted from the system, an applied positive gate voltage ($V_0 > 0$), tends to localize a fraction of the positive extra charge (a hole) closer to the molecule.

As an example, we consider the effect of a confining potential for the anion case ($Q = -1$, one electron added to the system). Fig. 12 shows the change in fractional charge that enters into the $\{Fe_4\}$ molecule as the strength of confining potential is increased, and the corresponding change in magnetic anisotropy barrier of the system. Clearly, as the voltage is increased, more of the added electron is pushed inside the molecule. As the charge fraction approaches unity, the anisotropy decreases and converges to the value obtained for the anionic state of the isolated $\{Fe_4\}$ SMM.

It turns out that not only the anisotropy barrier

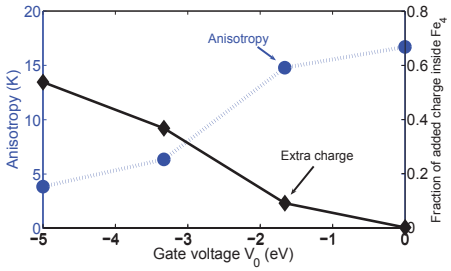

FIG. 12. (Color online) Fraction of the added charge (blue circles) confined inside $\{Fe_4\}$, as a function the confining potential strength, and corresponding change in the magnetic anisotropy (black diamonds) of the leads plus molecule system in the anion state, $Q = -1$. The external potential corresponds to an electric field along the z-direction. See Fig. 4.

but other magnetic properties converge to the properties of the anion state of the isolated $\{Fe_4\}$ as the extra charge, under the effect of the external potential, moves closer to the center of the molecule. The easy axis of the system, which in zero potential points perpendicular to the plane of the Fe_4 triangle and towards the leads, eventually rotates into the plane of the Fe_4 triangle, exactly as in the case of the anion state of the isolated $\{Fe_4\}$ SMM. Similarly, as the added charge moves inside the inner magnetic core of $\{Fe_4\}$, the total spin of the system is reduced from $S = 11/2$ to the value of the anion state of the isolated molecule, $S = 9/2$.

Similar results are obtained for the cation. As we apply an increasingly positive voltage, a larger fraction of a (negative) electron charge is pushed outside $\{Fe_4\}$, or equivalently, a larger fraction of (positive) hole is attracted inside the $\{Fe_4\}$. As a result, the anisotropy barrier increases and it reaches a value of 22.8 K for $V_0 = 5$ eV, with more than half of the extra (positive) charge now inside $\{Fe_4\}$. Similarly, the spin also switches from $S = 11/2$ at $V_0 = 0$ to $S = 9/2$ at $V_0 = 5$ eV. Again, this is consistent with both the spin and the anisotropy converging towards the corresponding values of the isolated cation state.

A summary of the dependence of the anisotropy barrier as a function of the external potential for all three charge state in shown in Fig. 13. While the anisotropy of neutral state displays a weak dependence on the field, the anisotropy of the two charged states is significantly affected. These calculations demonstrate that, for a SET with a $\{Fe_4\}$ SMM as a central island, by manipulating the position of the additional charge with a gate voltage, it is possible to modify the magnetic properties of the SMM. This in turn can have important effects on the tunneling transport of the device.

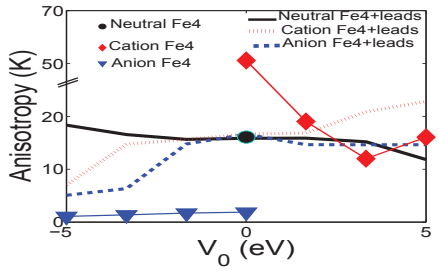

FIG. 13. Magnetic anisotropy as a function of a confining field for the molecule plus leads (Type 2) system, for the three charge states. The field is applied along the easy axis, that is, perpendicular to the plane of the molecule. The anisotropy for the the three charge states for the isolated molecule is included as a comparison (see diamond, circle and triangle symbols).

VI. COMPARISON WITH SET EXPERIMENTS

Recent SET experiments[16,18] have permitted the first measurements of the magnetic characteristics of the $\{Fe_4\}$ SMM weakly coupled to Au leads, for both neutral and charged states. Comparison with our theoretical results has be done with caution, since important details (e.g., the type of linker used, see below) might differ in the two cases. In a first study Zyazin *et al.*[16] have studied quantum transport in the inelastic cotunneling regime. By measuring the zero-field splitting of magnetic excitations and their dependence on the magnetic field, it was possible, with help of the model Hamiltonian of Eq. (2), to extract values of the giant spin S and the magnetic anisotropy barrier $\Delta = DS^2$ for three adjacent charge states, N (neutral), $N+1$ (anion) and $N-1$ (cation). For the neutral state, the spin of the molecule was found to be equal to expected value $S_N = 5$ and the anisotropy barrier to be consistent with the value in the bulk phase, $\Delta_N = 1.4$meV $= 16.24$K. These results are in good agreement with our theoretical estimate for the $Q = 0$ charge state, see Table III.

For the charged states, the situation is more complicated. For the reduced molecule (anion state, one electron added) the experimental measurements gave $S_{N+1} = 11/2$ for the spin and $\Delta_{N+1} =$

2.7meV = 31.30K for the anisotropy. For the oxidized molecule (cation state, one electron removed), the measurements gave $S_{N-1} = 9/2$ and $\Delta_{N-1} = 1.8\text{meV} = 20.90\ K$ respectively. Comparing these findings with the results of our calculations (see Table III)) we can see that, for a given choice of lead type (Type 1 or Type 2), the theoretical value of the spin is consistent with the experimental one for either cation or anion, but not for both. We can also conclude that the experiment typically finds larger values for the anisotropy barrier, for both reduced and oxidized states, than the values predicted by theory.

Several reasons can be responsible for these discrepancies. First, the functionalization of the molecule used in the experiment is slightly different from the one used in the calculations. In fact, in the experiments two different types of ligands were used. In one case (labeled as sample A) the $\{Fe_4\}$ SMM was connected to the Au lead the phenyl group. In the second case, (labeled as sample B) the $\{Fe_4\}$ was connected via a thiol group, C_9S. The coupling molecule-lead turns out to be weaker in sample A than in sample B.[41] As shown above, in all our calculations we have used a different type of linker, which was combination of a phenyl group and a thiol group.

Secondly, in experiment different charge states are achieved by adding or removing electrons to the central region of SET via a gate voltage. In the theoretical calculations, the two relevant charged states are constructing by adding or removing an electron to a system consisting of the $\{Fe_4\}$ connected to finite leads. The extra charge is allowed to relax in the self-consistent field, and it occupies regions away from the $\{Fe_4\}$, which affects the magnetic properties of the system. Indeed, confining on the SMM with an external gate modifies the anisotropy barrier.

Third, the evaluation of the magnetic properties from experiment done in Ref. 16 relies on the use of the model Hamiltonian of Eq. (2). The fitting of the experimental results maintains a degree of uncertainty and arbitrariness, and moreover it could be problematic in cases of level degeneracy at the Fermi level, not uncommon for charged states. In this case, we have seen the the giant-spin model of Eq. (2) might become inadequate.

Finally, the method of Ref. 16 relies on the measurement of inelastic cotunneling excitations, which is quite sensitive to the coupling between molecule and leads, and therefore it is a procedure not immune of uncertainties. Indeed, in a more recent paper Burzurí *et al.*[18] introduced a novel gate-voltage spectroscopy technique which permits the measurement of the anisotropy of an individual SMM in different charge states by tracking the dependence of the charge degeneracy point as a function of magnetic field. This method is much more sensitive and accurate than the method based on conventional transport spectroscopy employed in Ref. 16. The spin Hamiltonian provides a good fit of the data if $S_N = 5$, $\Delta_N = 16.2$K for the neutral state, $S_{N+1} = 9/2$ and $\Delta_{N+1} = 16.0$K for the reduced state and $S_{N-1} = 11/2$ and $\Delta_{N-1} = 16.5$K for the oxides state. Furthermore, the orientation of the easy axis is found to exhibit only small variations among different charge states. Although some details might differ,[42], these results are quite consistent with the small variations in anisotropy magnitude and the unchanged orientation of the easy axis that we find for the three charge states in our theoretical analysis. See Table III.

As we mentioned above, the small variation in the anisotropy for different charged states found in our calculations is related to the fact that any extra charge added to the molecule + leads system tends not to reside directly on the magnetic atoms, but mainly on the ligands and on the Au leads. We pointed out that this could be, in part, an artificial effect due to the way we constructed charged states in our finite-size system and to the delocalizing character of our DFT approach. On the other hand, it is interesting that our estimates for the magnetic anisotropy are essentially consistent with the experimental results of Ref. 18, which are obtained exactly at charge degeneracy points. At these special values of the external gate voltage the energy of two adjacent charge states is the same. We can imagine that at the degeneracy point the extra charge can swap energy-free from the electrodes and the molecule and might be localized primarily in region where the molecule is connected to the leads. If this were the case, the charge distribution shown in Fig. 8 could be in fact a more realistic description of the charge states than previously anticipated. We could also surmise that, exactly as it happens in our calculations when we apply an external confining potential, changing the gate voltage to move away from the degeneracy point and make a given charge state more stable could strongly affect the the magnetic anisotropy. Indeed the results of the the first experiment[16], where the anisotropy was not extracted at degeneracy points but in the middle of a Coulomb blockade diamond, show a significantly enhanced anisotropy for charged states. The two experimental results could simply indicate that in one case the extra charge is localized closer to the SMM than in the other, exactly as it happens in our theoretical modeling.

VII. CONCLUSIONS

In this paper we have studied the electronic and magnetic properties of a $\{Fe_4\}$ SMM in a single-electron transistor (SET) geometry, using DFT as implemented in NRLMOL. We have modeled the system by a $\{Fe_4\}$ functionalized with phenyl groups attached to two metals leads described by Au_{20} nanoclusters. Our calculations show that the magnetic structure of the neutral $\{Fe_4\}$ SMM, that is, its spin ordering and magnetic anisotropy, remains stable in the presence of metallic leads. Specifically the ground state spin is $S = 5$ and the anisotropy barrier is of the order of $16K$, like for the isolated $\{Fe_4\}$. This result is ascribed to the fact that, when attaching leads to $\{Fe_4\}$, any charge transfer between the molecule and the metal leads occurs primarily in the contact region and on the ligands, but does involve the magnetic core of the molecule.

Based on the properties of the HOMO and LUMO of the neutral system, when an electron is added or subtracted to the molecule-lead system, we find that the added charge ($Q = \mp 1$) is primarily located on the ligands and on the leads. As a result, while the total spin of this finite system changes by $\Delta S = \pm 1/2$, the magnetic anisotropy displays small variations both in magnitude and orientation with respect to the neutral state. In contrast, the anisotropy of the anion and cation states of an isolated $\{Fe_4\}$ is quite different from the values of neutral molecule, since the added extra charge penetrates the region of the Fe atoms. The theoretical study of charged states $Q = \pm 1$ for the molecule-leads system is technically challenging, due to occurrence of small HOMO-LUMO gaps and consequent fractional occupancies of the states around the Fermi level. Furthermore, DFT tends to overdelocalize any added charge in the peripheral parts of the system. Nevertheless, the analysis of these states presented here sheds light on the properties of a $\{Fe_4\}$ SET when individual electrons are added or subtracted to the "quantum dot" by overcoming the Coulomb charging energy with a gate voltage.

We have shown that an external electric potential, modeling a gate voltage, can be used to manipulate the charge on the molecule-leads system and with that the magnetic properties of the device. In particular, for the two charged states $Q = \pm 1$ when the extra charge, under the effect of the potential, is progressively removed from the ligands-leads region into the magnetic core of the molecule, the magnetic properties converge to the properties of the anion and cation states of the isolated $\{Fe_4\}$. This is an example of the electric control of magnetism of a SMM in a SET. The charged states of the molecule-leads system in the presence of external fields studied in this paper can be used to construct the transition matrix elements entering a quantum master equation describing tunneling transport in a SET. With the limitations inherent to the DFT approach mentioned above, these states incorporate charging effects for the SMM weakly coupled to metal leads.

We have compared the results of our numerical calculations with the results of two recent experimental studies of tunneling transport in a $\{Fe_4\}$ three-terminal device in the Coulomb blockade regime[16,18]. This comparison must be made with caution since some important details (e.g., the precise atomic and electronic structure of the ligands) are different and might explain some of the discrepancies between theory and experiment that we find. Nevertheless, one of these experiments[18] finds that the anisotropy for the two charged states $Q = \pm 1$ displays only small variations in magnitude and orientation from the corresponding values of the neutral states, in agreement with our theoretical findings. Interestingly enough, the experimental values are extracted by tracking the dependence of the charge degeneracy point between two adjacent charged states as a function of the magnetic field. Our numerical calculations show that the nearly-independence of the magnetic anisotropy on the charged states is related to the position of the added charge being far away from the magnetic core of the molecule. Thus the agreement between theory ad experiment might indicate that for a $\{Fe_4\}$ SET the charge of a added (subtracted) electron close to a charge-degeneracy point is primarily located on the ligands and in the contact region with the leads. If correct, this would be an example in which a magnetic property of SMM-based SET can provide information on the electronic properties of the charged states.

For molecule-lead systems with finite gaps, we expect our results to provide accurate predictions of experiment. However for those cases where HOMO-LUMO gaps are very small and the electronic states at the Fermi level are partially occupied, further understanding will require variationally accounting for the electronic occupations along the lines suggested in Ref.[31] Another point of view is that such fractionally occupied solutions are also strongly affected by self-interaction corrections and that accounting for such corrections will often significantly decrease the possibility of fractionally occupied solutions. Self-interaction corrections are also likely to provide a more complete understanding of the nature of charged states investigate in this paper. Addressing spin-dependent conductance in macro-

molecular to meso-scale devices will require efficient solutions to these problems and renewed efforts at extracting quantitative model Hamiltonians for such systems.

ACKNOWLEDGMENTS

This work was supported by the faculty of Natural Science and Technology at Linnaeus University, the Swedish Research Council under Grants No: 621-2007-5019 and 621-2010-3761, and the NordForsk research network 080134 "Nanospintronics: theory and simulations".

[1] A. R. Rocha, V. M. Garcia-Suarez, S. W. Bailey, C. J. Lambert, J. Ferrer, and S. Sanvito, Nat. Mater. **4**, 335 (2005).
[2] A. R. Rocha, V. M. Garcia-Suarez, S. Bailey, C. Lambert, J. Ferrer, and S. Sanvito, Phys. Rev. B **73**, 085414 (2006).
[3] M. Trif, F. Troiani, D. Stepanenko, and D. Loss, Phys. Rev. B **82**, 045429 (2010).
[4] W. Wernsdorfer and R. Sessoli, Science **284**, 133 (1999).
[5] L. Bogani and W. Wernsdorfer, Nat. Mater. **7**, 179 (2008).
[6] A. Candini, S. Klyatskaya, M. Ruben, W. Wernsdorfer, and M. Affronte, Nano Letters **11**, 2634 (2011).
[7] D. Gatteschi, R. Sessoli, and J. Villain, *Molecular Nenomagnets* (Oxford University Press, Oxford, 2006).
[8] H. B. Heersche, Z. de Groot, J. A. Folk, H. S. J. van der Zant, C. Romeike, M. R. Wegewijs, L. Zobbi, D. Barreca, E. Tondello, and A. Cornia, Phys. Rev. Lett. **96**, 206801 (2006).
[9] M.-H. Jo, J. E. Grose, K. Baheti, M. M. Deshmukh, J. J. Sokol, E. M. Rumberger, D. N. Hendrickson, J. R. Long, H. Park, and D. C. Ralph, Nano Lett. **6**, 2014 (2006).
[10] R. Sessoli, H. Tsai, A. Schake, S. Y. Wang, J. B. Vincent, K. Folting, D. Gatteschi, G. Christou, and D. N. Hendrickson, J. Am. Chem. Soc. **115**, 1804 (1993).
[11] M. Mannini, P. Sainctavit, R. Sessoli, C. Cartier dit Moulin, F. Pineider, M.-A. Arrio, A. Cornia, and D. Gatteschi, Chemistry A European Journal **14**, 7530 (2008).
[12] S. Accorsi, A.-L. Barra, A. Caneschi, G. Chastanet, A. Cornia, A. C. Fabretti, D. Gatteschi, C. Mortalo, E. Olivieri, F. Parenti, P. Rosa, R. Sessoli, L. Sorace, W. Wernsdorfer, and L. J. Zobbi, J. Am. Chem. Soc. **128**, 4742 (2006).
[13] L. Gregoli, C. Danieli, A.-L. Barra, P. Neugebauer, G. Pellegrino, G. Poneti, R. Sessoli, and A. Cornia, Chem.s Eur. J. **15**, 6456 (2009).
[14] M. Mannini, F. Pineider, P. Sainctavit, C. Danieli, E. Otero, C. Sciancalepore, A. Talarico, M.-A. Arrio, A. Cornia, D. Gatteschi, and R. Sessoli, Nat. Mater. **8**, 194 (2009).
[15] M. Mannini, F. Pineider, C. Danieli, F. Totti, L. Sorace, P. Sainctavit, M. A. Arrio, E. Otero, L. Joly, J. C. Cezar, A. Cornia, and R. Sessoli, Nature **468**, 417 (2010).
[16] A. S. Zyazin, J. W. G. van den Berg, E. A. Osorio, H. S. J. van der Zant, N. P. Konstantinidis, M. Leijnse, M. R. Wegewijs, F. May, W. Hofstetter, C. Danieli, and A. Cornia, Nano Letters **10**, 3307 (2010).
[17] A. S. Zyazin, H. S. J. van der Zant, M. R. Wegewijs, and A. Cornia, Synth. Met. **161**, 591 (2011).
[18] E. Burzurí, A. S. Zyazin, A. Cornia, and H. S. J. van der Zant, Phys. Rev. Lett. **109**, 147203 (2012).
[19] Ł. Michalak, C. M. Canali, M. R. Pederson, M. Paulsson, and V. G. Benza, Phys. Rev. Lett. **104**, 017202 (2010).
[20] S. Barraza-Lopez, K. Park, V. García-Suárez, and J. Ferrer, Phys. Rev. Lett. **102**, 246801 (2009).
[21] F. Rostamzadeh Renani and G. Kirczenow, Phys. Rev. B **85**, 245415 (2012).
[22] M. R. Pederson and S. N. Khanna, Phys. Rev. B **60**, 9566 (1999).
[23] J. Kortus, M. R. Pederson, T. Baruah, N. Bernstein, and C. Hellberg, Polyhedron **22**, 1871 (2003).
[24] A. V. Postnikov, J. Kortus, and M. R. Pederson, Phys. Stat. Sol. (b) **243**, 2533 (2006).
[25] M. R. Pederson and T. Baruah, *Handbook of Magnetism and Magnetic Materials*, edited by S. Parkin and H. Kronmullerr (J. Wiley and Sons, London, 2007) Chap. 9.
[26] T. Baruah and M. R. Pederson, Int. J. of Quant. Chem. **93**, 324 (2003).
[27] K. Park and M. R. Pederson, Phys. Rev. B **70**, 054414 (2004).
[28] C. van Wllen, J. Chem. Phys. **130**, 194109 (2009).
[29] P. J. S. Schmitt and C. v Wullen, J. Chem. Phys. **134**, 194113 (2011).
[30] J. F. Janak, Phys. Rev. B **18**, 7165 (1978).
[31] M. R. Pederson and K. A. Jackson, Phys. Rev. B **43**, 7312 (1991).
[32] M. R. Pederson and K. A. Jackson, Phys. Rev. B **41**, 7453 (1990).
[33] K. A. Jackson and M. R. Pederson, Phys. Rev. B **42**, 3276 (1990).
[34] J. P. Perdew, K. Burke, and M. Ernzerhof, Phys. Rev. Lett. **77**, 3865 (1996).
[35] S. Accorsi, A.-L. Barra, A. Caneschi, G. Chastanet, A. Cornia, A. C. Fabretti, D. Gatteschi, C. Mortal, E. Olivieri, F. Parenti, P. Rosa, R. Sessoli, L. Sorace, W. Wernsdorfer, and L. Zobbi, J. Am. Chem. Soc.

128, 4742 (2006).

[36] A. L. Barra, A. Caneschi, A. Cornia, F. Fabrizi de Biani, D. Gatteschi, C. Sangregorio, R. Sessoli, and L. Sorace, J. Am. Chem. Soc. **121**, 5302 (1999).

[37] J. Ribas-Arino, T. Baruah, and M. R. Pederson, J. Chem. Phys. **123**, 044303 (2005).

[38] J. Li, X. Li, H.-J. Zhai, and L.-S. Wang, Science **299**, 864 (2003).

[39] The fact that in Table III the spin magnetic moment of the $Q = -1$ charge state is not exactly equal to an integer is due to the fractional occupancy (approximately 15%) of the spin-down LUMO in our calculations, carried out with a finite smearing of the Fermi-Dirac distribution.

[40] Note however that the amplitude of the LUMO wavefunction is quite small in the central region. Therefore, an electron tunneling in from one of the leads would still find a bottleneck when tunneling out to the other lead.

[41] Note that in Ref. 16, the results reported for the anion and cation were obtained for sample A and B respectively.

[42] In general, in Ref. 18 it is found that upon reduction, either from $N \to N+1$ or from $N-1 \to N$, the spin S always *decreases* and the anisotropy parameter D, defined via $\Delta = DS^2$, always *increases*. The results of our calculations (see Table III) show that both the anion and the cation have preferably $S = 11/2$ for a lead of Type-2, whereas $S = 9/2$ for a lead of Type-1. However, states with swapped spin configurations $S = 11/2 \leftrightarrow S = 9/2$ are quite close in energy for both charged states.

9

Cotunneling signatures of spin-electric coupling in frustrated triangular molecular magnets

Cotunneling signatures of Spin-Electric coupling in frustrated triangular molecular magnets

J.F. Nossa[1,2] and C.M. Canali[1]

[1] *Department of Physics and Electrical Engineering, Linnaeus University, SE-39182 Kalmar, Sweden*
[2] *Solid State Physics/The Nanometer Structure Consortium, Lund University, Box 118, SE-221 00 Lund Sweden*

(Dated: August 2, 2013)

The ground state of frustrated (antiferromagnetic) triangular molecular magnets is characterized by two total-spin $S = 1/2$ doublets with opposite chirality. According to a group theory analysis [M. Trif *et al.*, Phys. Rev. Lett. **101**, 217201 (2008)] an external electric field can efficiently couple these two chiral spin states, even when the spin-orbit interaction (SOI) is absent. The strength of this coupling, d, is determined by an off-diagonal matrix element of the dipole operator, which can be calculated by *ab-initio* methods [M. F. Islam *et al.*, Phys. Rev. B **82**, 155446 (2010)]. In this work we propose that Coulomb-blockade transport experiments in the cotunneling regime can provide a direct way to determine the spin-electric coupling strength. Indeed, an electric field generates a d-dependent splitting of the ground state manifold, which can be detected in the inelastic cotunneling conductance. Our theoretical analysis is supported by master-equation calculations of quantum transport in the cotunneling regime. We employ a Hubbard-model approach to elucidate the relationship between the Hubbard parameters t and U, and the spin-electric coupling constant d. This allows us to predict the regime in which the coupling constant d can be extracted from experiment.

I. INTRODUCTION

Molecular nano-magnets (NMs)[1] represent a rich playground for exploring quantum mechanics at the nanoscale, and are intensively investigated both in condensed matter physics and chemistry. MMs, rationally designed and realized by chemical engineering,[2] are promising building blocks of electronic devices for molecular spintronics,[3,4] and for classical[5] and quantum information processing.[6–8] For applications in quantum computation, MMs with frustrated antiferromagnetic coupling between spins are particularly promising, since at low energies they behave effectively as magnetic two-level systems with long spin coherent times, which can be used as qbits to encode and manipulate quantum information.[2,8] One outstanding issue in quantum information processing is the need of realizing fast control and switching between quantum spin states. Standard spin-control techniques such as electron spin resonance (ESR), carried out by time dependent magnetic fields, have limitations, since in practice it is difficult to achieve switching times of the order of nanoseconds for large enough fields. The need to achieve spatial resolutions of the order of 1 nm represents another serious challenge for spin manipulations via magnetic fields. For these reasons, control via electric fields seems to be a much more promising alternative, since strong electric fields can be switched on and off fast, and applied selectively to nanoscale regions.[9–11]

Electric control and manipulation of magnetic properties is an important topic solid state physics, presently studied in multiferroic materials, dilute magnetic semiconductors and topological insulators. The electric control of nanomagnets presents both hard challenges and novel possibilities. Since electric fields do not couple directly to spins, electric control can typically occur only indirectly, e.g., via a manipulation of the spin-orbit interaction (SOI). Indeed, interesting spin-electric effects induced solely by SOI have been realized in semiconductor quantum dots.[12] The applicability of this procedure in MMs on the other hand is much harder, since the relative strength of the SOI scales with the volume of the system, implying that impractically large electric fields are required for systems of the order of a few nanometers. Therefore alternative schemes for efficient spin-electric coupling in MMs have been proposed. One example relies on the electric manipulation of the spin exchange constant[13,14] which can trigger various level crossings between magnetic states of a different total spin. Here we are interested in another type of spin-electric coupling, made it possible in certain antiferromagnetic MMs by the lack of inversion symmetry, as proposed by Trif *et al.*.[15] It turns out that in some of these antiferromagnetic molecules, such as the triangular $\{Cu_3\}$ and $\{V_3\}$ MMs,[16,17] and other odd-spin rings, an electric field can couple spin states through a combination of exchange and chirality of the spin-manifold ground state. For triangular MMs this coupling is nonzero even in the absence SOI.

The low-energy physics of a $\{Cu_3\}$ MM can be described by three identical spin $s = 1/2$ Cu cations, located at $\mathbf{r}_j$, $j = 1, 2, 3$, interacting via an antiferromagnetic (Heisenberg) exchange coupling (see Fig. 1). The ground state consists of two

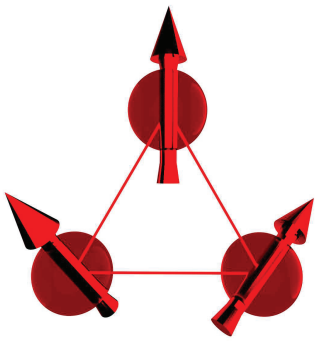

FIG. 1. Schematic representation of a triangular molecule.

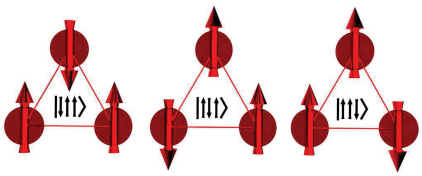

FIG. 2. The three independent spin configurations associated with total spin projection $S_z = 1/2$. The two GS chiral states $|E'_{\pm}, S_z = 1/2\rangle$ are linear combinations of these states.

total-spin $S = 1/2$ doublets, $|E'_{\pm}, S_z = \pm 1/2\rangle$, of opposite spin chirality, $E'_{\pm}$, which are degenerate in the absence of spin-orbit interaction. (Here E' refers to the two-dimensional irreducible representation (IR) of the D_{3h} symmetry group of the triangular MM, spanned by the two states, $|E'_{+}, S_z\rangle$ and $|E'_{-}, S_z\rangle$.) The states $|E'_{\pm}, S_z = 1/2\rangle$ can be written as linear combinations of the three frustrated spin configurations shown in Fig. 2.

According to an analysis based on group theory,[15,18] the matrix elements of the components of the operator $\mathbf{R} = \sum_{j=1}^{3} \mathbf{r}_j$ in the $\{Cu_3\}$ plane, $X_{\pm} = \pm X + iY$, between states of opposite chirality, do not vanish

$$e\langle E'_{+}, S_z|X_{-}|E'_{-}, S_z\rangle = e\langle E'_{-}, S_z|X_{+}|E'_{+}, S_z\rangle = 2id\,. \quad (1)$$

In Eq. 1 e is the electron charge, $i = \sqrt{-1}$, and the real number d has the units of an electric dipole moment. All the other matrix elements of $\mathbf{R}$ in the subspace spanned by $\{|E'_{\pm}, S_z = \pm 1/2\rangle\}$ are zero. The nonzero value of d is in fact related to the existence of a nonzero electric dipole moment in each of the three frustrated spin configurations of Fig. 2 that compose the chiral ground states.[19–22]

An electric field $\boldsymbol{\varepsilon}$ couples to the $\{Cu_3\}$ MM via $e\boldsymbol{\varepsilon} \cdot \mathbf{R}$. Then the non-zero matrix elements in Eq. 1 ensure that the amplitude of the spin-electric coupling between chiral states is *linear* in the field. Note that the electric-field–induced transitions conserve the total spin. However, in the presence of an additional small dc magnetic field that mixes the spin states, this spin-electric coupling can generate efficient electric transitions from one spin state to another.

The relevance of this spin-electric mechanism for qubit manipulation and qbits coupling clearly depends on the value of the electric dipole moment d. It has been proposed[15] that an experimental estimate of d can in principle be provided by ESR measurements in static electric fields. Nuclear magnetic resonance, magnetization and specific heat measurements have also been proposed to determine the strength of the coupling experimentally.[18] As far as we know these measurements have not yet been performed. Theoretically, a Hubbard model approach can provide understanding and a rough estimate of d in terms of a small number of Hubbard model parameters.[18]

In practice, a microscopic evaluation of d can only be provided by first-principles calculations. In fact, in Ref. 21 we have carried out Density Functional Theory (DFT) studies of a $\{Cu_3\}$ MM, and shown that d is of the order of $e10^{-4}a$, where a is the Cu separation. At electric fields of the order of 10^8 V/m, easily accessible in the vicinity of a scanning tunneling spectroscope (STM) tip, a d of this size would ensure transition times of the order of 1 ns. More recent DFT calculations[23] have shown that the value of d in other triangular molecules, such as $\{V_3\}$ $\{Cu_3O_3\}$ and $\{V_{15}\}$, can be one or two orders of magnitude larger than in $\{Cu_3\}$.

In this paper we carry out a theoretical study of quantum transport through an *individual* triangular antiferromagnetic MM displaying the spin-electric coupling, arranged in a single-electron transistor (SET) geometry. The main motivation of this work is to investigate whether the coherent coupling of the two spin chiral states induced and controlled by an electric field has detectable consequences on the transport properties of the MM. Our conclusion is that, in the cotunneling regime of Coulomb blockade transport, the GS energy splitting induced by the electric field should be easily accessible and should provide a direct estimate of the strength of the electric dipole moment parameter d. In this coherent regime, higher excited states of the MM could add as additional auxiliary states that can be exploited to perform quantum gates.[15] We also show that similar results could be obtained by performing inelastic electron tunneling spectroscopy through the MM adsorbed on surface by means of STM techniques. For the modeling of the MM we use the Hubbard model approach introduced in Ref. 18. This approach is quite convenient and transparent to address the effect of an applied electric field on the molecu-

lar orbitals of the molecule leading to the spin-electric coupling. The parameters of the model are extracted from our previous first-principles calculations on $\{Cu_3\}$. Quantum transport is studied by means of a quantum master equation including both sequential and cotunneling contributions. Transport studies on triangular systems using a similar formalism have been done recently.[24–28] But our motivation is different and an analysis of the spin-electric effect in this system has not been considered so far.

The paper is divided into the following. four sections. In Sec. II we introduce a Hubbard approach to model the effect of the electric field leading to the spin-electric coupling in terms of a few free parameters. In Sec. III we introduce the model and the formalism to study quantum transport and calculate the conductance in the sequential tunneling and cotunneling regime. In Sec. IV we present transport results. Finally, we summarize the conclusions of our work in Sec. V

II. HUBBARD MODEL APPROACH TO THE SPIN-ELECTRIC COUPLING

In this section we introduce the Hubbard model approach developed in Ref. 18 to analyze the spin-electric coupling. This approach is very useful for three reasons. Firstly, it describes the effect of the applied electric field on the orbital degrees of freedom of the MM, and therefore it elucidates the emergence of the spin-electric coupling at the microscopic level. Secondly, it permits the description of the spin-electric coupling in terms of a few parameters that can be evaluated by first-principles methods. Last but not least, it provides the natural framework to study later on quantum transport.

Before we introduce the Hubbard model, it is convenient to summarize the main results of the spin-electric coupling using the language of a spin Hamiltonian,[15] in part already anticipated in the introduction, which will then emerge again from the Hubbard model.

The ground-state manifold of a three-site spin $s = 1/2$ Heisenberg antiferromagnet, with isotropic exchange constant J, is given by the two doubly-degenerate chiral doublets

$$|E'_{\pm}, S_z = \frac{1}{2}\rangle = \frac{1}{\sqrt{3}}\big(|\downarrow\uparrow\uparrow\rangle + \epsilon_{\pm}|\uparrow\downarrow\uparrow\rangle + \epsilon_{\mp}|\uparrow\uparrow\downarrow\rangle\big)\ , \tag{2}$$

where $\epsilon_{\pm} = \exp(\pm 2\pi i/3)$. These states are eigenstates of the total spin $\mathbf{S^2}$ with eigenvalue $S = 1/2$, and of the total z component S_z, with eigenvalue $1/2$. The three spin configurations of Eq. 2 are shown in Fig. 2). Similar linear combinations can be written for the 2 eigenstates of S_z with eigenvalue $1/2$. These states are also eigenstates of the z-component of the chiral spin operator

$$C_z = \frac{4}{\sqrt{3}}\mathbf{s}_1 \cdot \mathbf{s}_2 \times \mathbf{s}_3\ , \tag{3}$$

with eigenvalue ± 1. (The $\pm$ in $E'_{\pm}$ refers to this quantum number.)

The lowest excited state, separated from the GS by an energy of order J, is the fourfold degenerate eigenstate of $\mathbf{S^2}$, with eigenvalue $3/2$. The element of this quartet that is an eigenstate of S_z with eigenvalue $1/2$, is written in terms of the same three spin configurations of Fig. 2 as

$$|A'_1, S_z = \frac{1}{2}\rangle = \frac{1}{\sqrt{3}}\big(|\downarrow\uparrow\uparrow\rangle + |\uparrow\downarrow\uparrow\rangle + |\uparrow\uparrow\downarrow\rangle\big)\ . \tag{4}$$

The four states $|A'_1, S_z\rangle$ form four A'_1 onedimensional IR of the symmetry group D_{3h}. Note that the expectation value of C_z for the states $|A'_1, S_z\rangle$ vanishes.

The SOI-induced Dzyaloshinskii-Moriya (DM) interaction splits the chiral GS manifold into two two-dimensional subspaces. As we discussed in the introduction, an electric field couples states of opposite chirality. These two interactions can be represented by the following low-energy effective spin Hamiltonian[15]

$$H_{\rm eff}^{\rm spin} = \Delta_{\rm SOI} C_z\, S_z + d\boldsymbol{\mathcal{E}} \cdot \mathbf{C}_{\parallel} \tag{5}$$

where $\mathbf{C}_{\parallel} \equiv (C_x, C_y, 0)$ is the component of the chiral operator in the xy plane. In Eq. 5 the energy $\Delta_{\rm SOI}$ is proportional to the SOI coupling strength, and turns out to be equivalent to the DM coupling constant D. The parameter d is the electric dipole moment introduced in Eq. 1. We will now see how this effective spin Hamiltonian emerges from the Hubbard model approach.[18]

The second quantized one-band Hubbard Hamiltonian reads

$$H_U = -\sum_{i,j}\sum_{\alpha}\Big\{t_{ij}c^{\dagger}_{i\alpha}c_{j\alpha} + \text{h.c.}\Big\} + \frac{1}{2}U\sum_{i} n_{i\uparrow}\, n_{i\downarrow}\ , \tag{6}$$

where $c^{\dagger}_{i\alpha}$ ($c_{i\alpha}$) creates (destroys) an electron with spin α at site i, $n_{i\alpha} = c^{\dagger}_{i\alpha}c_{i\alpha}$ is the particle number operator and t_{ij} is a spin-independent hopping parameter. More precisely the index i labels a Wannier function localized at site i. The first term represents the kinetic energy describing electrons hopping between nearest-neighbor sites i and j. For D_{3h} symmetry this term is characterized by a hopping parameter $t_{ij} = t$. The second-term is an on-site repulsion energy of strength U, which describe the energy cots associated with having two electrons of opposite spin on the same site. In this model the interaction energy between electrons which are not on the same site is completely neglected. The Hubbard model is the simplest

model describing the fundamental competition between the kinetic energy and the interaction energy of electrons on a lattice.

The spin-orbit interaction in the Hubbard model is described by adding the following spin-dependent hopping term[18,29–31]

$$H_{\rm SOI} = \sum_{i,j}\sum_{\alpha,\beta}\left\{c^\dagger_{i\alpha}\Big(i\frac{\mathbf{P}_{ij}}{2}\cdot\boldsymbol{\sigma}_{\alpha\beta}\Big)c_{j\beta}+\text{h.c.}\right\}, \quad (7)$$

where $\boldsymbol{\sigma} = \sigma_x\hat{x} + \sigma_y\hat{y} + \sigma_z\hat{z}$ is the vector of the three Pauli matrices. A commonly used notation for the Pauli matrices is to write the vector index i in the superscript, and the matrix indices as subscripts, so that the element in row α and column β of the the ith Pauli matrix is $\sigma^i_{\alpha\beta}$, with $i = x, y, z$. Here the vector $\mathbf{P}_{ij}$ is proportional to the matrix element of $\boldsymbol{\nabla}V \times \mathbf{p}$ between the orbital parts of the Wannier functions at sites i and j; V is the one-electron potential and $\mathbf{p}$ is the momentum operator. Clearly the spin-orbit term has the form of a spin-dependent hopping, which is added to the usual spin-independent hopping proportional to t. In Eq. (7), spin-orbit coupling induces a spin precession of magnitude about $\mathbf{P}_{ij}$ when an electron hops from site i to site j. This form of the spin-orbit interaction is a special case of Moriya's hopping terms[32] in the limit that all but one orbital energy is taken to infinity,[30] and it is consistent with our choice of a one-band Hubbard model. The x and y components of $\mathbf{P}_{ij}$ describe processes with different spin and because of the α_v symmetry, $\mathbf{P}_{ij} = p\mathbf{e}_z$. Therefore, because of the symmetry of the molecule the free Hubbard parameters are reduced to three, namely, t, U and p.

The final expression of the Hamiltonian describing the electrons in a triangular molecule, including the spin-orbit interaction, is

$$H_{U+\rm SOI} = \sum_{i,\alpha}\Big\{c^\dagger_{i\alpha}\big(-t + i\lambda_{\rm SOI}\alpha\big)c_{i+1\alpha}+\text{h.c.}\Big\} + \sum_{i,\alpha}\left(\epsilon_0 n_{i\alpha} + \frac{1}{2}U n_{i\alpha}\, n_{i\bar{\alpha}}\right), \quad (8)$$

where $\lambda_{\rm SOI} \equiv p/2 = \mathbf{P}_{ij}/2\cdot\mathbf{e}_z$ is the spin-orbit parameter, ϵ_0 is the on-site orbital energy, and $\bar{\alpha} = -\alpha$.

We want to treat the two hopping terms perturbatively on the same footing, by doing an expansion around the atomic limit t/U , $\lambda_{\rm SOI}/U \to 0$. In many molecular magnets $t \gg \lambda_{\rm SOI}$. This turns out to be the case also for $\{Cu_3\}$.[33] In other molecules the two hopping parameters are of the same order of magnitude.

We are interested in the half-filled regime. From second-order perturbation theory in t/U, an antiferromagnetic isotropic exchange term emerges and it splits the spin degeneracy of the low-energy sector of the Hubbard model, which is defined by the singly-occupied states.

The perturbative method requires the definition of the unperturbed states being the one-electron states

$$|\phi^\alpha_i\rangle = c^\dagger_{i\alpha}|0\rangle, \quad (9)$$

singly occupied three-electron states

$$|\psi^\alpha_i\rangle = \prod_{j=1}^{3} c^\dagger_{j\alpha_j}|000\rangle = \prod_{j=1}^{3}\left|\phi^{\alpha_j}_j\right\rangle, \quad (10)$$

with $\alpha_j = \alpha$ for $j \neq i$ and $\alpha_j = \bar{\alpha}$, for $j = i$. Finally the double-occupied three electron states

$$\left|\psi^\alpha_{ij}\right\rangle = c^\dagger_{i\uparrow}c^\dagger_{i\downarrow}c^\dagger_{j\alpha}|000\rangle, \quad (11)$$

with $i = 1, 2, 3$ and $j \neq i$. Note that the states in Eqs. (9)-(11) are eigenstates of the Hamiltonian, Eq. (8), only in the absence of the hopping and spin-orbit parameter and with energies ϵ_0, $3\epsilon_0$ and $3\epsilon_0 + U$, respectively. These states are not yet symmetry adapted states of the D_{3h} point group. Symmetry adapted states can be found using the the projector operator formalism.[18,34] One-electron symmetry adapted states can be written as a linear combinations of one-electron states, Eq. (9),

$$\left|\Phi^\alpha_{A'_1}\right\rangle = \frac{1}{\sqrt{3}}\sum_{i=1}^{3}|\phi^\alpha_i\rangle, \quad (12)$$

and

$$\left|\Phi^\alpha_{E'_\pm}\right\rangle = \frac{1}{\sqrt{3}}\sum_{i=1}^{3}\epsilon^{i-1}_{1,2}\,|\phi^\alpha_i\rangle \quad , \quad (13)$$

where A'_1 and $E'_\pm$ are one-dimensional and two-dimensional IR in D_{3h} point group, respectively and $\epsilon^k = \exp\left((2\pi i/3)^k\right)^{1,2}$ is a phase factor. The three-electron symmetry adapted states for singly-occupied magnetic centers can be written as

$$\left|\psi^{1\alpha}_{A'_1}\right\rangle = \frac{1}{\sqrt{3}}\sum_{i=1}^{3}|\psi^\alpha_i\rangle, \quad (14)$$

and

$$\left|\psi^{1\alpha}_{E'_\pm}\right\rangle = \frac{1}{\sqrt{3}}\sum_{i=1}^{3}\epsilon^{i-1}_{1,2}\,|\psi^\alpha_i\rangle, \quad (15)$$

The states $|\psi^{1\alpha}_{E'_+}\rangle$ and $|\psi^{1\alpha}_{E'_-}\rangle$ have total spin $S = 1/2$ and z-spin projection $S_z = \pm 1/2$. These states are formally identical to the chiral states given in Eq. (2), and are eigenstates of the Hubbard Hamiltonian when $t = \lambda_{\rm SOI} = 0$. The tunneling and SOI mix the singly-occupied and double-occupied states. Symmetry properties of D_{3h} point group dictates that the tunneling and SOI terms in the Hubbard Hamiltonian transform

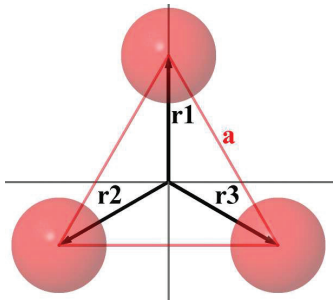

FIG. 3. Coordinates of magnetic centers in a triangular molecule. $\mathbf{r}_i$ is the coordinate of the ith electron.

as the IR A_1'. Therefore, only states transforming according to the same IR could be mixed. The first-order correction in t/U and $\lambda_{\rm SOI}/U$ is obtained by mixing in doubly-occupied states

$$|\Phi^{1\,\alpha}_{E'_\pm}\rangle \equiv |\psi^{1\,\alpha}_{E'_\pm}\rangle + \frac{(\epsilon^1_2-1)(t\pm\alpha\lambda_{\rm SOI})}{\sqrt{2}U}|\psi^{2\,\alpha}_{E'^1_\pm}\rangle + \frac{3\epsilon^1_1(t\pm\alpha\lambda_{\rm SOI})}{\sqrt{2}U}|\psi^{2\,\alpha}_{E'^2_\pm}\rangle\,, \tag{16}$$

where

$$|\psi^{2\,\alpha}_{E'^1_\pm}\rangle = \frac{1}{\sqrt{6}}\sum_{i=1}^{3}\epsilon^{i-1}_{1,2}\left(|\psi^\alpha_{i1}\rangle + |\psi^\alpha_{i2}\rangle\right)\,, \tag{17}$$

and

$$|\psi^{2\,\alpha}_{E'^2_\pm}\rangle = \frac{1}{\sqrt{6}}\sum_{i=1}^{3}\epsilon^{i-1}_{1,2}\left(|\psi^\alpha_{i1}\rangle - |\psi^\alpha_{i2}\rangle\right)\,, \tag{18}$$

are three-electron symmetry adapted states for double occupied magnetic centers.

In the small t/U , $\lambda_{\rm SOI}/U$ limit, we can resort to a spin-only description of the low-energy physics of the system. The ground state manifold (corresponding to the states Eq. (16)) is given by the two chiral spin states of Eq. (2). In this low-energy regime the orbital states correspond to the singly-occupied localized atomic orbitals. The lowest energy states have total spin $S = 1/2$ and chirality $C_z = \pm 1$. Using the same perturbative procedure, we can construct approximate Hubbard model states corresponding to the $S = 3/2$ excited-state quartet of Eq. 4. To first order in t/U and $\lambda_{\rm SOI}/U$ one obtains

$$|\Phi^{1\,\alpha}_{A'_1}\rangle = |\psi^{1\,\alpha}_{A'_1}\rangle \tag{19}$$

The energy of the $S = 3/2$ quartet is $3J/2$ higher in energy than the energy of the chiral GS doublets, with $J \approx 4t^2/U$.

We now introduce the effect of the external electric field. An external electric field $\boldsymbol{\varepsilon}$ can couple to the molecule via two mechanisms. The first mechanism that we will study is by the modification of the on-site energies ϵ_0 via the Hamiltonian

$$H^0_{d-\varepsilon} = \sum_\alpha\sum_{i=1}^{3}\left(-e\mathbf{r}_i\cdot\boldsymbol{\varepsilon}\right)c^\dagger_{i\alpha}c_{i\alpha}, \tag{20}$$

where $\mathbf{r}_i$ is the coordinate vector of the ith magnetic center. From Fig. 3, the on-site electric Hamiltonian can be written as

$$H^0_{d-\varepsilon} = -ea\sum_\alpha\left[\frac{\varepsilon^y}{\sqrt{3}}c^\dagger_{1\alpha}c_{1\alpha} - \frac{1}{2}\left(\varepsilon^x + \frac{\varepsilon^y}{\sqrt{3}}\right)c^\dagger_{2\alpha}c_{2\alpha} + \frac{1}{2}\left(\varepsilon^x - \frac{\varepsilon^y}{\sqrt{3}}\right)c^\dagger_{3\alpha}c_{3\alpha}\right], \tag{21}$$

where $\varepsilon^{x,y}$ are the in-plane coordinates of the electric field, e the electron charge and a the distance between magnetic centers.

The second mechanism is given by the modification of the hopping parameters t_{ii+1} and it can be written as

$$H^1_{d-\varepsilon} = \sum_\alpha\sum_{i=1}^{3}t^{\boldsymbol{\varepsilon}}_{ii+1,\alpha}c^\dagger_{i\alpha}c_{i+1\alpha} + \text{H.c.}, \tag{22}$$

where $t^{\boldsymbol{\varepsilon}}_{ii+1,\alpha} = \langle\phi^\alpha_i| - e\mathbf{r}\cdot\boldsymbol{\varepsilon}|\phi^\alpha_{i+1}\rangle$ are the modified hopping parameters due to the external electric field $\boldsymbol{\varepsilon}$, ϕ^α_i are the Wannier states localized on the ith magnetic center with spin α. These induced hopping parameters can be written as $t^{\boldsymbol{\varepsilon}}_{ii+1,\alpha} = \sum_q q^\alpha_{ii+1}\varepsilon_q$, with $q^\alpha_{ii+1} = -e\langle\phi^\alpha_i|q|\phi^\alpha_{i+1}\rangle$ and $q = x, y, z$. D_{3h} point group symmetry properties, given by the dipole selection rules, reduce the number of free parameters induced by the electric field. Finding these free parameters is not an easy task when the basis set are the localized Wannier orbitals. In order to investigate the effect of the electric field on the triangular molecule we switch from the localized Wannier basis set to the symmetry adapted basis set $\Gamma = A'_1, E'_\pm$. Then we apply the transition dipole selection rules to the new induced hopping parameters. In the symmetry adapted states, the hopping-Hamiltonian, Eq. (22), reads

$$H^1_{d-\varepsilon} = \sum_\alpha\sum_{\Gamma\Gamma'}t^{\boldsymbol{\varepsilon}}_{\Gamma,\Gamma',\alpha}c^\dagger_{\Gamma\alpha}c_{\Gamma'\alpha} + \text{H.c.}, \tag{23}$$

where $\Gamma, \Gamma' = A'_1, E'_+, E'_-$, $t^{\boldsymbol{\varepsilon}}_{\Gamma,\Gamma',\alpha} = \sum_q q^\alpha_{\Gamma\Gamma'}E_q$, with $q = x, y, z$ and $q^\alpha_{\Gamma\Gamma'} = -e\langle\phi^\alpha_\Gamma|q|\phi^\alpha_{\Gamma'}\rangle$. Here $c^\dagger_{\Gamma\alpha}(c_{\Gamma\alpha})$ creates (destroys) an electron in the adapted state Γ with spin α. Note that in Eq. (23) all the possible transitions are included, even those between states of the same symmetry adapted basis set. Dipole transition rules then will select the allowed transitions and the corresponding states. Although symmetry properties control the dipole transition rules, they do not allow us to calculate

the strength of the transitions. Detailed experimental measurements and/or accurate *ab*-initio calculations have to be carried out to determine them. In the D_{3h} point group the (x, y) and z coordinates span as E' and A_1' IR, respectively. We have grouped x and y because they form a degenerate pair within the E' representation. From character tables of D_{3h} point group we have the only allowed transitions correspond to

$$\begin{aligned}\left\langle \phi^{\alpha}_{E'_+}\right| x \left|\phi^{\alpha}_{E'_-}\right\rangle &= -i\left\langle \phi^{\alpha}_{E'_+}\right| y \left|\phi^{\alpha}_{E'_-}\right\rangle \equiv -\frac{d_{EE}}{e}\\ \left\langle \phi^{\alpha}_{A'_1}\right| x \left|\phi^{\alpha}_{E'_+}\right\rangle &= -i\left\langle \phi^{\alpha}_{A'_1}\right| y \left|\phi^{\alpha}_{E'_+}\right\rangle \equiv -\frac{d_{AE}}{e}\\ \left\langle \phi^{\alpha}_{A'_1}\right| x \left|\phi^{\alpha}_{E'_-}\right\rangle &= i\left\langle \phi^{\alpha}_{A'_1}\right| y \left|\phi^{\alpha}_{E'_-}\right\rangle \equiv -\frac{d_{AE}}{e}\end{aligned} \tag{24}$$

where d_{EE} and d_{AE} are the only two free parameters to be determined. Here we have used the symmetry rule that the product $f_1 \otimes f_2 \otimes f_3 \neq 0$ if it spans A_1 representation. All the other possible transitions are not allow within the D_{3h} symmetry group. Inserting these allowed transitions into the Hamiltonian, Eq. (23), we have

$$\begin{aligned}H^1_{d-\varepsilon} = \sum_{\alpha}\Big[&d_{AE}\left(\bar{\mathcal{E}}c^{\dagger}_{A'_1\alpha}c_{E'_-\alpha} + \mathcal{E}c^{\dagger}_{A'_1\alpha}c_{E'_+\alpha}\right)\\ &+ d_{EE}\bar{\mathcal{E}}c^{\dagger}_{E'_-\alpha}c_{E'_+\alpha}\Big] + \text{H.c.},\end{aligned} \tag{25}$$

where $\mathcal{E} = \varepsilon^x + i\varepsilon^y$ and $\bar{\mathcal{E}} = \varepsilon^x - i\varepsilon^y$. Note that the parameter d_{AE} and d_{EE} tell us about the possible dipole-electric transitions between states that span the A'_1-$E'_{\pm}$ and E'_+-E'_- IR, respectively. From Eq. (15) we can see that the chiral states also span the $E_{\pm}$ IR.

To take even more advantage of the symmetry of the triangular molecule, we now write the relationship between the second quantized operators $c^{\dagger}_{i\alpha}, c_{i\alpha}$ and the symmetry adapted operators $c^{\dagger}_{\Gamma\alpha}, c_{\Gamma\alpha}$. From Eqs. (9),(12) and (13), we have

$$\begin{pmatrix} c^{\dagger}_{A'_1\alpha}\\ c^{\dagger}_{E'_+\alpha}\\ c^{\dagger}_{E'_-\alpha}\end{pmatrix} = \begin{pmatrix}1 & 1 & 1\\ 1 & \epsilon & \epsilon^2\\ 1 & \epsilon^2 & \epsilon\end{pmatrix}\begin{pmatrix} c^{\dagger}_{1\alpha}\\ c^{\dagger}_{2\alpha}\\ c^{\dagger}_{3\alpha}\end{pmatrix}, \tag{26}$$

where we have used $\epsilon^4 = \epsilon$. From last equation we can write the localized second quantized operators as linear combination of symmetry adapted operators

$$\begin{pmatrix} c^{\dagger}_{1\alpha}\\ c^{\dagger}_{2\alpha}\\ c^{\dagger}_{3\alpha}\end{pmatrix} = \begin{pmatrix}1 & 1 & 1\\ 1 & \epsilon^2 & \epsilon\\ 1 & \epsilon & \epsilon^2\end{pmatrix}\begin{pmatrix} c^{\dagger}_{A'_1\alpha}\\ c^{\dagger}_{E'_+\alpha}\\ c^{\dagger}_{E'_-\alpha}\end{pmatrix}. \tag{27}$$

Now we can write the rest of the perturbed Hamiltonian, namely the $H^0_{d-\varepsilon}$ on-site electric field Hamiltonian (Eq. (21)) and H_{SOI} spin-orbit Hamiltonian (Eq. (7)), in terms of the symmetry adapted operators

$$\begin{aligned}H^0_{d-\varepsilon} = -\frac{iae}{2\sqrt{3}}\sum_{\alpha}\Big[&\bar{\mathcal{E}}c^{\dagger}_{E'_+\alpha}c_{A'_1\alpha} - \mathcal{E}c^{\dagger}_{E'_-\alpha}c_{A'_1\alpha}\\ &+\bar{\mathcal{E}}c^{\dagger}_{E'_-\alpha}c_{E'_+\alpha}\Big] + \text{H.c.},\end{aligned} \tag{28}$$

and

$$H_{\text{SOI}} = \sqrt{3}\lambda_{\text{SOI}}\sum_{\alpha}\alpha\left(c^{\dagger}_{E'_-\alpha}c_{E'_-\alpha} - c^{\dagger}_{E'_+\bar{\alpha}}c_{E'_+\bar{\alpha}}\right). \tag{29}$$

We conclude this section with the following important considerations

1. With the use of the symmetry properties of the triangular molecule, the Hubbard model in the presence of SOI (Eq. 29) and external electric field (Eqs. (25) and (28)), can be parametrized by five free parameters: t, U, λ_{SOI}, d_{EE} and d_{AE}. For a realistic MM, t, U, λ_{SOI} can be extracted from first-principles calculations, as for example done in Ref. 33 for $\{Cu_3\}$. An analogous determination of the single-particle parameters d_{EE} and d_{AE} has not been attempted so far. For localized orbitals, one expects $ea >> d_{EE}, d_{AE}$, and this the assumption that we will make in the paper.
2. Eqs. (25) and (28) and Eq. (29) are completely consistent with the effective spin Hamiltonian result of Eq. 5, in that they imply a splitting of the chiral GS by the SOI, and a linear coupling of the same states by an electric field. Note also that the SOI does not mix states of different chirality and/or spin.
3. Clearly Eqs. (25) and (28) and Eq. (29) are single-particle Hamiltonian. In order to extract the electric-dipole moment d and the DM splitting δ_{SOI} appearing in Eq. 5, one has to take matrix elements of these Hamiltonians between many-body states $|\Phi^{1\alpha}_{E'_{\pm}}\rangle$ defined in Eq. (16). For the matrix elements of the electric field Hamiltonian one finds[18]

$$\left|\left\langle \Phi^{1\alpha}_{E'_-}\right| H^0_{d-\varepsilon}\left|\Phi^{1\alpha}_{E'_+}\right\rangle\right| \simeq \left|\frac{t^3}{U^3}\mathcal{E}ea\right|, \tag{30}$$

$$\left|\left\langle \Phi^{1\alpha}_{E'_-}\right| H^1_{d-\varepsilon}\left|\Phi^{1\alpha}_{E'_+}\right\rangle\right| \simeq \left|\frac{4t}{U}\mathcal{E}d_{EE}\right|. \tag{31}$$

It follows that the electric-dipole moment d of the spin electric coupling is given by a combination of $\left|\frac{t^3}{U^3}ea\right|$ and $\left|\frac{4t}{U}d_{EE}\right|$.

4. In the presence of an electric field, the degenerate GS chiral manifold $\{|\Phi^{1\alpha}_{E'_{\pm}}\rangle\}$ is replaced by the coherent linear superpositions

$$\left|\chi^{\alpha}_{\pm}(\boldsymbol{\varepsilon})\right\rangle == \frac{1}{\sqrt{2}}\left(|\Phi^{1\alpha}_{E'_+}\rangle + \pm\frac{|\mathbf{d}\cdot\boldsymbol{\varepsilon}|}{\mathbf{d}\cdot\boldsymbol{\varepsilon}}|\Phi^{1\alpha}_{E'_-}\rangle\right) \tag{32}$$

with energies

$$\text{E}_{\pm}(\varepsilon) = \text{E}_{\pm}(0) \pm d\,\varepsilon/\sqrt{2} \tag{33}$$

Note that spin degeneracy is preserved, even when SOI is included. The electric-field–induced splitting of the chiral GS, $\Delta E(\varepsilon) \equiv E_+(\varepsilon) - E_-(\varepsilon)$, is proportional to ε, at least in this approximation, in agreement with the effective spin Hamiltonian approach. We will refer to the states $\left|\chi^{\alpha}_{\pm}(\boldsymbol{\varepsilon})\right\rangle$ as *mixed chiral states*. They will play a crucial role in transport.

5. Eqs. (25) and (28) show that an electric field, in fact, can couple $\{|\Phi^{1\,\alpha}_{E'_\pm}\rangle\}$ with $|\Phi^{1\,\alpha}_{A'_2}\rangle$. However this coupling, which in principle could affect Eq. 32 is not important, since these states are separated by an energy of order J. We will therefore disregard it.

In Figs. 4and 5 we plot the computed energy splitting of the chiral GS, $\Delta E(\varepsilon)$, induced by an electric field of strength ε, as a function of ε and t/U. The splitting is, as expected, linear in ε at small fields. This is the landmark of the spin-electric coupling. However, at larger field, we find also a quadratic dependence. Is seems that, despite the large value of U, the system has a sizable polarizability, leading to an rather strong induced electric dipole moment in the presence of a field. This is responsible for the quadratic contribution in $\Delta E(\varepsilon)$.

All the calculations on the model presented in the next section are obtained by exact diagonalization of the Hubbard model for $N = 2, 3, 4$ filling or *charge states*. It turns out, however, that for the values of the parameters relevant for $\{Cu_3\}$, the perturbative results in t/U are typically quite close to the exact results.

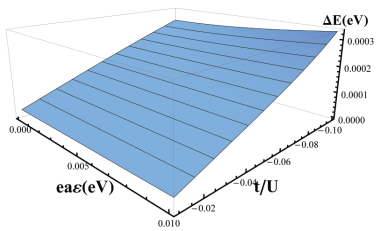

FIG. 4. (Color online) Electric-field–induced splitting $\Delta E(\varepsilon)$ of the chiral GS energy for a triangular MM at half-filling ($N = 3$), as a function of field strength ε and t/U. At these small/moderate values of the field, $\Delta E(\varepsilon)$ depends linearly on ε.

III. TRANSPORT MODEL AND MASTER EQUATION APPROACH

A. Transport setup

We are interested in studying quantum transport through a triangular MM, weakly coupled to conducting leads, gated, and with the possibility of an extra external electric field for control of the spin-electric coupling. The transport regime that we have in mind is predominately the one where transport is controlled by Coulomb blockade physics. Later in this section we will also comment on the possibility of employing inelastic electric tunneling spectroscopy without the presence of charging effects.

A possible transport geometry is schematically shown in Fig. 6. The MM is placed on a surface (semiconducting or insulating.). Two conducting coplanar leads acting as source (S) and drain (D) are constructed on the surface, for example using techniques recently to realize a single-atom transistor.[35] the molecule is weakly couple to S and D leads via ligands. Two in-plane gates (G1 and G2) are also patterned on either side of the transport channel. The orientation of the MM on the surface is such that the electric from the gate is orthogonal to the plane of the MM, and it is simply used as a capacitative coupling to control the chemical potential of MM. Alternatively, S and D nanoleads and gate electrodes can be constructed by nano-

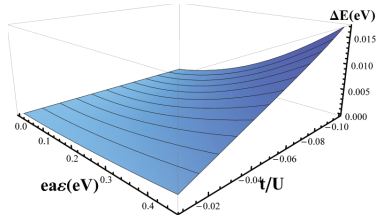

FIG. 5. (Color online) The same as in Fig. 4, but for larger values of the electric field, showing a quadratic dependence of $\Delta E(\varepsilon)$ due to an induced electric dipole moment.

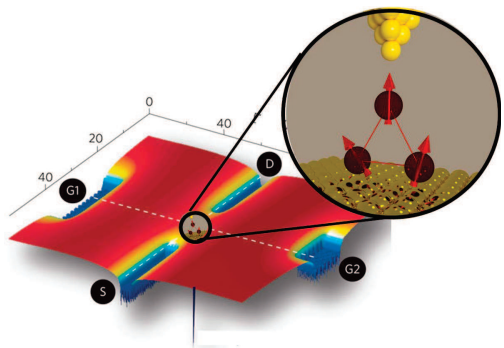

FIG. 6. Schematic representation of the transport geometry with a triangular MM. Picture modified from the original work by Fuechsle *et.al.*. Reprinted by permission from Macmillan Publishers Ltd: Nature Nanotechnology 7, 242246, copyright (2012)

lithography by depositing metal atoms (e.g., Au) on an insulating surface. Finally, a STM tip is positioned in the vicinity of the MM (see the blown-up region of the device close to the MM). This electrode is supposed to provide another *strong* and *localized* electric field to manipulate the MM states via the spin-electric coupling discussed in the previous section.

The construction of the device described here is very challenging. But we rely on recent progress in STM nano-lithography, and especially in funcionalizing MMs on surfaces.

A second possibility is to study transport in a single-electron transistor (SET) built in more traditional molecular electronic device. MMs are presently being successfully investigated with this techniques.[14,36? ? ,37] Here the challenge is to provide and independent extra gate electrode (besides the ordinary back gate) to reliably generate an in-plane electric field triggering the spin-electric coupling.

In the following we will assume that the following three features are present in our system: (i) source and drain leads weakly coupled to the molecule, providing a bias voltage V_b for electric transport; (ii) a gate voltage generating a variable potential V_g on the molecule able to manipulate its charge state; (iii) a third independent local electric field $\boldsymbol{\varepsilon}$, of strengths typically attainable in the vicinity of a STM, with a component in the plane of the MM.

B. Hamiltonian of the transport device

The Hamiltonian of the system, schematically represented in Fig. 6, is the sum of three terms

$$\mathcal{H} = \mathcal{H}_{L/R} + \mathcal{H}_{\rm mol} + \mathcal{H}^T_{L/R}\,, \qquad (34)$$

where

$$\mathcal{H}_{L/R} = \sum_{k\alpha} \varepsilon^{L/R}_k a^\dagger_{L/Rk\alpha} a_{L/Rk\alpha} \qquad (35)$$

describes free (*i.e.*, noninteracting) electrons in the left/right conducting lead (source/drain). Here, the operator $a^\dagger_{L/Rk\alpha}$ ($a_{L/Rk\alpha}$) creates (destroys) one electron with wave vector k and spin α in the left/right lead, respectively with energy $\varepsilon^{L/R}_k$. The tunnel junctions representing the coupling between leads and MM are described by the tunneling Hamiltonian

$$\mathcal{H}^T_{L/R} = \sum_{km\alpha} \left(T^{L/R}_{km\alpha} a^\dagger_{L/Rk\alpha} c_{m\alpha} + \text{H.c.} \right), \qquad (36)$$

where $T^{L/R}_{km\alpha}$ is the tunneling amplitude, $c^\dagger_{m\alpha}$ ($c_{m\alpha}$) creates (destroys) an electron in a single particle state with quantum numbers m and α inside the MM. The tunneling Hamiltonian $\mathcal{H}^T_{L/R}$ is treated as a perturbation to $\mathcal{H}_{\rm mol}$ and $\mathcal{H}_{L/R}$.

The general form of the MM Hamiltonian is given by

$$\mathcal{H}_{\rm mol} = \mathcal{H}_0 + \mathcal{H}_U + \mathcal{H}_t + \mathcal{H}_{\rm SOI} + \mathcal{H}_{\rm EF}, \quad (37)$$

where

$$\mathcal{H}_0 = \sum_j \sum_\alpha \left(\epsilon_j - e\,V_g\right) c^\dagger_{j\alpha} c_{j\alpha}, \qquad (38)$$

with V_g the gate voltage. $\mathcal{H}_U = U \sum_j n_{j\uparrow} n_{j\downarrow}$ with U the on-site Coulomb repulsion parameter and $n_{j\alpha} = c^\dagger_{j\alpha} c_{j\alpha}$ the number operator. $\mathcal{H}_t = t \sum_j \sum_\alpha c^\dagger_{j\alpha} c_{j+1\alpha} + \text{H.c.}$ the hopping Hamiltonian with t the hopping parameter. $\mathcal{H}_{\rm EF} = \mathcal{H}^1_{d-\varepsilon} + \mathcal{H}^0_{d-\varepsilon}$ the electric field Hamiltonian defined in Eqs. (25) and (28) and $\mathcal{H}_{\rm SOI}$ the spin-orbit Hamiltonian defined in Eq. (29).

We assume the Coulomb interaction between electrons in the MM and those in the environment, to be determined by a single and constant capacitance $C = C_L + C_R + C_g$, where $C_{L/R}$ and C_g are the capacitances of the right/left lead and the gate electrode, respectively. Another assumption is that the single-particle spectrum is independent of these interactions.

Quantum transport, e.g. the calculation of the tunneling conductance as a function of bias and gate voltages, can now be studied by means of a quantum master equation. General derivations of these equations have recently appeared in the literature,[38–40] together with several approximate solutions applied to SETs with quantum dots[41] and molecules,[39,40,42] including MMs.[38,43–46] The simplest strategy is to solve these equations perturbatively in the tunneling Hamiltonian.[47]

C. Coulomb blockade Regime, Sequential Tunneling

In the regime of weak coupling between leads and molecule, transport occurs via the so-called sequential tunneling.[47] We review here the main characteristics of this regime an the steps leading to the calculation of the current.[47] In this regime the conductance of the tunnel junctions should be much smaller than the quantum of conductance $\mathcal{G}_Q = 2e^2/h$. The electron tunneling rates Γ should be much smaller than the charging energy E_c of the molecule and the the temperature: $\hbar\Gamma \ll k_{\rm B}T \ll E_c$. The time between two tunneling events Δt is the longest time scale in the regime. In particular $\Delta t \gg \tau_\phi$, where τ_ϕ is the electron phase coherence. This guarantees that once the electron tunnels in, it has the time to loose its phase coherence before it tunnels out. Therefore the charge state can be treated classically and superposition

of different charge states is not allowed. Only one-electron transitions between leads and molecule occur in the system. These transitions are characterized by rates Γ_{ij}, where i, j are the initial and final system states of the system involved in the electron transfer. The system is described by stationary non-equilibrium populations $\mathcal{P}_i$ of the state i. These occupation probabilities can be obtained from the master equation

$$\frac{d}{dt}\mathcal{P}_i = \sum_{j(j\neq i)} \left(\Gamma_{ij}\mathcal{P}_j - \Gamma_{ji}\mathcal{P}_i\right) . \tag{39}$$

The first RHS term represents events where the electron tunnels into the state i from the state j, while the second RHS term represents events where the electron tunnels out from the state i into the state j. These probabilities obey the normalization condition

$$\sum_i \mathcal{P}_i = 1 . \tag{40}$$

In the steady state, the probabilities are time-independent $d\mathcal{P}_i/dt = 0$, therefore Eq. (39) can be written as

$$0 = \frac{d}{dt}\mathcal{P}_i = \sum_{j(j\neq i)} \left(\Gamma_{ij}\mathcal{P}_j - \Gamma_{ji}\mathcal{P}_i\right) . \tag{41}$$

In the regime of sequential tunneling the transition amplitudes are computed by first-order perturbation theory in the tunneling Hamiltonian $\mathcal{H}^T$, Eq. (36). Therefore the transition rates from state i to state j, through the left/right lead, are given by Fermi's golden Rule

$$\Gamma^{L/R}_{i\to j} = \frac{2\pi}{\hbar}\sum_{i,j}\left|\left\langle j\left|H^T_{L/R}\right|i\right\rangle\right|^2 W_i\delta(E_j - E_i) , \tag{42}$$

where W_i is a thermal distribution function and $E_j - E_i$ gives the energy conservation. The states $|i\rangle$ and $|j\rangle$ are the unperturbed system states and are defined as a product of the molecule and lead states $|i\rangle = |i_{mol}\rangle \otimes |i_l\rangle \otimes |i_r\rangle$. Transition rates depend on whether an electron is leaving or entering the molecule through the left or right lead. Inserting the tunneling Hamiltonian Eq. (36) into the Fermi's golden Rule, Eq. (42), the transition rates become[47,48]

$$\Gamma^{L/R,-}_{i\to j} = \gamma^{L/R,-}_{ji}\left[1 - f_{L/R}(E)\right] , \tag{43}$$

$$\Gamma^{L/R,+}_{i\to j} = \gamma^{L/R,+}_{ji}\left[f_{L/R}(E)\right] , \tag{44}$$

where

$$\gamma^{L/R,-}_{ji} = \Gamma^{L/R}\sum_{m,\alpha}\left|\langle j\left|c_{m,\alpha}\right|i\rangle\right|^2 \tag{45}$$

and

$$\gamma^{L/R,+}_{ji} = \Gamma^{L/R}\sum_{m,\alpha}\left|\langle j\mid c^\dagger_{m,\alpha}\mid i\rangle\right|^2 \tag{46}$$

are the transition matrix elements between the states j and i of the molecule (we have now dropped the label "mol"); $E = E_j - E_i$ is the energy difference between molecule many-electron states, and $f_{L/R}(E) = \left[e^{(E-\mu_{L/R})/k_BT} + 1\right]^{-1}$ is the Fermi function. Here the combination between the tunneling amplitudes $T^{L/R}_{m,\alpha}$ and the left/right lead density of states $D_{L/R}(i_{L/R})$ is assumed to be constant: $\Gamma^{L/R} = (2\pi/\hbar)\left|T^{L/R}_{m,\alpha}\right|^2 D_{L/R}(i_{L/R}) = (2\pi/\hbar)\left|T^{L/R}\right|^2 D_{L/R}(i_{L/R})$. The full transition matrix in the master equation, Eq. (39) is the sum of all contributions of electrons tunneling out or into the molecule, Eqs. (43) and (44):

$$\Gamma_{ij} = \Gamma^{L,+}_{ij} + \Gamma^{R,+}_{ij} + \Gamma^{L,-}_{ij} + \Gamma^{R,-}_{ij} . \tag{47}$$

The stationary rate equation, Eq. (41), is a system of linear equations and has to be solved numerically for a system of n many-electron states that are taking into account. We can rewrite it as a matrix equation

$$0 = \sum_j^n \Lambda_{ij}\mathcal{P}_j, \tag{48}$$

where

$$\Lambda_{ij} = \Gamma_{ij} - \delta_{ij}\sum_{k=1}^n \Gamma_{kj}. \tag{49}$$

There must exist a physical solution to Eq. (48). Therefore we replace the first line of of this equation by the normalization condition, Eq. (40), fixing $\Lambda_{1j} = 1$. Thus we can write

$$\delta_{1i} = \sum_j^n \Lambda_{ij}\mathcal{P}_j \tag{50}$$

instead Eq. (48). Because Coulomb blockade is typically studied at low temperatures some transitions rates might become exponentially small. This leads to numerical problems in solving Eq. 50. Then some of the states do not contribute and one has to develop a convenient truncation method.[44]

Finally, the current flowing through left lead coming into the molecule must be equal to the current flowing through right lead coming out from the molecule. Knowing the occupation probabilities, Eq. (41), the current through the system is defined as[41]

$$I \equiv I^{L/R} = (-/+)e\sum_{i,j(j\neq i)} \mathcal{P}_j\left(\Gamma^{L/R,-}_{ij} - \Gamma^{L/R,+}_{ij}\right) \tag{51}$$

This expression contains implicitly the bias and gate voltages. Therefore IV curves can be obtained for finite values of these voltages. The bias derivative of the current gives the differential conductance G. When plotted as a function of the bias V_b, the current has steps in correspondence of values of V_b at which new transitions involving two contiguous charge states are energetically allowed. At low voltages – smaller than the charging energy – this is not possible and the current is blocked. In correspondence of these transitions, the conductance as function of V_b displays peaks. When plotted simultaneously as a function of both V_b and V_g, the conductance displays a characteristic diamond pattern, the so called stability diagram: inside each diamond a given charge state is stable and the current is blocked.

D. Cotunneling Regime

When the coupling to the leads becomes stronger the description of transport based on incoherent sequential tunneling is no longer enough. In particular higher-order tunneling processes in which the electron tunnels coherently through classically forbidden charge states. As a result, for values of the voltages where sequential tunneling predicts a blocking of the current, a small leakage current is in fact possible though these processes.[47] The simplest example of these processes is second order in the tunneling Hamiltonian, and it is known as cooperative tunneling or cotunneling. Typically for the cotunneling regime $k_{\rm B}T < \hbar\Gamma \ll E_c$.

Cotunneling can be either elastic or inelastic. In the former case the energies of the initial and final state are the same, while in the latter the energies are different. Signatures for these processes have also been observed in single-molecule junctions.[14,36,37] Beyond the sequential tunneling regime, the tunneling Hamiltonian must be replaced by the T-matrix, which is given by[47]

$$T = \mathcal{H}^T + \mathcal{H}^T \frac{1}{E_j - \mathcal{H}_0 + i\eta} T \,, \qquad (52)$$

where E_j is the energy of the initial state $|j\rangle\,|n\rangle$, where $|j\rangle$ refers to the equilibrium state on the left and right lead and $|n\rangle$ is the initial molecular state, $\eta = 0+$ is a positive infinitesimal and $\mathcal{H}_0 = \mathcal{H}_{mol} + \mathcal{H}_{L/R}$. To second order, the transition rates from state $|j\rangle\,|n\rangle$ to $|j'\rangle\,|n'\rangle$ with an electron tunneling from lead α to the lead α' are given by

$$\Gamma^{nj;n'j'}_{\alpha\alpha'} = \frac{2\pi}{\hbar} \left| \langle j'|\,\langle n'|\,\mathcal{H}^T \frac{1}{E_{jn} - \mathcal{H}_0 + i\eta} \mathcal{H}^T\,|n\rangle\,|j\rangle \right|^2 \times \delta(E_{j'n'} - E_{jn}) \,, \qquad (53)$$

where $E_{j'n'}$ and E_{jn} are the energies of the final and initial states, respectively. Here $|j'\rangle\,|n'\rangle = a^\dagger_{\alpha'\mathbf{k}'\sigma'} a_{\alpha\mathbf{k}\sigma}\,|j\rangle\,|n'\rangle$. Inserting the tunneling Hamiltonian, Eq.(36), in last equation and after some algebra (see Appendix A) one can get the expression for the transition rates for processes from lead α till lead α' and from molecular state $|n\rangle$ to the state $|n'\rangle$:

$$\Gamma^{n;n'}_{\alpha\alpha'} = \sum_{\sigma\sigma'} \gamma^\sigma_\alpha \gamma^{\sigma'}_{\alpha'} \int d\varepsilon f(\varepsilon - \mu_\alpha)\left(1 - f(\varepsilon + \varepsilon_n - \varepsilon_{n'} - \mu_{\alpha'})\right) \times \left| \sum_{n''} \left\{ \frac{A^{\sigma *}_{n''n'} A^{\sigma'}_{n''n}}{\varepsilon - \varepsilon_{n'} + \varepsilon_{n''} + i\eta} + \frac{A^{\sigma'}_{n'n''} A^{\sigma *}_{nn''}}{\varepsilon + \varepsilon_n - \varepsilon_{n''} + i\eta} \right\} \right|^2 , \qquad (54)$$

where σ is the electron spin, $f(\varepsilon)$ is the Fermi distribution function, μ_α is the chemical potential of the lead α, $\mu_L - \mu_R = -eV/2$, $|n''\rangle$ is a virtual state, $A^{\sigma'}_{ij} = \langle i|\,c_{\sigma'}\,|j\rangle$ and $A^{\sigma *}_{ij} = \langle j|\,c^\dagger_\sigma\,|i\rangle$. Here γ^σ_α is the tunneling amplitude. Note that $|n\rangle$ and $|n'\rangle$ are states with the same number of particles. We have not taken into account processes changing the electron number by ± 2 units.[42,49]

The transition rates in Eq. 54cannot be evaluated directly because of the second-order poles in the energy denominators. A regularization scheme has been carried out to fix these divergences and obtain the cotunneling rates.[50,51] Here it is important to mention that these divergences are an artifact of the to the T-matrix approach rather than a real physical problem. The fourth-order Bloch-Redfield quantum master equation (BR) and the real-time diagrammatic technique (RT) approaches to quantum transport have been developed to avoid any divergences and therefore no *ad hoc* regularization to cotunneling is required.[39,40] Nevertheless, the T-matrix approach agrees with these two approaches and gives good reasonable results deep inside the Coulomb blockade region.[45] We expect to catch all the relevant physics for our system with the T-matrix approach. After the regularization scheme is implemented, we get the tunneling rates defined as (see Appendix B)

$$\Gamma^{n;n'}_{\alpha\alpha'} = \sum_{\sigma\sigma'} \gamma^{\sigma}_{\alpha}\gamma^{\sigma'}_{\alpha'} \Bigg[\sum_k \left(A^2 J(E_1, E_2, \varepsilon_{ak}) + B^2 J(E_1, E_2, \varepsilon_{bk}) \right) + 2 \sum_q \sum_{k\neq q} A_k A_q I(E_1, E_2, \varepsilon_{ak}, \varepsilon_{aq}) + 2 \sum_q \sum_{k\neq q} B_k B_q I(E_1, E_2, \varepsilon_{bk}, \varepsilon_{bq}) + 2 \sum_q \sum_k A_k B_q I(E_1, E_2, \varepsilon_{ak}, \varepsilon_{bq}) \Bigg] \quad (55)$$

where $A_k = A^{\sigma *}_{kn'} A^{\sigma'}_{kn}$, $B_k = A^{\sigma'}_{n'k} A^{\sigma *}_{nk}$, $\varepsilon_{ak} = \varepsilon_{n'} - \varepsilon_k$, $\varepsilon_{bk} = \varepsilon_k - \varepsilon_n$, $E_1 = \mu_\alpha$ and $E_2 = \mu_{\alpha'} + \varepsilon_{n'} - \varepsilon_n$. Here I and J are integrals that come out from the regularization scheme, and are defined in Eqs. (B1) and (B2), respectively.

The complete master equation, including both sequential and cotunneling contributions, finally reads

$$\frac{d}{dt}\mathcal{P}_i = \sum_{j(j\neq i)} \left(\Gamma_{ij}\mathcal{P}_j - \Gamma_{ji}\mathcal{P}_i \right) + \sum_{\alpha\alpha' j} \left(\Gamma^{ji}_{\alpha\alpha'}\mathcal{P}_j - \Gamma^{ij}_{\alpha\alpha'}\mathcal{P}_i \right) \quad (56)$$

and the current through the system is now given by

$$I \equiv I^{L/R} = (-/+)e \sum_{i,j(j\neq i)} \mathcal{P}_j \left(\Gamma^{L/R,-}_{ij} - \Gamma^{L/R,+}_{ij} \right) + (-/+)e \sum_{i,j(j\neq i)} \mathcal{P}_j \left(\Gamma^{ji}_{LR/RL} - \Gamma^{ij}_{RL/LR} \right) \quad (57)$$

As mentioned above, cotunneling gives rise to a small current inside a Coulomb-blockade diamond region of a given charge state. At small values of the bias voltage, smaller than any excitation energies for the given charge state, we are in the regime of *elastic cotunneling* and the current is proportional to the bias voltage. At voltages corresponding to the transition energy to the first excited state of the *same* charge state, a new cotunneling transport channel becomes available and the slope of the linear dependency of the current increases. This signals the first occurrence of *inelastic cotunneling*. Upon further increasing the bias, other upward changes of the slope of the current occur in correspondence to energies at which higher excited states become available. It follows that the differential conductance displays *steps* that resemble the IV curve in the sequential tunneling regime. Note however, that the nature of the two curves is very different: at low bias the conductance is finite (elastic cotunneling). Furthermore the width of the steps in the cotunneling conductance gives the energy difference between states of the *same* charge state, fixed by the specific Coulomb diamond of the stability diagram. Therefore, cotunneling is an excellent tool to investigate *directly* the excitation energies of a given charge state. Indeed cotunneling spectroscopy has been used to investigate electronic, vibrational and magnetic excitations in nanostructures such as a-few-electron semiconductor quantum dots,[52] carbon nanotube quantum dots,[53,54] metallic carbon nanotubes,[55] and single-molecule junctions.[56–58]

At this point, before analyzing the transport results of our model, it is useful to make a connection with inelastic electron tunneling spectroscopy (IETS), studied for example by electron tunneling from a STM tip through a molecule adsorbed on a surface[59,60]. The reader familiar with IETS easily recognizes that the differential conductance versus applied voltage for this case is very similar to the cotunneling conductance of Coulomb blockade. This similarity is not accidental: the physics is essentially the same in both cases, since involves the coherent electron tunneling through a finite system, whose internal degrees of freedom (e.g., vibrational, magnetic and electronic) can be excited by the process. The mathematical formulation of the problem is very similar in the two cases. There is one noticeable difference. In IETS by STM the coupling between the molecule and the (conducting) substrate is much stronger that the coupling between the STM tip and the molecule. Therefore typical IETS setups can be viewed as strongly asymmetric Coulomb-blockade systems, when these are studied in the cotunneling regime.

These considerations suggest an alternative way to investigate the spin-electric coupling in triangular MMs via quantum transport. In the setup of Fig. 6 we can imagine that transport through the MM occurs between the STM and the substrate. on which the MM is placed. Now the gates and leads constructed on the surface could provide the external electric field responsible for the spin-electric tunneling. For this purpose the plane of the triangular MM should be parallel to the surface of the substrate. In this case the detection and coherent manipulation of the low-energy chiral states of the MM would occur by means of IETS.

IV. RESULTS AND DISCUSSION

We now discuss quantum transport for the setup of Fig. 6

We first construct the relevant low-energy many-body states for the charge states containing $N = 2, 3, 4$ electrons. For this purpose we use he Hubbard model introduced in Sec. II. The parameters of the model are taken from the first-principles studies on the $\{Cu_3\}$ triangular MM by Ref. 21.

We have $t = -51$ meV, $U = 9.06$ eV, $\lambda_{\rm SOI} = 0.4$ meV. The model is solved exactly for $N = 2, 3, 4$. We label the many-body states with their electron number N (the charge state), total spin S and z-component of the total spin S_z[61] In case of additional degeneracy, we will use additional quantum numbers to specify the states. E.g., for the the chiral degeneracy for the $N = 3$ GS, we will add $E'_{\pm}$.

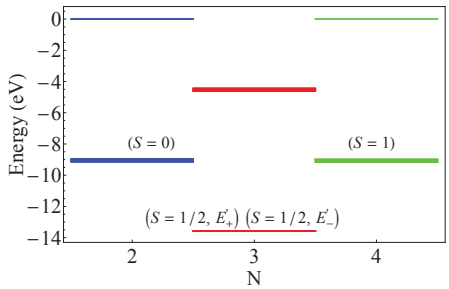

FIG. 7. Low-energy spectrum of the triangular molecular magnet, described by the Hubbard model of Eq. (8), for different charge states or electron filling, $N = 2, 3, 4$. Here the Hubbard model parameters, $t = -0.051$, $U = 9.06$, $\lambda_{\rm SOI} = 0.0004$ (all in eV), are taken from first-principles calculations[21] for the $\{Cu_3\}$ MN. A gate voltage $V_g = U/2$ has been added to rigidly shift the spectrum of the system for a given N. The total spin of the ground state (GS) for the different charge states is indicated in parenthesis. The GS for the $N = 3$-particle system corresponds to the chiral states, $E'_{\pm}$, defined in Eq. (16).

The low-energy levels for the three contiguous charge states are shown in Fig. 7. To the energies calculated with the Hubbard model, we have added a gate voltage term $-eV_g N = -U/2\,N$, which shifts rigidly the spectra of the different charge states with respect to each other. (This choice makes the spectra of the $N = 2$ and $N = 4$ charge states more symmetric with respect to the $N = 3$ states. We will also use this value of the gate voltage below, in the study of cotunneling transport, to make sure that the system is stable in the middle of the $N = 3$ Coulomb diamond.)

For the present choice of the Hubbard parameters, these states are well described by the perturbative analysis of Sec. II. As discussed there, the GS for the $N = 3$ charge state (lowest middle line) is four-fold degenerate, and it corresponds to the states defined in Eq. 16. In Fig. 7 the same line denotes the position of the $S = 3/2$ excited state, whose separation from the GS is not visible on this energy scale.

We now consider the presence of a strong and localized electric field, generated, for example, by a STM tip positioned nearby the MM. We will consider values of ε up to a maximum equal 0.1V/Å,

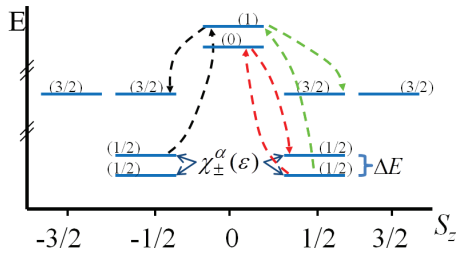

FIG. 8. (Color online). Schematic energy diagram of a triangular MM in the presence of an external electric field ε. Only the GS of the $N = 2, 3, 4$-particle system and the lowest excited states of the $N = 3$ system are included. The numbers in parenthesis corresponds to the total spin S. The electric field lifts the of the $N = 3$ GS degeneracy, and mixes the chiral states defined in Eq. (16). The "mixed chiral states", are now labeled by $\chi^{\alpha}_{\pm}$, with χ^{α}_{-} being the GS. The GS splitting ΔE is linear in ε at low fields. Here we have used the same parameters of Fig. 7, plus $ea\varepsilon = 0.487$eV, and $d_{EE}\varepsilon = 0.1ea\varepsilon$. The electric field is applied in the plane of the triangle, perpendicularly to line joining vertexes 1 and 2 of the triangle. Also shown in the figure with dashed-colored lines are allowed inelastic cotunneling transitions, occurring via $N = 2, 4$ virtual states. Red, black and green dashed lines correspond to transitions: $\chi_- \leftrightarrow \chi_+$ (ΔE), $\chi_+ \leftrightarrow S = 3/2$ and $\chi_- \leftrightarrow S = 3/2$, respectively.

which can be easily attained with STM.[62,63] For a $\{Cu_3\}$ MM, the distance between magnetic ions is $a = 4.87$Å. For a spin-electric coupling strength $d = ea$, which is the maximum value estimated in Ref. 15, the energy scale $ea\varepsilon$ is equal to 0.487 eV when $\varepsilon = 0.1$ V/Å. As discussed in Sec. II, we model the effect of the electric field in the Hubbard approach via the parameters a, d_{EE}, d_{AE} entering the single-particle Hamiltonians in Eqs. (25) and (28). Here we take $d_{EE} = 0.1ea$ and $d_{AE} = 0$. The effect of the field on the low energy spectrum of the MM is shown in Fig. 8, with the expected splitting and mixing of the GS chiral states for the $N = 3$ charge state. In the absence of SOI the "mixed chiral states" $|\chi^{\alpha}_{-}(\varepsilon)\rangle$ and $|\chi^{\alpha}_{+}(\varepsilon)\rangle$ (with $|\chi^{\alpha}_{-}(\varepsilon)\rangle$ being the GS) are still spin ($\alpha = \pm 1/2$) degenerate. As we saw, their splitting $\Delta E(\varepsilon)$ is proportional to ε. It is interesting to note that, the (small) spin-orbit coupling given in Eq. 29, mixes a little bit $|\chi^{\alpha}_{-}(\varepsilon)\rangle$ and $|\chi^{\alpha}_{+}(\varepsilon)\rangle$. However, since the effect is the same for $\alpha = \pm 1/2$, the double degeneracy of the GS and the first excited state is preserved, and the splitting remains of the order of $\Delta E(\varepsilon)$.

Shown on the same figure are also the four-fold degenerate (N= 3, $S = 3/2$) excited state and the $N = 2$ and $N = 4$ GS, having spin $S = 0$ and $S = 1$ respectively. The $N = 2(4)$ GS has total spin $S = 0(1)$ and spin projection $S_z = 0(0)$. The

rest of the energy spectrum is not shown in Fig. 8.

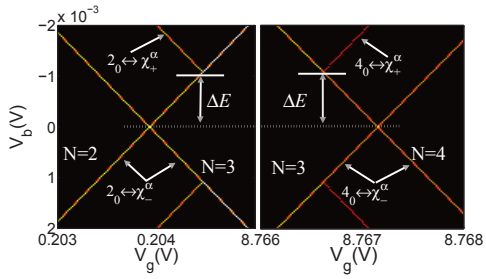

FIG. 9. (Color online) Differential conductance as a function of the bias and gate voltages in the sequential tunneling regime (stability diagram), showing the Coulomb diamonds for three contiguous charge states $N = 2, 3, 4$. Only the corners of the diamonds are shown. The arrows indicate the electron transitions responsible for peaks in the conductance. States are labeled following the notation of Fig. 8. The calculations are done for a symmetric device at temperature $T \sim 10^{-2}K$ ($k_BT \sim 0.001$meV). The parameters for the Hubbard model are the same of those in Fig. 8, A local electric field $\varepsilon = 0.1$ V/Å, is also included, causing a spin-electric coupling of the $N = 3$ chiral states and a GS splitting ΔE.

In Fig. 9 we plot the Coulomb blockade stability diagram, that is, the differential conductance in the sequential tunneling regime as a function of bias and gate voltages. The calculations are done for a symmetric device, where the capacitances and tunneling resistances for the two junctions are the same. The temperature is taken to be $T \sim 10^{-2}K$ ($k_BT \sim 0.001$meV). The calculations are done for the parameters of Fig. 8, and an electric field $\varepsilon = 0.1$ V/Å is included, generating a GS splitting ΔE for the $N = 3$ charge state. The picture displays familiar Coulomb diamonds for the three contiguous charge states $N = 2, 3, 4$, inside which the current is zero. The lines delimiting these diamonds represent the onset of tunneling current, where the conductance has peaks. They correspond to real transitions between states of two contiguous charge states $N \to N \pm 1$. The first lines where this happens involve the transition between the corresponding GSs. Other lines, parallel to these, involve transitions between excited states, which become occupied out of equilibrium. We do not include any energy or spin relaxation mechanism in these calculations.

We now consider cotunneling. In Fig. 10 we plot the differential conductance as a function of the bias voltage V_b, for $V_g = U/2$, which puts the system in the middle of $N = 3$ Coulomb diamond, that is, deep in the Coulomb blockade regime. Here the sequential tunneling current is suppressed, and transport is entirely due to cotunneling. The conductance is nonzero even at zero bias, due to elastic cotunneling. At $V_b \approx 1.1$ meV, the conductance has a first step, indicated by the red dashed line. The step signals the onset of inelastic cotunneling, which takes place when the bias voltage provides enough energy for the final occupation of the lowest excited state of the $N = 3$ charge state ($N = 3, \chi^\alpha_+$), via the virtual transition from the ($N = 3, \chi^\alpha_-$) GS to the ($N = 2, S = 0$) GS. Therefore, the width of this first step provides a direct estimate of the energy splitting between the mixed chiral states, ($N = 3, \chi^\alpha_+$) and ($N = 3, \chi^\alpha_-$), caused by the spin-electric coupling Increasing further the bias, other two cotunneling channels open up, causing the appearance of two other steps in the conductance. The first one, quite small, indicated by the black dashed line, is related with the first occupation of the ($N = 3, S = 3/2$) excited state, which occurs via the virtual transition from the ($N = 3, \chi^\alpha_+$) excited state to the ($N = 4, S = 1$) GS. Note that the state ($N = 3, \chi^\alpha_+$) is already occupied because of the first inelastic cotunneling transition. The second (higher) step, indicated by a green dashed line, is again due to the occupation of the ($N = 3, S = 3/2$) as a final state, but though the virtual transition from the ($N = 3, \chi^\alpha_-$) GS to the ($N = 4, S = 1$) GS.

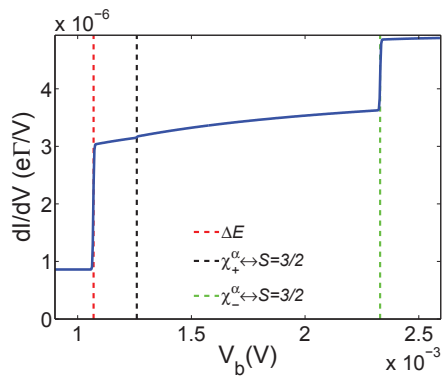

FIG. 10. (Color online) Cotunneling differential conductance as a function of the bias voltage for parameters as in Fig. 7. The states involved are labeled as in Fig.8. At low voltage transport is through elastic cotunneling. The red-dashed line corresponds to the first onset of inelastic cotunneling, due the occupation of the lowest excited state ($N = 3, \chi^\alpha_+$), through a virtual transition ($N = 3, \chi^\alpha_-$) GS $\to$ ($N = 2, S = 0$) GS. The black-dashed line and green-dashed line indicate inelastic cotunneling steps caused by the final occupation of the ($N = 3, S = 3/2$) excited state via the virtual transitions from ($N = 3, \chi^\alpha_\pm$) to the ($N = 4, S = 1$) GS.

The cotunneling conductance pattern depends on the external electric field ε. In Fig. 11 we plot

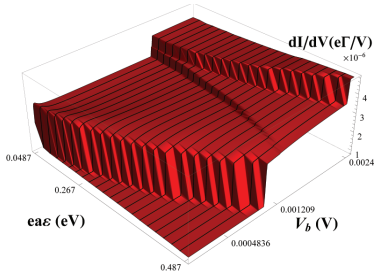

FIG. 11. Cotunneling differential conductance as a function of the bias voltage and the local electric field triggering the spin-electric coupling.

the conductance as function of ε and V_b. As expected, the value of the voltage where the first inelastic step occurs increases with the field. Variations of the position of the other two inelastic steps in the conductance as a function of ε are also visible: at low fields, where the splitting of the chiral GS vanishes, the other two inelastic steps involving the $(N = 3, S = 3/2)$ excited state occur at the same bias. Surprisingly, the height of the inelastic steps is *not* strongly affected by the electric field. The only exception is the second step, whose height becomes very small at the maximum value of ε, as also shown in Fig. 10.

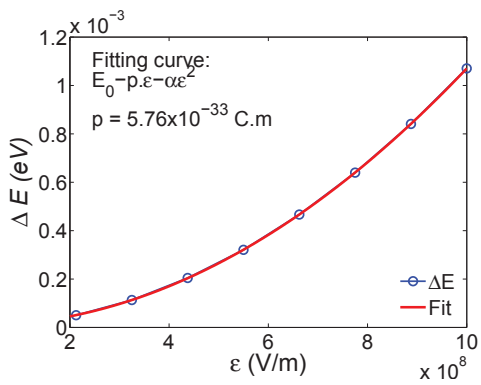

FIG. 12. Energy splitting of the $N = 3$ chiral GS, ΔE, caused by the spin-electric coupling, as a function of the external electric field. The values of ΔE correspond to the position of the first conductance step in Fig. 11. The fitting curve contains a linear term proportional to a dipole moment $p = 5.76\ 10^{-33}$ C m, in agreement with the first-principles calculations on $\{Cu_3\}$ of Ref. 21.

In Fig. 12 we plot ΔE, extracted from the position of first inelastic step, as a function of ε. A polynomial fitting of ΔE vs. ε finds, besides a quadratic contribution due to an induced electric dipole moment, a linear term, which dominates at low fields, and it is the landmark of the (linear) spin-electric coupling. Interestingly, the extracted value of the proportionality coefficient of the linear term, i.e. the "electric dipole moment" $p = d/\sqrt{2}$, is equal to $5.76\ 10^{-33}$ C m, which is consistent with the value found previously by *ab*-initio methods for Cu.[21] This indicates that our choice of the spin-electric parameter $d_{EE} = 0.1ea$ (see Eqs. (24) and (25)) is in the right ballpark. In principle, the curve plotted in Fig. 12 can be directly extracted from experimental measurements of the conductance in the cotunneling regime. From this curve, the strength of electric dipole moment d can be estimated.

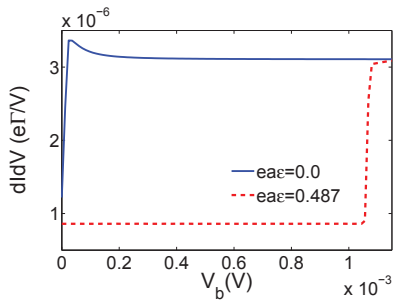

FIG. 13. Cotunneling differential conductance versus bias voltage with (dashed red line) and without (blue solid line) external electric field, causing the spin-electric coupling. Here we have used the same parameters of Fig. 8.

The cotunneling conductance for both $\varepsilon = 0$ (blue line) and $\varepsilon = 0.1$ V/Å (red dashed line) is plotted in Fig. (13). At zero field, the splitting of the $N = 3$ GS, controlling the onset of inelastic cotunneling, is brought about only by the SOI-induced Dzyaloshinskii-Moriya interaction, which splits the chiral states without mixing them. This splitting is predicted to be very small, both experimentally[15] ($\Delta_{\rm SOI} = 0.04$ meV) and theoretically ($\Delta_{\rm SOI} = 0.02$ meV)[33]. The value extracted from the cotunneling conductance of Fig. (13) is consistent with this estimate. A measurement of this splitting from cotunneling experiments is also in principle possible but probably very challenging. The value of the elastic cotunneling conductance is slightly larger when the ε-field is absent than in the presence of the field. However value of the inelastic conductance is the same with and without field. The fact that inelastic cotunneling sets in at very different thresholds with and without field suggests the possibility of using this system as a switching device, which can be controlled electrically, possibly by a time-dependent field.

V. CONCLUSIONS

In summary, we have carried out a theoretical study of quantum transport through an antiferromagnetic triangular molecular magnet (MM), in a single-electron transistor setup. The interplay of spin frustration and lack of inversion symmetry in this MM is responsible for the existence of an efficient spin-electric coupling, which can affect the non-linear transport. When a strong localized electric field is applied to the molecule, the spin-electric coupling causes a splitting between the two doubly-degenerate spin chiral states that compose the ground state of the MM. We have shown that this energy splitting and, consequently the strength of the spin-coupling, should be directly accessible experimentally by measuring the inelastic cotunneling conductance in the Coulomb blockade regime. Both SETs used in molecular spintronics and IETS of molecules on surfaces addressed with a STM could be employed to study this effect.

Our theoretical approach was based on a Hubbard model,[15,18] where the spin-electric coupling can be described in terms of a few microscopic parameters derivable from first-principles calculations. We have shown that the value of the strength of spin-electric coupling estimated from tunneling transport is consistent with the value calculated by first-principles methods.[21]

Antiferromagnetic molecules, like the one considered here, characterized by ground states composed of chiral pairs of spin-1/2 doublets, could be used to create pairs of quasi-degenerate qbits. The possibility of coherently coupling these two qbits electrically and detecting their quantum superposition state in electronic transport is an interesting topic that should further investigated.

The effect of an external magnetic field, not considered in this paper, can be used for gaining full control of the ground-state manifold. Furthermore, higher excited states of the system can play a role as auxiliary states employed to perform quantum gates. As we have shown in our study of the cotunneling conductance (see Fig. 11), these higher states can also be manipulated electrically and brought closer to or further apart from the ground-state manifold. One important issue that we have not discussed in this work is the effect of spin relaxation on transport. This certainly plays a crucial role in determining the robustness of the coherent superposition induced by the electric field.

ACKNOWLEDGMENT

We would like to thank D. Loss and D. Stepanenko for several important discussions and clarifications on the spin-electric coupling in molecular magnets, and M. Islam for an ongoing collaboration on the same subject. We would like to thank D. Magnus Paulsson for his help in developing the codes used in this work. This work was supported by the School of Computer Science, Physics and Mathematics at Linnaeus University, the Swedish Research Council under Grants No: 621-2007-5019 and 621-2010-3761, and the NordForsk research network 080134 "Nanospintronics: theory and simulations".

Appendix A: Explicit derivation of Eq. (54)

Here we demonstrate the Eq. (54). We study the transition rates up to four order. The transition rate from state $|j\rangle|n\rangle$ to $|j'\rangle|n'\rangle$ with one electron tunneling from lead α to the lead α' is given by

$$\Gamma_{\alpha\alpha'}^{nj;n'j'} = \frac{2\pi}{\hbar}\left|\langle j'|\langle n'|\mathcal{H}^T\frac{1}{E_{jn}-\mathcal{H}_0+i\eta}\mathcal{H}^T|n\rangle|j\rangle\right|^2\delta(E_{j'n'}-E_{jn})\,,$$

where $E_{j'n'}$ and E_{jn} are the energies of the final and initial states, respectively. $\mathcal{H}_T = \sum_{\alpha=L,R} t_\alpha \sum_{\mathbf{k}\sigma}\left(a_{\alpha\mathbf{k}\sigma}^\dagger c_\sigma + c_\sigma^\dagger a_{\alpha\mathbf{k}\sigma}\right)$ is the tunneling Hamiltonian Eq. (36) with $T_{km\alpha}^{L/R} = t_\alpha$. $\mathcal{H}_0 = \mathcal{H}_{mol} + \mathcal{H}_{leads}$ and η is a positive infinitesimal number. Here $|j'\rangle|n'\rangle = a_{\alpha'\mathbf{k}'\sigma'}^\dagger a_{\alpha\mathbf{k}\sigma}|j\rangle|n'\rangle$. $|j\rangle$ ($|n\rangle$) refers to the equilibrium state of the left and right Fermi sea (molecule). The total cotunneling rates for

transitions that involve virtual transitions between two n, n'-occupied molecule states are then given by

$$\begin{aligned}
\Gamma^{nj;n'j'}_{\alpha\alpha'} &= \frac{2\pi}{\hbar}\sum_{\mathbf{k}\mathbf{k}'\sigma\sigma'}\Bigg|\langle j|\langle n'|\, a^\dagger_{\alpha\mathbf{k}\sigma}a_{\alpha'\mathbf{k}'\sigma'}\sum_{\alpha'''}t^*_{\alpha'''}\sum_{\mathbf{k}'''\sigma'''}\left(a^\dagger_{\alpha'''\mathbf{k}'''\sigma'''}c_{\sigma'''}+c^\dagger_{\sigma'''}a_{\alpha'''\mathbf{k}'''\sigma'''}\right)\\
&\quad\times\frac{1}{E_{jn}-\mathcal{H}_0+i\eta}\sum_{\alpha''}t_{\alpha''}\sum_{\mathbf{k}''\sigma''}\left(a^\dagger_{\alpha''\mathbf{k}''\sigma''}c_{\sigma''}+c^\dagger_{\sigma''}a_{\alpha''\mathbf{k}''\sigma''}\right)|n\rangle\,|j\rangle\Bigg|^2\delta(E_{j'n'}-E_{jn})\\
&= \frac{2\pi}{\hbar}\sum_{\mathbf{k}\mathbf{k}'\sigma\sigma'}\Bigg|\langle j|\langle n'|\, a^\dagger_{\alpha\mathbf{k}\sigma}a_{\alpha'\mathbf{k}'\sigma'}\sum_{\alpha'''\mathbf{k}'''\sigma'''}\sum_{\alpha''\mathbf{k}''\sigma''}t^*_{\alpha'''}t_{\alpha''}\\
&\quad\times\Bigg(\underbrace{a^\dagger_{\alpha'''\mathbf{k}'''\sigma'''}c_{\sigma'''}\frac{1}{E_{jn}-\mathcal{H}_0+i\eta}a^\dagger_{\alpha''\mathbf{k}''\sigma''}c_{\sigma''}}_{=\,0,\ n\text{-2 states}}+a^\dagger_{\alpha'''\mathbf{k}'''\sigma'''}c_{\sigma'''}\frac{1}{E_{jn}-\mathcal{H}_0+i\eta}c^\dagger_{\sigma''}a_{\alpha''\mathbf{k}''\sigma''}\\
&\quad+c^\dagger_{\sigma'''}a_{\alpha'''\mathbf{k}'''\sigma'''}\frac{1}{E_{jn}-\mathcal{H}_0+i\eta}a^\dagger_{\alpha''\mathbf{k}''\sigma''}c_{\sigma''}+\underbrace{c^\dagger_{\sigma'''}a_{\alpha'''\mathbf{k}'''\sigma'''}\frac{1}{E_{jn}-\mathcal{H}_0+i\eta}c^\dagger_{\sigma''}a_{\alpha''\mathbf{k}''\sigma''}}_{=\,0,\ n\text{+2 states}}\Bigg)\\
&\quad\times|n\rangle\,|j\rangle|^2\,\delta(E_{j'n'}-E_{jn})
\end{aligned}$$

$$\begin{aligned}
\Gamma^{nj;n'j'}_{\alpha\alpha'} &= \frac{2\pi}{\hbar}\sum_{\mathbf{k}\mathbf{k}'\sigma\sigma'}\Bigg|\langle j|\langle n'|\, a^\dagger_{\alpha\mathbf{k}\sigma}a_{\alpha'\mathbf{k}'\sigma'}\sum_{\alpha'''\mathbf{k}'''\sigma'''}\sum_{\alpha''\mathbf{k}''\sigma''}t^*_{\alpha'''}t_{\alpha''}\Big\{c^\dagger_{\sigma'''}a_{\alpha'''\mathbf{k}'''\sigma'''}\,\frac{1}{E_{jn}-\mathcal{H}_0+i\eta}a^\dagger_{\alpha''\mathbf{k}''\sigma''}c_{\sigma''}\\
&\quad+a^\dagger_{\alpha'''\mathbf{k}'''\sigma'''}c_{\sigma'''}\frac{1}{E_{jn}-\mathcal{H}_0+i\eta}c^\dagger_{\sigma''}a_{\alpha''\mathbf{k}''\sigma''}\Big\}\,|n\rangle\,|j\rangle\Bigg|^2\delta(E_{j'n'}-E_{jn})\\
&= \frac{2\pi}{\hbar}\sum_{\mathbf{k}\mathbf{k}'\sigma\sigma'}\Bigg|\sum_{\alpha'''\mathbf{k}'''\sigma'''}\sum_{\alpha''\mathbf{k}''\sigma''}t^*_{\alpha'''}t_{\alpha''}\Big\{\\
&\quad\langle j|\langle n'|\, a^\dagger_{\alpha\mathbf{k}\sigma}a_{\alpha'\mathbf{k}'\sigma'}c^\dagger_{\sigma'''}a_{\alpha'''\mathbf{k}'''\sigma'''}\frac{1}{E_{jn}-\mathcal{H}_0+i\eta}a^\dagger_{\alpha''\mathbf{k}''\sigma''}c_{\sigma''}\,|n\rangle\,|j\rangle\\
&\quad+\langle j|\langle n'|\, a^\dagger_{\alpha\mathbf{k}\sigma}a_{\alpha'\mathbf{k}'\sigma'}a^\dagger_{\alpha'''\mathbf{k}'''\sigma'''}c_{\sigma'''}\frac{1}{E_{jn}-\mathcal{H}_0+i\eta}c^\dagger_{\sigma''}a_{\alpha''\mathbf{k}''\sigma''}\,|n\rangle\,|j\rangle\Big\}\Bigg|^2\delta(E_{j'n'}-E_{jn})
\end{aligned}\tag{A1}$$

Here n and n' are states with the same number of particles. Now we take a look at the denominator terms

$$\begin{aligned}
\langle j|\, a^\dagger_{\alpha\mathbf{k}\sigma}a_{\alpha'\mathbf{k}'\sigma'}a_{\alpha'''\mathbf{k}'''\sigma'''}a^\dagger_{\alpha''\mathbf{k}''\sigma''}\,|j\rangle &= -\,\langle j|\, a^\dagger_{\alpha\mathbf{k}\sigma}a_{\alpha'''\mathbf{k}'''\sigma'''}a_{\alpha'\mathbf{k}'\sigma'}a^\dagger_{\alpha''\mathbf{k}''\sigma''}\,|j\rangle\\
&= -f\left(\varepsilon-\mu_\alpha\right)\delta_{\alpha\alpha'''}\delta_{\mathbf{k}\mathbf{k}'''}\delta_{\sigma\sigma'''}\\
&\quad\times\left(1-f\left(\varepsilon+\varepsilon_n-\varepsilon_{n'}-\mu_{\alpha'}\right)\right)\delta_{\alpha'\alpha''}\delta_{\mathbf{k}'\mathbf{k}''}\delta_{\sigma'\sigma''}
\end{aligned}$$

and

$$\begin{aligned}
\langle j|\, a^\dagger_{\alpha\mathbf{k}\sigma}a_{\alpha'\mathbf{k}'\sigma'}a^\dagger_{\alpha'''\mathbf{k}'''\sigma'''}a_{\alpha''\mathbf{k}''\sigma''}\,|j\rangle &= \langle j|\, a^\dagger_{\alpha\mathbf{k}\sigma}a_{\alpha'\mathbf{k}'\sigma'}\left(\cancelto{0}{\delta_{\alpha'''\alpha''}\delta_{\mathbf{k}'''\mathbf{k}''}\delta_{\sigma'''\sigma''}}-a_{\alpha''\mathbf{k}''\sigma''}a^\dagger_{\alpha'''\mathbf{k}'''\sigma'''}\right)|j\rangle\\
&= -\,\langle j|\, a^\dagger_{\alpha\mathbf{k}\sigma}a_{\alpha'\mathbf{k}'\sigma'}a_{\alpha''\mathbf{k}''\sigma''}a^\dagger_{\alpha'''\mathbf{k}'''\sigma'''}\,|j\rangle\\
&= \langle j|\, a^\dagger_{\alpha\mathbf{k}\sigma}a_{\alpha''\mathbf{k}''\sigma''}\,|j\rangle\,\langle j|\, a_{\alpha'\mathbf{k}'\sigma'}a^\dagger_{\alpha'''\mathbf{k}'''\sigma'''}\,|j\rangle\\
&= f\left(\varepsilon-\mu_\alpha\right)\delta_{\alpha\alpha''}\delta_{\mathbf{k}\mathbf{k}''}\delta_{\sigma\sigma''}\\
&\quad\left(1-f\left(\varepsilon+\varepsilon_n-\varepsilon_{n'}-\mu_{\alpha'}\right)\right)\delta_{\alpha'\alpha'''}\delta_{\mathbf{k}'\mathbf{k}'''}\delta_{\sigma'\sigma'''}
\end{aligned}$$

Here we have used a Taylor series expansion on the operator $1/(E_{jn}-H_0)=(1/E_{jn})\sum_{l=0}^{\infty}(H_0/E_{jn})^l$. Taking into account last delta rules, we have

$$\langle n'|\, c^\dagger_{\sigma'''}c_{\sigma''}\,|n\rangle=\sum_{n''}\langle n'|\, c^\dagger_{\sigma}\,|n''\rangle\,\langle n''|\, c_{\sigma'}\,|n\rangle=\sum_{n''}\left(\langle n''|\, c_{\sigma}\,|n'\rangle\right)^\dagger\,\langle n''|\, c_{\sigma'}\,|n\rangle=\sum_{n''}A^{\sigma *}_{n''n'}A^{\sigma'}_{n''n}$$

and

$$\langle n'|\, c_{\sigma'} c_{\sigma}^{\dagger}\, |n\rangle = \sum_{n''} \langle n'|\, c_{\sigma'}\, |n''\rangle \langle n''|\, c_{\sigma}^{\dagger}\, |n\rangle = \sum_{n''} \langle n'|\, c_{\sigma'}\, |n''\rangle \left(\langle n|\, c_{\sigma}\, |n''\rangle\right)^{\dagger} = \sum_{n''} A^{\sigma'}_{n'n''} A^{\sigma *}_{nn''}$$

where $A^{\sigma'}_{n'n''} = \langle n'|\, c_{\sigma'}\, |n''\rangle$ and $A^{\sigma *}_{nn''} = \langle n''|\, c_{\sigma}^{\dagger}\, |n\rangle$. Here n'' represents a intermediate state.

Thus Eq. (A1) becomes

$$\begin{aligned}
\Gamma^{nj;n'j'}_{\alpha\alpha'} = \frac{2\pi}{\hbar} \sum_{\mathbf{k}\mathbf{k}'\sigma\sigma'} \Bigg| & \sum_{\alpha'''\mathbf{k}'''\sigma'''} \sum_{\alpha''\mathbf{k}''\sigma''} t^{*}_{\alpha'''} t_{\alpha''} \Big\{ \\
& - \langle j|\, \langle n'|\, a^{\dagger}_{\alpha\mathbf{k}\sigma} a_{\alpha'\mathbf{k}'\sigma'} a_{\alpha'''\mathbf{k}'''\sigma'''} c^{\dagger}_{\sigma'''} \frac{1}{\varepsilon_{n'} - \varepsilon_{n''} - \varepsilon + i\eta} c_{\sigma''}\, |n\rangle\, a^{\dagger}_{\alpha''\mathbf{k}''\sigma''}\, |j\rangle \\
& + \langle j|\, \langle n'|\, a^{\dagger}_{\alpha\mathbf{k}\sigma} a_{\alpha'\mathbf{k}'\sigma'} a^{\dagger}_{\alpha'''\mathbf{k}'''\sigma'''} c_{\sigma'''} \frac{1}{\varepsilon_{n} - \varepsilon_{n''} + \varepsilon + i\eta} c^{\dagger}_{\sigma''}\, |n\rangle\, a_{\alpha''\mathbf{k}''\sigma''}\, |j\rangle \Big\} \Bigg|^2 \delta(E_{j'n'} - E_{jn}) \\
\Gamma^{n;n'}_{\alpha\alpha'} = 2\,|t_{\alpha}|^2\,|t_{\alpha'}|^2 \sum_{\sigma\sigma'} \nu_{\alpha}(\sigma)\nu_{\alpha'}(\sigma') & \int \mathrm{d}\varepsilon f\left(\varepsilon - \mu_{\alpha}\right)\left(1 - f\left(\varepsilon + \varepsilon_{n} - \varepsilon_{n'} - \mu_{\alpha'}\right)\right) \\
& \times \left| \sum_{n''} \left\{ \frac{A^{\sigma *}_{n''n'} A^{\sigma'}_{n''n}}{\varepsilon - \varepsilon_{n'} + \varepsilon_{n''} + i\eta} + \frac{A^{\sigma'}_{n'n''} A^{\sigma *}_{nn''}}{\varepsilon + \varepsilon_{n} - \varepsilon_{n''} + i\eta} \right\} \right|^2 \\
= \sum_{\sigma\sigma'} \gamma^{\sigma}_{\alpha} \gamma^{\sigma'}_{\alpha'} & \int \mathrm{d}\varepsilon f\left(\varepsilon - \mu_{\alpha}\right)\left(1 - f\left(\varepsilon + \varepsilon_{n} - \varepsilon_{n'} - \mu_{\alpha'}\right)\right) \\
& \times \underbrace{\left| \sum_{n''} \left\{ \frac{A^{\sigma *}_{n''n'} A^{\sigma'}_{n''n}}{\varepsilon - \varepsilon_{n'} + \varepsilon_{n''} + i\eta} + \frac{A^{\sigma'}_{n'n''} A^{\sigma *}_{nn''}}{\varepsilon + \varepsilon_{n} - \varepsilon_{n''} + i\eta} \right\} \right|^2}_{Q}
\end{aligned} \tag{A2}$$

Appendix B: Explicit derivation of Eq. (55)

The absolute value in Eq. (A2) can be written as

$$\begin{aligned}
Q &= \left| \sum_{n''} \left\{ \frac{A^{\sigma *}_{n''n'} A^{\sigma'}_{n''n}}{\varepsilon - \varepsilon_{n'} + \varepsilon_{n''} + i\eta} + \frac{A^{\sigma'}_{n'n''} A^{\sigma *}_{nn''}}{\varepsilon + \varepsilon_{n} - \varepsilon_{n''} + i\eta} \right\} \right|^2 \\
&= \left(\frac{A^{\sigma' *}_{1n} A^{\sigma}_{1n'}}{\varepsilon - \varepsilon_{n'} + \varepsilon_{1} - i\eta} + \frac{A^{\sigma}_{n1} A^{\sigma' *}_{n'1}}{\varepsilon + \varepsilon_{n} - \varepsilon_{1} - i\eta} + \frac{A^{\sigma' *}_{2n} A^{\sigma}_{2n'}}{\varepsilon - \varepsilon_{n'} + \varepsilon_{2} - i\eta} + \frac{A^{\sigma}_{n2} A^{\sigma' *}_{n'2}}{\varepsilon + \varepsilon_{n} - \varepsilon_{2} - i\eta} \right. \\
&\quad \left. + \frac{A^{\sigma' *}_{3n} A^{\sigma}_{3n'}}{\varepsilon - \varepsilon_{n'} + \varepsilon_{n''} - i\eta} + \frac{A^{\sigma}_{n3} A^{\sigma' *}_{n'3}}{\varepsilon + \varepsilon_{n} - \varepsilon_{3} - i\eta} \right) \\
&\quad \times \left(\frac{A^{\sigma *}_{1n'} A^{\sigma'}_{1n}}{\varepsilon - \varepsilon_{n'} + \varepsilon_{1} + i\eta} + \frac{A^{\sigma'}_{n'1} A^{\sigma *}_{n1}}{\varepsilon + \varepsilon_{n} - \varepsilon_{1} + i\eta} + \frac{A^{\sigma *}_{2n'} A^{\sigma'}_{2n}}{\varepsilon - \varepsilon_{n'} + \varepsilon_{2} + i\eta} + \frac{A^{\sigma'}_{n'2} A^{\sigma *}_{n2}}{\varepsilon + \varepsilon_{n} - \varepsilon_{2} + i\eta} \right. \\
&\quad \left. + \frac{A^{\sigma *}_{3n'} A^{\sigma'}_{3n}}{\varepsilon - \varepsilon_{n'} + \varepsilon_{n''} + i\eta} + \frac{A^{\sigma'}_{n'3} A^{\sigma *}_{n3}}{\varepsilon + \varepsilon_{n} - \varepsilon_{3} + i\eta} \right) \\
&= \sum_{k} \left(\frac{(A^{\sigma *}_{kn'} A^{\sigma'}_{kn})^2}{(\varepsilon - \varepsilon_{n'} + \varepsilon_{k})^2 + \eta^2} + \frac{(A^{\sigma'}_{n'k} A^{\sigma *}_{nk})^2}{(\varepsilon + \varepsilon_{n} - \varepsilon_{k})^2 + \eta^2} \right) \\
&\quad + 2Re \sum_{q} \sum_{k<q} \left(\frac{A^{\sigma *}_{qn'} A^{\sigma'}_{qn}}{\varepsilon - \varepsilon_{n'} + \varepsilon_{q} + i\eta} \frac{A^{\sigma *}_{kn'} A^{\sigma'}_{kn}}{\varepsilon - \varepsilon_{n'} + \varepsilon_{k} - i\eta} + \frac{A^{\sigma'}_{n'q} A^{\sigma *}_{nq}}{\varepsilon + \varepsilon_{n} - \varepsilon_{q} + i\eta} \frac{A^{\sigma'}_{n'k} A^{\sigma *}_{nk}}{\varepsilon + \varepsilon_{n} - \varepsilon_{k} - i\eta} \right) \\
&\quad + 2Re \sum_{q} \sum_{k} \left(\frac{A^{\sigma *}_{kn'} A^{\sigma'}_{kn}}{\varepsilon - \varepsilon_{n'} + \varepsilon_{q} - i\eta} \frac{A^{\sigma'}_{n'k} A^{\sigma *}_{nk}}{\varepsilon + \varepsilon_{n} - \varepsilon_{k} - i\eta} \right)
\end{aligned}$$

Thus Eq. (54) becomes

$$\begin{aligned}
\Gamma_{\alpha\alpha'}^{n;n'} &= \sum_{\sigma\sigma'}\gamma_{\alpha}^{\sigma}\gamma_{\alpha'}^{\sigma'}\int \mathrm{d}\varepsilon f\left(\varepsilon-\mu_{\alpha}\right)\left(1-f\left(\varepsilon+\varepsilon_{n}-\varepsilon_{n'}-\mu_{\alpha'}\right)\right)\\
&\quad\times\left|\sum_{n''}\left\{\frac{A_{n''n'}^{\sigma*}A_{n''n}^{\sigma'}}{\varepsilon-\varepsilon_{n'}+\varepsilon_{n''}+i\eta}+\frac{A_{n'n''}^{\sigma'}A_{nn''}^{\sigma*}}{\varepsilon+\varepsilon_{n}-\varepsilon_{n''}+i\eta}\right\}\right|^{2}\\
&= \sum_{\sigma\sigma'}\gamma_{\alpha}^{\sigma}\gamma_{\alpha'}^{\sigma'}\int \mathrm{d}\varepsilon f\left(\varepsilon-\mu_{\alpha}\right)\left(1-f\left(\varepsilon+\varepsilon_{n}-\varepsilon_{n'}-\mu_{\alpha'}\right)\right)\\
&\quad\times\left[\sum_{k}\left(\frac{(A_{kn'}^{\sigma*}A_{kn}^{\sigma'})^{2}}{(\varepsilon-\varepsilon_{n'}+\varepsilon_{k})^{2}+\eta^{2}}+\frac{(A_{n'k}^{\sigma'}A_{nk}^{\sigma*})^{2}}{(\varepsilon+\varepsilon_{n}-\varepsilon_{k})^{2}+\eta^{2}}\right)\right.\\
&\quad+2Re\sum_{q}\sum_{k<q}\left(\frac{A_{qn'}^{\sigma*}A_{qn}^{\sigma'}}{\varepsilon-\varepsilon_{n'}+\varepsilon_{q}+i\eta}\frac{A_{kn'}^{\sigma*}A_{kn}^{\sigma'}}{\varepsilon-\varepsilon_{n'}+\varepsilon_{k}-i\eta}+\frac{A_{n'q}^{\sigma'}A_{nq}^{\sigma*}}{\varepsilon+\varepsilon_{n}-\varepsilon_{q}+i\eta}\frac{A_{n'k}^{\sigma'}A_{nk}^{\sigma*}}{\varepsilon+\varepsilon_{n}-\varepsilon_{k}-i\eta}\right)\\
&\quad\left.+\,2Re\sum_{q}\sum_{k}\left(\frac{A_{kn'}^{\sigma*}A_{kn}^{\sigma'}}{\varepsilon-\varepsilon_{n'}+\varepsilon_{q}-i\eta}\frac{A_{n'k}^{\sigma'}A_{nk}^{\sigma*}}{\varepsilon+\varepsilon_{n}-\varepsilon_{k}-i\eta}\right)\right]\\
&= \sum_{\sigma\sigma'}\gamma_{\alpha}^{\sigma}\gamma_{\alpha'}^{\sigma'}\int \mathrm{d}\varepsilon f\left(\varepsilon-E_{1}\right)\left(1-f\left(\varepsilon-E_{2}\right)\right)\\
&\quad\times\left[\sum_{k}\frac{A^{2}}{(\varepsilon-\varepsilon_{ak})^{2}+\eta^{2}}\right.\qquad\text{(Integral type J)}\\
&\quad+\sum_{k}\frac{B^{2}}{(\varepsilon-\varepsilon_{bk})^{2}+\eta^{2}}\qquad\text{(Integral type J)}\\
&\quad+2Re\sum_{q}\sum_{k<q}\frac{A_{k}}{\varepsilon-\varepsilon_{ak}+i\eta}\frac{A_{q}}{\varepsilon-\varepsilon_{aq}-i\eta}\qquad\text{(Integral type I)}\\
&\quad+2Re\sum_{q}\sum_{k<q}\frac{B_{k}}{\varepsilon-\varepsilon_{bk}+i\eta}\frac{B_{q}}{\varepsilon-\varepsilon_{bq}-i\eta}\qquad\text{(Integral type I)}\\
&\quad\left.+\,2Re\sum_{q}\sum_{k}\frac{A_{k}}{\varepsilon-\varepsilon_{ak}+i\eta}\frac{B_{q}}{\varepsilon-\varepsilon_{bq}-i\eta}\right]\qquad\text{(Integral type I)}
\end{aligned}$$

where $A_k = A_{kn'}^{\sigma*}A_{kn}^{\sigma'}$, $B_k = A_{n'k}^{\sigma'}A_{nk}^{\sigma*}$, $\varepsilon_{ak} = \varepsilon_{n'} - \varepsilon_k$, $\varepsilon_{bk} = \varepsilon_k - \varepsilon_n$, $E_1 = \mu_\alpha$ and $E_2 = \mu_{\alpha'} + \varepsilon_{n'} - \varepsilon_n$.

Integral type I

$$\begin{aligned}
I(E_1,E_2,\varepsilon_1,\varepsilon_2) &= Re\int \mathrm{d}\varepsilon f(\varepsilon-E_1)\left[1-f(\varepsilon-E_2)\right]\frac{1}{\varepsilon-\varepsilon_1-i\gamma}\frac{1}{\varepsilon-\varepsilon_2+i\gamma}\\
&= \frac{n_B(E_2-E_1)}{\varepsilon_1-\varepsilon_2}Re\left\{\psi\left(\frac{1}{2}+\frac{i\beta}{2\pi}\left[E_2-\varepsilon_1\right]\right)-\psi\left(\frac{1}{2}-\frac{i\beta}{2\pi}\left[E_2-\varepsilon_2\right]\right)\right.\\
&\quad\left.-\psi\left(\frac{1}{2}+\frac{i\beta}{2\pi}\left[E_1-\varepsilon_1\right]\right)+\psi\left(\frac{1}{2}-\frac{i\beta}{2\pi}\left[E_1-\varepsilon_2\right]\right)\right\}
\end{aligned}\tag{B1}$$

Here ψ is the digamma function, n_B is the Bose function and $\beta = 1/k_BT$.

Integral type J

$$\begin{aligned}
J(E_1,E_2,\varepsilon_1) &= \int \mathrm{d}\varepsilon f(\varepsilon-E_1)\left[1-f(\varepsilon-E_2)\right]\frac{1}{(\varepsilon-\varepsilon_1)^2+\eta^2}\\
&= \frac{\beta}{2\pi}n_B(E_2-E_1)Im\left\{\psi'\left(\frac{1}{2}+\frac{i\beta}{2\pi}\left[E_2-\varepsilon_1\right]\right)-\psi'\left(\frac{1}{2}+\frac{i\beta}{2\pi}\left[E_1-\varepsilon_1\right]\right)\right\}
\end{aligned}\tag{B2}$$

Thus Eq. (B1) becomes

$$\Gamma^{n;n'}_{\alpha\alpha'} = \sum_{\sigma\sigma'} \gamma^{\sigma}_{\alpha}\gamma^{\sigma'}_{\alpha'} \Bigg[\sum_{k} \left(A^2 J(E_1, E_2, \varepsilon_{ak}) + B^2 J(E_1, E_2, \varepsilon_{bk}) \right) + 2 \sum_{q} \sum_{k\neq q} \left(A_k A_q I(E_1, E_2, \varepsilon_{ak}, \varepsilon_{aq}) + B_k B_q I(E_1, E_2, \varepsilon_{bk}, \varepsilon_{bq}) \right) + 2 \sum_{q} \sum_{k} A_k B_q I(E_1, E_2, \varepsilon_{ak}, \varepsilon_{bq}) \Bigg] \tag{B3}$$

[1] D. Gatteschi, R. Sessoli, and J. Villain, *Molecular Nanomagnets* (Oxford University Press, Oxford, 2006).
[2] C. J. Wedge, G. A. Timco, E. T. Spielberg, R. E. George, F. Tuna, S. Rigby, E. J. L. McInnes, R. E. P. Winpenny, S. J. Blundell, and A. Ardavan, Phys. Rev. Lett. **108**, 107204 (2012).
[3] L. Bogani and W. Wernsdorfer, Nat Mater **7**, 179 (2008).
[4] S. Sanvito, Chem. Soc. Rev. **40**, 3336 (2011).
[5] M. Affronte, J. Mater. Chem. **19**, 1731 (2009).
[6] M. N. Leuenberger and D. Loss, Nature **410**, 789 (2001).
[7] J. Lehmann, A. Gaita-Arino, E. Coronado, and D. Loss, Nat Nano **2**, 312 (2007).
[8] A. Ardavan, O. Rival, J. J. L. Morton, S. J. Blundell, A. M. Tyryshkin, G. A. Timco, and R. E. P. Winpenny, Phys. Rev. Lett. **98**, 057201 (2007).
[9] A. Andre, D. DeMille, J. M. Doyle, M. D. Lukin, S. E. Maxwell, P. Rabl, R. J. Schoelkopf, and P. Zoller, Nat Phys **2**, 636 (2006).
[10] C. F. Hirjibehedin, C. P. Lutz, and A. J. Heinrich, Science **312**, 1021 (2006).
[11] A. C. Bleszynski-Jayich, L. E. Frberg, M. T. Bjrk, H. J. Trodahl, L. Samuelson, and R. M. Westervelt, Phys. Rev. B **77**, 245327 (2008).
[12] K. C. Nowack, F. H. L. Koppens, Y. V. Nazarov, and L. M. K. Vandersypen, Science **318**, 1430 (2007).
[13] N. Baadji, M. Piacenza, T. Tugsuz, F. D. Sala, G. Maruccio, and S. Sanvito, Nat. Mat. **8**, 813 (2009).
[14] E. A. Osorio, K. Moth-Poulsen, H. S. J. van der Zant, J. Paaske, P. Hedegård, K. Flensberg, J. Bendix, and T. Bjørnholm, Nanolett. **10**, 105 (2010).
[15] M. Trif, F. Troiani, D. Stepanenko, and D. Loss, Phys. Rev. Lett. **101**, 217201 (2008).
[16] K.-Y. Choi, Y. H. Matsuda, H. Nojiri, U. Kortz, F. Hussain, A. C. Stowe, C. Ramsey, and N. S. Dalal, Phys. Rev. Lett. **96**, 107202 (2006).
[17] T. Yamase, E. Ishikawa, K. Fukaya, H. Nojiri, T. Taniguchi, and T. Atake, Inorg. Chem. **43**, 8150 (2004).
[18] M. Trif, F. Troiani, D. Stepanenko, and D. Loss, Phys. Rev. B **82**, 045429 (2010).
[19] L. N. Bulaevskii, C. D. Batista, M. V. Mostovoy, and D. I. Khomskii, Phys. Rev. B **78**, 024402 (2008).
[20] D. I. Khomskii, Journal of Physics: Condensed Matter **22**, 164209 (2
[21] M. F. Islam, J. F. Nossa, C. M. Canali, and M. Pederson, Phys. Rev. B **82**, 155446 (2010).
[22] D. Khomskii, Nat Commun **3**, 904 (2012).
[23] J. F. Nossa, M. F. Islam, C. M. Canali, and M. R. Pederson, "Electric control of spin states in frustrated triangular molecular magnets," (2013), unpublished.
[24] B. R. Bulka, T. Kostyrko, and J. Luczak, Phys. Rev. B **83**, 035301 (2011).
[25] I. Weymann, B. R. Bulka, and J. Barnas, Phys. Rev. B **83**, 195302 (2011).
[26] J. Luczak and B. R. Bulka, Journal of Physics: Condensed Matter **24**, 375303 (2012).
[27] C.-Y. Hsieh, Y.-P. Shim, M. Korkusinski, and P. Hawrylak, Reports on Progress in Physics **75**, 114501 (2012).
[28] Y.-C. Xiong, J. Huang, and W.-Z. Wang, Journal of Physics: Condensed Matter **24**, 455604 (2012).
[29] J. Friedel, P. Lenglart, and G. Leman, J. Phys. Chem. Solids. **25**, 781 (1964).
[30] T. A. Kaplan, Z. Phys. B - Condensed Matter **49**, 313 (1983).
[31] N. E. Bonesteel, T. M. Rice, and F. C. Zhang, Phys. Rev. Lett. **68**, 2684 (1992).
[32] T. Moriya, Phys. Rev. **120**, 91 (1960).
[33] J. F. Nossa, M. F. Islam, C. M. Canali, and M. R. Pederson, Phys. Rev. B **85**, 085427 (2012).
[34] S. T. Boris, *Group Theory in Chemistry and Spectroscopy.* (Dover publications, INC, 2006).
[35] M. Fuechsle, J. A. Miwa, S. Mahapatra, H. Ryu, S. Lee, O. Warschkow, L. C. L. Hollenberg, G. Klimeck, and M. Y. Simmons, Nature Nanotechnology **7**, 242 (2012).
[36] H. B. Heersche, Z. de Groot, J. A. Folk, H. S. J. van der Zant, C. Romeike, M. R. Wegewijs, L. Zobbi, D. Barreca, E. Tondello, and A. Cornia, Phys. Rev. Lett. **96**, 206801 (2006).
[37] M.-H. Jo, J. E. Grose, K. Baheti, M. M. Deshmukh, J. J. Sokol, E. M. Rumberger, D. N. Hendrickson, J. R. Long, H. Park, and D. C. Ralph, *Nano Letters*, Nano Lett. **6**, 2014 (2006).
[38] F. Elste and C. Timm, Phys. Rev. B **71**, 155403 (2005).
[39] M. Leijnse and M. R. Wegewijs, Phys. Rev. B **78**, 235424 (2008).
[40] S. Koller, M. Grifoni, M. Leijnse, and M. R. Wegewijs, Phys. Rev. B **82**, 235307 (2010).
[41] D. Weinmann, W. Husler, and B. Kramer,

Phys. Rev. Lett. **74**, 984 (1995).
[42] M. Leijnse, M. R. Wegewijs, and M. H. Hettler, Phys. Rev. Lett. **103**, 156803 (2009).
[43] C. Timm and F. Elste, Phys. Rev. B **73**, 235304 (2006).
[44] F. Elste and C. Timm, Phys. Rev. B **73**, 235305 (2006).
[45] F. Elste and C. Timm, Phys. Rev. B **75**, 195341 (2007).
[46] C. Timm, Phys. Rev. B **76**, 014421 (2007).
[47] H. Bruus and K. Flensberg, *Many body quantum theory in condensed matter physics* (Oxford Graduate Texts, 2004).
[48] M. Tews, Annalen der Physik **13**, 249 (2004).
[49] J. Koch, M. E. Raikh, and F. von Oppen, Phys. Rev. Lett. **96**, 056803 (2006).
[50] M. Turek and K. A. Matveev, Phys. Rev. B **65**, 115332 (2002).
[51] J. Koch, F. von Oppen, Y. Oreg, and E. Sela, Phys. Rev. B **70**, 195107 (2004).
[52] R. Schleser, T. Ihn, E. Ruh, K. Ensslin, M. Tews, D. Pfannkuche, D. C. Driscoll, and A. C. Gossard, Phys. Rev. Lett. **94**, 206805 (2005).
[53] J. V. Holm, H. I. Jørgensen, K. Grove-Rasmussen, J. Paaske, K. Flensberg, and P. E. Lindelof, Phys. Rev. B **77**, 161406 (2008).
[54] J. Paaske, A. Rosch, P. Wolfle, N. Mason, C. M. Marcus, and J. Nygard, Nat Phys **2**, 460 (2006).
[55] S. Sapmaz, P. Jarillo-Herrero, J. Kong, C. Dekker, L. P. Kouwenhoven, and H. S. J. van der Zant, Phys. Rev. B **71**, 153402 (2005).
[56] N. Roch, S. Florens, V. Bouchiat, W. Wernsdorfer, and F. Balestro, Nature **453**, 633 (2008).
[57] J. J. Parks, A. R. Champagne, G. R. Hutchison, S. Flores-Torres, H. D. Abruña, and D. C. Ralph, Phys. Rev. Lett. **99**, 026601 (2007).
[58] E. A. Osorio, K. O'Neill, M. Wegewijs, N. Stuhr-Hansen, J. Paaske, T. Bjrnholm, and H. S. J. van der Zant, *Nano Letters*, Nano Lett. **7**, 3336 (2007).
[59] M. Galperin, M. A. Ratner, and A. Nitzan, J. Phys.: Condens. Matter **19**, 103201 (2007).
[60] M. A. Reed, Materials Today **11**, 46 (2008).
[61] In principle, because of the presence of the spin-orbit interaction, states with different total S are coupled. However the mixing is of the order of the DM parameter $D \propto t\lambda_{\rm SOI}/U$, which, for the parameters used here, is very small on the scale of the exchange constant separating states with different S. Therefore, in practice, S and S_z are good quantum numbers.
[62] N. Mingo and F. Flores, Thin Solid Films **318**, 69 (1998).
[63] K. Stokbro, U. Quaade, and F. Grey, Applied Physics A **66**, S907 (1998).

Printed by Media-tryck, Lund 2013, Sweden

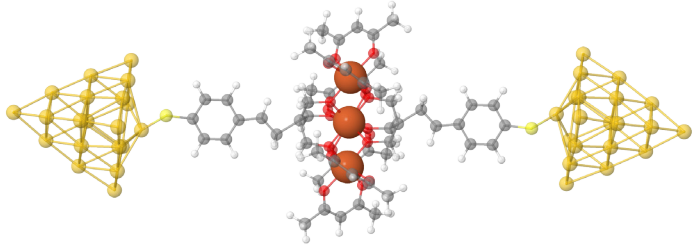

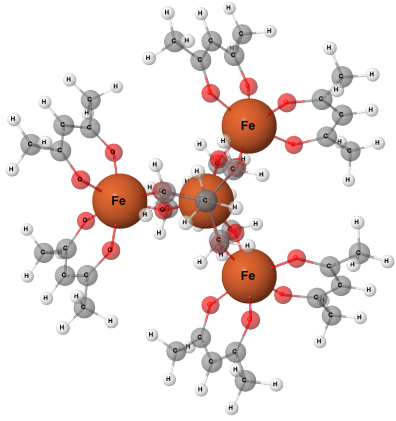

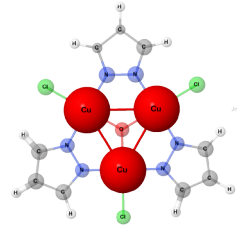

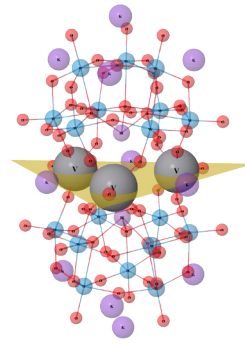

LUND UNIVERSITY

DIVISION OF SOLID STATE PHYSICS
LUND INSTITUTE OF TECHNOLOGY
LUND UNIVERSITY, SWEDEN
ISBN 978-91-7473-547-5